EESAT
PROCEEDINGS 2017

Electrical Energy Storage Applications And Technologies

GATEWAY TO THE FUTURE

Sandia National Laboratories is a multimission laboratory managed and operated by National Technology & Engineering Solutions of Sandia, LLC, a wholly owned subsidiary of Honeywell International Inc., for the U.S. Department of Energy's National Nuclear Security Administration under contract DE-NA0003525.

New Approaches to Increase Ultracapacitor Energy, Power and Efficiency

Y. Maletin, N. Stryzhakova, S. Zelinsky, S. Chernukhin, D. Tretyakov, and S. Tychina

Yunasko-Ukraine, Henerala Naumova St, 13, Kyiv, Ukraine, 02000

***Abstract*- New approaches aimed at increasing the ultracapacitor (UC) energy and power densities are described and discussed. An increase in energy has been achieved due to so-called parallel hybridization of the electrode/electrolyte system, wherein both positive and negative electrodes contain nanoporous carbon and Li-intercalated metal oxides as balanced mixtures. The organic electrolyte is also compatible with both UC and battery electrode components. This technology enables to reach the specific energy of about 35 Wh/kg for a packaged cell that can be charged within 2-3 minutes. Yet another approach based on studying the electrolyte in-pore mobility in positive and negative electrodes enables to substantially increase the UC power output and efficiency.**

***Keywords*- hybrid ultracapacitor, energy density, in-pore mobility, efficiency**

I. Introduction

Ultracapacitor (UC) is one of the names used for an electrochemical capacitor that can store large energy density, as compared with other types of capacitors, resulting from charge separation in the electrical double layer at the electrode electrolyte interface [1-3]. Large electrostatic capacitance and, hence, energy is due to the choice of nanostructured carbon materials (nanoporous activated carbon, carbon nanotubes, graphene, etc.) that are typically used in UC electrodes, the materials having a huge surface area of the order of 1000… 2000 m^2/g.

UC devices have an obvious advantage in high power applications, in particular, if very fast and repeatable charge/discharge events are critical like, e.g., in regenerative braking or stop & start systems in hybrid cars, in pitch-controlled wind turbines, in portable spot or stud welding machines, etc. For many of those applications the UC internal resistance should further be reduced from the currently available level in order to maximize their efficiency and power output, and thus to give a chance to reduce the size (hence, also cost) of the entire solution. Besides, an increase in the energy density from currently available level of 5-7 Wh/kg for pure UC or 10-14 Wh/kg for hybrid devices could obviously expand their application areas but still remains a good challenge.

Our approach aimed at a substantial increase in the UC power density and efficiency is based on the fact that the electrolyte mobility in nanopores of various carbons can differ significantly. Besides, the electrochemical stability of electrolytes in positive or negative potential range depends on the carbon used to fabricate the corresponding electrode. Bearing this in mind, special techniques were developed to select the most appropriate positive and negative electrode materials, which can typically be different [4]. As a result, the UC devices of superior power capability (up to 100 kW/kg) and high efficiency were developed with their performance being verified in several recognized laboratories [5, 6, 7] and also by some automobile producers.

Yet another approach was used [8, 9] to substantially increase the specific energy of UC devices while maintaining their high power output, efficiency and quick charge. To achieve such a challenging goal, both positive and negative electrodes were hybridized, namely, comprised mixtures of nanoporous carbon and lithiated metal oxide powders with thoroughly matched operating potential ranges and energy/power ratio of the mixture components. This design, which can be called a parallel Li-ion capacitor (//LIC) or otherwise a nanocarbon-enhanced Li-ion battery, does provide the energy density of 30-40 Wh/kg with high power output and charging time within 2-3 min.

II. UC Power Density and Efficiency

High power output and high efficiency, along with the long cycle life, safe operation and wide operating temperature range, are the key advantages of UC devices today that open the doors to more and more market niches. Since both power and efficiency values increase with decreasing the UC internal resistance, R_{in}, all the contributions to the R_{in} value should thoroughly be analyzed and minimized. A simple equivalent circuit to describe the contributions can be presented by Eq. (1) and illustrated at a UC schematic cross section in Fig. 1.

$$R_{\text{in}} = R_1 + R_2 + R_3 + R_4 + R_5, \quad (1)$$

where R_1 is the ohmic resistance of current collectors and current leads, R_2 is the contact resistance at the "current collector – active electrode layer" interface, R_3 is the ohmic resistance of the active electrode layer, R_4 is the electrolyte resistance in nanopores of the active electrode layer, and R_5 is

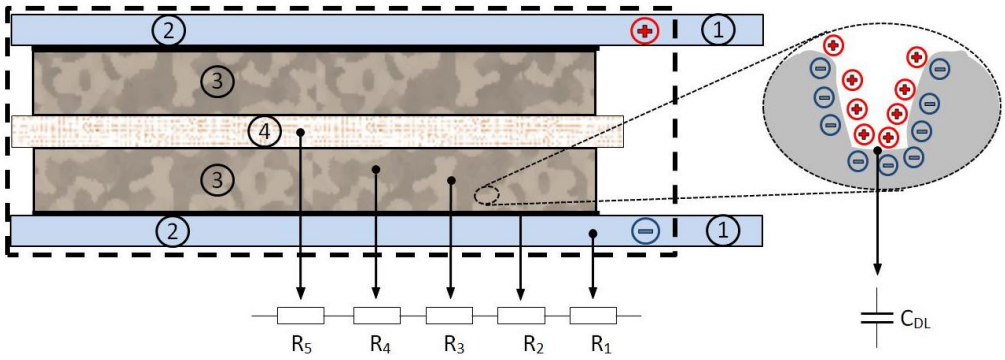

Fig. 1. Schematic cross section of a UC cell: 1 – current leads; 2 – current collectors; 3 – active electrode layers; 4 – porous insulating film (separator). In the enlarged zone on the right, the formation of a double electric layer with a capacitance C_{DL} in a separate slit-like nanopore is illustrated. The zones related with resistances R_1… R_5, as in Eq. 1 are also indicated.

the electrolyte resistance in macropores of the active electrode layer and separator. The contributions of these components to the total R_{in} value are obviously unequal, so consider them one by one.

The R_1 value can easily be minimized by varying the length and cross section of aluminum current collectors and leads/terminals, and this resistance is, no doubt, the lowest and in many cases negligible term in the right part of Eq. 1. The contact resistance, R_2, and ohmic resistance of the active electrode layer, R_3, can be measured with the use of 4-wire method according to the procedure [10], and it was found that R_3 value does not typically contribute more that 5% to the total R_{in} value and, if it is higher for some types of nanoporous carbons, it can easily be reduced to this level by adding the carbon black to the electrode composition. It is also worth noting, that if the nano-sized spherical carbon black is used (e.g., SuperP-Li, Timcal, grain size of about 40 nm), the carbon black particles fill in the voids among the much larger nanoporous carbon grains (typically of a few micron size) and thus do not practically reduce the electrode volumetric capacitance. On the other hand, it has been found [10] that with plain Al foil as a current collector, the contact resistance, R_2, can contribute significantly to UC internal resistance due to the native insulating oxide layer on the Al surface. In order to reduce the contact resistance, the area of contact between the current collector and active electrode layer can substantially be increased by etching the Al foil surface, and there are many companies throughout the world producing such etched foils. Yet another method to reduce the R_2 value was offered in [10, 11], the method providing the local fusion of conductive graphite particles into the plain Al foil surface with the use of electric spark treatment. Both methods - local fusion of conductive particles and etching the current collector surface - result in significant decrease in the R_2 value that does not typically exceed 1-2% of the total R_{in} value.

The electrolyte conductivity in the electrode and separator macro-pores is practically the same as in bulk solution, and therefore, the electrolyte resistance R_5 value can be evaluated from the known electrolyte conductivity and electrode/separator thickness. Our estimations show that R_5 value can contribute approximately 20% to the total R_{in} value. Thus, the sum of four terms in Eq. 1, namely, $R_1 + R_2 + R_3 + R_5$ contributes about 30% only to the UC internal resistance, while the electrolyte resistance in electrode nanopores, R_4, obviously, dominates and gives approximately 70%. Therefore, one of key objectives of our study was to measure the electrolyte in-pore mobility in various carbons in order to select the most appropriate materials for positive and negative UC electrodes.

As is well known [12], the ion mobility and, correspondingly, the electrolyte conductivity are proportional to the diffusion coefficients of ions. A significant reduction in electrolyte diffusion coefficients inside carbon nanopores can be accounted for by at least two major factors. Kalugin et al. [13] with the use of molecular dynamic calculations have shown that the spatial confinement in carbon nanotubes can result in slow diffusion of solvent molecules. Electrostatic and/or Van-der-Waals interactions between the electrolyte species and conductive pore walls can be yet another factor, though these interactions can hardly be evaluated quantitatively because of complexity of the system. On the other hand, two experimental methods have recently been developed [4] that enable to estimate and compare the electrolyte in-pore mobility in various nanoporous carbons in order to best match the nanoporous electrode and organic electrolyte.

The first method is actually a version of the well known technique based on pulsed field-gradient NMR spectroscopy [14], which is widely used for measuring the diffusion coefficients in liquids. In [4] similar measurements were carried out using the nanoporous carbon powders impregnated with typical EDLC electrolytes. Of course, the diffusion coefficients thus obtained reflect some averaged (effective) values due to rather wide distribution of pore size. So, to verify this result, yet another method was used [4], namely, cyclic voltammetry measurements if a porous rotating disc electrode (PRDE) was used as a working electrode. Obviously, in this case the compounds capable to participate in redox

transformations should be involved [4] followed by plotting the diffusion current value versus the electrode rotation rate as in [15]. Both methods give similar results, and indeed, they demonstrate a significant slowdown of electrolyte diffusion in carbon nanopores. Besides, a good correlation of effective diffusion coefficients for cations and anions of organic electrolytes impregnating different nanoporous carbons with the R_{in} value for UC devices containing the corresponding electrode materials was observed [4]. Further this approach was used to select the most appropriate electrode materials for UC with extremely low internal resistance and RC constant value of the order of 0.1 - 0.2 s [16], as was also confirmed by comparative tests in JME [6] and Wayne State University [7]. Some of the test results [7] are listed in Table 1. Here it is worth noting that yet another advantage that results from very low internal resistance and can also be seen in Table 1 is the high efficiency of Yunasko UC cells. In our opinion, it is very important since during a quick discharge the heat generation inside the Yunasko UC cell is about 1-2% of the stored energy only and three-four times less than for best competing cells. This can be of particular importance if a number of repeatable charge-discharge events are needed, and, obviously, lower heat generation implies lower requirements to a cooling system and improved safety.

Thus, provided that carbon materials for positive and negative electrodes are chosen in accordance with the electrolyte mobility in their nanoporous structure, the internal resistance of UC cells can be reduced substantially, and even further reduction in the R_{in} value is possible, in our opinion, by a factor of approximately two.

TABLE I

INTERNAL RESISTANCE AND EFFICIENCY AT CONSTANT POWER (CP) DISCHARGE WITHIN 10 OR 5 SECONDS FOR TWO 1200F UC CELLS [7]

UC cell 1200F	Internal resistance, mΩ	Efficiency @ CP 10 s discharge, %	Efficiency @ CP 5 s discharge, %
Best-on-market	**0.40**	**96.7**	**93.9**
Yunasko	**0.09**	**99.2**	**98.3**

III. UC ENERGY DENSITY: HOW IT CAN BE INCREASED SIGNIFICANTLY

As is known, the energy density of about 7 Wh/kg as reached today [17] or further projected for carbon-carbon UC devices is still low for many applications, and some new approaches should be pursued to increase it significantly. As one of those approaches, the hybridization of the electrochemical system can be implemented, the system thus comprising the nano-structured carbons and some battery-type materials – see, e.g., in [2].

The first hybrid devices were invented by ESMA, Russia in mid-1990s [18], the devices comprising a positive electrode (nickel oxide) from alkaline battery technology and negative electrode (nanoporous carbon) from UC technology. Similar hybridization but "UC and lead-acid battery" has been realized by Axion Power in Canada [19]. A more recent and promising technology is aimed at hybridizing UC and Li-ion battery [20], and a number of various modifications is known today by the general name of LIC (Li-ion capacitor) – e.g., see [21, 22]. One of the best commercial LIC devices is currently produced by JM Energy by the trade name of ULTIMO [23].

All types of hybridization mentioned above provide an increase in specific energy up to 10-15 Wh/kg, and in many cases at the expense of much lower power density and efficiency as compared with typical UC. Such a modest improvement in the UC performance can be accounted for the following reason. All these hybrid technologies combine a high-energy electrode (that of battery type) with a low-energy one (that of UC type) connected in series, and in such a serial combination the low-energy electrode obviously limits the total energy. To avoid this limitation, a different design has recently been developed [8, 9] that can be called a parallel combination of Li-ion and UC electrode components. This technology is denoted as //LIC below and can be presented in more detail as follows:

- Electrodes, both positive and negative, are fabricated with the use of mixtures of nanoporous carbon powder and lithiated metal oxides/phosphates as active ingredients to meet the chemistry requirements of both UC and Li-ion battery technologies. As an example, the negative electrode comprises lithium titanate (LTO), while the positive one comprises lithiated manganese oxide (LMO) and lithium iron phosphate (LFP), both electrodes also containing Kuraray YP50F carbon powder.
- These active electrode ingredients should thoroughly be adjusted by their mass and potential range in order to best match their electrochemical characteristics and provide smooth charge-discharge processes.
- Beside the active electrode ingredients, some kind of binder and conductive particles, e.g., polyvinylidene fluoride (PVdF) and carbon black should be added followed by fabricating the corresponding electrodes.
- From all the organic electrolytes known in Li-ion and UC technologies, acetonitrile is preferred as a solvent to provide the high conductivity and wide operating temperature range. The salts in the electrolyte typically contain both Li^+ and R_4N^+ ions known in both technologies.

Fig. 2-1 illustrates typical charge-discharge curves of thus fabricated //LIC cells packaged in a laminated pouch-type shell (total mass of 85 g). For comparison purposes the same figure also illustrates the charge-discharge curves for a UC cell of the same mass of 85 g (see Fig. 2-2). Both curves were obtained

under the same 20A constant current (CC) conditions. As can be seen from Fig. 2-1, the //LIC charge-discharge curves include an obvious plateau, which is not typical for UC devices, and the curve looks like that for batteries at high C-rates. The specific energy stored in those //LIC cells is about 35 Wh/kg, which is notably higher than that for UC cells or for currently known hybrid technologies mentioned above. It is also worth noting that after charging the //LIC device with the current of 20 A (or ca. 15C-rate), it can be discharged with currents up to 100 A (or ca. 77C-rate) or even higher still demonstrating a smooth slope on a discharge curve. So, as an alternative, this hybrid technology can be called as a "nanoporous carbon enhanced Li-ion battery".

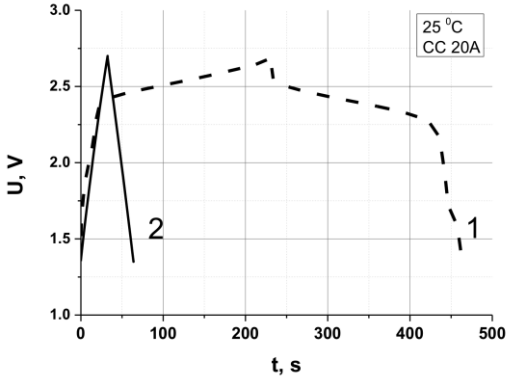

Fig. 2. Charge-discharge curves of a //LIC cell (1) and a UC cell (2) under 20A constant current (CC) conditions at 25 °C; both cells have the same mass of 85 g.

Performance of //LIC prototypes is also illustrated in Fig. 3, wherein the Ragone plots for three different technologies are compared. The upper curve (3) for high power Li-ion batteries illustrates the values presented in a recent comprehensive review [24] and averaged by us. As can be seen from Fig. 3, //LIC devices give a chance to substantially increase the energy density as compared with UC while their power output exceeds that of Li-ion batteries significantly if the efficiency is taken into account.

In Fig. 3 the discharge time for these three different technologies is also shown to demonstrate that high power Li-ion batteries are effective if the discharge time is about 10 min or more. On the other hand, UC devices can most efficiently be employed if the high power pulses of short duration (from fractions of a second to ca. 20 s) are needed. The niche between the two well-known technologies can be filled with //LIC that can most effectively be used between ca. 20 s and 10 min. It is worth noting that //LIC can fully be charged within ca. 3 min, which is much faster than in battery technologies. The cycle life of //LIC devices is also intermediate between Li-ion battery and UC and reaches 30K deep charge-discharge cycles.

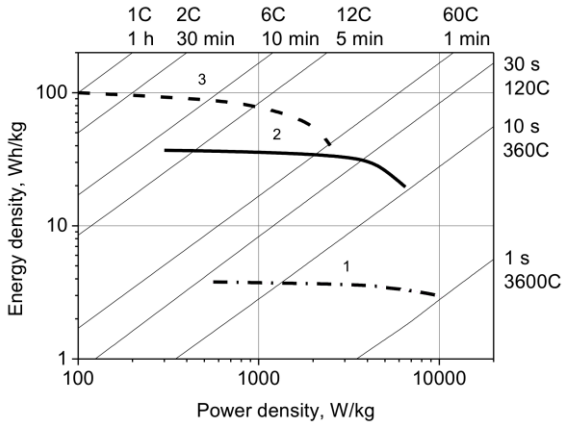

Fig. 3. Ragone plots for high power UC (1), //LIC hybrid device (2), and high power Li-ion battery (3).

IV. Conclusions

1. The ultracapacitor (UC) power output and efficiency are due to its low internal resistance, which in its turn is mostly determined by the electrolyte mobility in carbon electrode nanopores. Since the in-pore mobility of anions and cations can differ significantly, different nano-structured carbons should preferably be chosen for UC positive and negative electrodes.

2. A proprietary technology with both positive and negative electrodes being hybridized (//LIC) gives a chance to increase the UC energy density up to 30-40 Wh/kg while maintaining the power output typical for UC, namely, 3-4 kW/kg at the efficiency above 80%. The electrode components borrowed from UC and Li-ion technologies to fabricate hybrid //LIC electrodes should thoroughly be balanced by their energy stored and charge-discharge potential range.

3. UC devices can most efficiently be employed if the high power pulses of short duration (from fractions of a second to ca. 20 seconds) are needed, while longer pulses (from 20 s to 10 min) can be covered by //LIC devices. The latter can also be fully charged within ca. 3 minutes and can withstand about 30K deep charge-discharge cycles.

Acknowledgements

The test results from Dr. Andrew F. Burke, Dr. John R. Miller and Dr. Dennis Corrigan as well as stimulating discussions with them are very much appreciated.

References

[1] B. E. Conway, *Electrochemical Supercapacitors: Scientific Fundamentals and Technological Appl.*, New York, NY: Kluwer-Plenum Press, 1999.

[2] F. Béguin and E. Frackowiak, *Supercapacitors: Materials, Systems, and Applications*, G. M. Lu, Ed. Weinheim, Germany: Wiley-VCH.

[3] P. J. Grbović, *Ultra-Capacitors in Power Conversion Systems: Appl., Anal. and Design from Theory to Practice*, Hoboken, NJ: Wiley IEEE Press, 2014.

[4] Y. Maletin, V. Strelko, N. Stryzhakova, *et al.*, "Carbon based electrochemical double layer capacitors of low internal resistance," *Energy and Environment Res.*, vol. 3, no. 2, pp. 156-165, Oct. 2013.

[5] A. Burke, Z. Liu, and H. Zhao, "Present and future applications of supercapacitors in electric and hybrid vehicles," in *Proc. of IEEE Int. Electric Vehicle Conf.*, 2014, pp. 1-8.

[6] J. R. Miller, S. M. Butler, and S. McNeal, "Life performance of large electrochemical capacitors," *Proc. of 46th Power Sources Conf.*, 2014, pp. 380-381.

[7] S. Ghosh and D. Corrigan, "Directed Research Report on Performance Comparison of Commercial Supercapacitors," Wayne State University, Detroit, 2014.

[8] Y. Maletin, N. Stryzhakova, S. Zelinskyi, et al., "New approach to ultracapacitor technology: What it can offer to electrified vehicles," *J. of Energy Power Eng.*, vol. 9, pp. 585-591, June 2015.

[9] S. Chernukhin, D. Tretyakov, and Y. Maletin, "Hybrid electrochemical energy storage device," U.S. Pat. Appl. 2014/0085773 A1, Mar. 27, 2014.

[10] Y. Maletin, S. Podmogilny, N. Stryzhakova, et al., "Electrochemical double layer capacitor," U.S. Pat. Appl., 2008/0151472 A1, Jun. 26, 2008.

[11] Y.A. Maletin, O.M. Shembel, Novak P., et al. "Method to manufacture electrodes with low contact resistance for batteries and electric double layer capacitors," U.S. Patent 90448, 2010.

[12] A. J. Bard and L. R. Faulkner, *Electrochemical Methods: Fundamentals and Applications*, 2nd ed., New York, NY: Wiley, 2001.

[13] O. N. Kalugin, V. V. Chaban, V. V. Loskutov, et al., "Uniform diffusion of acetonitrile inside carbon nanotubes favors supercapacitor performance," *Nano. Lett.*, vol. 8, pp. 2126-2130, Jul. 2008.

[14] Y. Cohen, L. Avram, and L. Frish, "Diffusion NMR spectroscopy in supramolecular and combinatorial chemistry: An old parameter—new insights," *Angewandte Chemie Int. Ed,*. vol. 44, no. 4, pp. 520-554, Jan. 2005.

[15] R. T. Bonnecaze, N. Mano, B. Nam, and A. Heller, "On the behavior of the porous rotating disk electrode," *Journal of the Electrochemical Society*, vol. 154, no. 2, pp. F44-F47, 2007.

[16] Y. Maletin, N. Stryzhakova, S. Zelinskyi, et al., "Method for selecting nanoporous carbon material for polarizable electrode, method of manufacturing such polarizable electrodes and method of manufacturing electrochemical double layer capacitor," U.S. Patent 9 524 830, December 20, 2016.

[17] (2018) Maxwell Technologies DuraBlue Ultracapacitor Technology. [Online]. Available: http://www.maxwell.com/products/ultracapacitors/durablue

[18] A.B. Stepanov, I.N. Varakin, V.V. Menukhov, et al., "Double layer capacitor," U.S. Patent 6 181 546, Jan. 30, 2001.

[19] (2016) Axion Power. [Online]. Available: http://www.axionpower.com

[20] S. Tasaki, N. Ando, M. Nagai, et al., "Lithium ion capacitor," U.S. Patent 7 697 264, Apr. 13, 2010.

[21] G. G. Amatucci, F. Badway, A. Du Pasquier, et al., "An asymmetric hybrid nonaqueous energy storage cell," *Journal of the Electrochemical Soc.*, vol. 148, no. 8, pp. A930-A939, 2001.

[22] K. Naoi, S. Ishimoto, J. Miyamoto, et al., "Second generation 'nanohybrid supercapacitor': Evolution of capacitive energy storage devices," *Energy Environmental Sci.*, vol. 5, pp. 9363-9373, 2012.

[23] (2009) ULTIMO Prismatic cell. Front runner of Lithium Ion capacitor. JM Energy Corporation. [Online]. Available: http://www.jmenergy.co.jp/en/products_cell_can.html

[24] H. Budde-Meiwes, J. Drillkens, B. Lunz, et al., "A review of current automotive battery technology and future prospects," *Proc. of the Institution of Mechanical Engineers Part D: J. of Automobile Eng.*, vol. 227, no. 5, pp. 761-776, 2013.

Feasibility Analysis and Testing of a Utility Grade Advanced Power Inverter (API)

Bruce Pilvelait,[1] Dustin Lackey,[1] Ben Cameron,[1] Jack McCarthy,[2] Gysler Castelino,[2] Chip Palombini[2]
[1]*Creare LLC, Hanover, NH, United States*
[2]*Dynapower Company, South Burlington, VT, United States*

***Abstract*- Increased electricity demand amid infrastructure development restrictions continues to foster innovation for distributed generation. However, advances in power converter efficiency, power density, and flexibility are required to enable competitive distributed generation methods to be realized. Wide Band Gap (WBG) semiconductors offer benefits of increased efficiency, higher power density, and simplified thermal management at utility power levels. We aim to use these emerging devices to improve the value proposition of energy storage based distributed generation by increasing power density and eliminating 60 Hz magnetics as well as liquid cooling. Creare is developing a full-scale, containerized grid tie energy storage system with greater than twice the power density over existing converters. This technology will find immediate commercial application to distributed electrical power generation equipment. Elimination of 60 Hz magnetics and liquid cooling provide benefits of reduced cost, greater revenue potential, increased source flexibility, and improved efficiency.**

***Keywords*- silicon carbide, energy storage, utility**

I. Introduction/Background

Energy storage units that provide distributed power generation are becoming desirable for grid stabilization and revenue growth [1]. However, large equipment size, high capitalization cost, and unacceptable reliability have created an opportunity to develop an innovative solution to satisfy market needs. The goal of this project is to develop an innovative Advanced Power Inverter (API) that enables penetration into these markets. The API technology (Fig. 1) addresses one of the largest needs in grid-tied energy storage units: incorporation of a smaller, lower cost, higher reliability inverter to improve their value proposition. Fig. 1 illustrates the approach for developing the API inverter, which is a combination full-bridge DC-DC converter and Three-Level Neutral-Point-Clamped (3LNPC) inverter using emerging high-voltage SiC MOSFETs [2, 3, 4, 5]. Our product is an SiC MOSFET-based API that we will incorporate into an existing grid tied energy storage container product line aimed at the utility industry. While existing power inverters use traditional silicon semiconductors such as IGBTs, our inverter utilizes Wide Band Gap (WBG) SiC MOSFETs that can operate at higher voltage, temperature, and frequency. These attributes will enable direct connection between the inverter and grid interface, and reduce overall cost and size of the inverter. Fig. 2 shows a computer model of the electronics module as well as a concept for how the electronics module is integrated with other components to form the API. The API is only 1.75 m^3 in size, and achieves substantial size reductions when compared with existing products by replacing the liquid cooling with forced air convection cooling and the large 60 Hz transformer with a high frequency transformer having one-tenth the size.

Table 1 compares API size with commercially available inverters. In addition, existing inverters have 480 V or 208 V outputs that require an additional transformer, such as the Temco medium voltage transformer (480:12.47 kV, three-phase 500 KVA, 5.3 m^3, $32,000) to achieve 12.47 kV. This roughly doubles the required size and substantially increases cost.

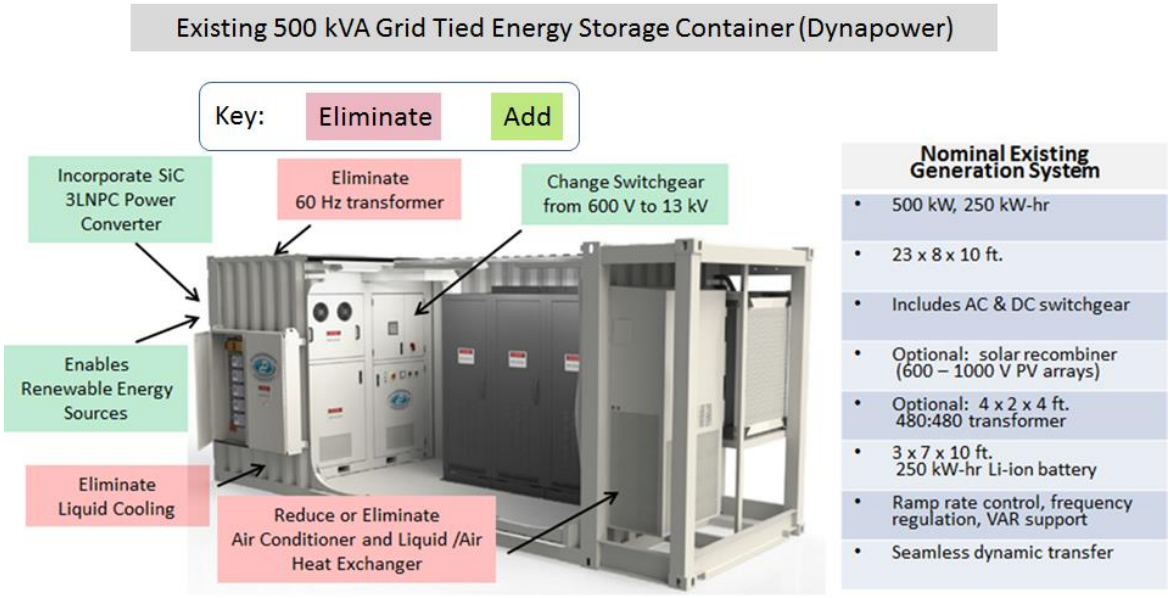

Fig. 1. A transformerless medium voltage grid-tied inverter uses a novel power conversion architecture and SiC semiconductors to eliminate the 60 Hz transformer and liquid cooling.

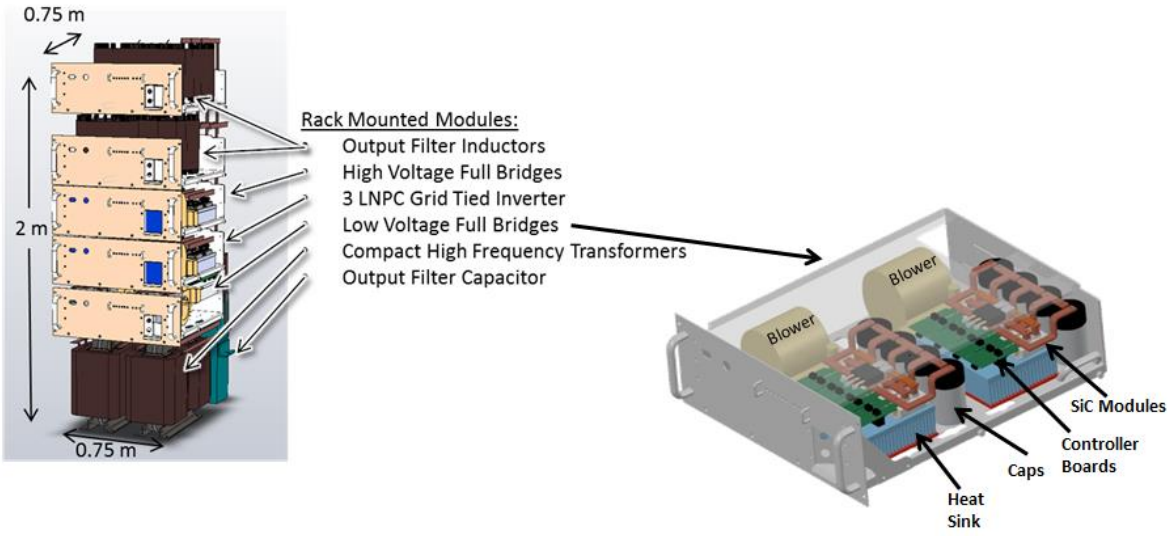

Fig. 2 Creare's API – Packaging details. Substantial size reduction is achieved by elimination of liquid cooling and transformer.

TABLE I
INVERTER SIZE
COMPARISON

Manufacturer	Size (m^3)	Voltage	Power (kW)
Creare	1.75	12.47kV	500
Dynapower	4.6	480V	500
Advanced Energy AE500NX	4.8	480V	500
Solectria SGI500	5.9	208V	500
SMA America 500	7.0	480V	500
Satcon Tech. PVS500	9.4	480V	500

II. RELATED WORK

Six important aspects establish a sound basis for this work. First, the U.S. Department of Energy (DOE) and others have presented data that show the markets for containerized energy storage inverter systems are expanding, and availability of power dense and cost effective power converters will assist these market expansions [1]. The cited report points out that to be cost effective in the near term, system capital cost must be less than $250/kWh, levelized cost must be under 20 ¢/kWh/cycle, system efficiency must be better than 75%, cycle life must exceed 4,000 cycles, and capital costs must be less than $1,750/kW. We believe the API will meet or exceed all of these objectives. Second, data from several researchers have demonstrated that SiC MOSFETs outperform Si IGBTs for medium grid-tie applications [5]. Data indicate that SiC MOSFETs achieve higher frequencies (reducing magnetics size), greater power density, and less loss than series connected Si devices. Third, 10 – 15 kV SiC MOSFETs are available for this work, and we have received and successfully tested 10 kV MOSFETs [5, 6]. Fourth, prior work has successfully demonstrated the use of high-voltage SiC MOSFETs for transformerless grid-tie inverters [7] using bridge-type inverters and boost-type converters. Fifth, using a 3LNPC inverter and novel control algorithms can achieve better harmonic and efficiency performance than a traditional two-level inverter [4]. Finally, while some companies already offer medium-voltage utility interfaces using Si IGBTs, there is no complete system available that incorporates high-voltage SiC power conversion to improve power density, efficiency, and cost [2,3,8]. Taken as a whole, prior work by our team and others establishes a sound basis for the proposed work.

III. CREARE'S API

A. Conventional Utility Inverter Architecture

A schematic of a conventional grid-tied inverter is shown in Fig. 3 where a two-level, three-phase inverter converts 1 kV DC to 480 V AC output voltage. A low-voltage to high-voltage 60 Hz transformer is then used to interface to the 12.47 kV AC electric grid. A primary goal in this work was to take advantage of the high-voltage capability, fast switching speed, and high temperature operation of SiC semiconductors to eliminate the 60 Hz transformer and the liquid cooling system.

The packaging strategy is modeled on the Dynapower Powerskid system, which is widely marketed. This is a 1 MW+, 12.47 kV AC standalone inverter in a separate enclosure from the battery system. Power levels of 500 kW to 1 MW+ are appropriate for the 12.47 kV interconnect, so this approach is believed to be broadly marketable. Since the inverter and the battery are separable, the inverter can be truly "battery agnostic," which also improves marketability. There is already a proven market for these container systems, since Dynapower has built and sold 12.47 kV AC systems at this power level using 60 Hz interconnect transformers. Choosing this approach enables concentration on demonstrating the benefits of SiC to make the most compact grid-tied inverter that is compatible with any battery system.

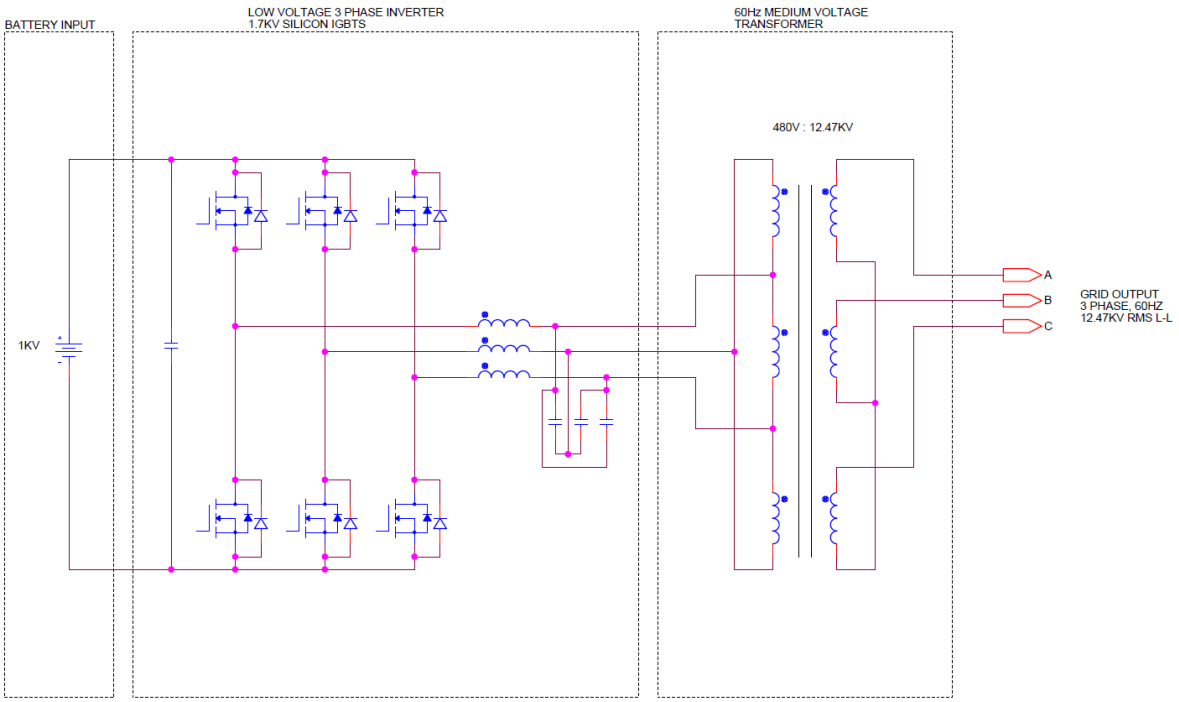

Fig. 3. Conventional two-level three-phase inverter commonly used for utility inverters

B. Advantages of SiC MOSFETS

Currently available semiconductor technologies have required most battery storage systems in the U.S. for utility applications in the 100 kVA to several MVA power range to use batteries with a nominal voltage near 1000 VDC even though the ultimate goal is to achieve medium voltage levels of 13 kV AC. This approach is necessary due to the limited voltage capability using 1700V Si IGBTs. This allows easy interface to a 3-phase 480 VAC electric grid and the use of commercially available ancillary components that have been tested and certified for DC applications. However, while this approach allows use of lower voltage semiconductors, use of a 60 Hz step-up transformer is still required. This incurs substantial cost and space, and the 60 Hz transformer may be on the same order of size as the battery bank itself.

Further restricting the design of existing containerized energy storage systems is the relatively low efficiency and low frequency restrictions of existing high-voltage IGBTs (Figure 4). The literature shows the clear advantage of high-voltage SiC MOSFETs over existing Si IGBTs by comparing maximum system power as a function of switching frequency for Si IGBTs and 10 kV and 15 kV SiC MOSFETs [5]. This advantage of SiC MOSFETs over Si IGBTs exists because (1) high-voltage commercial Si IGBTs are limited in blocking voltage range to about 6.5 kV, which mandates series connected devices to achieve higher grid compatible voltages; (2) IGBTs are inherently less capable of high switching frequency; and (3) SiC power MOSFETs have almost a 30x reduction in switching loss compared to the Si IGBTs. Taken as a whole, SiC MOSFETs enable greater power throughput, better efficiency, and smaller size than equivalent Si IGBTs.

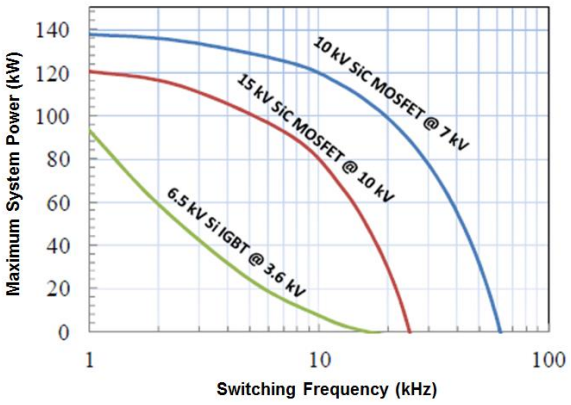

Fig. 4. Comparison of maximum system power as a function of switching frequency for Silicon IGBTs and SiC MOSFETs [5].

C. Design Approach

Creare's API takes advantage of the improved characteristics of SiC semiconductors to enable use of a novel transformerless topology while decreasing the total footprint of a battery energy storage system that directly connects to the 12.47 kV AC grid. A system will be designed with the goal of incorporating the inverter at power levels above 500 kW.

D. Creare's API Architecture

Creare's architecture relies on a Dual Active Bridge (DAB) to boost the battery voltage to a suitable DC link voltage, and a 3LNPC to create the three phase output voltage from the

DC link voltage. This architecture was chosen to take advantage of the high-voltage SiC MOSFETs currently available from a number of manufacturers.

A benefit of the 3LNPC topology is that since the 3LNPC can create three voltage levels at the grid interface (+VDC, -VDC, 0V) instead of two voltage levels, as in the standard two-level converter, this topology also creates fewer current harmonics (roughly half) for the same switching frequency [4]. This enables the use of less semiconductor area and a smaller LC filter, and resulting in better efficiency.

One of the complexities of a 3LNPC topology is that the DC link voltage must remain equally balanced around the "clamp-point." This can be achieved with switching strategies or by topology variations, as described below. To create this maximum 20 kV DC voltage, a number of options were considered. Our preferred option for converting the battery voltage (roughly 1 kV) to a larger DC link voltage (roughly 20 kV) is a two-phase DAB, as shown in Fig. 5. The bridges on the low-voltage side are wired in parallel to share current. The bridges on the high-voltage side are wired in series and operated to ensure the 20 kV DC bus remains balanced around the neutral point. The benefit of this topology is that each transformer has half the total power, so the low-voltage windings have reduced current and the high-voltage windings have reduced voltage. The two DAB pairs can generally be operated independently.

The API architecture relies upon modular subsections to achieve the DC-DC conversion and DC-AC inversion necessary. This topology has the advantage that each MOSFET only blocks half the DC link voltage and exhibits reduced current harmonics leading to smaller grid side filters. Also, this architecture lends itself well to modular testing, which enables subsystem verification and integration toward a fully functional API system.

E. Computer Simulations and Analysis

A computer-based simulation was developed to evaluate performance of the power electronics and controls. This provided a basis for evaluation of the voltage and current waveforms of the semiconductors to calculate losses. The simulation results also provided basis for specifying the values of the DC link capacitors and output filter components. The simulation was developed in the software tool, PSIM. The high level block diagram is shown in Fig. 6. The main components are two DAB blocks and one 3LNPC inverter block. The input is a DC voltage source, the output is a three-phase AC voltage source, and a power meter is wired to the output.

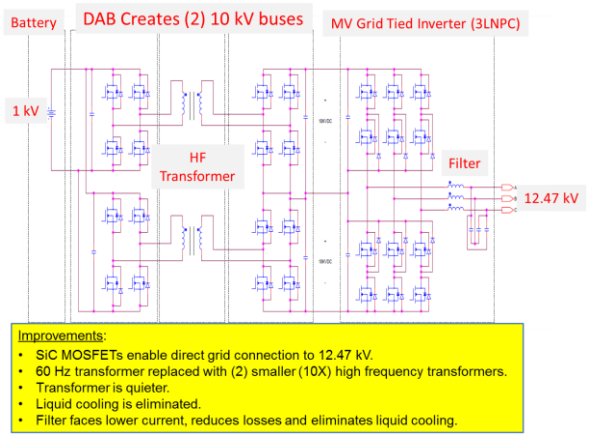

Fig. 5. Creare's API architecture based on a Dual Active Bridge Three-Level Neutral-Point-Clamp.

Fig. 7 shows the details of the DAB blocks. The main components are the MOSFET half-bridge circuits, the high-frequency transformer with winding ratio 1:15, and the 30 µF DC link capacitor on the high-voltage side. The DC link capacitor is sized to maintain reasonable ripple voltage and transient voltage during load changes. Figure 8 shows the details of the inverter block. The main components are the 3LNPC semiconductors and the grid tied output LCL filter. The output filter is designed to maintain current harmonics within the limits defined by IEEE 519/IEEE 1547.

Each DAB operates near 50% duty cycle with a 20 kHz switching frequency. This frequency is higher than possible with IGBTs, substantially reducing audible noise. Power flow from one side of the transformer to the other is controlled by phase-shifting the high and low side drive waveforms with respect to each other. Each DAB is controlled to maintain 10 kV DC across its high-side bus. This creates the balanced 20 kV DC bus required for the 3LNPC output inverter.

The three-phase 3LNPC grid inverter is controlled using conventional carrier-based techniques with the modulating signal controlled in the dq0 reference frame using Park transformations. The grid voltage is sensed to synchronize the output waveform to the grid, and the output current is controlled to create a sinusoidal waveform at the desired power factor. The 3LNPC inverter also switches at 20 kHz.

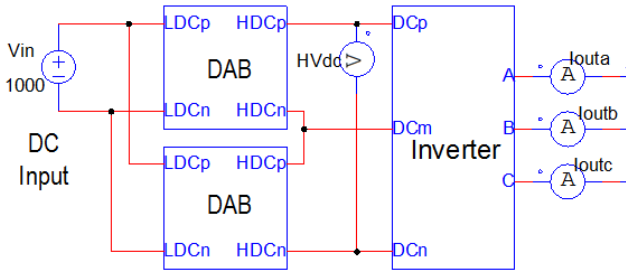

Fig. 6. Computer-based simulation model used to design and analyze the inverter.

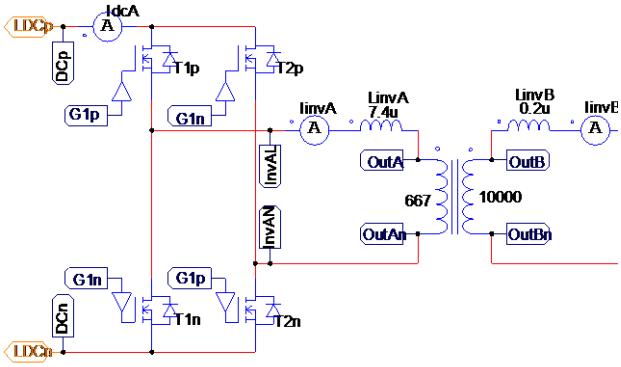

Fig. 7. Dual-Active Bridge block details.

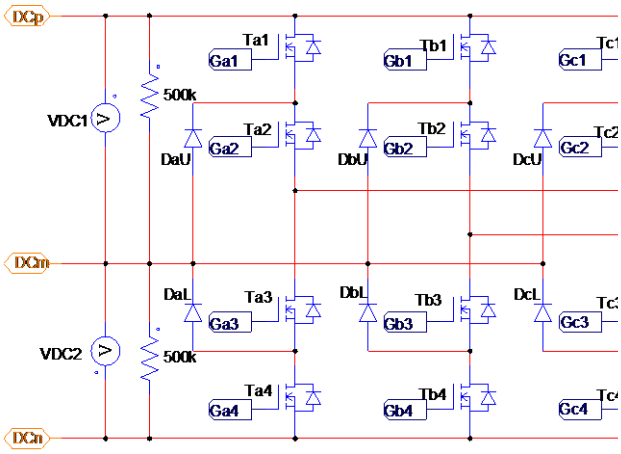

Fig. 8. Inverter block details.

Fig. 9 shows example simulation results that demonstrate system performance. The waveform labelled “HVdc” in the top panel shows that the DC link voltage only changes by 0.1% (± 200 V) with full power step changes, showing good voltage transient suppression. The red waveform labelled “OutP” in the next lower panel is the total output power of the inverter. The power increases to + 500 kW (exporting power to the grid), then decreases to - 500 kW (absorbing power from the grid), then returns to 500 kW, then drops to 0 kW. The waveforms labeled “Iouta,” “Ioutb,” and “Ioutc” show the output currents at the grid connection. They show that the grid currents rapidly respond to changes in power command and reactas expected, even with full power step transitions. The bottom panel shows the three-phase output voltage, which is 12.47 kV line-to-line. These computer simulations were validated with laboratory prototype tests. Fig. 10 shows the harmonic distortion of the output current, displayed as a percentage of the peak value. These harmonics are well below the requirements defined by IEEE 519/IEEE 1547. For example, the 5th harmonic at 300 Hz is roughly 0.7%, where the maximum allowed is 4%. The 11th harmonic at 660 Hz is roughly 0.6%, where the maximum allowed is 2%. The THD is below 1.5%, where the maximum allowed is 5%.

F. Efficiency Analysis

1) Low Voltage Section: Fig. 11 shows an example current waveform from the PSIM simulation for one of the low-voltage MOSFETs while the system is exporting 500 kW to the grid. In this waveform, the switching frequency is 20 kHz and the RMS current in the low-voltage side MOSFETs is roughly 300 A. Analysis using these simulation results shows that two half-bridge devices are needed in parallel to operate reliably at full power (250 kW per DAB). With two MOSFETs in parallel, there is a loss of 300 W per MOSFET, for a total of 300 W * 8 * 2 = 4.8 kW, roughly 1% of the output power.

2) High Voltage DAB: Fig. 12 shows an example current waveform for one of the high-voltage MOSFETs while the system is exporting 500 kW to the grid. In this waveform the time scale is 0.2 ms/division and the RMS current in the high-voltage side MOSFETs is roughly 20 A. Analysis using the simulations shows that a single MOSFET can be used reliably in each location on the high-voltage side (250 kW per DAB). With this configuration, there is roughly 300 W of loss per MOSFET, for a total of 300 W * 8 = 2.4 kW. This is roughly 0.5% of the output power.

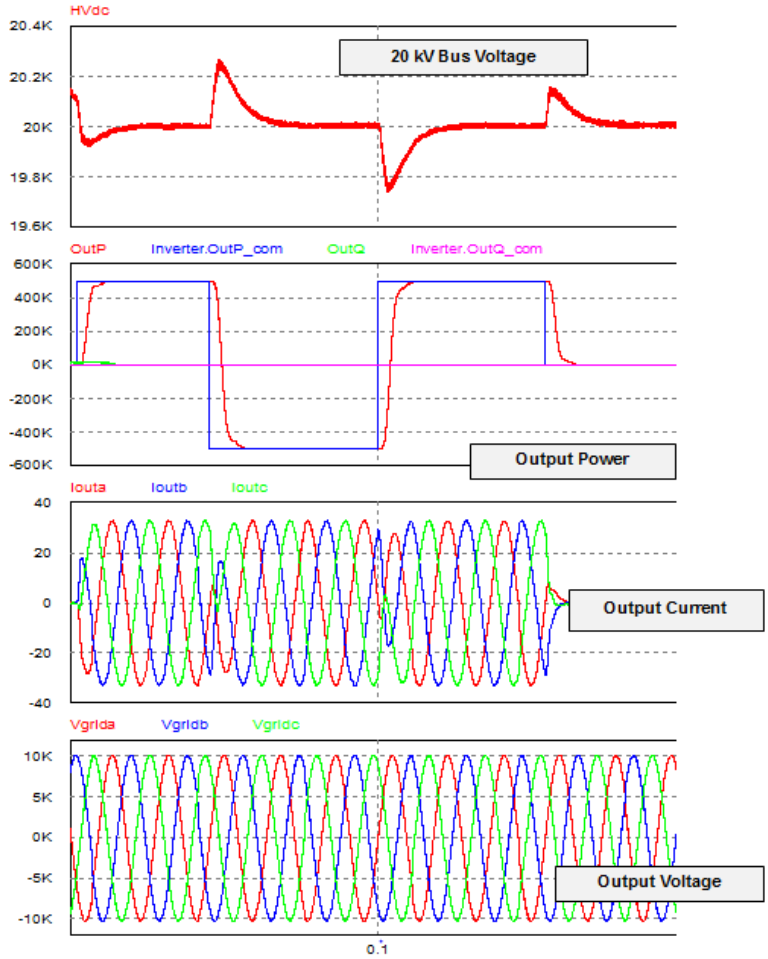

Fig. 9. Simulation results. As output power varies from +500 kW to -500 kW, the DC bus voltage, output current, and output voltage are all well behaved.

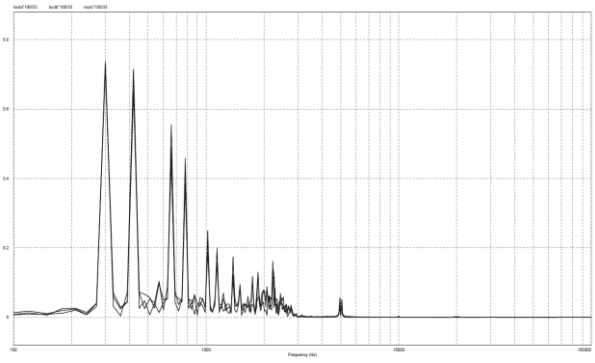

Fig. 10. Total Harmonic Distortion Simulation Results. The THD is below 1.5%, where the maximum allowed is 5%.

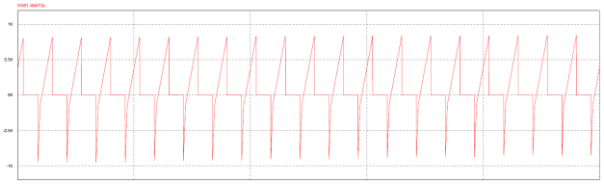

Fig. 11. Low-Voltage MOSFET Current. Total power dissipation in the low-voltage MOSFETs represents roughly 1% of the total output power.

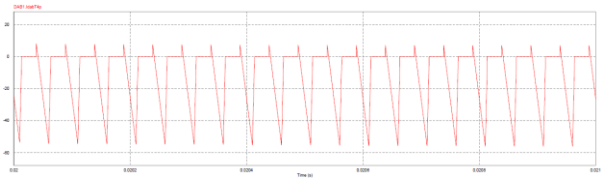

Fig. 12. High-Voltage Dual-Active Bridge MOSFET Current. Total power dissipation in the high-voltage MOSFETs represents roughly 0.5% of the total output power.

3) 3LNPC Inverter: Fig. 13 shows example current waveforms for the high-voltage 3LNPC MOSFETs and diodes while the system is exporting 500 kW to the grid. This waveform shows three cycles of 60 Hz current and the timescale is 10 ms/division. The red waveform shows the current in one of the clamp diodes (DaU), the blue waveform shows the current in one of the outer transistors (Ta1), and the green waveform shows the current in one of the inner transistors (Ta2). Fig. 14 shows the results for a longer duration where the power flow varies in both direction and power factor. Note the distribution of current among these devices varies strongly with power factor. The image shows the same waveforms while the power output varies from +

500 kW (exporting) to - 500 kW (absorbing) to + 500 kVAR to - 500 kVAR. In

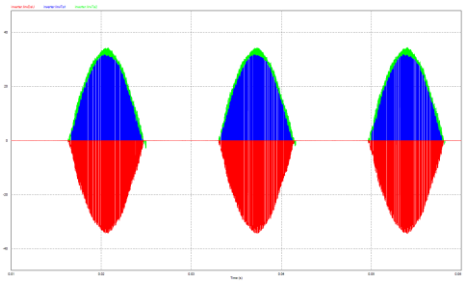

Fig. 13. High-Voltage MOSFET Current. The red waveform shows the current in one of the clamp diodes (DaU), the blue waveform shows the current in one of the outer transistors (Ta1), and the green waveform shows the current in one of the inner transistors (Ta2).

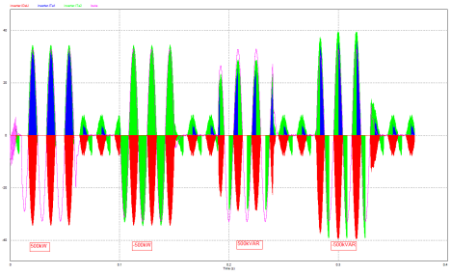

Fig. 14. High-Voltage MOSFET Current. Plot shows the effect of power flow direction and power factor on current split between the clamp diodes and transistors.

this waveform, the pink trace is the grid output current. Depending on power factor, the RMS current in the worst case high-voltage side MOSFET is 15 A. Analysis using the simulations shows that a single MOSFET can be used reliably in each location of the 3LNPC topology. With this configuration, there is roughly 300 W maximum loss in each MOSFET, with a total loss of roughly 3.6 kW. This is roughly 0.7% of the output power.

4) Overall Efficiency: Using the computer simulations, we examined efficiency and losses at a typical output power condition of 500 kW. Semiconductor losses total 10.2 kW, or 2% of total output power. Transformer losses are estimated to be 1% and filter losses are estimated to be 1%. Thus, overall efficiency is estimated to be roughly 96%. This is a significant achievement and enables elimination of the liquid cooling system. Table II summarizes the losses and efficiency.

TABLE II
POWER LOSS AND EFFICIENCY SUMMARY. THE SUMMARY IS BASED ON 500 KW OUTPUT POWER.

Component	Loss
Low-Voltage DAB	4.8 kW (1%)
High-Voltage DAB	2.4 kW (0.5%)
3LNPC	3.6 kW (0.7%)
Transformer	5 kW (1%)
Filters	5 kW (1%)
TOTAL LOSS	21 kW
Output Power	500 kW
Efficiency	96%

IV. PERFORMANCE EXPERIMENTS

A. Low Voltage Architecture Testing

Subsystem hardware testing, to date, includes the DAB modules, and to evaluate the DC-DC conversion performance, these modules were tested in the benchtop test facility shown in Fig. 15. Fig. 16 shows input and output waveforms during testing for a DAB module. During this test effort, we successfully demonstrated the DAB at frequencies up to 20 kHz at subscale voltages.

B. DAB/3LNPC Controller Testing

A combined DAB/3LNPC controller was also successfully tested using a surrogate 6 kHz silicon IGBT prototype while the SiC hardware is being developed. The following figures illustrate laboratory test results intended to validate the previously described computer simulations. Fig. 17 shows a block diagram of the controller, and Fig. 18 shows a photograph of the test facility. The controller was developed to enable configuration as a 20 kHz controller for testing with SiC components, once completed. The implemented control firmware functionality currently includes control for all modules in the API architecture and includes features to operate in a standalone (UF) mode or a grid-tied (PQ) mode. Both hardware and software were successfully demonstrated in UF and PQ modes, and Fig. 19 shows the results for the PQ grid-tied mode at 10 kW.

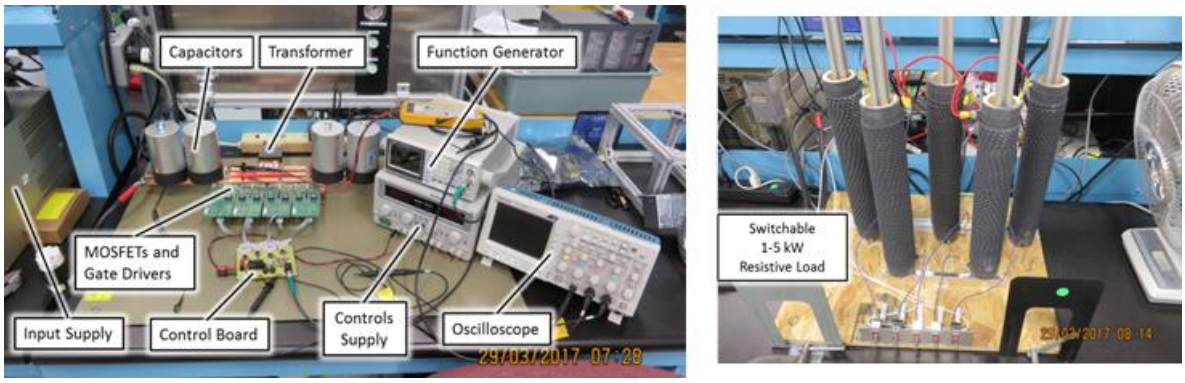

Fig. 15. Low Voltage section of the DAB.

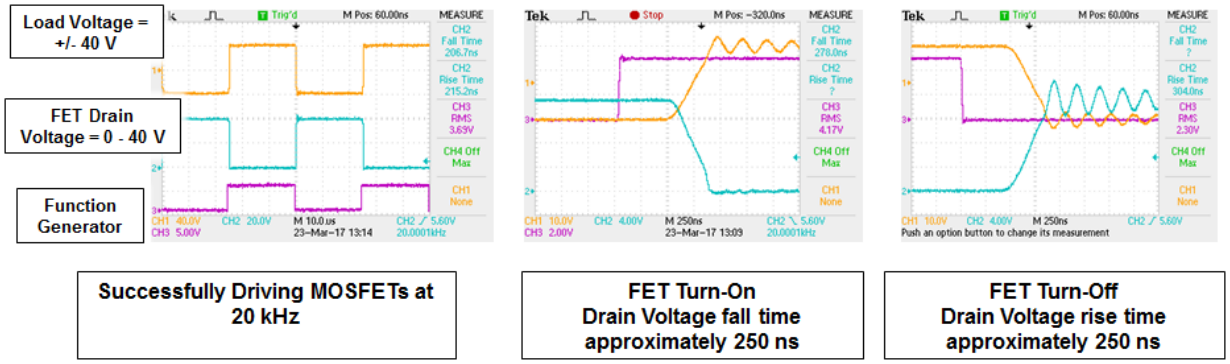

Fig. 16. Low Voltage section test results.

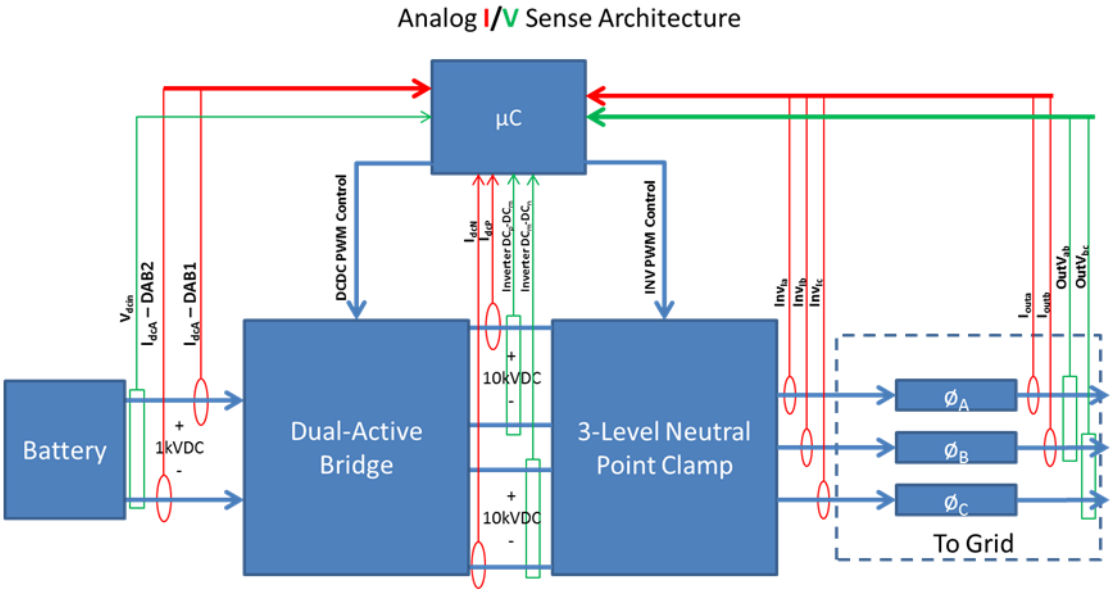

Fig. 17. Controller architecture.

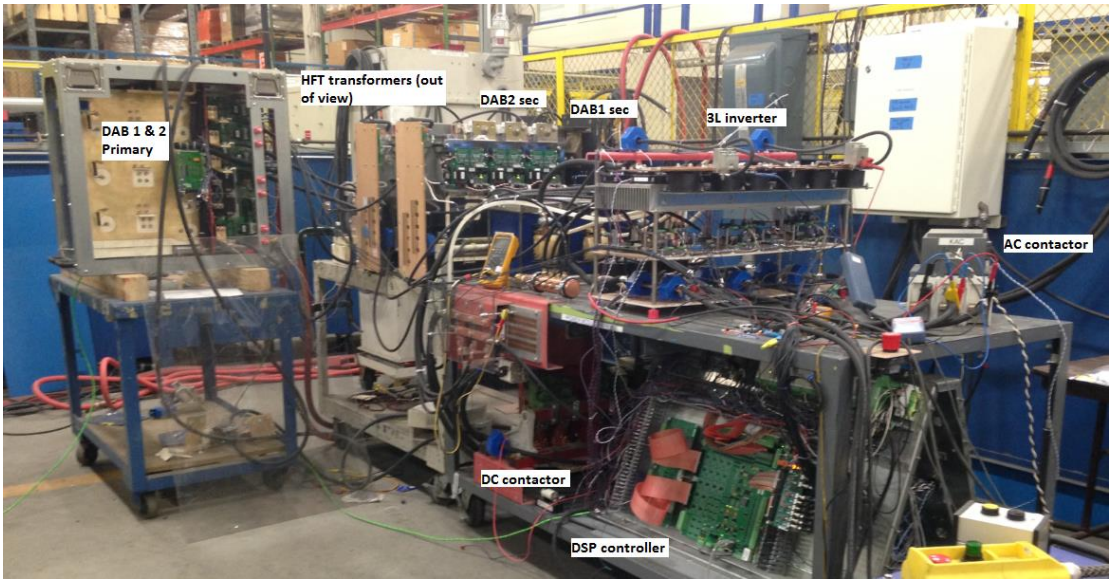

Fig. 18. Photograph of the controller, DAB, and 3LNPC hardware.

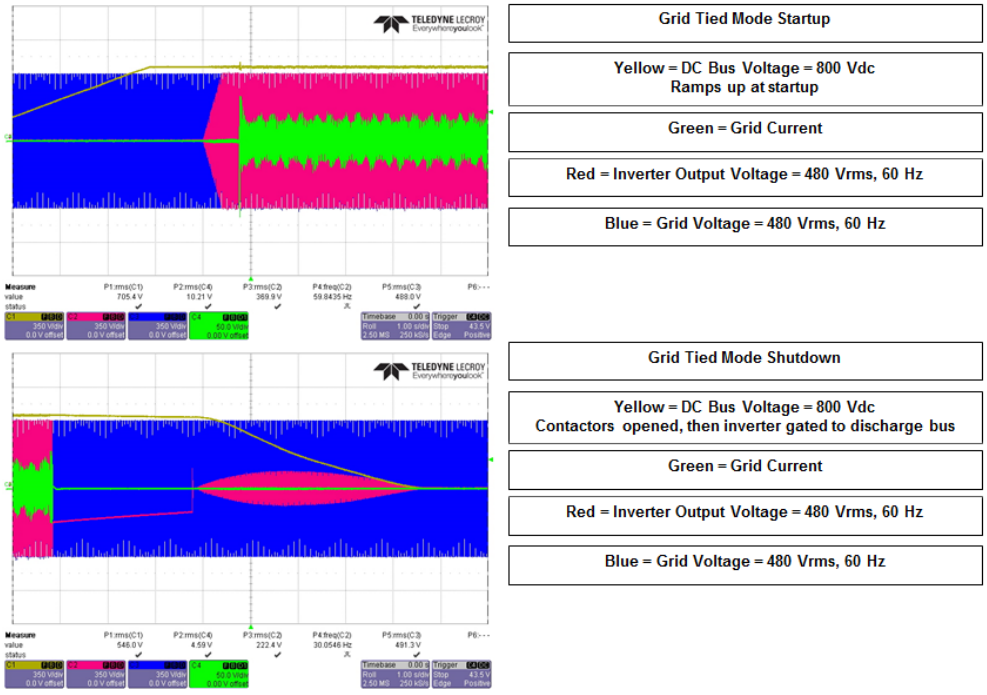

Fig. 19. PQ Grid-Tied mode test results.

V. Discussion

Fig. 20 compares a conventional inverter with Creare's DAB 3LNPC inverter. Benefits of Creare's API include elimination of the 60 Hz transformer and liquid cooling, increased power density, and reduced audible noise. Fig. 21 illustrates the cost and power density comparison between SiC MOSFETs and Si IGBTs. Overall, we expect the cost to be about the same, and the power density to be improved by at least two times when compared with the silicon inverter.

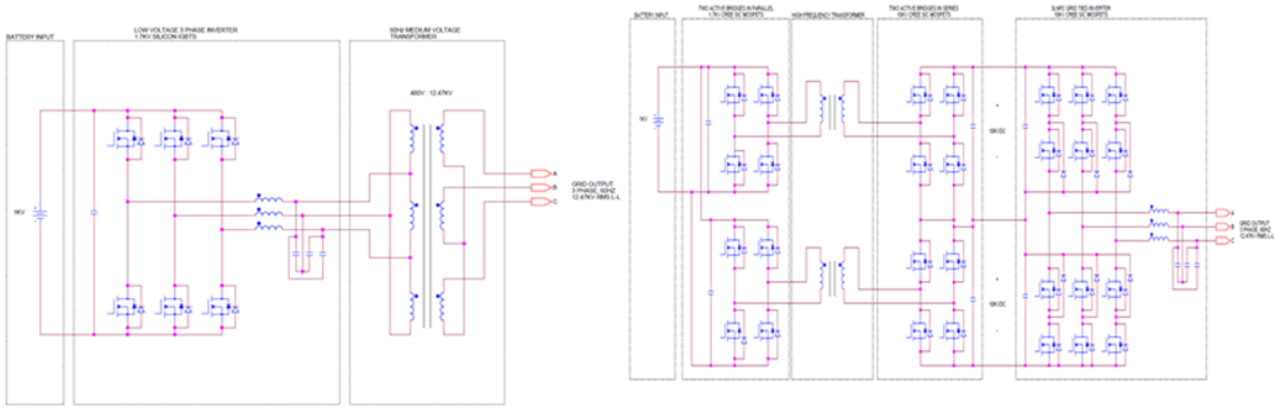

Limitations of this design:
- Requires 480 : 12.47 kV transformer for grid connect.
- Silicon MOSFETs or IGBTs require liquid cooling (~ 50 °C).
- Filter is large and also requires liquid cooling.
- 60 Hz transformer emits acoustic noise.

Improvements:
- SiC MOSFETs enable direct grid connection to 12.47 kV.
- 60 Hz transformer replaced with (2) smaller (10X) high frequency transformers.
- Transformer is quieter.
- Liquid cooling is eliminated.
- Filter faces lower current, reduces losses and eliminates liquid cooling.

Fig. 20. Comparison of conventional inverter with Creare's DAB 3LNPC Inverter.

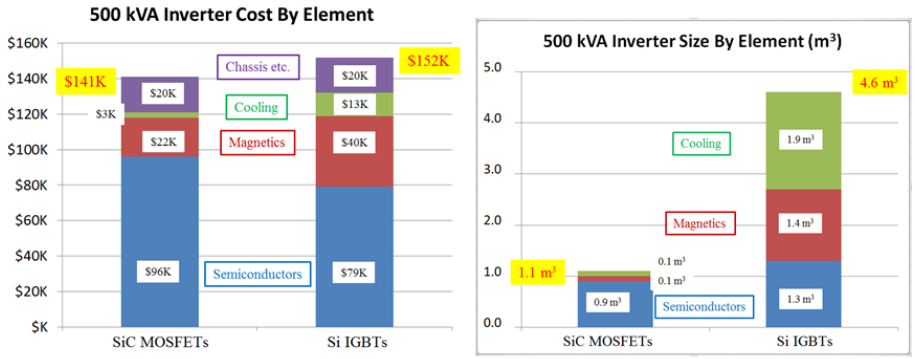

Per unit material costs are comparable ($141K vs. $152K). New design: SiC costs are higher, but magnetics and cooling costs are lower. **SiC costs are likely to reduce.**

Size of the inverter which uses SiC MOSFETs is much smaller, with 4.3X power density.

Fig. 21. Cost and power density comparison.

VI. Conclusions

Our work, thus far, has successfully proven the feasibility of deploying this high-performance inverter. Specifically:

- SiC MOSFETs are superior to silicon IGBTs because (1) high-voltage commercial silicon IGBTs are limited in blocking voltage; (2) IGBTs are limited to lower switching frequency; and (3) SiC power MOSFETs have lower loss.
- SiC MOSFETs will eliminate the need for a liquid-cooled system and 60 Hz transformer. Overall power density is expected to be at least two times greater with SiC MOSFETs than for silicon IGBTs.
- SiC MOSFETs are available to accomplish these goals. Testing of low and high voltage SiC MOSFETs has demonstrated adequate switching times to enable use of a high-frequency transformer.

VII. Recommendation

Based on these positive feasibility demonstrations, Creare plans to continue to develop this API technology. Key future accomplishments are expected to include: (1) fabrication of a fully functional prototype based on this design; (2) initial laboratory testing to verify design expectations; and (3) application of the prototype for initial energy storage applications.

VIII. Future Work

The project began in 2015 as a Phase I SBIR project. Thus far, the year long Phase I project and the first of 2 years of the Phase II project have been completed. The project is roughly two-thirds complete. During the next year of the program, we plan to fabricate and test the fully functional API prototype. We will review and refine the control firmware used during prior testing and acquire critical system components such as the high-voltage SiC devices. We will fabricate subsystem sections individually, then integrate them to form the entire system. Final versions of the high-frequency transformer and inductor will be fabricated. Controller testing will be completed, and the controller will be integrated with the hardware for testing.

Acknowledgements

Creare greatly appreciates the support of Dr. Imre Gyuk and Dr. Stan Atcitty through DOE SBIR Grant DE-SC0013765. Sandia National Laboratories is a multi-program laboratory managed and operated by Sandia Corporation, a wholly owned subsidiary of Lockheed Martin Corporation, for the U.S. Department of Energy's National Nuclear Security Administration under Contract DE-AC04-94AL85000.

References

[1] (2013) Grid Energy Storage. [Online]. Available at: http://energy.gov/sites/prod/files/2013/12/f5/Grid%20Energy%20Storage%20December%202013.pdf

[2 <http://www.dynapowerenergy.com/products/ips-500-solar-storage-systems/>

[3] <http://www.dynapower.com/PDF/Dynapower%20EMS%20MFG%20%20CAST_FOR%20WEBSITE.pdf>

[4] M. Schweizer, T. Friedli, and J.W. Kolar, "Comparative evaluation of advanced three-phase three-level inverter/converter topologies against two-level systems," *IEEE Trans. Ind. Electron.*, vol. 60, no. 12, pp. 5515–5527, Dec. 2013.

[5] V. Pala, E.V. Brunt, L. Cheng, M. O'Loughlin, J. Richmond, A. Burk, *et al.*, "10 kV and 15 kV silicon carbide power MOSFETs for next-generation energy conversion and transmission systems," in *Proc. 2014 IEEE Energy Conversion Congr. and Expo.*, 2014, pp. 449-454.

[6] M. K. Das, C. Capell, D. E. Grider, S. Leslie, J. Ostop, R. Raju, *et al.*, "10 kV, 120 A SiC half H-bridge power MOSFET modules suitable for high frequency, medium voltage applications," *Proc. IEEE Energy Conversion Congr. and Expo.*, 2011, pp. 2689-2692.

[7] S. Chakraborty, and M. A. Razzak, "Design of a transformer-less grid-tie inverter using dual-stage buck and boost converters," *Int. J. of Renewable Energy Res.*, vol. 4, no. 1, pp. 1-8, 2014.

[8] (2017) Grid Tied Inverter (2 Port) - GTIB 30 - Princeton Power Systems. [Online]. Available: http://www.princetonpower.com/GTIB-30.php

Switching Reliability Characterization of Vertical GaN PiN Diodes

O. Slobodyan[1], S. Sandoval[1], J. Flicker[1], R. Kaplar[1], C. Matthews[1], M. van Heukelom[1], and S. Atcitty[1]
[1]*Sandia National Laboratories, Albuquerque, NM, USA*
rjkapla@sandia.gov

Abstract **Vertical GaN (v-GaN) power semiconductor devices offer potential advantages compared to today's state-of-the-art Si, SiC, and lateral GaN power devices, including an enhanced unipolar figure-of-merit, and high-voltage and –current operation have been demonstrated for v-GaN PiN diodes. However, few reliability studies have been performed on such devices, particularly in a realistic switching environment. In this paper, we report on the development of a system for v-GaN power device reliability characterization under switching conditions. The system is based a double-pulse test circuit (DPTC). The paper describes how the DPTC was modified to apply a continuous stream of stress pulses, as opposed to the traditional long-short double-pulse sequence typically used for device characterization. Initial test results on a v-GaN PiN diode show good robustness under switching stress.**

Keywords– **Gallium Nitride, v-GaN, reliability, power switching, wide bandgap, power diode, double-pulse testing**

I. Introduction

Power conversion systems are necessary to process electrical energy (e.g., conversions between AC/DC, frequency, and voltage) in a wide variety of applications. Power semiconductor devices are the heart of the electrical conversion system and tend to be limited by voltage or current ratings. Historically, silicon (Si) has been the main electronic material used to fabricate these devices, and remains so today. However, Si power devices are approaching the limits imposed by the material, and a drive for ever-improving system-level performance has prompted the development of power semiconductor devices based on alternative materials, notably wide-bandgap (WBG) semiconductors. The most mature of these for high-voltage (> 1200 V) applications is silicon carbide (SiC) [1], while power switching devices based on gallium nitride (GaN) have primarily been high electron mobility transistors (HEMTs) targeted at lower voltages (< 600 V) [2]. However, recently vertical GaN (v-GaN) devices have emerged as a possible alternative to SiC for high-voltage power electronics [3], and research into a number of device types is ongoing [4-7].

Interest in v-GaN devices is motivated by the material properties of GaN, which are perhaps most simply (if incompletely) summarized by the unipolar figure of merit (UFOM), shown in Fig. 1. It is seen that for a given breakdown voltage, a GaN drift region has a lower on-resistance than SiC. This is due to the high critical electric field of GaN, which is believed to exceed 4 MV/cm [8]. However, v-GaN power device research has historically been hindered by a lack of high-quality native GaN substrates. Indeed, this lack of native substrates is one factor that has motivated the development of GaN power HEMTs grown on Si substrates. Unfortunately, the high defect densities associated with GaN-on-Si heteroepitaxial growth, as well as non-idealities such as surface breakdown in lateral devices, have limited the achievable voltage rating. While the low-voltage market is quite large and such devices excel in applications requiring very high switching frequencies (> 1 MHz), homoepitaxial vertical drift regions are required if GaN is to realize the potential indicated by the UFOM and compete with SiC in the > 1200 V range. Fortunately, the availability of native GaN substrates has increased substantially in recent years, leading to a large amount of research on v-GaN devices. PiN diodes are perhaps the most mature of these devices, with high breakdown voltages (> 3.7 kV) and high currents (> 400 A) demonstrated [4]. Moreover, the breakdown of such devices is consistent with an avalanche mechanism [4], which is important for avalanche ruggedness. With such performance demonstrated, it is now feasible to consider using v-GaN PiN diodes in high-voltage applications, which may challenge the position of SiC.

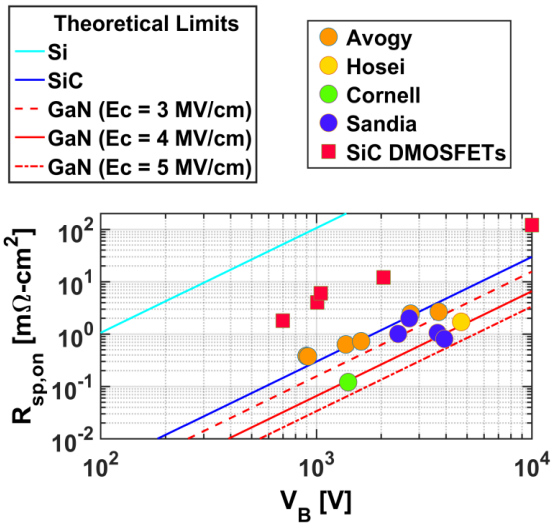

Fig. 1. Theoretical UFOM for Si, SiC, and GaN (lines) as well as reported values for SiC and GaN devices (symbols).

However, there have been few studies on the reliability of v-GaN PiN diodes [9]. Demonstrating high reliability is critical if circuit designers are to adopt such devices. Indeed, the ability to demonstrate high reliability has been one of the major factors that has determined the rate at which WBG power devices of all types have been adopted thus far. As such, this paper reports on reliability studies of v-GaN PiN diodes. Prior to conducting the reliability studies, extensive electrical characterization measurements were performed to verify the diodes' performance, e.g. temperature-dependent current-voltage (I-V) studies of both the forward and reverse bias regimes. Because these diodes are designed to operate in a switching environment in a power conversion circuit, the majority of our reliability characterization has focused on switching stress. For this, we have built on our previous work on characterization of reverse-recovery transients in v-GaN devices [10], and have adapted the double-pulse experimental setup used in that work to apply continuous pulsed stress under inductively-loaded conditions.

The devices investigated in this paper were fabricated by Avogy Inc., and characterization measurements and reliability testing were performed at Sandia National Laboratories.

II. Devices, Experimental Setup, and Results

A. *Vertical GaN Device Characterization*

A schematic of a basic PiN v-GaN diode is drawn in **Error! Reference source not found.**. In addition to the drift region and *p*-type anode, these devices incorporate edge termination structures to control the magnitude of the electric field at the device periphery to prevent early breakdown below that dictated by the intrinsic critical electric field. The diodes used in this study are true vertical structures grown on high-quality GaN substrates. They are rated for 5 A continuous forward current in a 0.72 mm^2 active device area, to yield a conduction current density of nearly 700 A/cm^2. As seen in Fig. 2, the devices consist of an n^+ GaN substrate, with the n^- drift region and p^+ anode homoepitaxially grown on top of it. Varying the thickness and doping of the drift region controls the breakdown voltage of the diode, in conjunction with the design of the edge termination.

Characterization of unpackaged die was done on a manual high-temperature (300°C), high-voltage (10 kV), and high-current (20 A_{DC}) probe station. Humidity was not controlled or monitored during measurement. I-V sweeps were separately performed on the same die in forward and reverse bias, because the high current and voltage capabilities are supported by different instruments and probe setups. Reverse bias measurements were done with the die immersed in Fluorinert FC-70 to prevent arcing.

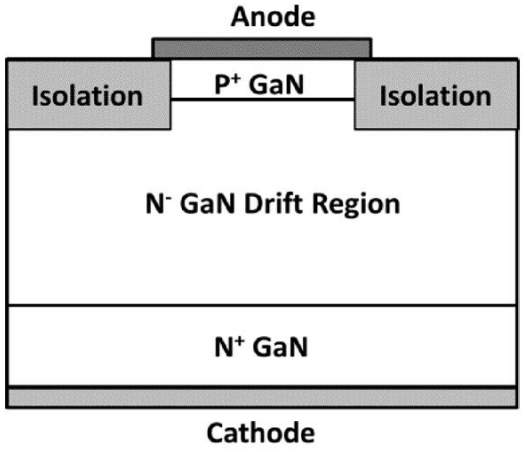

Fig. 2. Schematic drawing of v-GaN PiN diode.

Forward bias sweeps from 25°C to 150°C in 25°C steps are shown in **Error! Reference source not found.**. The turn-on voltage decreases going from 25°C to 150°C, consistent with previous measurements by Avogy [4]. Reverse-bias sweeps taken from 25°C to 125°C in 25°C steps are shown in Fig. 2. The leakage current increases with increasing temperature, consistent with [4]. The breakdown voltage also increases, but not in a linear manner. From 25°C to 125°C, the breakdown voltages are: 1657, 1652, 1675, 1706, and 1711 V.

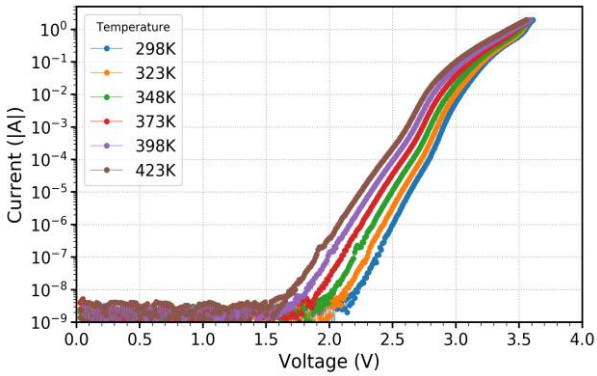

Fig. 3. Forward bias temperature-dependent I-V curves of v-GaN PiN diodes.

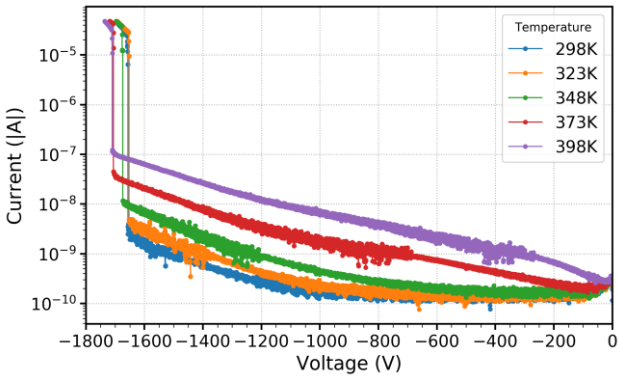

Fig. 2. Reverse bias temperature-dependent I-V curves of v-GaN PiN diodes, demonstrating temperature dependence of breakdown consistent with an avalanche mechanism.

Fig. 3 shows the breakdown voltage plotted as a function of temperature. The breakdown voltage shows a clear positive temperature coefficient of breakdown, which is characteristic of an avalanche process. While the dependence of breakdown voltage on temperature is approximately linear, a hysteresis effect is apparent for the first measurement at room temperature. This may be due to a burn-in effect, e.g., due to changes in the contacts.

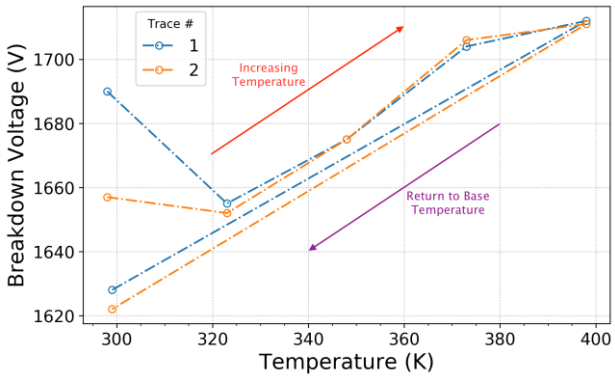

Fig. 3. Measured breakdown voltage as a function of temperature.

B. *Switching Relability Test Set-Up*

DC step-stress experiments are often performed to study degradation and reliability of power devices, and can provide good insight into mechanisms of degradation. However, on their own, and even combined with switching characterization between stressing sequences, these tests are not fully illustrative of typical operating conditions for power devices, where the device is continuously toggling between off- and on-states. Therefore, to better assess realistic degradation of power devices, a different test must be developed, and for this purpose we have focused on the development of pulse stressing using a modified double-pulse test circuit (DPTC).

The circuit diagram of the DPTC is shown in Fig. 4. This circuit is typically used to characterize switching behavior of power transistors under inductively-loaded conditions [11]. However, the DPTC can be adapted to test diodes, and has previously been used by our group to obtain switching characteristics of Avogy v-GaN diodes as well as baseline SiC and Si diodes [10]. The circuit is based on a board available from GeneSiC Semiconductor [12].

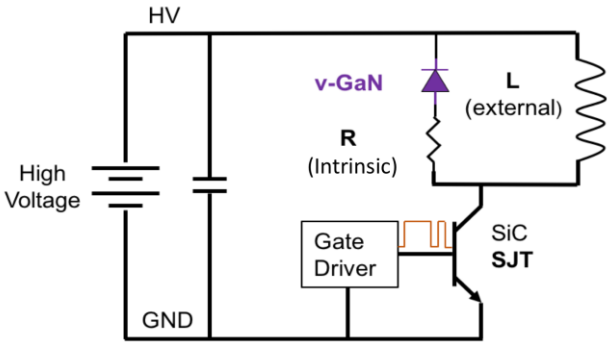

Fig. 4. DPTC used for switching stress of v-GaN diodes.

A photo of the test circuit is shown in Fig. 5. The typical mode of operation for a DPTC is a long-short double-pulse waveform that can be used to determine switching transition speed. However, the DPTC can be thought of as a conventional buck circuit with the output and input tied together [11]. This makes it possible to operate the DPTC in both a steady-state switching mode as well as the traditional double-pulse characterization mode, and the same circuit can be utilized to stress a device via long-term steady-state operation, as well as to periodically characterize the device's switching characteristics via the traditional double-pulse mode.

Fig. 5. Photograph of DPTC used for switching stress of the v-GaN diodes.

For an ideal DPTC operating in continuous operation mode, the current increases without bound because the inductor/diode circulation loop is ideally lossless. However, in a real circuit, the presence of resistance in the circulation loop (Fig. 4) degrades the circulating current while the switch is off. To operate in steady-state mode, the off-time of the switch must be large enough such that the circulating current in the inductor/diode loop decays to its starting value before the previous switching event (i.e., the current increase during the switch-on cycle must equal the current loss during the switch-off cycle). If the circulating current does not decay by a sufficient amount, then the net current flow through the circuit will increase with each switching cycle in a runaway event. Fig. 6 shows such an event. The switch current (pink trace) increases with each switching event, because the off-

time is not long enough for the circulating current to decay to its value at the start of the previous switch-on cycle.

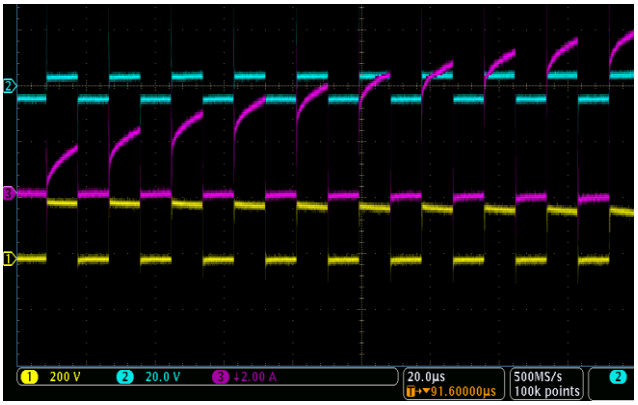

Fig. 6. Waveforms for DPTC in steady-state mode. The switch current (pink trace) shows a net increase with each switching cycle, since the off time is not long enough for the current to decay sufficiently. Yellow trace is diode voltage and blue trace is switch gate voltage.

The value of the inductor and the resistance in the inductor/diode loop therefore determine the switching duty cycle and frequency required to achieve steady-state mode. During the switch on-time, the current flow through the inductor increases linearly. The on-time required to achieve a given change in inductor current (ΔI_L) is determined by the input voltage (V_{in}) and inductance (L) via:

$$t_{on} = \frac{\Delta I_L \cdot L}{V_{in}} \tag{1}$$

When the switch turns off, the current through the diode/inductor pathway decays according to:

$$I_L(t) = I_{Lmax} \cdot e^{-\frac{R}{L}t} \tag{2}$$

Here, I_{Lmax} is the inductor current at the beginning of the switch off-time (this should be no more than the smallest of the current ratings of the inductor, diode, and switch). The off-time required for the current to decay by an amount ΔI_L is therefore equal to:

$$t_{off} = -\frac{L}{R}\ln\left(1 - \frac{\Delta I_L}{I_{Lmax}}\right) \tag{3}$$

Combining Eqs. (1) and (3) yields a relationship between t_{on} and t_{off}, subject to the values of L, R, V_{in}, and I_{Lmax}:

$$t_{off} = -\frac{L}{R}\ln\left(1 - \frac{t_{on} \cdot V_{in}}{L \cdot I_{Lmax}}\right) \tag{4}$$

The DPTC used in this work utilized three 1 mH inductors wired in series. No external resistance was intentionally added to the inductor/diode loop, so the total resistance was the sum of the intrinsic resistances from wiring, traces, and the socket used to mount the diode, as well as the intrinsic diode resistance. To apply rated current to the diode at an input voltage of 1000 V, the value of t_{on} was 2 µs. To prevent a condition of current runaway as dictated by Eq. (4), the switch off-time (978 µs) was kept significantly above the switch on-time (2 µs). Using Eqs. (1)-(4), this implies a parasitic resistance in the system of at least 1 Ω. The long off-time limited the steady-state stress-mode switching frequency to f = 1 kHz.

C. *Switching Reliability Testing Results*

Die situated in a standard TO220 package were tested using the DPTC shown in Fig. 4. A persistent issue during continuous operation of the circuit was overheating. Due to the lack of sufficient heatsinking on the DPTC setup, the device stress was de-rated from 5 A_{pk} to 2.2 A_{pk} to limit packaging-related failure mechanisms that are unrelated to intrinsic device operation (installation of heatsinking sufficient to enable stress/characterization at rated current/voltage is currently being implemented). This de-rating was accomplished by lowering the input voltage in the DPTC circuit. The lower peak current value was achieved using a steady-state operation with V_{in} = 500 V, t_{on} = 3.5 µs, and f = 1 kHz.

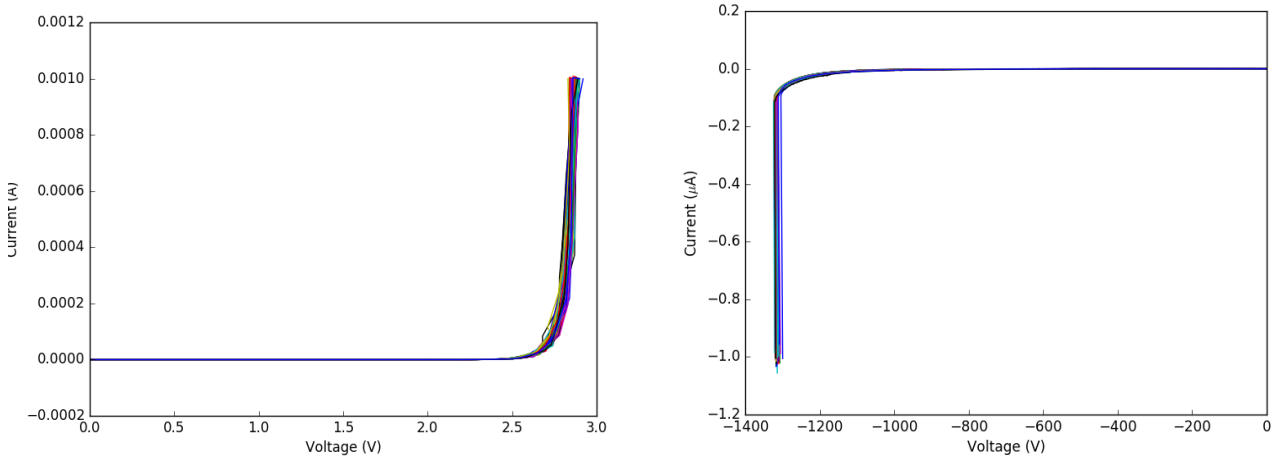

Fig. 7. Forward (left) and reverse (right) I-V curves taken at regular intervals during the first 800 minutes of steady-state switching stress.

To stress and characterize the devices under switching conditions, the DPTC was operated in steady-state mode and the diodes were subsequently characterized *in-situ* via a double-pulse waveform. The double-pulse waveform consisted of two pulses of 15 μs and 4 μs, respectively, separated by a 4 μs off-time. Following the double-pulse characterization, the devices were removed and characterized using forward and reverse I-V curves. The devices were then returned to the DPTC for the next round of steady-state-mode stressing. This process was repeated multiple times. The forward and reverse I-V curves (71 total) for the first 800 minutes of stress on one v-GaN diode are shown in Fig. 9.

These I-V curves show very little variation in the electrical characteristics of the diodes during the extent of the testing. Data analysis was carried out on the I-V curves as a function of total stress time (Fig. 10). In the blocking regime, the breakdown voltage (defined as a current of 1 μA, see Fig. 9) shows little degradation over the stress time measured. After an initial burn-in period where the breakdown voltage increases from an initial value of 1270 V to 1317 V, it stays fairly constant over the remaining duration of the test. There is some increase in the leakage current at a reverse bias of 1,000 V and, although the relative size of the change is significant (~50%), the absolute magnitude of the change in leakage is extremely small (< 3 nA). In the forward direction, the turn-on voltage (defined at a current of 1 mA, again see Fig. 9) shows negligible change as a function of stress time (differences in measured voltage shown in Fig. 10 are due to discretization of the voltage signal). Similarly, the forward current measured at a forward voltage of 2.16 V (picked for convenience due to data sampling) has no dependence on the stress time. Both the initial and final double-pulse characterizations are shown in Fig. 11. The measured switch current is the pink trace, the diode voltage is the yellow trace, and the switch voltage is the blue trace. The double-pulse waveform after 800 minutes of switching stress appears to be indistinguishable from the initial double-pulse waveform, indicating negligible degradation of the v-GaN diode.

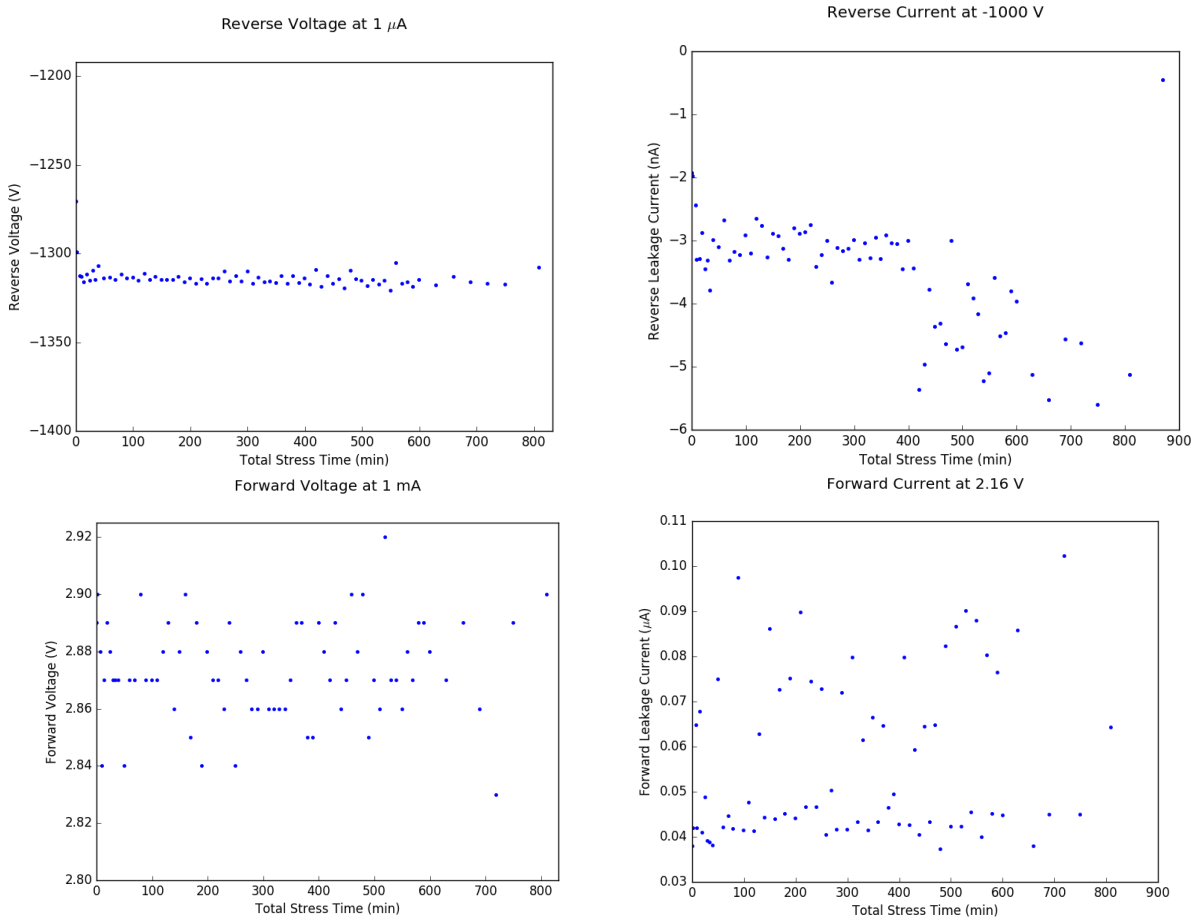

Fig. 10. Extracted data from forward and reverse I-V curves during stress. The reverse breakdown voltage (upper-left) and reverse leakage at 1,000 V (upper-right) throughout the stress time show little deviation from the initial values. The forward voltage (lower-left) at 1 mA and the leakage current at 2.16 V similarly show little signs of degradation.

III. Conclusion

In this work, we verified the electrical performance of v-GaN PiN diodes by characterizing the reverse and forward I-V characteristics of bare die as a function of temperature. The reverse breakdown voltage of the diodes increases as temperature increases, consistent with an avalanche-induced breakdown process.

The primary goal of the work was to demonstrate the utility of a DPTC operating in continuous mode for reliability

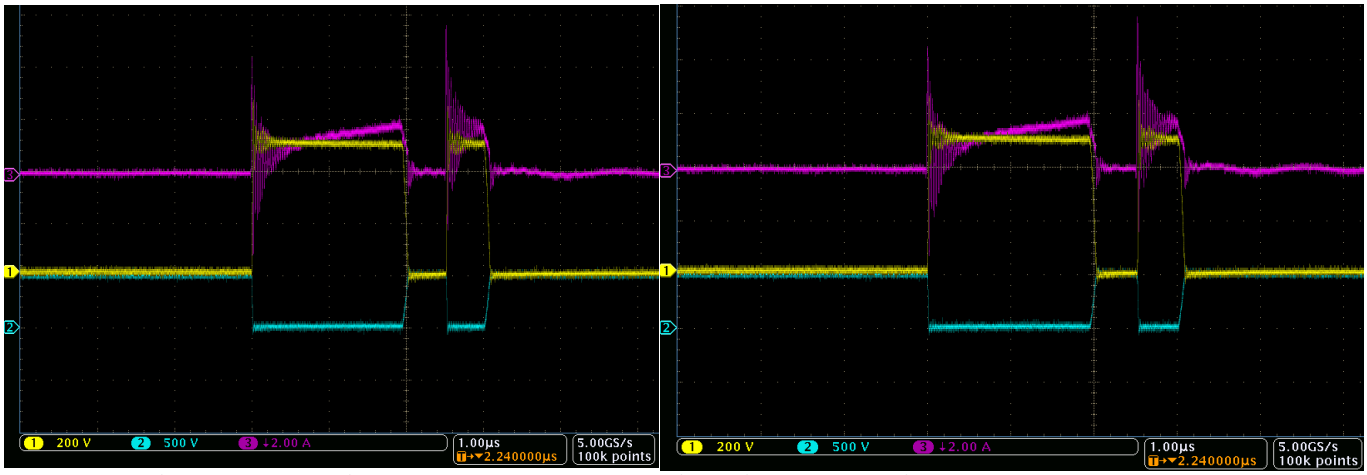

Fig. 11. Initial (left) double-pulse waveforms compared to double-pulse waveforms after 800 minutes of switching stress (right). Pink trace is switch current, yellow trace is diode voltage, and blue trace is switch voltage.

characterization. This allows for *in-situ* stressing and characterization of a packaged device in a realistic loaded switching circuit. A v-GaN die was stressed and repeatedly characterized over the length of the stress time via both DC I-V curves as well as non-continuous, traditional double-pulse characterization. Throughout the extent of the tests, the v-GaN diode showed no significant change in reverse and forward I-V curves, nor in the double-pulse switching characterization waveforms.

ACKNOWLEDGMENTS

The authors thank I. Kizilyalli and O. Aktas, both formerly of Avogy Inc., for providing the diodes studied in this work. The characterization work at Sandia was supported by the Energy Storage Program managed by Dr. Imre Gyuk of the DOE Office of Electricity, and the fabrication work at Avogy was supported by the SWITCHES program managed by Dr. Tim Heidel of ARPA-E. Sandia National Laboratories is a multi-mission laboratory managed and operated by National Technology and Engineering Solutions of Sandia LLC, a wholly owned subsidiary of Honeywell International Inc., for the U.S. Department of Energy's National Nuclear Security Administration under contract DE-NA0003525.

REFERENCES

[1] D. K. Schroder, "Progress In SiC Materials/Devices and Their Competition," *Int. J. of High Speed Electron. and Syst.*, vol. 21, no. 1, p. 1250009, 2012.

[2] M. J. Scott *et al.*, "Merits of Gallium Nitride Based Power Conversion," *Semiconductor Science and Tech.*, vol. 28, no. 7, p. 074013, 2013.

[3] E. A. Jones, F. F. Wang, and D. Costinett, "Review of Commercial GaN Power Devices and GaN-based Converter Design Challenges," *IEEE J. of Emerging and Selected Topics in Power Electronics*, vol. 4, no. 3, pp. 707-719, 2016.

[4] I. C. Kizilyalli, A. P. Edwards, O. Aktas, T. Prunty, and D. Bour, "Vertical Power p-n Diodes Based on Bulk GaN," *IEEE Trans. on Electron Devices*, vol. 62, no. 2, pp. 414-422, 2015.

[5] A. D. Koehler *et al.*, "Vertical GaN Junction Barrier Schottky Diodes," *ECS J. of Solid State Science and Technol.*, vol. 6, no. 1, pp. Q10-Q12, 2017.

[6] D. Ji *et al.*, "Normally OFF Trench CAVET With Active Mg-Doped GaN as Current Blocking Layer," *IEEE Trans. on Electron Devices*, vol. 64, no. 3, pp. 805-808, 2017.

[7] C. Gupta *et al.*, "In Situ Oxide, GaN Interlayer-Based Vertical Trench MOSFET (OG-FET) on Bulk GaN Substrates," *IEEE Electron. Device Lett.*, vol. 38, no. 3, pp. 353-355, 2017.

[8] A. M. Armstrong *et al.*, "High Voltage and High Current Density Vertical GaN Power Diodes," *Electron. Lett.*, vol. 52, no. 13, pp. 1170-1171, 2016.

[9] I. C. Kizilyalli, P. Bui-Quang, D. Disney, H. Bhatia, and O. Aktas, "Reliability Studies of Vertical GaN Devices Based on Bulk GaN Substrates," *Microelectronics Reliability*, vol. 55, no. 9–10, pp. 1654-1661, 2015.

[10] C. Matthews *et al.*, "Switching Characterization of Vertical GaN PiN Diodes," *IEEE Wide Bandgap Power Device and Appl. (WiPDA)*, pp. 135-138, 2016.

[11] S. R. Bahl, D. Ruiz, and D. S. Lee, "Product-Level Reliability of GaN Devices," *IEEE Int. Reliability Physics Symp. (IRPS)*, p. 4A-3, 2016.

[12] "Double Pulse Switching Board (GA100SBJT12-FR4) Datasheet," GeneSiC Semiconductor, Dulls, VA.

Integrating Multiple Energy Harvesting Systems for Department of Defense Applications

Joseph Swanner[1], Jo Bito[2], Gregory Nichols[1], Xuanke He[2], Joel Hewett[1], and Manos M. Tentzeris[2]
Homeland Defense and Security Information Analysis Center, Oak Ridge, U.S.A.
Georgia Institute of Technology, Atlanta, U.S.A.

***Abstract*- As modern warfare has grown increasingly reliant on mission-critical electronics over the past two decades, the United States warfighter has had to carry an increasingly heavy burden of equipment, armor, and batteries. In this study, we review the properties and potential efficacy of energy harvesting technologies across several modalities: solar, radio frequency/electromagnetic, thermal, and piezo/tribo-electric. Finally, we discuss how a hybrid energy harvesting system could combine multiple modalities and extend the life of Soldier-worn batteries by 40 to 60 percent over the course of a 72-hour patrol.**

***Keywords*- energy harvesting, battery charging, power integration, hybrid system**

I. Introduction

A top research and development priority for the U.S. Department of Defense (DoD) is to reduce the total weight of supplies and equipment that the warfighter must carry into combat. In May 2017, the federal Government Accountability Office found that the average load for Army and Marine Corps dismounted ground combat personnel totaled 120 pounds [1]. Such a heavy load hinders warfighter mobility and maneuverability in combat, and may result in musculoskeletal injury [2].

DoD has highlighted rising battery weight totals as a key domain where engineering research and development can significantly aid the warfighter. Concurrent to reducing battery weights is the goal of increasing the amount of mobile power/electricity available per pound to those deployed in the field. Whether that solution is a more efficient battery, or the provision of novel technologies that harvest or scavenge energy mid-mission—as this paper discusses—an improvement in power supply increases operational mobility and reduces reliance on forward operating bases and costly logistics requirements. As a recent U.S. Army report noted, “every time we deliver fuel or batteries on the battlefield, we put Soldiers at risk [3].”

Energy harvesting (EH) systems have the potential to solve the challenge of powering the warfighter in the field. An individual EH system draws from one of two types of low-intensity energy sources freely present in the environment: ambient power sources (e.g., solar radiation, or Radio Frequency/Electromagnetic [RF/EM] waves) or metabolic energy sources (e.g., thermal power, piezoelectric, or triboelectric electricity) (see Figure 1). Advancements in textile manufacturing, three-dimensional (or additive) printing techniques, and flexible circuitry have made the concept of an energy-self-sufficient combat uniform/kit that hosts multiple EH systems seem feasible. Such a multimodal, or hybrid EH system may be capable of providing a substantial amount of power to a soldier’s rechargeable battery.

This study surveys the operating principles of each harvesting method, based on research performed by the Homeland Defense and Security Information Analysis Center (HDIAC), and discusses recent research performed by engineers at the Georgia Institute of Technology (Georgia Tech) and other institutions. Georgia Tech addressed a combined RF/solar energy harvester device and a hybrid triboelectric/solar woven structured textile. This study concludes with a discussion on how these advancements in EH research point toward the feasibility of a fieldable hybrid EH system.

II. Modes of Energy Harvesting

Each ambient energy source exhibits distinct characteristics that bear upon its potential use in a hybrid EH system (see Table I). The power density per square meter of many ambient energy sources is small, often in the range of microWatts (μW) [4]. Operating alone, each energy source falls below the mark for providing a viable, consistent electricity flow useful for trickle charging a high energy density battery built into a combat suit. For instance, to generate useful amounts of power, solar cells can operate only during the day and must be oriented toward the sun, while thermoelectric devices require a temperature differential between two ends of a material. Other limitations, such as output variability and low energy-to-electricity conversion efficiency apply across the board, making sole-source exploitation of these sources unfeasible for harnessing useful amounts of electricity.

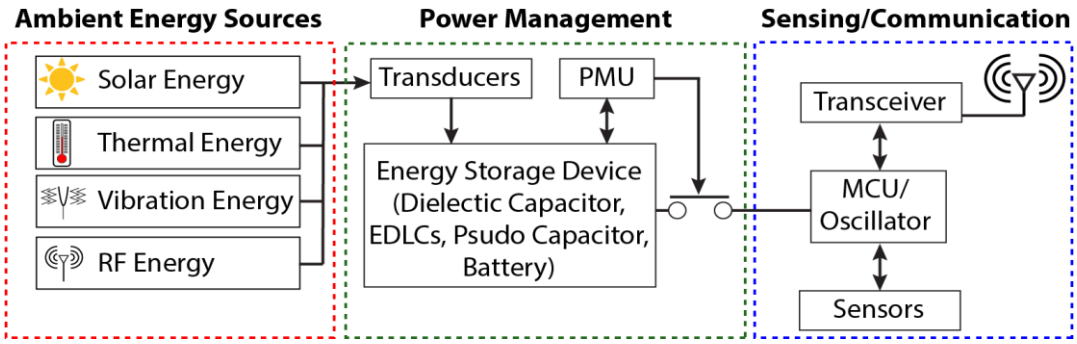

Fig. 1. Block diagram of a typical multiform, energy harvesting-enabled autonomous sensor device. Adapted from [4].

A. Solar

Solar energy has high power availability [4], making it a promising source of energy to integrate into a multimodal/hybrid EH system. It has a high power density of 100 mW/cm^2 during the daytime and 100 μW/cm^2 in an indoor environment, with a maximum conversion efficiency of more than 45 percent [5]. In a wearable context, the most promising solution for solar EH is through the utilization of polymer-based photovoltaic fibers and/or low-cost ink-jet printed solar cells.

1) Radio Frequency/Electromagnetic: RF/EM energy has a relatively low power density compared to other ambient energy sources [6]. The implementation of a high gain antenna into the EH system, however, greatly increases the amount of energy generated [6]. The energy levels available for collection heavily rely on the strength of the transmission and the distance between the RF harvester and the source [6]. In terms of energy conversion efficiency, rectifiers for ultrahigh frequency band have achieved more than 80 percent of conversion efficiency, with an optimal load and input RF power above 20 decibel-milliwatts (dBm) [7]. This is much higher than the other energy transducers for ambient EH – the highest conversion efficiency of a solar cell does not exceed 50 percent. Since the available ambient RF energy density in the far-field is very low (below 1 mW), diodes with a low threshold voltage and fast switching speed are preferable for ambient EH. From this perspective, Schottky diodes have been mainly used for RF EH.

B. Thermal

Thermal energy is readily available for use through wearable EH systems. Thermoelectric devices generate energy in the presence of a temperature gradient along the transducer itself [8]. Energy is available as long as a temperature gradient exists, but efficiently converting this energy relies on the degree of the differential as heat flows from a warmer area to a colder one [6]. In general, when a human body is a heat source, a thermoelectric generator produces an energy density of 20 to 60 μW/cm^2, yielding an approximate 18 to 25°C temperature difference between room temperature. Thermoelectric devices can continuously operate as long as the temperature gradient is maintained, but the energy conversion efficiency is low if the difference in temperature between the human body and the ambient environment is minimal. Typically, the conversion efficiency is below 1 percent when a human body is the heat source and the ambient environment is temperate. However, when thermoelectric EH is employed in desert environments (which offer extreme heat in the day and extreme cold at night-providing substantial temperature gradient with a human body), a higher energy conversion efficiency may be achieved.

C. Piezo- or tribo-electric

Vibration energy harvesters harness mechanical energy of a lower quality and at a lower frequency than traditional electromagnetic generators [9]. Nanogenerators that harvest mechanical energy use triboelectricity (energy generated from physical friction) and piezoelectricity (energy generated from compression). Triboelectric nanogenerators are a possible power source for wearable electronics, as they utilize common materials to convert almost all forms of mechanical energy, such as airflow, raindrops, rotations, and more into electricity [10]. Piezoelectric materials generate electricity when placed under physical stress or deformation and are also applicable in wearable platforms.

TABLE I
AMBIENT ENERGY SOURCES FOR ENERGY HARVESTING [4].

	Solar Energy	Thermal Energy	RF/EM Energy	Piezoelectric Energy	
				Vibration	*Compression*
Available Time	Daytime (4~8 Hrs)	Continuous	Continuous	Activity Dependent	Activity Dependent
Pros	•Large amount of energy •Well-developed technology	• Always available	•Antenna can be integrated into frame •Widely available source	•Lightweight •Well-developed technology	•Lightweight •Well-developed technology •Small volume
Cons	•Needs large area •Noncontinuous •Relies heavily on orientation	•Needs large area •Low power •Rigid & brittle	•Distance dependent •Reliant on available RF	•Need large area •Highly variable output	•Low conversion efficiency (high volt/low amps) •Highly variable output

D. Hybrid Triboelectric/ Solar System

Other research and development work has shown the promise of hybrid systems that use a different combination of EH sources. In 2016, a collaboration between engineers from Chongqing University, the Beijing Institute of Nanoenergy and Nanosystems, and Georgia Tech demonstrated the feasibility of developing a lightweight and fully flexible textile that integrated triboelectric and solar EH systems. This device, like the RF/solar discussed above, could harvest energy from one of the systems independently (i.e., from the triboelectric system, while the textile was indoors) or in a combined manner. The study was successful in producing a thin, highly deformable, breathable textile able to generate usable amounts of electricity.

The study also compared the fabric's performance through three different "electrical connection strategies": in series, in parallel, and when regulated by unidirectional blocking diodes [11]. Interestingly, a connection in series caused the triboelectric system to overwhelm the solar power circuit, reducing the system's total electrical output. A connection in parallel resulted in the opposite outcome, making the triboelectric system "ineffective" for EH [11]. Once a diode was introduced as an inter-component connection, the two energy sources were combined in an optimized manner that produced the most power (see Fig. 2).

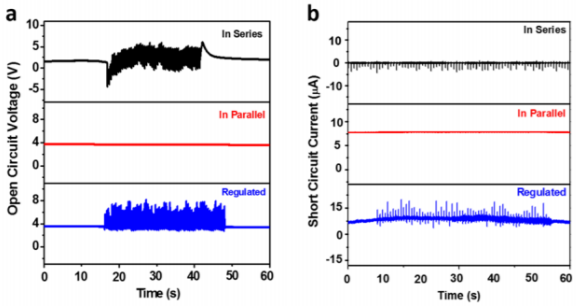

Figure 2. Power output of the triboelectric/solar hybrid textile, under different electrical connections [12].

E. Hybrid Radio Frequency/Solar System

Earlier this year, a student team from the School of Electric and Computer Engineering at Georgia Tech designed a novel hybrid EH and communication system, combining solar and radio frequency EH systems [12]. This research focused on a potential application for a stationary sensor, which would combine the ever-present but low-power RF energy with the strong but variable solar power input. The system is mainly composed of a 2.4 GHz custom dual-port antenna, an RF rectifier, a solar cell, a bq25504 Power Management Unity (PMU), a MSP430 Microcontroller (MCU), and a cc2500 transceiver. The hybrid RF/solar harvester receives -12.6 dBm of RF input power and achieves a 40% reduction in capacitor charging time when compared to the power generated from the solar cell alone.

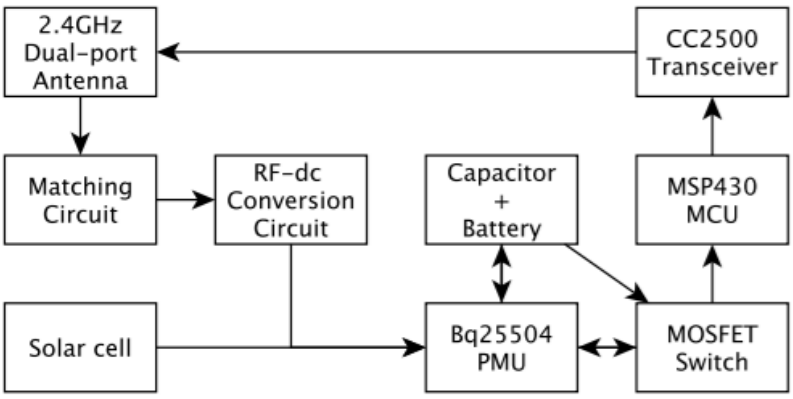

Fig. 3. Block diagram of a hybrid RF solar powered autonomous mote [11].

This work significantly improved upon previous efforts to combine an RF energy harvester with a solar cell, achieving a higher sensitivity of the hybrid system. Moreover, the study confirmed that the two EH systems together produced more usable electricity when combined into a hybrid system than when operating independently [12].

III. Multimodal/Hybrid Energy Harvesting System for Remote Battery Charging

The aforementioned research articles from Georgia Tech and its collaborating universities highlight a proof-of-concept: a hybrid EH system capable of generating usable amounts of power for small-scale electronics. Furthermore, this concept also demonstrates a promising method for charging high-energy-density batteries in remote environments.

The BB-3525 is a military-grade standard high-energy-density battery commonly used in dismounted warfighter operations [13]. Because the average patrol duration is approximately 72 hours, a dismounted warfighter will consume around 48 Whr before the first battery is drained and must be switched out with a new one.

In a hybrid EH system, the majority of the power available to charge a BB-3525 will be solar power, since its energy density is higher than the rest of the proposed energy sources (RF, thermal electric generator [TEG], and piezoelectric generator). Solar power will be obtained from a 12 cm x 12 cm flexible solar panel mounted on a helmet and operating at 18 percent efficiency. Energy from an RF device will be collected from a harvester attached to a typical two-way talk radio commonly used in operational scenarios. A typical radio outputs 36 dBm, of which 20 dBm can be recycled back into charging the BB-3525 battery without compromising the integrity of the communication link [14]. A TEG will be placed close to the body in order to establish a temperature gradient with the ambient environment—which, particularly in a desert climate, can easily reach a temperature gradient of 15° to 20°C, especially at night. Piezoelectric transducers placed on both feet can generate 59mW each, continuously, as long as the warfighter remains in motion [15].

This model of a proposed hybrid EH assumes a mission in which the warfighter conducted the patrol for at least 3 hours a day in the sun, moved/walked for 6 hours a day, and used the two-way talk function on the radio for 2 hours a day. This study also assumes an ambient temperature either higher or lower than the warfighter's body temperature by at least 15°C—a differential typical for desert climates. Table 2 further describes the proposed process for a multimodal/hybrid EH system.

Table II
Estimated total energy generated over a 72-hour patrol mission [16].

Energy source	**Power (W) per sq. cm**	**Area on Soldier sq. cm**	**Watts Generated (Including Efficiency)**	**Time Harvesting (hours)**	**Watt-hour Generated**
Solar	0.1	144	2.59	9	23.33
RF (Two-way talk radio) [14]	N/A	68.75	0.06	6	0.37
TEG	0.00019	232	0.04	72	3.17
Piezoelectric Generator [15]	0.00181	18.75	0.12	18	2.12
Total Energy					**29.0**

Based on the data presented in Table 2, it is estimated that the life of a soldier-worn BB-3525 battery can be extended by approximately 60 percent (from 48 Whrs to 77 Whrs) over the period of an average patrol. Such an increase in battery life could result in a drastic reduction in the number of batteries warfighters carry during dismounted operations.

IV. Conclusion

Recently, the use of wearable EH technologies for low-power electronics has become well established. However, ability to deliver usable energy at greater quantities is being realized. The RF/solar and triboelectric/solar systems demonstrate how multiple EH systems can be combined in close quarters with minimal to no interference, reducing energy loss. Finally, our proposed EH method for the remote charging of a high-energy density battery demonstrates a potential efficacy for multimodal/hybrid systems to meet larger energy demands.

Efficiently merging energy flows from multiple sources (or transducers) is not an easy endeavor. As has been discussed elsewhere, finding the right electrical architecture for how multiple EH sources combine within a hybrid system is a critical facet of applications, like a combat suit-integrated EH system [17]. For example, components like power management units run more efficiently with higher power or, as anticipated, when drawing from multiple EH sources. Multispectrum, unified hybrid EH systems may attain optimal performance depending on how they are wired.

References

[1] U.S. Government Accountability Office (GAO), "Personal protective equipment: Army and Marine Corps are pursuing efforts to reduce the weight of items worn or carried in combat," GAO, Washington, D.C., Rep. No. GAO-17-431, 2017. [Online]. Available: http://www.gao.gov/assets/690/684514.pdf.

[2] Holmes, A. (2017) "Army, Marine Corps look to lighten load for combat troops." [Online]. Available: http://www.military.com/daily-news/2017/05/17/army-marine-corps-look-lighten-load-combat-troops.html

[3] Deputy Chief of Staff, G-4, United States Army. "Operational energy brochure 'The power is in your hands'," [Online]. Available: https://www.army.mil/e2/c/downloads/269569.pdf.

[4] S. Kim, R. Vyas, J. Bito, K. Niotaki, A. Collado, A. Georgiadis, and M. M. Tentzeris, "Ambient RF energy-harvesting technologies for self-sustainable standalone wireless sensor platforms," in *Proc. of the IEEE*, 2014, vol. 102, no. 11, pp. 1649-1666.

[5] T. N. Tibbits, P. Beutel, M. Grave, C. Karcher, E. Oliva, G. Siefer, *et al.*, "New efficiency frontiers with wafer-bonded multi-junction solar cells," *in Proc. 29th European Photovolt. Solar Energy Conf. and Exhibition*, 2014, pp. 1975-1978.

[6] ATHENA Group, "Energy harvesting for self-sustainable autonomous system," unpublished.

[7] X. Lu, P. Wang, D. Niyato, D. I. Kim, and Z. Han, "Wireless networks with RF energy harvesting: A contemporary survey," *IEEE Commun. Surveys & Tutorials*, vol. 17, no. 2, pp. 757–789, Nov. 2014.

[8] J. H. We, S. J. Kim, and B. J. Cho, "Hybrid composite of screen-printed inorganic thermoelectric film and organic conducting polymer for flexible thermoelectric power generator," *Energy*, vol. 73, pp. 506–512, Aug. 2014.

[9] Y. Zi, H. Guo, Z. Wen, M. Yeh, C. Hu, and Z. L. Wang, "Harvesting low-frequency (<5 Hz) irregular mechanical energy: A possible killer application of triboelectric nanogenerator," *ACS Nano.*, vol. 10, no. 4, pp. 4797–4805, Apr. 2016.

[10] J. Wang, Z. Wen, Y. Zi, P. Zhou, J. Lin, H. Guo, Y. Zu, and Z. L. Wang, "All-plastic-materials based self-charging power system composed of triboelectric nanogenerators and supercapacitors," *Advanced Functional Materials*, vol. 26, no. 7, pp. 1070–1076, Feb. 2016.

[11] J. Chen, Y. Huang, N. Zhang, H. Zou, R. Liu, C. Tao, X. Fan, and Z. L. Wang, "Figure 7: Power output of the hybrid textiles with different electrical connections," In "Micro-cable structured textile for simultaneously harvesting solar and mechanical energy," *Nature Energy*, vol. 1, no. 10, p. 16138, Sept. 2016.

[12] J. Bito, R. Bahr, J. G. Hester, S. A. Nauroze, A. Georgiadis, and M. M. Tentzeris, "A novel solar and electromagnetic energy harvesting system with a 3-D printed package for energy efficient internet-of-things wireless sensors," *IEEE Trans. Microw. Theory Techn.*, vol. 65, no. 5, pp. 1831–1842, Feb. 2017.

[13] M. Huffman, "DoD ground expeditionary power & energy needs," presented at NextFlex Workshop- Powering the Internet of Everything, Atlanta, GA, Nov. 6-8, 2017.

[14] T.-H. Lin, J. Bito, J. G. Hester, J. Kimionis, R. A. Bahr, and M. M. Tentzeris, "Ambient energy harvesting from two-way talk radio for on-body autonomous wireless sensing network using inkjet and 3D printing," *in IEEE MTT-S Int. Microw. Symp. Dig.*, pp. 1034–1037, Jun. 2017.

[15] Mide Technology, Medford, MA, "PPA-4011 datasheet," in *PPA Products Datasheet and User Manual*, 2016. [Online]. Available: https://www.mouser.com/datasheet/2/606/ppa-piezo-product-datasheet-844547.pdf

[16] He, X, "Hybrid energy harvesting system," unpublished.

[17] M. Dini, A. Romani, M. Filippi, V. Bottarel, G. Ricotti, & M. Tartagni, "A nanocurrent power management IC for multiple heterogeneous energy harvesting sources," *IEEE Trans. Power Electron.*, vol. 30, no. 10, pp. 5665-5680, Oct. 2015.

BOUNDS OF SUPERCAPACITOR OPEN-CIRCUIT VOLTAGE CHANGE AFTER CONSTANT POWER EXPERIMENTS

Hengzhao Yang
California State University, Long Beach
Email: hengzhao.yang@csulb.edu

This paper examines the lower and upper bounds of the supercapacitor open-circuit voltage change after a constant power experiment, which is mainly due to the charge redistribution process and the equivalent series resistance (ESR). To derive the bounds, a simplified equivalent circuit model is developed based on the supercapacitor datasheet. Comprehensive constant power experiments are performed to verify the bounds. Results show that the bounds are valid for supercapacitor samples with different rated capacitance and voltage. This paper provides a tool to quickly estimate the supercapacitor open-circuit voltage change after a constant power process.

Keywords: supercapacitor modeling, charge redistribution, constant power experiment, equivalent series resistance (ESR), open-circuit voltage.

INTRODUCTION

Supercapacitors, also known as ultracapacitors, electric double layer capacitors (EDLCs), or electrochemical capacitors, are capacitors with large capacitances so that they can be used as secondary power sources. Supercapacitor-based energy storage systems have been employed by a variety of applications including electric and hybrid vehicles [1], smart grid [2], wireless sensor networks [3], and biomedical devices [4] due to the attractive characteristics of supercapacitors [5] such as long cycle life and high power density. To better utilize this energy storage technology, many aspects of supercapacitors have been investigated and several examples are system sizing [1], impedance characteristics [6], aging diagnosis [7], and state of charge (SOC) estimation [8]. Supercapacitor voltage is a vital parameter, which can be used an indicator of the supercapacitor SOC. Supercapacitor voltage is also utilized in cell balancing circuits. Multiple supercapacitor cells need to be connected in series to boost the voltage for microgrid applications. The individual cell voltage usually differs because of the manufacturing tolerance. To ensure safe and long-time operation of the supercapacitor bank, the cell voltages need to be equalized. When it comes to the supercapacitor voltage behavior, self-discharge [9-11] has been of great interest because it causes voltage drop and energy loss. While this characteristic is responsible for the long-term decay of the supercapacitor open-circuit voltage, the short-term behavior of the supercapacitor open-circuit voltage [12] is mainly determined by the charge redistribution process and the equivalent series resistance (ESR). A detailed study of the supercapacitor voltage behavior during charge redistribution [12-14] has been conducted using the supercapacitor variable leakage resistance (VLR) model [10, 11]. The impact of supercapacitor charge redistribution on power management in wireless sensor networks [15-17] has been illustrated by considering the task scheduling problem.

While the supercapacitor VLR model is a powerful tool for studying the open-circuit voltage behavior in detail, an estimate of the supercapacitor voltage change bounds also reveals critical information. On the other hand, the VLR model requires a relatively complex process to determine its parameter values. However, in some occasions the manufacturer datasheet is the only available resource to characterize the supercapacitor. Therefore, this paper aims to provide explicit formulas to estimate the bounds of the supercapacitor open-circuit voltage change after a constant power process based on information extracted from the supercapacitor datasheet.

The remainder of this paper first illustrates the supercapacitor open-circuit voltage change during charge redistribution and introduces a simplified supercapacitor model based on the manufacturer datasheet, then derives the lower and upper bounds of the supercapacitor open-circuit voltage change after a constant power action. After that, it presents the design and results of constant power experiments for four supercapacitor samples and concludes that the derived bounds apply to these samples.

BOUNDS OF SUPERCAPACITOR OPEN-CIRCUIT VOLTAGE CHANGE

Supercapacitor Charge Redistribution

To examine the supercapacitor open-circuit voltage change after a constant power process, Fig. 1 shows two charge redistribution experiments using a 10 F supercapacitor sample (manufacturer: Maxwell, model: BCAP0010, and rated voltage: 2.7 V): the “Ch” curve represents a charging process followed by charge redistribution and the “Dis” curve describes charge redistribution after a discharging action. In the “Ch” experiment, the supercapacitor is charged from 0.3004 to 1.2002 V by a constant power source of 0.4 W. At the end of the charging phase (t=15.735 s), the charging power is removed and the supercapacitor undergoes charge redistribution during the following 600 s, as shown in Fig. 1(a). The voltage change caused by the ESR is shown in Fig. 1(b). As denoted by circle A, the supercapacitor first experiences a sharp voltage drop immediately following the removal of the charging power because of the ESR: the voltage drops from 1.2002 (t=15.735 s) to 1.1765 V (t=15.740 s). The 0.005 s delay is the time resolution of the supercapacitor tester. Beginning at t=15.740 s, the supercapacitor experiences charge redistribution during

the next 600 s and its voltage decreases to 1.0708 V at t=615.740 s. Taking the supercapacitor voltage (1.2002 V) at t=15.735 s as the initial value and the voltage (1.0708 V) at t=615.740 s as the final value, the voltage change is therefore -0.1294 V, which is composed of a drop of 0.0237 V (from 1.2002 to 1.1765 V) because of the ESR and a drop of 0.1057 V (from 1.1765 to 1.0708 V) because of charge redistribution.

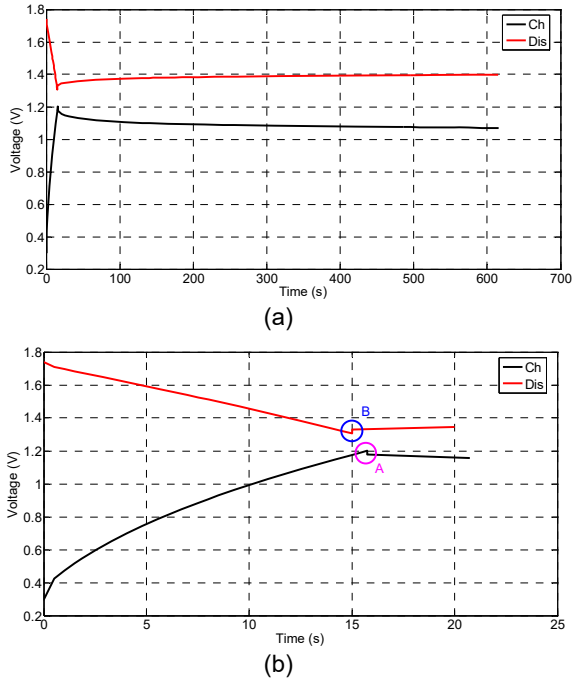

Fig. 1. Supercapacitor charge redistribution experiments. (a) Overview. (b) Voltage change due to ESR.

As for the "Dis" experiment, the supercapacitor is discharged from 1.7413 to 1.3049 V by a constant power source of 0.4 W in 15 s. After that, the discharging power is removed and the supercapacitor first experiences a sudden voltage boost because of the ESR, as denoted by circle B in Fig. 1(b): the voltage increases from 1.3049 (t=15 s) to 1.3290 V (t=15.005 s). The supercapacitor then undergoes charge redistribution during the following 600 s and the voltage increases to 1.3993 V at t=615.005 s, as shown in Fig. 1(a), which results in a voltage change of 0.0944 V after the discharging power is removed: a boost of 0.0241 V (from 1.3049 to 1.3290 V) because of the ESR and a boost of 0.0703 V (from 1.3290 to 1.3993 V) because of charge redistribution.

A Simplified Supercapacitor Model

While the VLR model shown in Fig. 2(a) is good for analyzing the detailed supercapacitor voltage behavior during charge redistribution, it is not well-suited for deriving explicit formulas to estimate the bounds of the supercapacitor open-circuit voltage change. To provide a better tool for predicting the supercapacitor voltage change because of charge redistribution and the ESR, this paper modifies the VLR model. As shown in Fig. 2(b), the simplified model in the dashed-line block consists of two RC branches: R_1 and C_1 for the first branch; R_2 and C_2 for the second branch. This model modifies the VLR model in four aspects. First, the variable leakage resistor R_3 is removed because the effect of self-discharge on the supercapacitor voltage change in the short term is insignificant [10, 11]. Second, the first branch capacitor C_1 is modeled as a constant capacitor. This is a reasonable assumption because charge redistribution takes place between the two RC branches [12-14] and the charge stored in each branch capacitor determines the supercapacitor voltage change. Therefore, the simplified model does not differentiate the charge stored in the first branch constant capacitor and the voltage-dependent capacitor. Third, the capacitances of the two branch capacitors are related by $C_2=\alpha C_1$, where α is a parameter typically ranging between 0.11 and 0.25. This assumption is based on [18] in which it is revealed that the slow branch capacitance (C_2) of a supercapacitor is a significant percentage of the total capacitance (C_1+C_2) and for most supercapacitor samples this percentage is between 0.1 and 0.2. A simple conversion gives the range of α: $0.11\leq\alpha\leq0.25$. Fourth, the resistance of the first branch resistor R_1 is represented by the ESR value specified in the supercapacitor datasheet because the experimentally determined value of R_1 is close to the ESR value [19, 20].

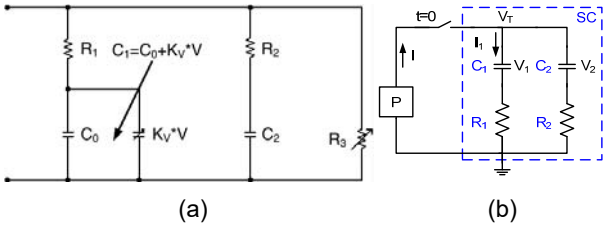

Fig. 2. Supercapacitor models. (a) VLR model. (b) Simplified model.

Bounds of Supercapacitor Voltage Change

The simplified supercapacitor model shown in Fig. 2(b) is used to derive the bounds of the supercapacitor open-circuit voltage change, which is defined as the difference between the final voltage and the initial voltage. The initial voltage is the supercapacitor terminal voltage right before the charging/discharging power is removed. The final voltage is the supercapacitor terminal voltage when the charge redistribution process terminates. As shown in Fig. 2(b), the supercapacitor is connected to the power source P for t<0. At t=0, the switch is opened and the power source is disconnected. The supercapacitor terminal voltage V_T right before the switch is opened is denoted as $V_T(0-)$, which is written as

$$V_T(0-) = V_1(0-) + I_1(0-)R_1 \quad (1)$$

where $V_1(0-)$ is the voltage across the capacitor C_1 and $I_1(0-)$ is the current through the first branch. The charging/discharging power P is related to $V_T(0-)$ and I by

$$P = V_T(0-)I \quad (2)$$

Since the first branch is the main branch of the supercapacitor and the majority of the current flows through this branch [12, 13], it is then assumed that $I_1(0-)=I$. Additionally, based on the fact that the R_1 value is close to the ESR value, it is further assumed that $R_1=R$, where R is the ESR value extracted from the supercapacitor datasheet. Therefore, (1) is rewritten as

$$V_T(0-) = V_1(0-) + IR \quad (3)$$

The supercapacitor final voltage is evaluated when the charge redistribution process terminates, which means that the two branch capacitor voltages are equal and no current flows through the two branches. At this time, the supercapacitor terminal voltage equals the two branch capacitor voltages: $V_T(\infty)=V_1(\infty)=V_2(\infty)$. Assuming that the supercapacitor charge is conserved during the charge redistribution process, the final voltage $V_T(\infty)$ is then written as

$$V_1(0-)C_1 + V_2(0-)C_2 = V_T(\infty)(C_1 + C_2) \quad (4)$$

Given that $C_2=\alpha C_1$, the final voltage is determined as

$$V_T(\infty) = \big(V_1(0-) + \alpha V_2(0-)\big)/(1+\alpha) \quad (5)$$

The supercapacitor voltage change is therefore

$$\Delta V_T = V_T(\infty) - V_T(0-) \quad (6)$$

To estimate the bounds of the supercapacitor voltage change, the key is to evaluate $V_1(0\text{-})$ and $V_2(0\text{-})$, which cannot be experimentally measured by the supercapacitor tester. Therefore, it is necessary to relate them to the measurable supercapacitor terminal voltage right before the charging/discharging power is removed, which is denoted as V_M for clarity:

$$V_T(0-) = V_M \quad (7)$$

Together with (3), $V_1(0\text{-})$ is then written as

$$V_1(0-) = V_M - IR \quad (8)$$

As for $V_2(0\text{-})$, it can only be assumed that it is between 0 and the supercapacitor rated voltage V_R because its exact value is dependent on the previous charging/discharging process and cannot be readily related to the supercapacitor terminal voltage:

$$0 \le V_2(0-) \le V_R \quad (9)$$

Combining (2), (6), (8), and (9), the lower bound of the supercapacitor voltage change is

$$\Delta V_{TL} = (-\alpha V_M - PR/V_M)/(1+\alpha) \quad (10)$$

and the upper bound is

$$\Delta V_{TU} = (\alpha(V_R - V_M) - PR/V_M)/(1+\alpha) \quad (11)$$

As shown in (10) and (11), the following information is needed to estimate the bounds of the supercapacitor voltage change: (1) V_R and R: the rated voltage and ESR value extracted from the supercapacitor datasheet, (2) V_M and P: the measured supercapacitor terminal voltage and power right before the charging/discharging power is disconnected, and (3) α: a parameter typically ranging between 0.11 and 0.25 for most supercapacitors. Although the exact value of α cannot be determined without characterizing the supercapacitor, its range still provides useful information. The effects of the α value on the bounds can be illustrated using the simplified model. Physically, a higher α value means a larger C_2 value, a larger portion of charge to be transferred during the charge redistribution process, and ultimately a more significant voltage change.

SUPERCAPACITOR CHARGE REDISTRIBUTION EXPERIMENTS AND RESULTS

Experiments

To verify the supercapacitor voltage change bounds, the constant power experiments presented in [14] are analyzed, which are performed using the four supercapacitor samples listed in Table 1. The rated capacitance (C_R) varies from 0.1 to 100 F with a scale factor of 10. The rated voltage (V_R) includes two values: 2.7 and 5 V.

Table 1. Supercapacitor samples.

Sample	1	2	3	4
Manufacturer	Cooper Bussmann	Maxwell	Maxwell	Maxwell
Model	PB-5R0V104-R	BCAP0001	BCAP0010	BCAP0100
C_R (F)	0.1	1	10	100
V_R (V)	5	2.7	2.7	2.7

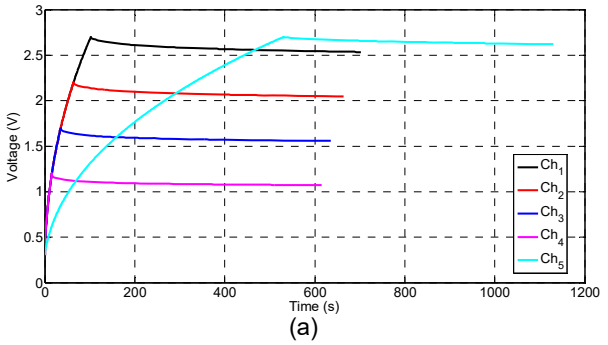

(a)

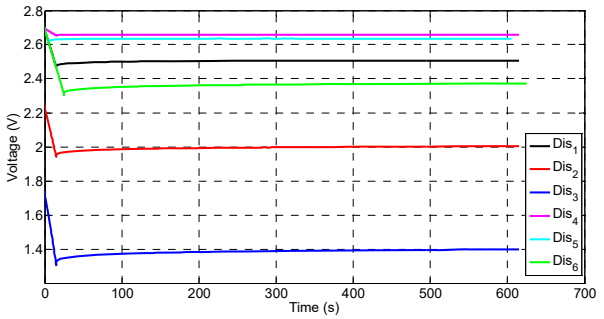

(b)

Fig. 3. Charge redistribution experiments for 10 F supercapacitor sample. (a) Constant power charge experiments. (b) Constant power discharge experiments.

The design of constant power experiments is similar for all samples. Take the 10 F sample for instance. Fig. 3 shows the charge redistribution experiments: Fig. 3(a) for five constant power charge experiments and Fig. 3(b) for six constant power discharge experiments. Depending on the parameter swept, the experiments shown in Fig. 3(a) are divided into two groups: group 1 includes Ch_1 through

Ch_4 and group 2 consists of Ch_1 and Ch_5. In group 1, the charge termination voltage is swept. The supercapacitor is charged by the same constant power of 0.4 W from the same initial voltage of 0.3 V to different final voltages: 2.7, 2.2, 1.7, and 1.2 V. The group 2 experiments are performed to study the impact of power while fixing the initial voltage of 0.3 V and termination voltage of 2.7 V: 0.4 W for Ch_1 and 0.08 W for Ch_5. The supercapacitor charge redistribution phase is 600 s for all experiments.

As shown in Fig. 3(b), six constant power discharge experiments are performed to sweep three parameters: discharge beginning voltage, power, and time, which are examined by three groups, respectively. Group 1 includes experiments Dis_1 through Dis_3. At the beginning of each experiment, the supercapacitor is conditioned to different initial voltages: 2.7, 2.2, and 1.7 V for experiments Dis_1 through Dis_3, respectively. Then the supercapacitor is discharged by a constant power of 0.4 W for 15 s. After that, the power is removed and the supercapacitor experiences charge redistribution during the following 600 s. Experiments Dis_1 and Dis_4 form group 2. The discharge beginning voltage is fixed at 2.7 V for both experiments. The discharging power for Dis_4 is 0.08 W. The discharge time and charge redistribution duration remain the same. The group 3 experiments Dis_1, Dis_5, and Dis_6 sweep the discharge time, which is 15, 5, and 25 s, respectively. The discharge beginning voltage (2.7 V), discharging power (0.4 W), and charge redistribution duration (600 s) apply to these three experiments.

Results

The supercapacitor voltage change bounds calculated using (10) and (11) as well as the measured values are shown in Fig. 4. The measurements are labeled as “Mea.”. The lower and upper bounds calculated using α=0.11 are denoted by “L11” and “U11”, respectively. Similarly, “L25” and “U25” are for α=0.25.

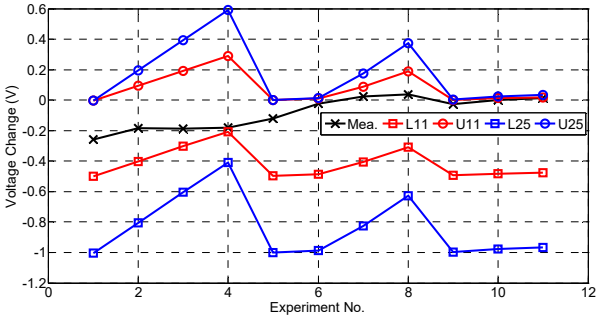

(a)

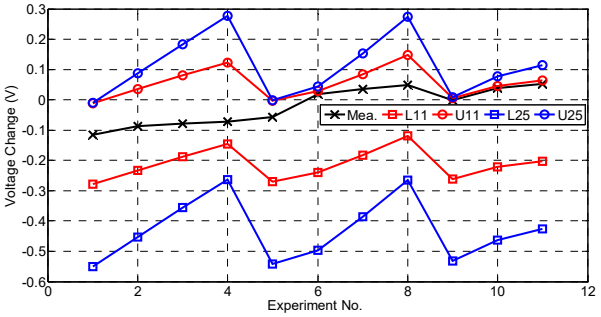

(b)

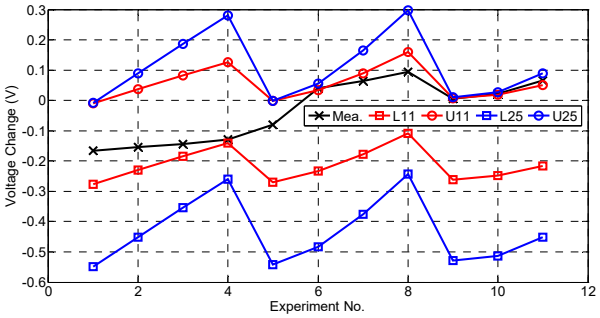

(c)

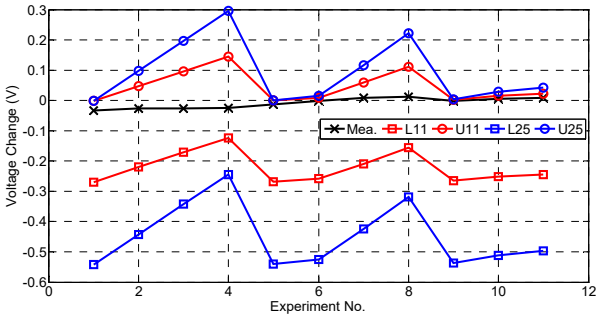

(d)

Fig. 4. Measured and estimated supercapacitor voltage changes. (a) 0.1 F. (b) 1 F. (c) 10 F. (d) 100 F.

Two observations can be made based on the results shown in Fig. 4. First, for the 0.1, 1, and 100 F samples, the measured supercapacitor voltage changes are within the bounds calculated using α=0.11, which is the minimum value of the typical range of the parameter α. Second, for the 10 F sample, although the measured values for experiments no. 6, 10, and 11 are not confined by the bounds when α=0.11, they are within the bounds when α =0.25, which is the maximum value of the typical range of α. For the remaining experiments, the measured values are within the bounds when α=0.11. These observations lead to the following conclusions. First, the supercapacitor open-circuit voltage change bounds derived based on the simplified supercapacitor model are valid for the supercapacitor samples and constant power experiments examined in this paper. Therefore, the bounds can be used to provide a quick estimate of the supercapacitor voltage behavior without going through the complex procedure to characterize the supercapacitor by performing and analyzing multiple experiments. Second, while all the other information needed for estimating the bounds can be extracted from the supercapacitor datasheet and the constant power experiment setup, the parameter α is only specified by a typical range between 0.11 and 0.25 and there is no obvious approach to relate this parameter to the supercapacitor specifications. In fact, even for samples with the same model number from the same manufacturer, a certain level of variation exists [18]. Therefore, more work needs to be conducted to further study this parameter.

CONCLUSION

This paper investigates the bounds of the supercapacitor open-circuit voltage change after a

constant power process, which is mainly resulted from the charge redistribution process and the ESR. Explicit mathematical formulas for the lower and upper bounds are derived using a simplified supercapacitor model based on the information extracted from the manufacturer datasheet. Multiple constant power experiments are analyzed to verify the bounds. Results show that the bounds are valid for supercapacitor samples with different rated capacitance and voltage. Therefore, the derived formulas can be used to estimate the supercapacitor open-circuit voltage change bounds.

Acknowledgment

Research reported in this publication was supported in part by the National Institute of General Medical Sciences of the National Institutes of Health under Award Number 5UL1GM118979-04. The content is solely the responsibility of the author and does not necessarily represent the official views of the National Institutes of Health. This work was also supported in part by California State University, Long Beach under the ORSP and RSCA programs.

References

[1] A. Kuperman, M. Mellincovsky, C. Lerman, I. Aharon, N. Reichbach, G. Geula, and R. Nakash, "Supercapacitor sizing based on desired power and energy performance," *IEEE Transactions on Power Electronics*, vol. 29, no. 10, pp. 5399–5405, 2014.

[2] R. K. Varma, V. Khadkikar, and R. Seethapathy, "Nighttime application of PV solar farm as STATCOM to regulate grid voltage," *IEEE Transactions on Energy Conversion*, vol. 24, no. 4, pp. 983–985, 2009.

[3] D. Brunelli, C. Moser, L. Thiele, and L. Benini, "Design of a solar-harvesting circuit for batteryless embedded systems," *IEEE Transactions on Circuits and Systems I: Regular Papers*, vol. 56, no. 11, pp. 2519–2528, 2009.

[4] C. Wentz, J. Bernstein, P. Monahan, A. Guerra, A. Rodriguez, and E. Boyden, "A wirelessly powered and controlled device for optical neural control of freely-behaving animals," *Journal of Neural Engineering*, vol. 8, no. 4, pp. 046 021:1–046 021:10, 2011.

[5] M. Farhadi and O. Mohammed, "Energy storage technologies for high-power applications," *IEEE Transactions on Industry Applications*, vol. 52, no. 3, pp. 1953–1961, 2016.

[6] L. Zhang, X. Hu, Z. Wang, F. Sun, and D. G. Dorrell, "Experimental impedance investigation of an ultracapacitor at different conditions for electric vehicle applications," *Journal of Power Sources*, vol. 287, pp. 129–138, 2015.

[7] A. Oukaour, N. Omar, H. Gualous, A. Rachid, P. V. D. Bossche, and J. V. Mierlo, "Electrical double-layer capacitors diagnosis using least square estimation method," *Electric Power Systems Research*, vol. 117, pp. 69–75, 2014.

[8] A. Nadeau, M. Hassanalieragh, G. Sharma, and T. Soyata, "Energy awareness for supercapacitors using Kalman filter state-of-charge tracking," *Journal of Power Sources*, vol. 296, pp. 383–391, 2015.

[9] B. Ricketts and C. Ton-That, "Self-discharge of carbon-based supercapacitors with organic electrolytes," *Journal of Power Sources*, vol. 89, no. 1, pp. 64–69, 2000.

[10] Y. Zhang and H. Yang, "Modeling and characterization of supercapacitors for wireless sensor network applications," *Journal of Power Sources*, vol. 196, no. 8, pp. 4128–4135, 2011.

[11] H. Yang and Y. Zhang, "Self-discharge analysis and characterization of supercapacitors for environmentally powered wireless sensor network applications," *Journal of Power Sources*, vol. 196, no. 20, pp. 8866–8873, 2011.

[12] H. Yang and Y. Zhang, "Analysis of supercapacitor energy loss for power management in environmentally powered wireless sensor nodes," *IEEE Transactions on Power Electronics*, vol. 28, no. 11, pp. 5391–5403, 2013.

[13] H. Yang and Y. Zhang, "A study of supercapacitor charge redistribution for applications in environmentally powered wireless sensor nodes," *Journal of Power Sources*, vol. 273, pp. 223–236, 2015.

[14] H. Yang, "Analysis of supercapacitor charge redistribution through constant power experiments," in *Proceedings of the 2017 IEEE Power & Energy Society General Meeting (PESGM 2017)*, 2017, p. in press.

[15] H. Yang, "Task scheduling in supercapacitor based environmentally powered wireless sensor nodes," *Ph.D. dissertation*, Georgia Institute of Technology, 2013.

[16] H. Yang and Y. Zhang, "A task scheduling algorithm based on supercapacitor charge redistribution and energy harvesting for wireless sensor nodes," *Journal of Energy Storage*, vol. 6, pp. 186–194, 2016.

[17] H. Yang and Y. Zhang, "Power management in supercapacitor-based wireless sensor nodes," in *Supercapacitor Design and Applications*, ISBN 978-953-51-2749-9, DOI: 10.5772/64987, pp. 165–179, 2016.

[18] J. W. Graydon, M. Panjehshahi, and D. W. Kirk, "Charge redistribution and ionic mobility in the micropores of supercapacitors," *Journal of Power Sources*, vol. 245, pp. 822–829, 2014.

[19] H. Yang and Y. Zhang, "Estimation of supercapacitor energy using a linear capacitance for applications in wireless sensor networks," *Journal of Power Sources*, vol. 275, pp. 498–505, 2015.

[20] H. Yang and Y. Zhang, "Characterization of supercapacitor models for analyzing supercapacitors connected to constant power elements," *Journal of Power Sources*, vol. 312, pp. 165–171, 2016.

Hybrid Thermal and Electric and Energy Storage System

Stephane Bilodeau[1], Michael Carty[1], Chris Mashburn[2] and Ross Quick[2]
[1]*Advanced Engineering & Technology Department, Novacab Inc., 18 Paul Gauguin, Candiac, QC, Canada J5R 6X1*
[2]*U.S. Head Office, Novacab Inc.,11701 Bee Cave Rd, Suite 124, Austin, Texas 78738*

***Abstract*- Electric Energy Storage (EES) and Thermal Energy Storage (TES) have been integrated in a hybrid approach to optimize energy efficiency and load leveling. This integration is allowing for significant improvement and stability in the operation in critical applications such as hospital, datacenters, military facilities, manufacturing plants, and other critical thermal + electric demand-side management. Using the extensive experience in the hybrid energy storage for vehicles and mobile applications, a special Synthetic Phase Change Material (SPCM) has been developed to act as a shock absorber in stationary thermal processes. The Hybrid Thermal and Electrical Energy Storage System (HTEES) maximizes the flexibility and the overall performance of the equipment on the grid. Monitoring in a datacenter has shown that optimum results are obtained when initial fluctuating conditions were observed. Improved performance and stability were measured and have shown that ramp up and ramp down of the equipment are reduced and the supply and return process temperatures are stabilized. It allows for performance improvement and more reliability in the operation. For the grid, the impact would also be substantial: smoothing the load profile and optimizing demand side management; and improved redundancy and predictability of the energy distribution. The integration and combined outcomes of the HTEES system is highlighted in the paper, including onsite operational data, Power Usage Effectiveness (PUE), reliability, and performance.**

***Keywords*- hybrid system, thermal energy storage, phase change material, renewable energy, smart grid**

I. Introduction

A. Background

The continuously rising cooling demand represents a challenge for existing electrical networks and future smart grids since it contributes to electricity peak demand, which is increasing substantially. In this context, well integrated in the electric supply, thermal energy storage can play an important role in shaving the peak demand, burdening the electrical grid. Hybrid energy storage can be used to develop demand-side management strategies able to shift the load from peak to off-peak hours (exploiting potential for price arbitrage) even in the presence of renewable energy production. Hybrid-demand side management is a mean to increase the overall efficiency of the entire electricity network - from generation to the end use - which consists of optimizing the allocation of resources, limiting the peak demand, and shaping the demand depending on the necessity of the grid.

B. Foregoing and Related Works

This paper presents hybrid systems, integrating Electric Energy Storage (EES) and Thermal Energy Storage (TES) that have been implemented in order to optimize energy efficiency and load leveling for Renewable Energy and Critical Processes.

Using the extensive experience in the hybrid energy storage for vehicles, a special Synthetic Phase Change Material (SPCM) has been developed.

What we generally see in the energy storage field, is that the different storage technologies are considered only as competitors and not as potential collaborators. Seeing the different technologies in a competitive mode; this is the paradigm. In fact, no single technologies could easily compete with the energy density of the cheap fossil fuel. It is important to find ways for these technologies to make the new technologies to work together. That would not only help to increase the efficiency of the whole process, but also it would lead to better energy management. This is what this paper is all about: integrating two storage complementary technologies in a hybrid approach: the HTEES.

II. Technology Description

A. Hybridization with Regulation Strategy Combining Thermal and Electric Capacities

Using this joint/collaborative approach and using our work in the hybrid energy storage for vehicles, we have developed special SPCM and the HTEES.

The control of the system is based on an anticipatory regulation strategy using fuzzy logic and a combined feedforward plus feedback control that can handle,

simultaneously, the storage and retrieval of electricity and solar energy. It takes into account the operating conditions such as load and outside air temperature, and optimizes the off- and on-peak periods for electrical heating. The combined strategy can significantly improve performance over simple feedback control whenever there are fluctuations or disturbances. The regulation strategy depends on a PID

controller that regulates the air flow from an electric fan to maintain the room temperature at the set point.

Fig. 1. Feedforward HTEES Control strategy.

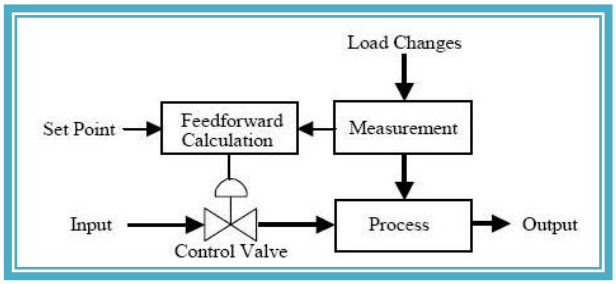

In a dynamic system, the Total Energy Storage Capacity "Σ" is the sum of the actual Thermal Energy Storage "τ, the actual Electrical Energy Storage "ε" and a supplementary useful equivalent storage capacity "δ":

$$\Sigma = \tau + \varepsilon + \delta \quad (1)$$

It is important to note that "τ" and "ε" in Eq. (1) are not the nominal (theoretical) values, but rather the actual capacities, taking into account the operational conditions. They represent the useful portion of the nominal capacity in the context (e.g., temperature, cycling, heat rejections, ramp up, and ramp down

In such a dynamic system, the Total Energy Storage Capacity "Σ" can be assimilated to an Electrical + Thermal "Uninterruptible" Supply (UPS+UTS) that is considering the system in which it is operating.

As a consequence, the Projected (or predicted) Energy Storage Capacity "Σp(t)" is not only a summation of the nominal capacities. It is the value that is changing in real time, a dynamic value:

$$\Sigma p(\tau) = \tau(\tau) + \varepsilon(\tau) + \delta(\tau) \quad (2)$$

The supplementary useful equivalent storage capacity "δ(t)" is the sum of the additional energies sources at time "t" (e.g., reduced losses, improved capacities due to temperature management, and equipment efficiencies). This new parameter is introduced in the feedforward control. The operation is integrating an optimized "Charge Mode" during off-peak hours, when outside temperature is more favorable. It is using the grid when it is more effective and using a "Discharge Mode" during on-peak hours, when it can absorb transient increases in datacenter cooling load, avoiding startup of additional chillers and reducing the load on the grid.

This "predictive" approach is allowing for a better use of the Energy Storage, but also for a better integration of EES and TES to maximize:

- Operational flexibility and stability
- Performance improvement in the operation
- Demand-Side management with predictability
- Reliability in the operation.

B. Thermal Energy Storage with SPCM

Developed to be operated on a 24/7 basis, the SPCM act as a buffer to mitigate the fluctuations in the load. The SPCM used in conjunction with the electric storage media is a Synthetic Phase Change Material. The phase change taking place in the thermal storage is from liquid to solid and vice-versa. This change in phase allows for managing (absorbing or releasing) a large quantity of energy in small volume, compared to conventional electric storage.

Through the last 2 decades, Novacab has developed 30 different SPCM mixtures with a melting point from -40°F to + 250°F; unlike only 32°F like for the liquid water to ice phase change. And also unlike water or even eutectic salt that have a substantial expansion factor (while solidifying), SPCM has a small negative expansion factor in the solid phase that results in negligible stress on components. These mixtures need very low maintenance and have a life span of up to 15,000 cycles while they are non-toxic, non-corrosive, nonbio-accumulative, and non-carcinogen.

III. Performance Experiments and On-Site Monitoring

The HTEES were implemented and monitored in various facilities (e.g., Fig. 2). The results show that they might have a significant impact on the grid itself. Datacenters were quickly identified amongst the good applications of the technology because their energy consumption is huge and growing fast, although they are consuming electricity and cooling.

Fig. 2. Implemented system.

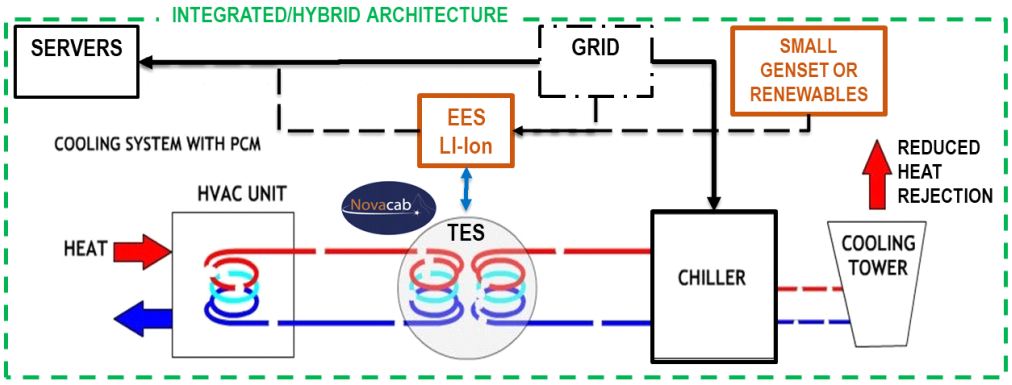

Fig. 4. HTEES integrated architecture/configuration.

A. Applications in Datacenters

The thermal and electrical loads are critical for the datacenters operation. In fact, the cooling systems are often the largest single consumers of power. In many cases, it is also one of the most inefficient systems in a datacenter. While the servers are becoming more and more efficient, their growing numbers (in terms of capacity and power) reverse the effect, and the consumption is still growing. According to the U.S. Department of Energy (2016 report), it will reach 73 billion kWh/year in 2020.

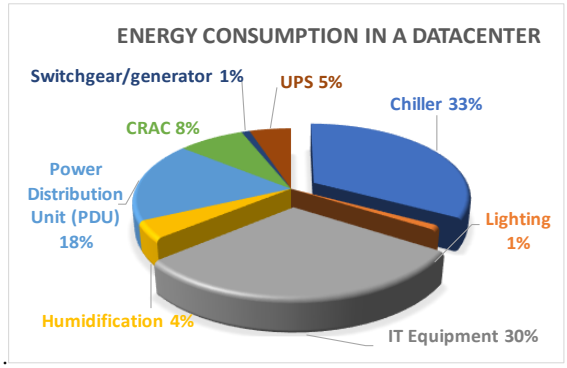

Fig. 3. Datacenters distributed power consumption.

As illustrated in Fig. 3, the cooling systems (33 percent for chiller and cooling tower) are the largest consumers of power that support the datacenter – in many cases it is the most inefficient. The chiller plant is often over-provisioned for redundancy, resulting in partially loaded equipment and energy inefficiencies.

To better understand, we look at how many datacenters operate today. The electric components are separated from the thermal (cooling) components that are considered "support" systems. Doing so, the biggest consumption point of the datacenter (the cooling) is often set apart from the main backup system. The hotter the outside temperature, the harder the chillers and cooling towers must work and the more difficult it is for the electric grid. Chiller size must account for such extreme conditions that they are often over-designed. Consequently, the variability in a datacenter cooling load leads to partially-loaded, inefficient chiller operation. Because cooling is required and critical to the operation, over-designed generators would be installed to compensate for that risk. A server room would fall down if the temperature rises too fast. It is difficult to do real climate controls to optimize operation with systems that are less efficient when the demand is higher. In short, the outside weather conditions are controlling the efficiency of the process.

As a response to these issues, an HTEES device is installed between the chillers and the datacenter (see Fig. 4). Chillers can be run at optimal utilization for highest efficiency. It is "Charged" during off-peak hours, when the outside temperature is more favorable and using the grid when it more effective. It is "Discharged" during on-peaks hours, when it can absorb transient increases in datacenter cooling load, avoiding startup of additional chillers and reducing the load on the grid.

B. Power Usage Effectiveness

Power usage effectiveness (PUE) is a common indicator representing the energy efficiency of a datacenter. PUE reflects how much of the facility's power consumption is used for the primary computing purpose, as opposed to support functions like cooling.

PUE is the ratio of the total amount of annual power usage of the datacenter to the annual power usage of IT equipment, as described by Eq. (3).

$$PUE = \frac{T}{IT} = \frac{K + Y + O + IT}{IT} \quad (3)$$

PUE = Power Usage Effectiveness
T = Total Energy Consumption; IT = IT Energy
K = Cooling Energy; Y = UPS Energy
O = Other Energy Consumption (i.e., PDU, lighting, etc.)

To better characterize the impact of the outside conditions on the efficiency, Mechanical Power usage effectiveness (PUEm) is a special indicator representing the energy efficiency of the mechanical cooling in a datacenter. PUEm is the ratio of

the total amount of annual power usage of the cooling systems to the annual power usage of IT equipment, as described by Eq. (4).

$$PUEm = \frac{K}{IT} \quad (4)$$

PUEm = Mechanical Power Usage Effectiveness
IT = IT Energy; K = Cooling Energy (i.e., chillers, pumps, cooling towers, air handling, etc.)

Reducing Part Load is an example of how an integrated HTEES with feedforward control can improve PUE. The performance curve in Eq. (5) represents actual measurements (with R^2=0.94) of the impact of Part Load on efficiency (kW/Ton) from a centrifugal chiller operating with constant 70°F entering condenser water and 42°F exiting evaporator water.

$$kW/Ton = -0.66\,\lambda^3 + 1.98\,\lambda^2 - 1.85\,\lambda + 1.11 \quad (5)$$

kW/Ton = Chiller Efficiency
λ = (Part) Load = Demand/Capacity

The idea here is to optimize the PUE through the chiller electric supply in regular operations (see Fig. 5 for the substantial impact of outside temperature on PUE and PUEm), and in fail safe-mode (e.g., during a power or mechanical failure).

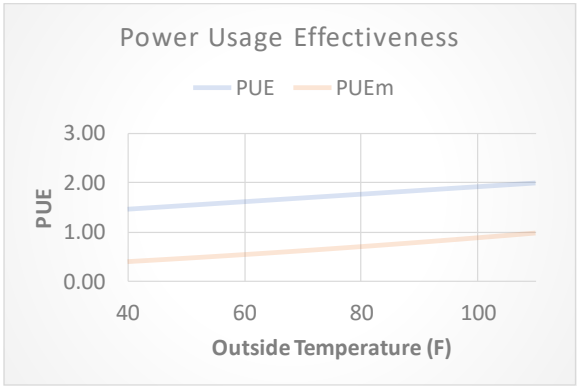

Fig. 5. PUE & PUEm as a function of outside temperature.

C. Onsite Monitoring

An implementation with extensive monitoring has been deployed at a major datacenter, located in ahigh rise building. Eighteen units in two sets: one for energy efficiency purposes, including peak shaving, and the other for safety reasons, as a redundancy for the server cooling. A hybrid approach that integrated the solution with a central power manager was the only viable solution; ultimately, the program successfully met all of its goals. The onsite monitoring shows a 10 percent to 23 percent reduction of the electricity consumption for the cooling. That represents approximately 2 Million kWh per year and up to 0.8 MW in peak shaving.

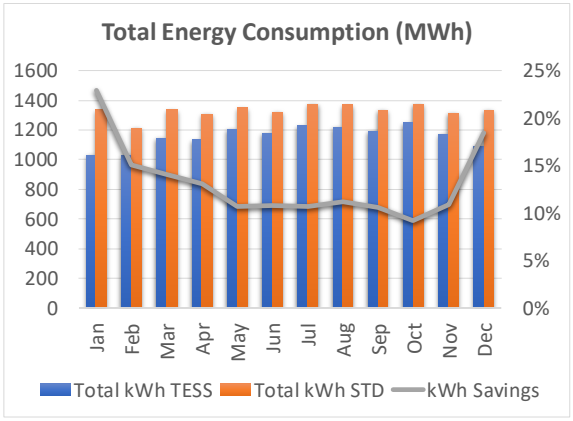

Fig. 6. Energy Consumption for Standard and HTEES.

With the HTEES, the cooling load from server racks is reduced substantially for all the OA conditions. In addition, the power consumption has a significant lower impact on the total datacenter power consumption with the HTEES. The Fig. 7 shows that Electric Peak can be improved (shaved) from 617 kW to 913 kW by the proposed system, under the given operating conditions.

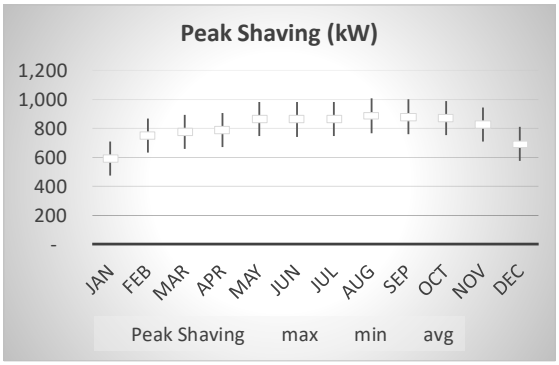

Fig. 7. Peak shaving with HTEES.

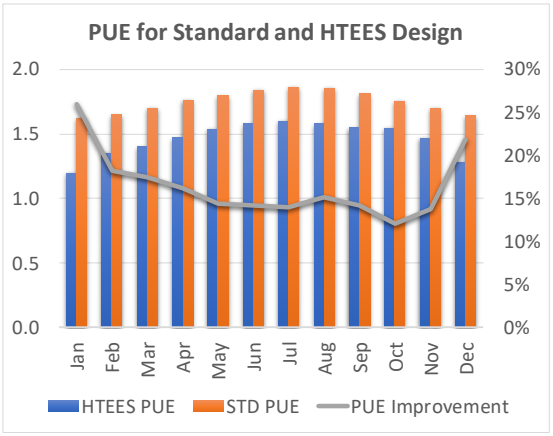

Fig. 8. PUE for Standard and HTEES Configuration.

The results illustrated in Fig. 7 show that the monthly averaged PUE values vary significantly because of the variation in mechanical cooling needs depending upon OA conditions. Figure? also shows that the average PUE with the standard

design is above 1.7, whereas the monthly PUE values with the HTEES are averaging a value lower than 1.6, regardless of OA conditions.

Fig. 8 outlines that the PUE can be improved from 12% to 27% by the proposed system, under the given operating conditions.

IV. Discussions

A. Implementation and Outcomes of Onsite Monitoring

The HTEES was designed with energy efficiency and sustainability in mind, setting it up to be 47% more efficient for cooling than typical datacenters, and from 10% to 23% more efficient than state-of-the-art facilities operating today. Almost 80% of the energy is going directly to its core purpose.

Ramp up and ramp down of the equipment are reduced and the Supply and Return process temperatures are stabilized. To summarize, the Measured Operational Cost Savings and other benefits of using an HTEES in the field are as follows:

- Peak shaving of up to almost 1000 kW
- Reduction of 13 % in the yearly overall electric consumption (35% reduction for cooling)
- 2 GWH/year and 0.8 MW average load leveling.

Other applications of the HTEES include industrial plants and hospitals that need electric and thermal energy. In such critical processes, a significant portion of the fluctuations in the load is taken by the HTEES. The SPCM is acting as a shock absorber in the thermal process.

With the HTEES, the PUE index is designed to stay under 1.5 as much as possible. This means that less than 20% of the energy for the entire complex will go to functions outside of the computing itself. Typical modern datacenters have a PUE index around 1.7 to 1.8, with many facilities operating at 2.0. The HTEES hybridization not only helps the end-user/operator, but also the energy provider; the utility itself unlocking on-peak power for other use.

In addition, the data can already allow for an evaluation of the Return on Investment of such an implementation. The simple Payback is ranging from 2.8 to 4.2 years, while the Net Present Value (NPV) is averaged to $2.7M over 10 years (with an average 4% discount rate extrapolated over the period). Longterm data collection (for more than a decade) would be required to allow for an even more accurate value of the NPV or of the life cycle costs (LCC) since the Lifespan of such a system is estimated to be around 20 to 25 years.

From the extensive monitoring, many items can be outlined for the stakeholders:

The end-user or the facility manager:

- Reduces peak loads (kW) and energy consumption (kWh)
- Allows for better energy efficiency, incremental peak shaving, and boosted free cooling
- Minimizes equipment Stops and Starts, Overdesign, and Part Loads
- Improves the PUE, reducing the total power, consumed by a datacenter, to get closer to the power consumed by the IT equipment of the facility.

The utility or the smart-grid operator:

- Smooth load profile optimization
- Demand-side management
- Redundant and predictable energy distribution.
- Lower energy consumption and transmission losses
- Lower operating costs and improved asset utilization
- Deferred construction and capital expenditure requirements.

The energy storage industry has just begun exploring grid-scale hybrid solutions that combine two or more energy storage technologies with complementary characteristics to provide an optimal solution not achievable by any one technology. The implementation and monitoring that were achieved here are a good example of the potential of such a strategy.

The tested systems include storage technologies that separately cover sprinter loads required for fast response or marathon loads required for peak shaving and load shifting. By combining two technologies, the HTEES makes this issue much less of a concern. In addition, the hybrid system has demonstrated that it could simultaneously provide multiple services that allow for two value streams concurrently.

V. Conclusion

The project has shown that the integration of Electric and Thermal components in the HTEES allows for saving electricity and surviving power failure. The outcomes of the HTEES was highlighted by the monitoring, including onsite operational data, PUE, reliability, and performance.

Monitoring in a datacenter has shown that optimum results are obtained when initial fluctuating conditions were observed. Improved performance and stability were measured and have shown that ramp up and ramp down of the equipment are reduced and the Supply and Return process temperatures are stabilized. With the HTEES, the PUE index would stay under 1.5, starting from value up to 2.0. This means that less than 20% of the energy for the entire complex will go to functions outside of computing, while the cooling consumption is reduced by more than 35%. It is also allowing to reduce the size of the generator or other backup power.

The same hybrid approach merits exploration for providing stationary energy storage solutions for other applications. The combined systems, properly controlled,

would allow for significant improvement and stability in the operation in a critical application such as hospitals, datacenters, military facilities, manufacturing plants, and other critical processes.

The measured advantages are lower cost, increased system efficiency, and increased system lifetime due to optimized operation and the ability for hybrids to do more and last longer with less overall storage capacity. Hybrid systems could open up even more revenue streams for facility managers, operators and smart-grids not currently possible with a single energy storage technology.

The HTEES merit a closer look for many other stationary applications as part of comprehensive energy storage deployment strategies. HTEES technology has demonstrated the potential to achieve double-digit percent decreases in CAPEX and OPEX, increase system operating life, and boost revenues by simultaneously providing multiple services. This hybrid solution may be a change in the 'single storage' paradigm. Of course, the energy management hardware and software needed to manage two different storage technologies for multiple use cases are not trivial, and development will definitely continue with the new applications coming in.

ACKNOWLEDGEMENTS

This Demonstration and Deployment project was partially supported by Austin Energy, Simon Property Group, DB Foundation, and other Private Donors. We would like to extend a special thank you to the Simon Property Group and Novacab Team for providing us with World class talent, vision and the necessary momentum to advance our exciting world of RE projects. This Team effort will generate much better efficiencies, thermal energy storage, demand response and other great benefits to our environment and businesses alike. We would also like to show our gratitude to the G. Dennis Vaughan, Rear Admiral U.S. Navy (Ret.), Art Vatsky, PE, James Babb, PE U.S. Navy Cdr.(Ret.) and James Pitchford, Former U.S. Marine and PAO for the Chief of the U.S. Navy Reserve for sharing their pearls of wisdom with us during the course of this project.

REFERENCES

[1] A. Shehabi, S. J. Smith, D. A. Sartor, R. E. Brown, *et al.*, "United States Data Center Energy Usage Report 2016," Lawrence Berkeley National Laboratory, Berkley, CA, rep. no. LBNL-1005775, pp. 1-65, 2016.

[2] IEA-ETSAP and A. Hauer, "Thermal energy storage: Technology brief," International Renewable Energy Agency (IRENA), Abu Dhabi, United Arab Emirates, pp 1-24, Jan. 2013.

[3] Renewable Energy Policy Network for the 21st Century (REN21) Steering Committee, "Renewables 2016 global status report," REN21, Paris, France, 2016. [Online]. Available: http://www.ren21.net/wp-content/uploads/2016/10/REN21_GSR2016_FullReport_en_11.pdf

[4] A. Datas and C. Algora, "Development and experimental evaluation of a complete solar thermophotovoltaic system," *Prog. Photovolt: Res. Appl.*, vol. 21, no. 5, pp. 1025–1039, Apr. 2012.

[5] A. Ramos, I. Guarracino, A. Mellor, D. Alonso-Alvarez, P. Childs, N. J. Ekins-Daukes, *et al*., "Solar-thermal and hybrid photovoltaic-thermal systems for renewable heating," Grantham Institute, London, UK, briefing paper no. 22, May 2017.

[6] X. P. Chen, Y. D. Wang, H. D. Yu, D. W. Wu, Y. Li, and A. P. Roskilly, "A domestic CHP system with hybrid electrical energy storage," *Energy and Buildings*, vol. 55, pp. 361-368, Dec. 2012.

[7] G. Comodi, F. Carducci, B. Nagarajan, and A. Romagnoli, "Application of cold thermal energy storage (CTES) for building demand management in hot climates," *Applied Thermal Eng.*, vol. 103, pp. 1186–1195, Jun. 2016.

Stephane Bilodeau, Eng., Ph.D., FEC, CTO, Founder/Chairman

Professional Engineer, PhD in Energy & Advanced Thermodynamics with a Master in Applied Sciences. He is a Fellow of Engineers Canada and his Vice-President of the Public Affairs Advisory Committee; he was Director on its Board from 2013 to 2016. Member of the Board at the OIQ (more than 60 000 professional engineers) from 2006 to 2015, he has been involved actively in many standing committees and serves notably as Vice-President from 2009 to 2014 and President in 2014. In the last 20 years, Dr. Stephane Bilodeau has driven many top tier projects related to Thermal Energy Storage and Energy Management with various teams including IBM, Natural Resources Canada, Johnson Controls, Kruger, Honeywell, Hydro-Quebec, Bombardier, Volvo Bus, etc.

Michael L. Carty, President/CEO

Michael brings decades of corporate leadership along with experience in development of new technologies, he has more than 40 years of experience in business and product development, marketing, strategic deployment, and event organizer. Vast experience in sales and merchandising in Canada and USA. Projects and product development with Northern Telecom production of printed circuits Bell Canada. Entrepreneur in the automotive industry, car dealership owner (General manager and Vice President of a Chrysler Dealership), and trainer for Manufacturers. Michael L. Carty can rely on the services of expert partners in different fields of activities worldwide.

Chris Mashburn, VP/General Manager

Former Captain with the Texas Highway Patrol and Detail Leader for President Bush's Executive Protection Detail. Prior to joining Novacab, served as CEO and President of Penfield's Office Solutions since 2006, a specialty business center tailored for the hospitality industry. Prior to that, he founded a private physical security and outsourced staffing firm in 2001, serving as President and CEO, expanded the company's growth in the airline and commercial industries, and drove development of internal processes and controls resulting in a fully ISO 9000 compliant company.

Ross Quick, VP/CSO

With Novacab since 2015, he has been previously involved in the commercial industry cultivating sales teams for fortune 500 companies over the last 20 years. Ross worked as a broker for Strategic Energy, Reliant Energy and others while building and training a team of 34 representatives resulting in $200 million in contract value. With his previous partners in Admiral Energy, LLC back in 2007, he won the $1.6 billion dollars project to rebuild the former Clark Air Force Base located in the Philippines.

Fast Response Flywheel Energy Storage Technology for Virtual Power Plants and Microgrids

Thilo Engelmann, Rainer vor dem Esche, Reddy Tudi

Stornetic GmbH, Stetternicher Str. Staatsforst, 52428 Jülich, Germany

I. SUMMARY

The continued expansion of renewable energy sources like wind power and photovoltaics is gradually reducing short and long-term grid stability, especially as more and more conventional thermal power plants are retired and taken offline. Power to gas, power to heat, battery storage and flexible load management provide a solution to deal with the challenges of long-term (5 to 12 hours) grid stability, while fast response storage technologies such as Flywheel Storage provides an efficient and affordable solution to manage the short-term (0 seconds to 5 minutes) challenges of grid stability.

The EFRE project Quirinus [1] and the EDF concept grid [2] are two demonstration projects being tested in Europe, based on a combination of flywheels, gas engines, and renewable generation. They explore the ability to stabilize local grids in critical states, as well as the potential to reduce cost of transition to future grids with carbon free generation and a very high level of power quality and reliability. The intent of this paper is to introduce and present the findings of these demonstration projects.

Today conventional synchronous generators, with their ability to provide inertia and adjust to load changes instantaneously, are key for grid stability. When these conventional generators are replaced by renewables, system inertia is reduced, negatively affecting grid stability. A good example is Ireland having a weakly inter-connected <8GW island grid and a renewable penetration growing above 50%. Currently the renewable growth is limited by grid stability constraints requiring the Irish grid operator to invent new market mechanisms and tools to stabilise the grid before the next step to 75% renewable share [3]. Similar problems occur in smaller island or micro-grids partly operating on renewable generation, but still requiring conventional generation for grid stability. The limited size of these grids in combination with load changes makes them sensitive to short-term power quality issues. Typically, customers, particularly power intensive industrials, require a high power quality. With the increasing decentralized solar generation in distribution grids, power quality becomes a challenge and these demonstration projects aim to mitigate these challenges.

Fig. 1 shows how fast response Flywheel Storage technology like Stornetic's DuraStor system can provide reliable and efficient solutions without having the need to operate many synchronous generators to stabilise the grid frequency. This is the basis for the current demonstration projects with EDF and Quirinus. This paper also shows that the investments needed to provide sufficient synthetic inertia can be financed by the savings from not operating synchronous inertia for the sake of grid stabilisation.

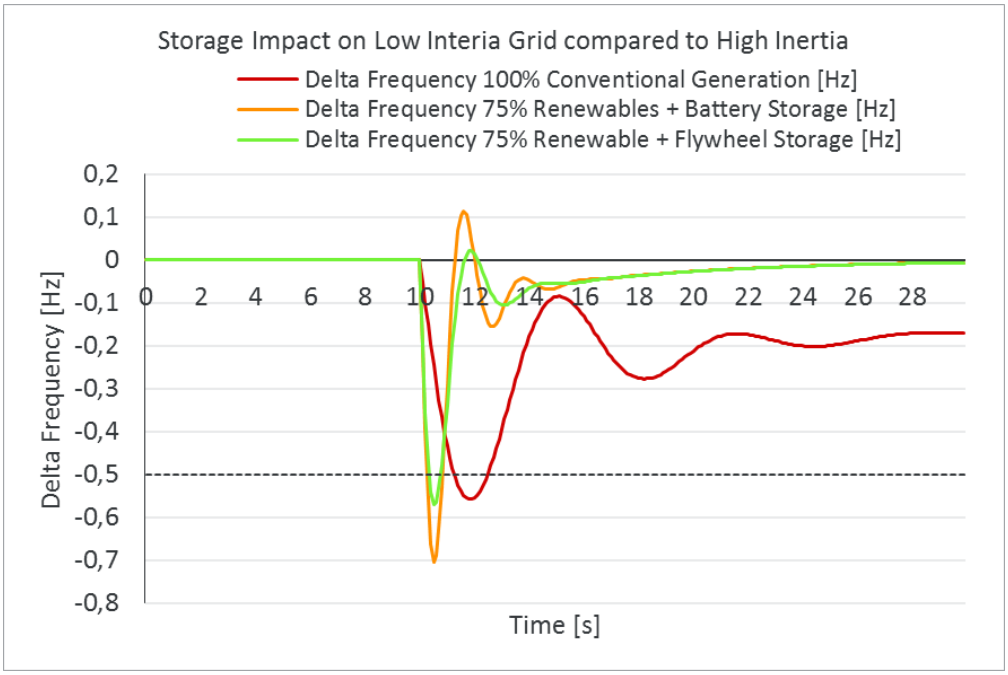

Fig. 1. Comparison of flywheels, batteries and conventional generators during grid fault event.

II. Introduction/ Quirinus-Project

The government of North Rhine-Westfalia initiated the Quirinus project [1] with funding from the European Regional Development Funds EFRE in an area of traditional lignite mining. 10 GW of lignite electricity generation is paired with a high number of energy–intensive industrial loads. Based on greenhouse emission targets, the plan is to substitute the lignite plants stepwise with renewables. Quirinus will address the challenges to maintain grid stability (i.e., power quality such as voltage sags and frequency deviation) at the high level of renewable penetration while supporting critical industrial loads:

- Renewables sited in medium and low voltage distribution grids (50/50) instead of large lignite plants feeding top down via the transmission grid
- Ancillary services provided by distribution grids without overloading lines and devices like transformers
- Management of intermittent renewable generation and its power fluctuations with storage and CHPs/gas generators
- Compensation of missing inertia of large generators with storage
- Locally-managed grid area changes with features like automatic islanding, black start, and resync capabilities.

Three scenarios are being prepared for up to four distribution girds starting with a lignite-mining pit as “sand box environment”:

1. Traffic light concept to detect overloading of grid elements combined with mitigation strategies
2. Ancillary services management provided by distribution grids rather than transmission grids (i.e., to other regional distribution grids)
3. Securing the supply of critical areas with micro-grid features like automatic islanding and black start to support a quick, regional-grid restoration process.

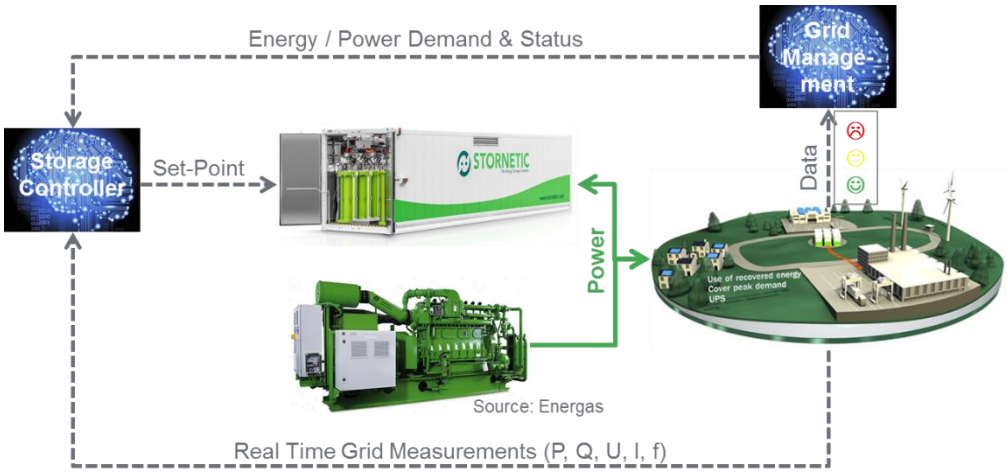

Fig. 2. Typical setup with DuraStor & gas-motor short term stabilising the Microgrid.

Advanced grid management systems are required to provide these functions for a further transition to renewable generation, see Fig. 2. Its task is to manage the energy balance of the entire system based on the health state of the relevant grid areas. The DuraStor energy storage systems has three key functions:

1. Manage the local grid stability, optional together with gas-motor(s), to maintain frequency and voltage.
2. Support the regional energy balance by charging/discharging electricity on demand
3. Prepare and perform on demand grid recovery together with the gas motor (Black-Start).

A) Grid Stabilisation Challenges: Systems with reduced grid inertia are more sensitive against load changes, [4], [5]. Fig. 3 shows the response of a typical gas-motor to a significant load change. One can see that the current adjusts automatically, resulting in an instantaneous power increase. However, thereafter, the frequency, voltage, current and power start to drift away. After about 2 seconds, the system stabilises at a frequency ≈5Hz lower and starts recovering, driven by the increasing motor torque. After about 10-15 seconds, all parameters are stabilised. Voltage and frequency exceeded critical thresholds.

Typically, a frequency corridor of <±0,5Hz and a voltage corridor <±5% around nominal would be acceptable for industrial grids. International standards for gas-motors permitted today to have dynamic frequency deviations from -15% to 18% and voltage deviations from -25% to 35% as defined in [6].

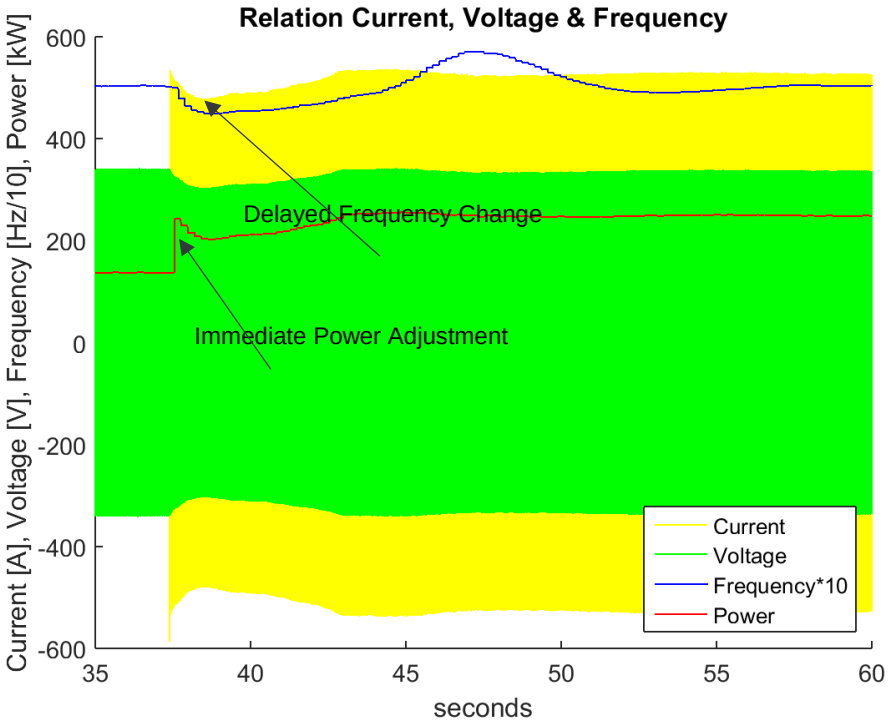

Fig. 3. Dynamic response of a gas-motor to a load step.

Additionally, it is predicted that in future even in interconnected grids, some regions have to have the ability to operate in island mode [1], [7]. This will be required to avoid larger black-outs when grids become unstable and will also be needed to restore grids after local or regional failures. In the future, local grids, grids with more decentralized renewable generation and with less system inertia, will need to have more elasticity to support grid restoration. This requires that local or micro-grids should support:

- Grid following operation when grid connected supporting regular grid codes and providing regular grid services
- Swift movement from grid following into island mode when the superordinate grid gets instable and if required by grid management
- Formation and operation of a micro-grid, with different grid codes, with operation of critical equipment like gas-motor and energy storage
- Resynchronization and reconnection to the public grid if required by the grid management system

The same demand occurs for “private” micro-grids like industrial grids that want to operate in island mode during instabilities. Studies have shown that the fast response time of flywheel and battery storage systems, compared to conventional generators, have a positive influence on grid stability and ancillary service costs [8] while also reducing the CO_2 emission by some percent [9].

III. High-Level Solutions

Today multiple solutions are in discussion to cover the upcoming problem of grid stability due to reduced inertia. In general, the assumption is that systems will become more and more decentral and with smaller individual power producers. First steps have been taken to force renewable sources to provide system stability services. Table 1 provides an overview of discussed solutions providing short-term grid stabilisation services.

TABLE I
SUITABILITY OF VARIOUS TECHNOLOGIES STABILIZING THE GRID

Solution	Pros.	Cons.
Adjust renewable generation at over and under-frequency (Curtailment)	• Low cost solution mainly introduced by software changes • Relatively easy to implement • Provides service proportional to the renewable share • Number of installations is increasing.	• It's only available during renewable generation => less predictable and not manageable • It can only provide low frequency support if continuous curtailment is accepted • Increased pay-back times because of opportunity losses • It is not immediate as it needs to balance the interest of energy supply vs. system stability (up to 1 second delay).
Use of gas-motors like Biomass or CHP systems	• It's real inertia, thus, instantaneous • Biomass is more baseload power, and therefore, predictable and manageable • Number of installations are increasing • Resynchronization is possible • Black-Start is possible.	• Due to the slow response characteristic of gas motors and little mechanical inertia, service is limited • If providing primary frequency regulation, the owner can have opportunity losses.
Battery storage	• Can be combined with mid- and long-term storage • Relative responsive (100 to 1,000 ms), and thus, good fast frequency control.	• No real inertia and does not provide support for the first 100 to 500 ms • In continuous frequency control load cycles reduce battery lifetime.
Synchronous flywheels	• It's real inertia, and thus, instantaneous • Provide a lot of power for a few seconds.	• Can only provide energy for a few seconds (H-Factor < 2 s) • Relatively expensive and specialised • Continuing losses.
EnWheels (non-synchronous flywheels)	• Provide a lot of power for a few minutes • Very responsive (toggle from charging to discharging in 10 ms, and thus, reliable and very fast frequency control • Load cycle resistance and long lifetime • Support resynchronization and Blackstart.	• Non-synchronous grid inertia • Limited to a few minutes of grid support.
Hybrid solutions with EnWheels and Generators or turbines	• Provide real synchronous inertia • Very Responsive (toggle from charging to discharging in 10 ms, and thus, reliable and very fast frequency control • Load cycle resistance and long lifetime • Resynchronization and Blackstart possible.	• In combination with gas motors only providing synchronous inertia as long the gas motor is in operation • Continuing losses of around 7% to 10%

Error! Reference source not found. shows the benefit of synchronous reserve, but also the benefit of very fast responding systems on grid stability. The combination of both would allow enhancing grid stability at the lowest investment levels. In addition, most of these systems can be installed in a decentralized manner, solving local constraints and being more adaptive.

IV. SYSTEM DESIGN

To judge the capabilities of the various solutions, it is necessary to understand where constraints originate. This finally will also explain the physical gap between synchronous and non-synchronous solutions, and the remaining risks of losing more and more synchronous reserve.

A) Functioning of Synchronous Generators: A rotor with a magnetic field is passing stator coils connected to an AC supply producing a rotating field. At synchronous speed (the grid frequency (f)), the rotor poles lock to the rotating magnetic field. The rotor is typically driven by a motor or turbine that creates the required mechanical energy, power, and torque. See Fig. 4.

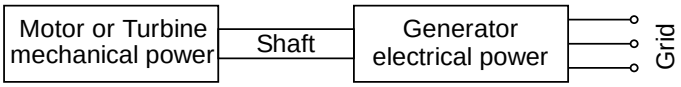

Fig. 4. Schematic of the power transfer from Motor/Turbine to Generator and Grid.

If load changes, the changed current also flows through the stator coils of the generator, which changes the electro-magnetic counter-field (B_{Stator}), and with this, the electro-magnetic torque of the stator (T_{el}), see next formula with k being a generator constant.

$$T_{el} = \frac{k}{2 * \pi * f} * B_{Stator} * B_{Rotor} * \sin \delta(t) \qquad (1)$$

To achieve again a new electro-magnetic energetic equilibrium, the angle ($\sin \delta(\tau)$) changes until the magnetically transferred energy equals the electrical energy. This will change the electrical torque (T_{el}). Now the equilibrium between the electrical Torque (Tel) and the mechanical torque (T_{mech}) of the motor/turbine gets disturbed. As a consequence, the speed/frequency of the generator changes. This change will only stop when the mechanical torque (T_{mech}) is adjusted to the electrical torque and a new equilibrium is achieved. The mechanical part of this process is described by the "swing equation" [10]. J is the mechanical inertia of the turbine-generator set.

$$J * \dot{\omega}(t) = T_{mech} - T_{el} \qquad (2)$$

The formula describes that mechanical energy is taken out of the rotating mechanical inertia (J) until by other means/adjustments the mechanical and electrical torque equilibrium is achieved again. Consequently, the shaft accelerates or decelerates ($\dot{\omega}$). In a micro-grid this influences the grid frequency immediately because J can be small compared to the torque change.

This service is called "Synchronous Grid Inertia" and is a very important factor for grid stability. The swing equation also shows that the change of grid frequency (ω) is by definitions a consequence of load change always being delayed compared to the load step, also shown in **Error! Reference source not found.**.

A) Inverter Based Systems and Their Behaviour Stabilising the Grid: All systems producing energy without using a synchronous generator need inverters to deliver electrical power into the grid. Examples are solar and battery systems as well as most wind power systems or battery storage systems.

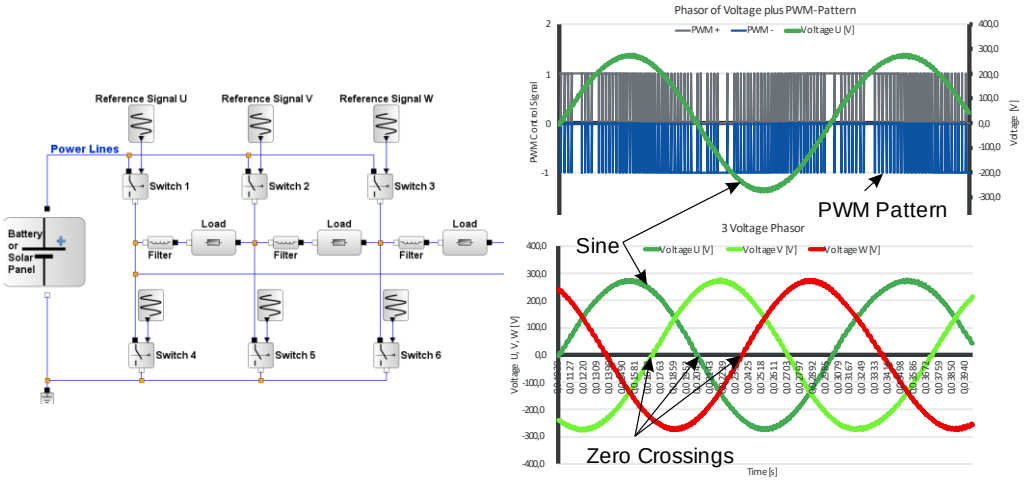

Fig. 5. H-Bridge creating 3 Phase Voltage [11].

The inverter uses DC current and voltage, and creates a sinus like AC voltage and current using power electronic switches, chopping the DC-current into rectangular pulses with a moduled length. This method is called “Pulse Width Modulation” (PWM). A typical design is shown in Fig. Based on a reference signal for every phase, a dedicated PWM pattern is generated that switches the semiconductors. Typically, grid-connected inverters measure and predict constantly the three grid phasors and create, out of this, the reference signal controlling the semiconductors.

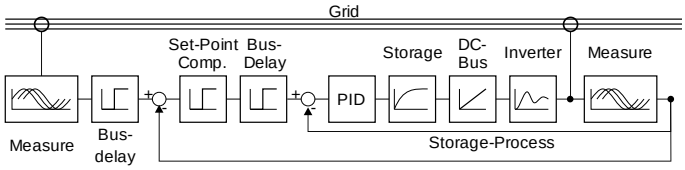

Fig. 6. Typical control loop of an inverter based storage system.

As long as conditions are not changing significantly, the phasors can be predicted. If conditionschange, some interpolations are needed before the phasor change is characterised properly in amplitude, angle, and speed. These measurements take time. Therefore, inverter driven systems have the following fundamental difference compared with synchronous generators:

- Inverter based systems always respond with a delay and do not support the grid immediately
- All interactions and changes are based on computations, are conscious and not coming from physical effects
- Depending on the DC source additional reaction delays can exist
- The sine is not perfect and can have harmonics.

Table II highlights the differences between synthetic inertia and synchronous inertia at different points in time after an event occurs. Compared to the case with high grid inertia, inverter based systems have disadvantages within the first second. These disadvantages are strongly related to the response time of the system. Systems with short response times and short dead times compensate fast. Systems with response times longer 1,000ms do not contribute to short term grid stability. Dependent on the storage/generation technology as part of the inverter-based system the grid is allowed to recover faster compared to pure synchronous reserves.

TABLE II
GRID SUPPORT OF SYNCHRONOUS AND INVERTER BASED GENERATION AT VARIOUS TIMEFRAMES

Timeframe[1]	Synchronous Inertia[2]	Inverter Based (synthetic) Inertia[3]
0 ms up to ≈ 30 ms	• Provides required power based on Ohm’s law • Grid frequency change hardly visible.	• No support.
≈ 30 ms up to ≤ 1 s	• Provides required power • Frequency starts changing visibly.	• Provides power ramping up, based on technology and control algorithm within ≈ 50 ms up to ≤ 1 s.
≤ 1 s up to ≈ 5 s	• Provides required power • Depending on load step strong change of frequency visible • Mechanical torque starts to adjust.	• Delivers required power • Stops frequency drift • Based on control algorithm frequency, drift starts to recovers.
≈ 5 s up to ≈ 30 s	• Provides required power • Torque adjustment stops frequency drift.	• Delivers required power • Grid frequency is recovering.
≈ 30 s up to ≈ 5 min	• Provides required power • Torque adjustment helps to recover frequency.	• Delivers required power • Grid frequency is recovered.

For grid services, it is key to further reduce the reaction time of the inverter based systems, allowing to further close the gap to synchronous generation within the first second and allow stable grid operation with less synchronous generation.

B) Improved Responsiveness of Inverter Based Storage Systems: Table II show the benefits of fast responding inverter based resources for grid stability. Storage systems, in particular, allow compensating bi-directional load changes while currently renewable generation curtailment is mainly used to stabilise high frequency scenarios. Fast response with

[1] Timeframe can vary based on technology and vendor. Fig.s are indicative representing typical solutions existing today or requirements from typical grid codes.
[2] Statements is assuming sufficient power installed
[3] Statements is assuming sufficient power installed. Fig.s are indicative representing typical solutions existing today.

little delay time helps grids recovering because of two main effects:

- Fast adjustment of power obviously leads to faster achieving a new equilibrium giving grid stability
- Little response and delay times allow for faster and more robust control-loop designs.

To understand system response and its impact on grid frequency, it is helpful to analyse the system, including measurements, computation, system component responses, and control loop designs.

Critical processes are the grid measurements, the computation times and the storage response. Depending on the measurements methods chosen, measurement times can vary from < 10 ms up to > 0.5 s. The response of the storage itself depends on technologies and has often limited ramp rates or slopes. Overall, control loops can get very long, limiting the use of energy storage systems for frequency regulation; but it is possible to design fast control systems.

To achieve shorter to very short reaction times, system operators have to make a choice. Currently non-synchronous frequency regulation services are typically designed with a corridor of no action (dead band), followed by a proportional correction action (P-Controller). A long slope time (I-Controller with long integration time) is usual before a service is fully triggered. A different control behaviour is needed to replace inertia with synthetic inertia, acting proportionally with reasonably short integration time, but in addition, maybe even acting differentially on the rate of change (PI(D)-Controller).

Fig shows the response of a simulated grid to a RoCoF event of 13% of the nominal grid capacity at various levels of inertia and with storage support. Within the first second, a small difference exists between a high inertial grid and a grid supported with fast storage. Nevertheless, if the amount of storage power installed is sufficient and acting fast, the total frequency drop is about the same as the one with a high inertia grid. The storage supported grid recovers after one second much faster than a usual grid with high inertia. To achieve this, the system requires fast responding control loops with 50 ms response times and ramp rates of 20MW/s per installed MW. This results in demanding load profile for the storage with constant current flows in and out.

-

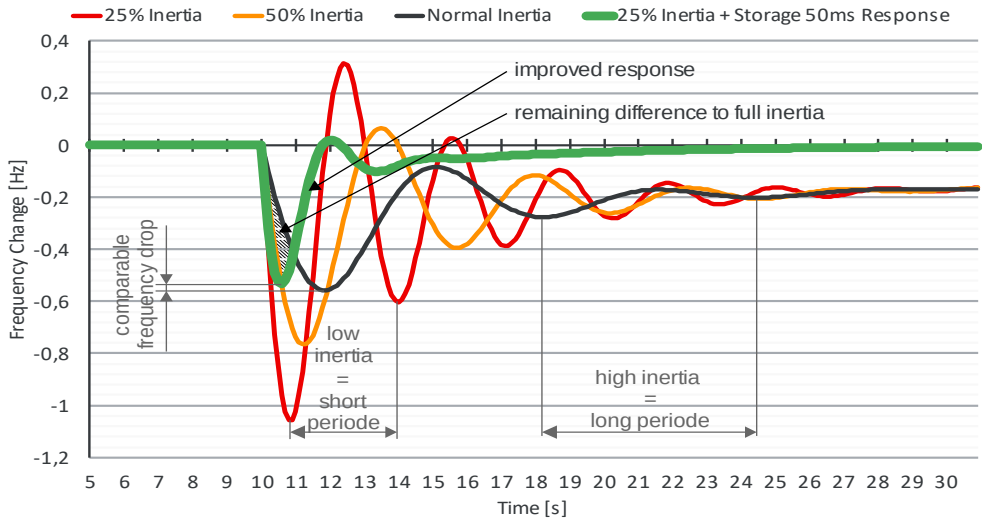

Fig. 7. Frequency change of grid two generators to a 10% load step based on different rate of inertia and storage support.

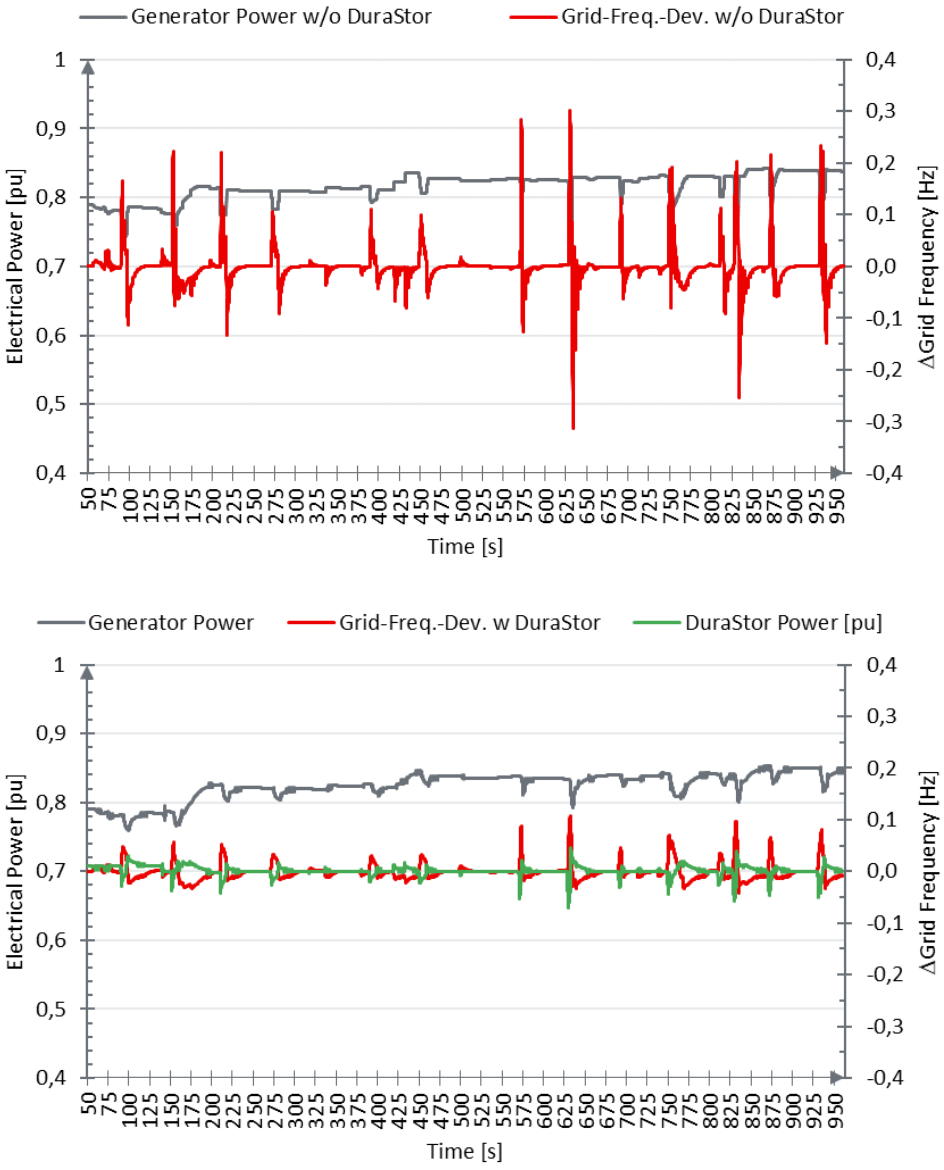

Fig. 8. Frequency variation in a microgrid with and without responsive storage.

The graphs in Fig show the response a gas-motor storage in a grid with statistical load variations in the range of ≤ 5% of the nominal grid load. The system consists of a 1MW gas motor and a 240kW DuraStor® flywheel system. The results are compared to the grid without storage.

The grid frequency is in general more stable by a factor 3. Additionally, the generators have to provide less primary and secondary frequency regulation service, and therefore, run more smoothly.

To achieve this stabilisation performance with storage systems, fast reacting control loops are keeping the storage systems constantly in duty reacting against every load change. This will stress the storage system much more than usual with today's systems in operation.

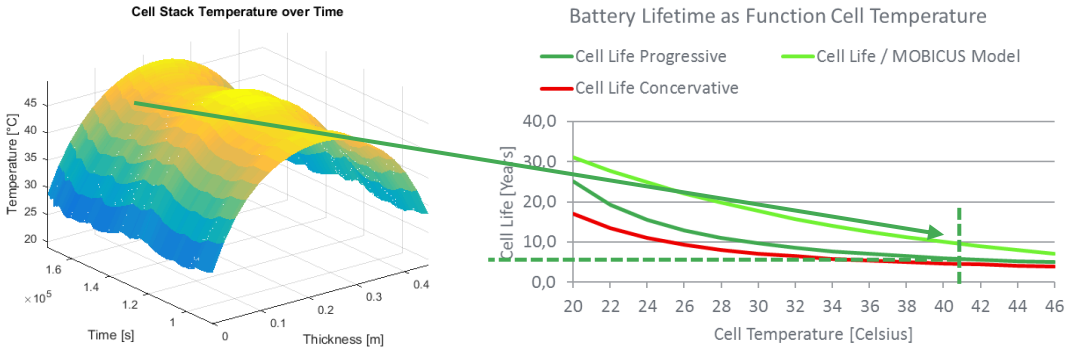

Fig. 9. Temperature inside a battery cell pack operating in continuous stabilisation mode [15], [16], [17].

V. Business Case

The challenge with energy storage business cases for frequency regulation is the fact that they need to replace existing generation technologies typically operating for many years and often fully depreciated. In many countries, steam power plants are providing this service today, and in some countries like Ireland, some steam units are already declared as must-run-systems for grid stability.

Economically, the fast reacting storage investment needs to be valued against the must-run cost of generators kept online for grid stability purposes. Steam power-plants today have boundary costs in the area of 40€/MWh when running partial load [12], while diesel generators have operating costs of > 100€/MWh [13], and gas-motors are around 60€/MWh. Most systems cannot produce less than 30% of the nominal power. Assuming in a micro-grid a 300kW gas-motor could be shut down because it's must-run capacity is not needed anymore for grid stability purpose, it would save around 160k€ operating costs per year (365days*24h*0.3MW*60€/MW).

To replace the must-run in this example, around 250kW of storage capacity is needed. At capital costs less than 1,000€/MW, break even can be achieved in less than 2 years with high power quality allowing a transition into energy production with much less CO_2 emissions.

Experience exists with battery and flywheel storage systems providing frequency stabilisation service mainly in the United States and Ireland [3]. The PJM grid has a relatively demanding load characteristic [14], but still less demanding than needed to replace the real inertia as described in this document.

Because of the extreme cyclic profile needed for short-term grid stabilization, aging of storage technology is the main challenge. The lifetime of batteries is mainly driven by temperature coming from constant load flows and inner resistance rather than from energy exchange. **Error! Reference source not found.** shows that already after a few hours in operation battery temperature becomes quite high peaking >40°C (>105F) and resulting in replacement patterns <5 years. Nevertheless, batteries lifetime is close to the payback period giving an advantage for flywheels systems lasting significantly longer.

Another advantage of flywheels vs. batteries is the increased specific power ramp rate of flywheels. Flywheels can provide full power in less than 50 ms, whereas batteries typically ramp within 200 to 500 ms. The specific ramp rate per installed MW for Stornetic flywheels is 1MW/0.05s=20MW/s, compared to 1MW/0.2= max 5MW/s for batteries.

Further reductions are possible with the development of more powerful flywheels systems offering system cost below 600k€/MW in the near future. Because of the extended lifetime, flywheel technology additionally offers higher return on investments as for example shown in [17].

VI. Outlook

This paper shows the capabilities of storage systems on short-term electricity grid stabilization. With more and more renewable energy systems in the grid replacing conventional turbines, this topic becomes more and more relevant. Independent from the storage technology chosen, fast response times are key if today's grid stability criteria should be maintained in the future. Today, research starts to focus on this topic, but needs to be intensified. The following areas especially require further research and development work:

- AC/DC grid inverter responsiveness requiring improved control loop design and faster data acquisition
- AC/DC grid inverter power ratings, requiring higher current and voltage levels in combination with fast switching times maybe using SiC semiconductor technologies
- Fast grid frequency detection with improved metrology algorithms and predictors.

VII. STORNETIC GMBH

Stornetic GmbH, a Germany based company, is building flywheel energy storage systems called DuraStor®. Stornetic is introducing hybrid energy storage solutions to service multiple grid services. The technology is characterised by its:

- Proven safety
- Durability, designed to operate continuously at 100% power
- Responsiveness to load changes
- Full power and capacity throughout the lifetime
- Efficiency
- Containerized system for quick installation or relocalization

REFERENCES

[1] RegioNETZ GmbH, Eschweiler, Germany, "QUIRINUS – Regionales Virtuelles Flächenkraftwerk für Versorgungs-sicherheit und Stromnetzstabilität," 2017. [Online]. Available: https://www.leitmarktagentur.nrw/lw_resource/datapool/_items/item_414/pdb_kvk-1-012.pdf

[2] PR Newswire, (2016) "EDF and STORNETIC Start Project on Advanced Smart Grids Storage Solutions" [Online]. Available: http://www.prnewswire.com/news-releases/edf-and-stornetic-start-project-on-advanced-smart-grids-storage-solutions-601626585.html

[3] EirGrid Group, (2015). DS3 Programme. [Online]. Available: http://www.eirgridgroup.com/how-the-grid-works/ds3-programme/

[4] C. Rehtanz, M. Greve, T. Noll, and J. Schwippe, "Bedarfund Erbringung von Momentanreserve 2030," German Energy Agency (DENA), Berlin, Germany, article no. 9142, 2016.

[5] Renewable Energy Federation, *The Integration of Renewable Energy Sources Into the Distribution Grid.* German, H. Loew. Berlin, Türk-Alman Enerji Inovasyon Forumu 2013 : Bunderverband Eneuerbare Energie e.V., 2013.

[6] International Organization for Standardization. *Reciprocating internal combustion engine driven alternating current generating sets - Part 5: Generating sets.* ISO 8528-5. 2013. ISO/TC 70 Internal combustion engines, Beijing, China

[7] ENTSO-E. (2014). Current practices in Europe on Emergency and Restoration: Drafting Team for the Network Code on Emergency and Resoration. [Online]. Available: https://www.entsoe.eu/Documents/Network%20codes%20documents/NC%20ER/140527_NC_ER_Current_practices_on_Emergency_and_Restoration.pdf

[8] K. Vu, R. Masiello, and R. Fioravanti, "Benefits of fast-response storage devices for system regulation in ISO markets," in *Proc. 2009 IEEE Power & Energy Society General Meeting*, pp. 1-8.

[9] M. Atanacio, R. Fioravanti, W. Katzenstein, and K. Vu, "Emission II study of advanced storage used for frequency regulation," Sandia National Laboratories, Albuquerque, NM, Sandia Negotiation 96362, 2012.

[10] E. Ørum, M. Kuivaniemi, M. Laasonen, A. I. Bruseth, E. A. Jansson, *et al.*, "Nordic report furture system inertia," European Network of Transmission System Operators for Electricity (ENTSO-E), Brussels, Belgium, 2013.

[11] Steinbeis, S. Rupp, "Modellierung von Analgen und Systemen, Teil 2 - Antriebe und Systeme," Baden-Wuerttemberg Cooperative State University, Center for Advanced Studies, Heilbronn, Germany, rep. no. TM20305.2, 2018.

[12] P. Graichen and M. M. Kleiner, "Erneuerbare vs. fossile Stromsysteme: ein Kostenvergleich," Agora Energiewende, Berlin, Germany, rep. no. 105/02-A-2017/DE, 2017.

[13] J. Irlenborn, "Simulationsprogramm zur Optimierung eines Inselnetzes mit Photovoltaikanlagen, Dieselgeneratoren und Batteriespeichern, " M.S. thesis, Univ. of Applied Sciences, Technical Univ. of Cologne, Cologne, Germany, Jul. 2014.

[14] PJM, (2017) PJM - Synchrophasor Technology. [Online] Available: http://www.pjm.com/markets-and-operations/ops-analysis/synchrophasor-technology.aspx

[15] NREL, K. Smith, et. al., "Predictive Models of Li-ion Battery Lifetime," in *Proc. IEEE Conf. on Reliability Sci. for Advanced Materials and Devices*, 2014, NREL/PR-5400-62813.

[16] Renault SAS, P. Gyan, "Battery aging tests and modelling under calendar, cacling and mixed conditions," in *Proc. IQPC 2nd Conf. Automive Battery Manage. Syst.*, 2016.

[17] R. vor dem Esche and R. Tudi, "Benefits of hybrid storage system with flywheels," Stornetic GmbH, Jülich, Germany, Oct. 2016. doi: 10.13140/RG.2.2.29623.93606

Hybrid Power Generation for Improved Fuel Efficiency and Performance

James Kersey, Michael Sprengel, Guy Babbitt, and Travis Johnson
Czero, Inc., Fort Collins, CO, USA

***Abstract*- This paper provides an overview of the analysis and design of a hybrid power system, including trade studies and analyses performed to define the system architecture and the performance and fuel economy benefits (predicted and test results) of the system. This system provides a new approach to deployable power generation to overcome key weaknesses of conventional diesel power generation. The hybrid system architecture developed improves lower load performance and fuel efficiency while maintaining similar fuel efficiencies to conventional diesel generators at higher loads. Test results have demonstrated fuel efficiency improvements of greater than 40% at low loads and greater than 60% at very low loads. Furthermore, the system architecture supports renewable energy inputs from sources such as solar and wind, which can further increase overall energy efficiency.**

***Keywords*- Hybrid power; energy efficiency; lithium iron phosphate**

I. Background and Motivation

Fuel cost is the largest single contributor to lifecycle cost for power generation in island power scenarios. This cost is amplified in remote areas where the cost to deliver the fuel can greatly increase the total (delivered) cost per gallon. In military wartime scenarios, fuel delivery also comes with a risk of loss of life. The Army Environmental Policy Institute estimated one casualty per 24 fuel convoys in FY2007. In that year alone, there were over 6,000 fuel convoys between Iraq and Afghanistan, equating to 250 casualties directly related to fuel delivery that year [1].

Conventional diesel generators have good fuel efficiency at higher loads. However, specific fuel consumption increases for loads less than 40%, as shown in Fig. 1. Because generator systems for island power are traditionally sized to meet peak power demand, small island power installations may operate significant amounts of time at loads less than 40%, resulting in increased fuel consumption. Even in larger installations, power reliability requirements for critical facilities may require significant spinning reserve, thus, further reducing average generator load and forcing engines to operate in areas of lower fuel efficiency. Running at low loads can also increase maintenance costs due to a condition called "wet stacking," where the diesel fuel does not fully combust and begins to accumulate in exhaust system components.

Renewable energy sources can provide a means to reduce fuel consumption. However, the potential variability of renewables can sometimes have a counterproductive effect, where the generator cannot be downsized yet the renewable energy sources further decrease the load on the generator. This can cause an unexpected increase in fuel consumption. Micro-grid systems and hybrid power generation systems that also incorporate energy storage can mitigate this issue [2]. Such systems available today are made up of multiple separate components rather than a single, self-contained system. While this may not be an issue for permanent installations, it limits the deployability of these systems for temporary installations.

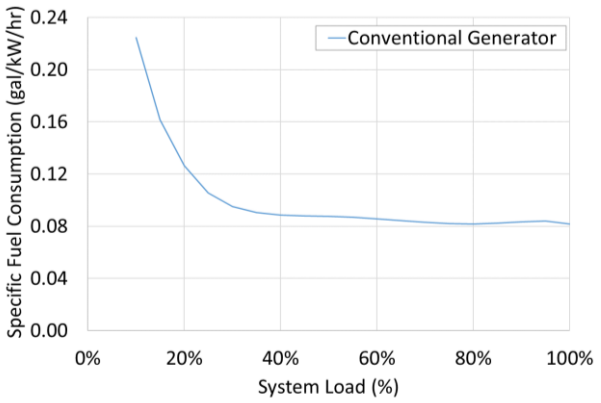

Fig. 1. Specific fuel consumption for a typical conventional diesel-powered generator.

Based on the above and additional commercial and technical factors, the key goals were to:

1. Significantly improve specific fuel consumption over conventional diesel generators at lower loads
2. Maintain efficiency similar to conventional diesel generators at higher loads
3. Maximize power output within a compact, deployable package
4. Support 50% single-step load changes
5. Support operation in high-temperature, desert environment, with minimal to no derating.

II. Analysis-Led Design Process

A systems engineering process incorporating analysis-led design and extensive modeling was used for this development. Key design tensions were identified early between power output, thermal management, and space constraints. Thermal management is critical to reliable operation in desert environments. However, maximizing power output within the

fixed space constraints requires making use of all available space. These competing requirements required careful analysis during the design process. The following summarizes the analysis performed and tools used in the development.

1. ANSYS Fluent was used for thermal and airflow modeling in two areas:
    a. Air flow and heat distribution throughout the engine compartment – through inlet louvers and radiators, over the engine and aftertreatment components, through the outlet louvers
    b. Air conditioning flow distribution and heat transfer within the energy storage system.
2. ANSYS Mechanical FEA was used for stress modeling of the mechanical structure to ensure the system met all applicable transportation requirements.
3. Dynamic modeling of liquid cooling circuits was performed in Simulink to inform cooling circuit layout and ensure sufficient coolant flow distribution.
4. SolidWorks was used for component and system design, component FEA, and preliminary mechanical structure FEA.

III. System Architecture Design and Analysis

System level design and analysis was performed prior to detailed engineering to define the architecture best suited to the system requirements. Four key design attributes were considered:

1. Constant vs. variable speed prime mover
2. Permanent magnet vs. synchronous generator
3. Number of engine-generator sets
4. Energy storage.

A. Constant vs. Variable Speed Prime Mover

Conventional generators run at fixed speed (i.e., 1800RPM for 60 Hz, 1500RPM for 50 Hz), regardless of the electrical demand. Operating at high speed and low load is not fuel efficient and can cause maintenance issues such as wet stacking, as previously discussed. A variable speed engine, however, can be slowed down in response to reduced electrical demand. This allows the engine to operate in regions with better fuel efficiency and with fewer maintenance issues. While Fig. 2 is for an automotive application, the same trends hold true in diesel power generation applications.

Low loads can be met in multiple ways. In the example below, 20HP can be achieved by the engine at high engine speed and low BMEP (and torque) (Point #1) or at low engine speed and high BMEP (Point #2). However, these points provide very different fuel efficiency. Specific fuel consumption for the high speed point (#1) is ~400g/kW/hr while the lower speed point (Point #2) is significantly reduced (~220g/kW/hr). Because conventional gensets operate at a fixed speed, they cannot benefit from the improved fuel efficiency at lower loads that can be obtained by running at a slower speed.

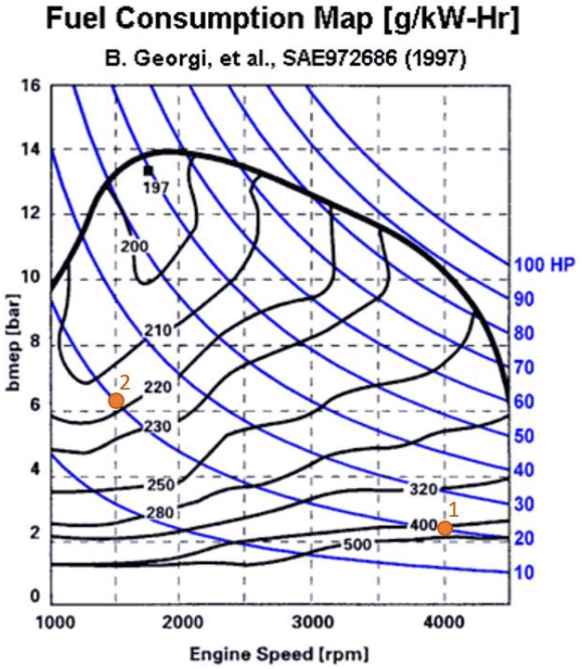

Fig. 2. Example diesel BSFC map [3].

Two key items must be addressed with variable speed operation. A generator connected to a variable speed engine will produce “wild” AC with varying voltage and frequency. This must be rectified and inverted to produce usable AC power (e.g. 480V, 60 Hz). In addition, variable speed engines generally suffer from poor transient response as the engine must be accelerated to meet an increased load demand [4]. One method for addressing this is through the addition of energy storage, which is discussed more in the energy storage section below.

B. Permanent Magnet vs. Synchronous Generator

Synchronous AC generators are the norm for power generation. Synchronous AC generators are readily available at relatively low cost, but efficiency can vary multiple percentage points as the load changes. They are best suited for constant speed operation. These machines are also typically air-cooled, which results in a relatively large footprint to ensure sufficient cooling airflow.

A Permanent Magnet Generator (PMG) uses permanent magnets rather than field coils to generate the magnetic field in the rotor. This allows for much stronger magnetic fields and allows PMGs to be more power dense than synchronous AC generators. PMGs are better suited for variable speed operation and can achieve higher, near constant efficiency throughout the load range. PMGs are also typically liquid-cooled, which

further reduces the footprint compared to synchronous machines. As such, PMGs combined with variable speed prime movers offer potential for improved efficiency in a smaller footprint than conventional generators, as shown in Fig. 3. However, PMGs are not as readily available as synchronous AC generators and are more expensive due to the use of rare earth magnets.

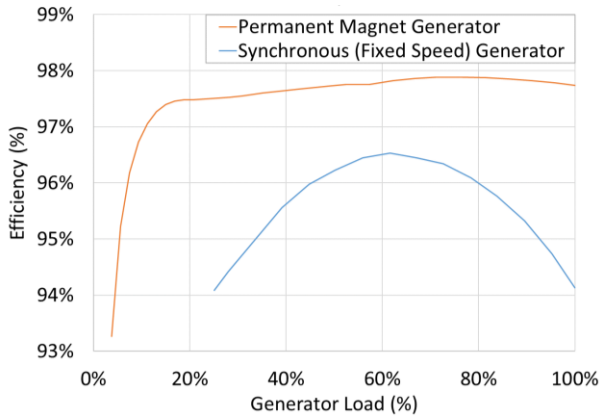

Fig. 3. Generator efficiency comparison.

C. Number of Engine-Generator Sets

Incorporating multiple smaller engine-generator sets can also reduce fuel consumption and maintenance issues at lower system loads. This is done by operating only as many engine-generators sets as needed to support the load, thus, putting a higher load on each individual engine. System architectures ranging from one to four engine-generator were considered for the hybrid power system.

Using multiple engine-generators reduces fuel consumption at lower system loads. For fixed-speed engine-generator sets, two to four sets produced near constant specific fuel consumption down to 20% load. Increasing the number of generator sets continued to improve specific fuel consumption below 20% load, as shown in Fig. 4.

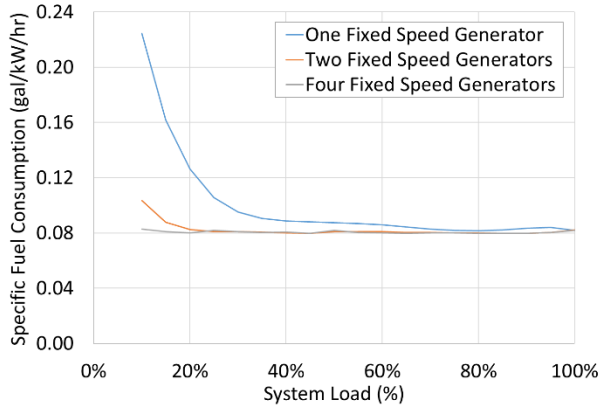

Fig. 4. Fuel consumption variation for multiple fixed speed generators.

With variable speed engine-generator sets, the fuel consumption at lower loads for a single unit is already greatly improved compared to a fixed-speed engine-generator (as discussed previously). As such, the relative improvement with increasing number of units is reduced. Two to four variable speed engine-generator sets offer similar fuel consumption across all loads, as shown below.

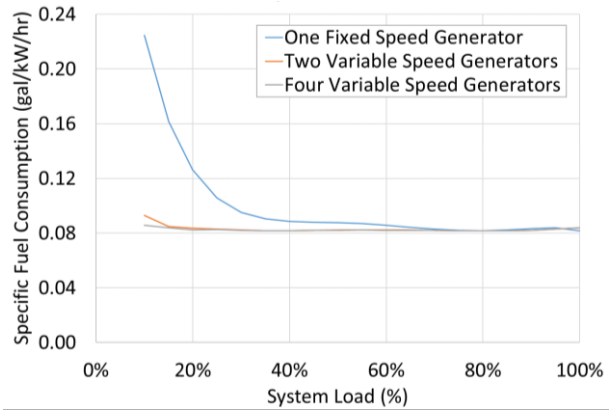

Fig. 5. Fuel consumption variation for multiple variable speed generators.

D. Energy Storage

Energy storage can be used in a wide variety of ways in a hybrid power system. Each use has different benefits, but also creates different requirements for the system that must be considered. In addition, there are a number of energy storage technologies available with different performance characteristics, and one technology may be better suited for a particular use than another. As such, several energy storage use cases were first identified and evaluated as part of the design. Then, different energy storage technologies were evaluated against these use cases.

1) Energy Storage Use Cases: The following use cases were identified and evaluated for energy storage in the system:

1. Silent hours operation and Uninterruptable Power Supply (UPS) operation (energy storage only, no engines used)
2. Load leveling/shifting
3. Peak shaving and step load change capability.

While silent hours or UPS operation may be desirable capabilities of the system, they do not directly provide any fuel savings. In addition, if energy storage is required for other capabilities (i.e., peak shaving), the system design and control must ensure that sufficient energy storage is reserved to meet these requirements. While any energy storage technology will allow for silent hours operation, more energy dense technologies are best suited for this requirement as they can provide longer run times for a given volume of energy storage.

Load leveling or shifting generally refers to charging the energy storage during periods of lighter load and discharging this energy during higher load periods to augment the generation. Generally, this is performed on a daily cycle. If the

load profile is known *a priori* and enough energy storage can be incorporated into the design, it is possible to use load leveling to enable downsizing the engine-generator(s), meeting peak demand with a combination of generation and energy storage. However, this results in a time limitation on peak power output. This approach was deemed unacceptable for deployable power generation as the load profile is not known ahead of time and may vary significantly across different applications.

Peak shaving can be implemented at several different timescales. At longer, daily timescales, peak shaving is similar to load leveling, but with reduced capacity, as shown in Fig. 6.

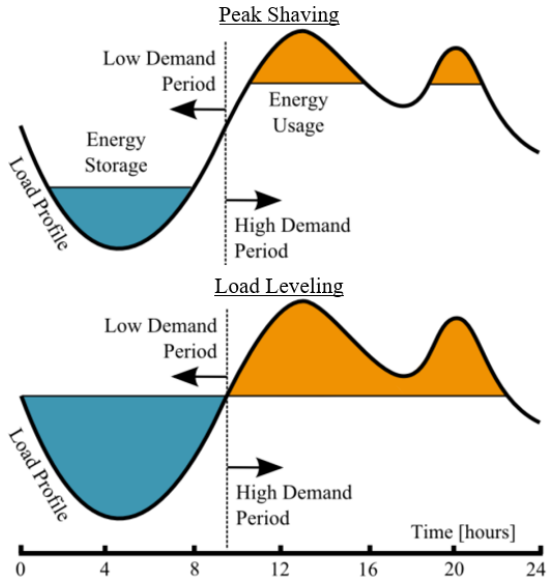

Fig. 6. Peak shaving vs. load leveling [5].

However, peak shaving can also be used on shorter timescales. Particularly when multiple engine-generator sets are employed, energy storage can be used for peak shaving to meet short-term load demand, without the need to start an additional engine-generator. This can improve fuel economy by keeping generators at higher load and also reduces wear and tear and associated maintenance by reducing the number of engine starts.

The key performance issue noted when using variable speed engines for power generation is poor load response [4]. This is due to the time and engine torque required to accelerate the engine to a higher speed to support the increased load. Load response can also be an issue if multiple engine-generator sets are used due to the time required to bring the next unit online. As such, architectures with variable speed engines and/or with multiple engine-generator sets require a certain amount of stored energy that can be supplied at sufficient power levels in order to meet the system step load requirements. The time required for an engine to increase speed is on the order of 1 to 10 seconds, while the time required to bring an additional unit online may be on the order of 30 to 120 seconds.

2) Energy Storage Chemistries/Technologies: Because of the benefits of running variable speed and with multiple units described previously, peak shaving and step load response became key use cases for the energy storage. As such, preference was given to chemistries with high power density so the power output required for these cases could be provided in a compact, space efficient package. This quickly eliminated Lead Acid and other low power density chemistries, such as Sodium Nickel Chloride.

Ultracapacitors were investigated for their high discharge rates, however, the time scale required for the power discharge to meet system requirements (e.g., 30 to 120 seconds) would require a significant number of parallel strings of ultracapacitors to provide the required energy due to their extremely low energy density. This was deemed to not be a cost-effective approach in this application.

As such, the focus quickly narrowed to Lithium chemistries. Three chemistries were investigated for their performance characteristics and availability from reputable suppliers: Lithium Titanate (LTO), Lithium Nickel Manganese Cobalt Oxide (NMC), and Lithium Iron Phosphate (LiFePO4). All three chemistries can meet the power and energy requirements for the key use cases identified in a compact package.

LTO chemistry offers the highest peak discharge rates, which initially made it a very attractive option. However, LTO has a high cost premium compared to the other two options. Lithium NMC and LiFePO4 have similar performance characteristics at similar costs. LiFePO4 was selected for this application based on commercial factors.

E. Overall System Architecture

A system architecture was finalized based on the above analysis. Variable speed architectures using PMGs provide significant efficiency improvements at lower load and also offer increased power density compared to designs incorporating synchronous AC generators. This was a key goal for the project.

The architecture uses two variable speed engine-generator units as this provides the same fuel efficiency benefits as architectures with more units and results in a simpler system and reduced capital cost.

A simplified, high-level diagram of the selected system architecture is shown below. The output from the two generators is rectified; and then joined on a DC bus with the energy storage before inverting to AC output.

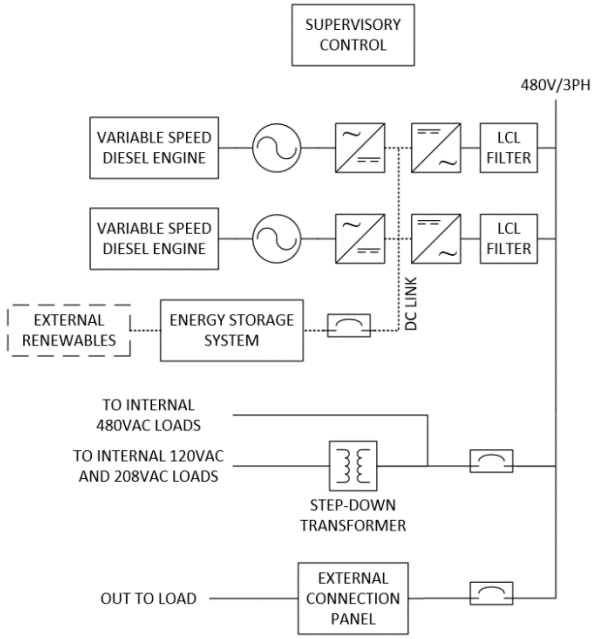

Fig. 7. Simplified high-level system architecture.

III. Electrical Design

The electrical system design was divided into two areas:

1. Power subsystem, including generator, energy storage, and power electronics
2. Support subsystems, including power distribution to internal loads and supervisory control.

Design of the support subsystems will not be covered here.

The power subsystem is at the core of the design. The system architecture shown previously was further developed on collaboration with key vendors and partners on specific hardware capabilities.

Transformerless inversion to 480VAC requires a DC voltage of 725V or higher. However, the inverters selected have a maximum DC voltage limit of 800V. This would result in a range of only 75V for the energy storage to operate if placed directly on the DC bus. It was determined that this would drastically reduce the usable energy from the batteries.

As such, a DC/DC converter was added to extract as much usable energy from the energy storage as possible. This also allows the battery voltage to be lower than the DC bus and allows for a larger change in voltage in the batteries, as the DC/DC converter will boost the voltage to the desired voltage of 750V. The DC/DC converter has a high efficiency (~99%), which introduces only minimal losses for power flow into and out of the energy storage.

For the energy storage system, precertified, factory tested battery modules were used rather than building a custom pack from the cell level. This greatly reduced the development required while ensuring a robust, safe design. The design team partnered with CIE Solutions for proprietary packaging and energy storage system integration to suit the design. The system can incorporate 110kWh to 220 kWh of usable energy storage for different applications.

The system uses a proprietary supervisory control system. Off-the-shelf hardware was chosen on capabilities and system inputs and outputs required. This was packaged into a custom enclosure for improved maintenance and quality control. This approach offers reduced cost compared to a custom hardware solution. Software algorithms were developed for monitoring and controlling the system. These can be broken into categories:

1. Monitoring and safety
2. System start-up and shutdown
3. Power delivery and management.

Algorithms developed to date use pre-defined logic, not learning or adaptive algorithms. Further development to implement adaptive algorithms is expected to provide even further versatility and fuel economy benefits over the existing implementation.

The final electrical architecture is shown in Fig. 8. This system is expected to be able to provide 800kW/1000KVA power output from a compact, deployable package.

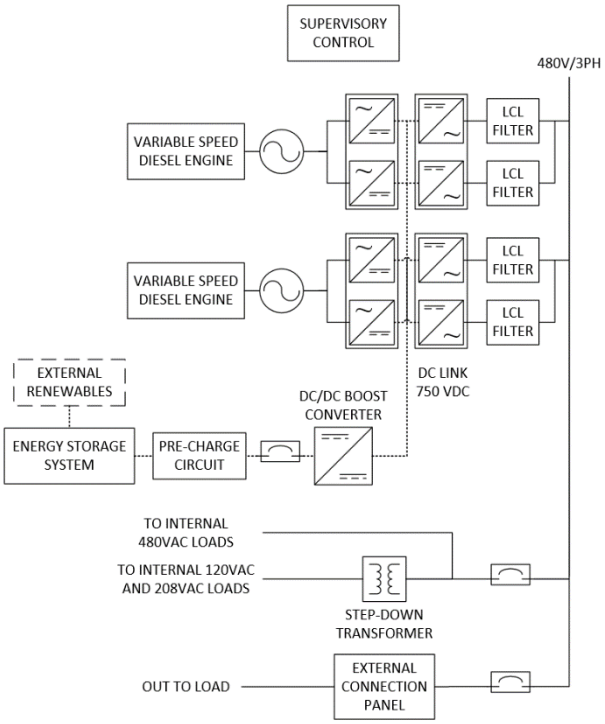

Fig. 8. Final high-level system architecture.

IV. Mechanical Design

The mechanical design was divided into three interrelated areas:

1. Power Module
2. Electrical packaging
3. Overall mechanical structure.

Design in these areas occurred in parallel and in close collaboration with multiple design iteration loops to meet the demanding packaging constraints of the system. The overall mechanical structure design and analysis will not be covered in this paper.

A. Power Module Design

The Power Module consists of:

1. One variable speed engine-generator unit
2. One Energy Storage Module, which contains half of the total system energy storage
3. Related subsystems (e.g., cooling).

There are two Power Modules in the current design, though the architecture is extensible from one to many Power Modules.

The Power Module was designed with a Tier 4 Final engine to provide compliance with latest emissions standards. Compact packaging was essential to meet the space constraints of the design, but the design still ensures access to key maintenance items. The Energy Storage Module is a sealed, temperature-controlled environment designed to be factory-serviced to prevent access and maintenance by untrained personnel.

There are multiple cooling subsystems in the Power Module. The engine and related components are cooled with an engine driven water pump, as with conventional engine-generators. The engine radiator and charge air cooler are cooled with an engine driven fan. Liquid-cooled electrical components are cooled with an electrically driven pump and separate radiator cooled with VFD controlled fans to limit parasitic loads. The energy storage is air-cooled with a purpose-built integrated air conditioning unit.

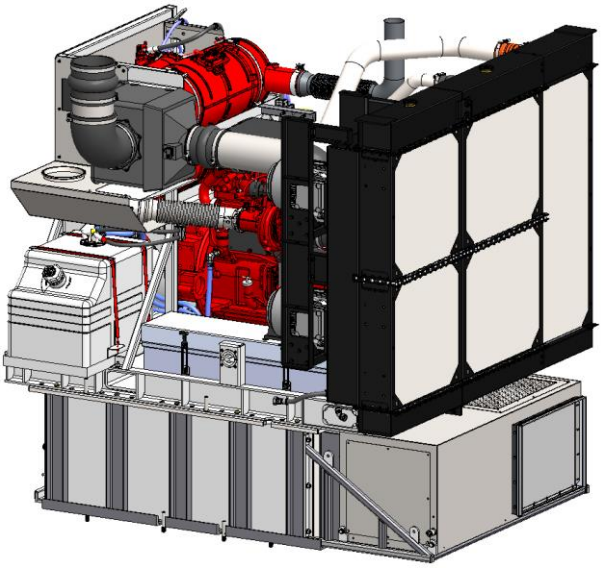

Fig. 9a. Left view of Power Module and cooling system.

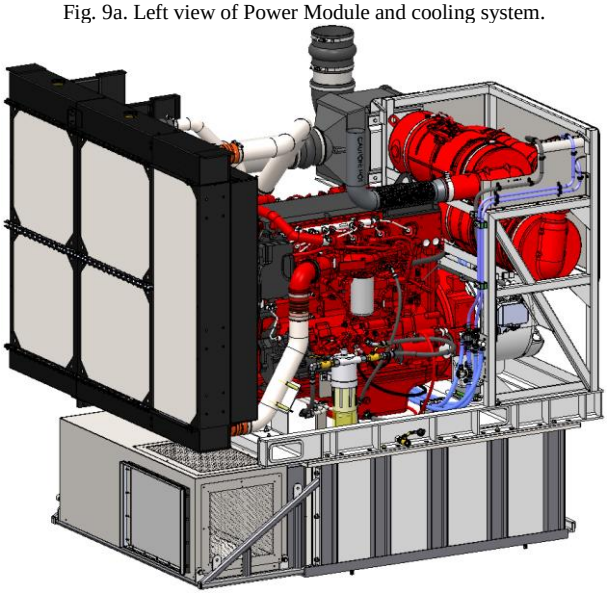

Fig. 9b. Right view of Power Module and cooling systems.

CFD was performed using ANSYS Fluent to study the airflow over radiators and through the engine compartment area to confirm sufficient cooling given the tight space constraints and high ambient operating temperatures. Initial results were used to influence mechanical structure design to optimize airflow. Fig.s 10a and 10b show air temperature in the engine compartment. Some hotspots can be seen, particularly on the Diesel Particulate Filter behind the engine, but all temperatures are within component specifications.

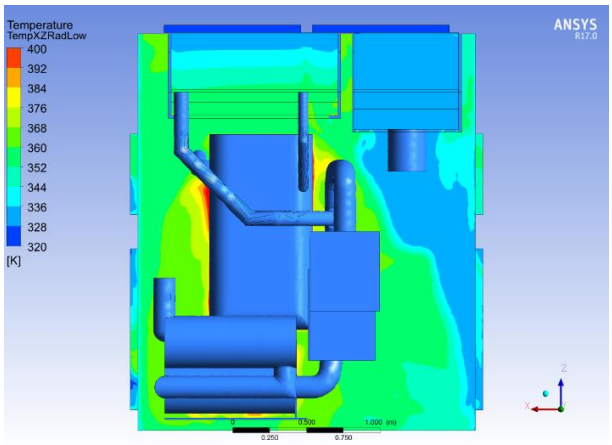

Fig. 10a. CFD results from engine compartment (top view).

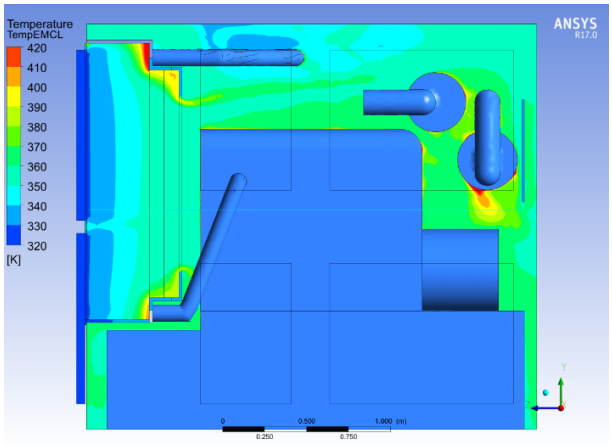

Fig. 10b. CFD results from engine compartment (side view).

CFD was also performed on the cooling airflow within the Energy Storage Module. The compact packaging required introduced a risk of poor airflow distribution and regions with insufficient cooling. Compact plenums on both sides of the energy storage were designed to create even pressure distribution to help provide relatively uniform flow throughout the system. Fig. 11 shows air velocities through the cooling passages. The flow is not perfectly uniform but is sufficient to prevent any localized hot spots.

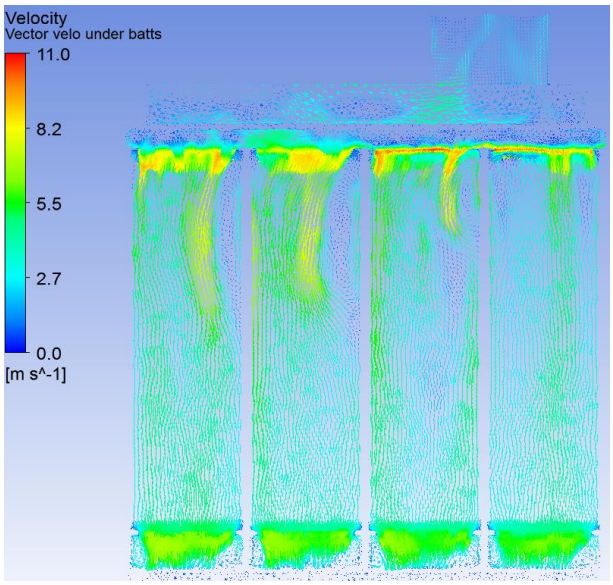

Fig. 11. CFD results from Energy Storage Module.

B. Electrical Packaging

The hybrid system architecture results in additional electrical equipment beyond that found in conventional generator units. This, coupled with the goal of maximizing power density while still achieving maintainability and power resiliency, created challenges with respect to the packaging of the electrical equipment as very limited space was available for this equipment.

This electrical section is divided into two areas for power electronics and for control equipment and support subsystems. Packaging challenges for the power electronics were primarily due to the size of the equipment, large power cables with limited bend radii, and hoses required for liquid.

The key challenge for control equipment and support subsystems was accessibility for maintenance given the limited space available. It was important to keep all breakers readily accessible while also allowing for access to other equipment that may need to be replaced over time. A hinged panel system was designed that allows easy access to breakers will still providing access to equipment packaged behind the breakers. The HMI is housed in this area, but is accessed from outside the structure via a separate panel.

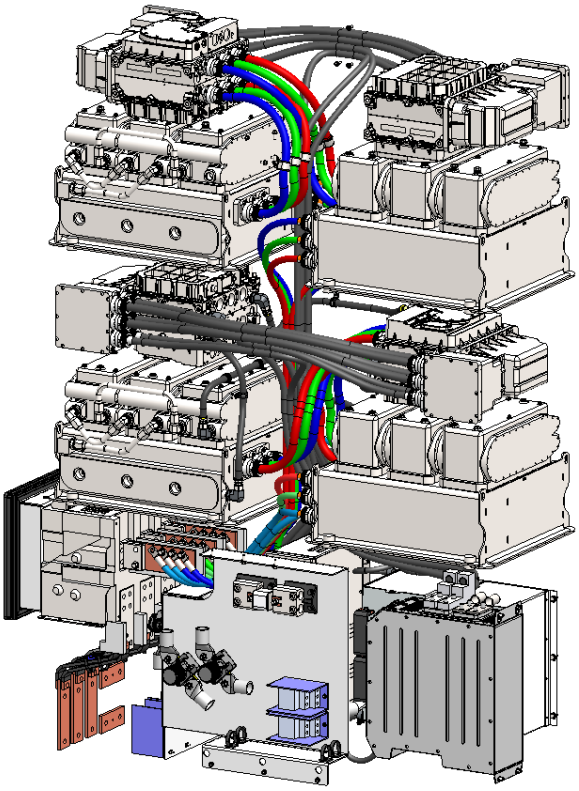

Fig. 12. Compact packaging of electrical equipment.

V. Test Results

A partial system with one engine-generator was built for testing to prove the concepts and benefits of the design. The Test System architecture is shown in Fig. 13.

The focus, to date, has been on functional and preliminary performance testing. The test results below demonstrate variable speed operation with power output from 5kW to over 400kW. The results also demonstrate the energy storage providing step load response while the variable speed engine responds on a slower timescale.

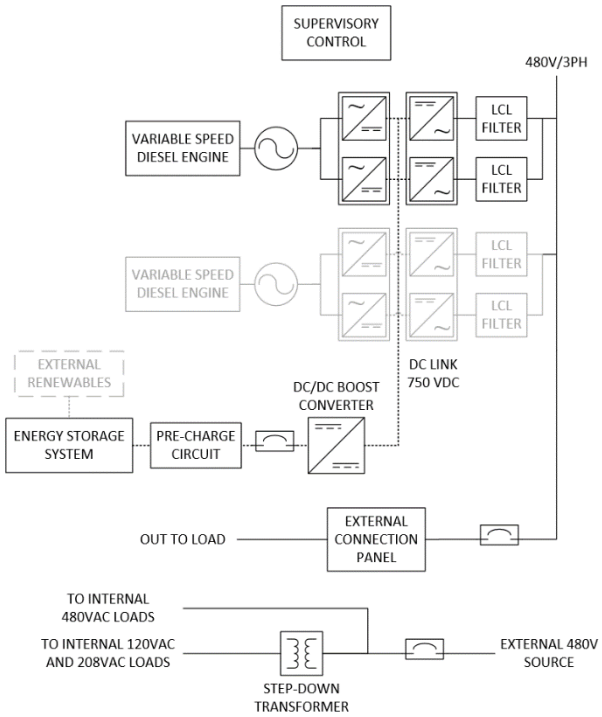

Fig. 13. Test system architecture.

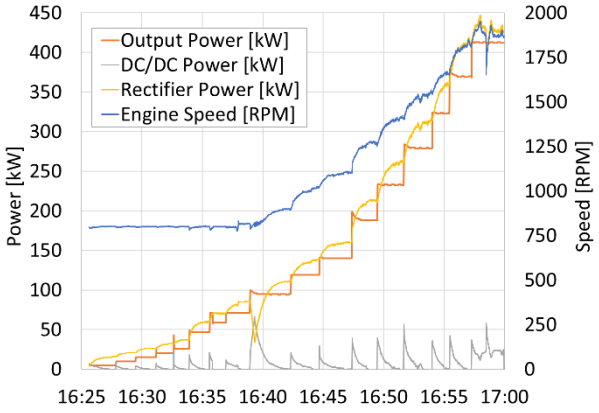

Fig. 14. Test results from power ramp up to full load.

Fuel consumption results from testing, shown in Fig. 15 (in green), exceed the efficiency estimated during preliminary analyses. This is due to three primary factors:

1. Lower engine BSFC than originally estimated
2. Lower parasitic internal loads than originally estimated
3. Higher PMG efficiency than originally estimated

Expected behavior for the full system has been extrapolated and is shown with the dashed green line. At very low loads, the system will run off battery power only to maintain system efficiency. Test results show greater than 60% reduction in fuel consumption at 100 kW and greater than 40% reduction in fuel consumption at 200 kW compared to a standard diesel genset. This reduction is expected to provide large fuel cost savings for generators that run a significant

number of hours, particularly in remote locations where total delivered fuel cost may be substantially increased.

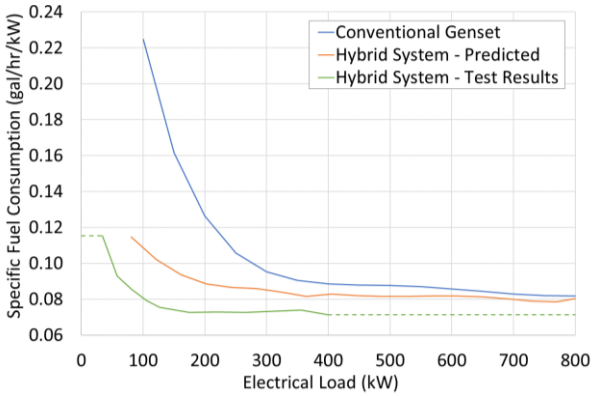

Fig. 15. Fuel consumption test results.

Step load testing is ongoing and has demonstrated up to 35% single-step changes. Software changes have been identified to enable the system to meet the 50% single-step target. No hardware changes are expected to achieve this.

VI. Conclusions

Several project goals were identified at the start of development. A number of these have been achieved and proven during testing, specifically:

- Significant reductions in fuel consumption at lower loads compared to conventional diesel generators
- Fuel consumption at higher loads that is better than conventional diesel generators.

This performance will result in significant reductions in fuel used and significant associated cost savings. Two key areas have not yet been proven. Step load performance does not currently meet the 50% single step target, but is expected to by the completion of the current testing program. In addition, high ambient temperature performance has not yet been confirmed.

References

[1] D. S. Eady, S. B. Siegel, S. Bell, and S. H. Dicke, "Sustain the mission project: Casualty factors for fuel and water resupply convoys," National Defense Center for Energy and Environment, Johnstown, PA, September 2009. [Online]. Available: http://www.dtic.mil/dtic/tr/fulltext/u2/b356341.pdf

[2] P. Journeay-Kaler, and L. Mofor, "Pacific lighthouses: Hybrid power systems," *International Renewable Energy Agency (IRENA)*, August 2013. [Online]. Available: https://www.irena.org/DocumentDownloads/Publications/Hybrid-power-systems.pdf

[3] B. Georgi, S. Hunkert, J. Liang, and M. Willmann, "Realizing future trends in diesel engine development," in *Proc. 1997 SAE Future Transportation Technol. Conf. and Expo.*, paper no. 972686, pp. 67-79.

[4] P. A. Stott, "Renewable variable speed hybrid system," Ph.D. dissertation, Dept. Eng., Univ. Edinburgh, Scotland, UK, 2010.

[5] S. Sabihuddin, A. E. Kiprakis, and M. Mueller, "A numerical and graphical review of energy storage technologies," *Energies*, vol. 8, no. 1, pp. 172-216, Jan. 2015.

An Economic Assessment of Portland General Electric's Salem Smart Power Center Energy Storage System

Patrick Balducci[1], Jan Alam[1], Vilayanur Viswanathan[1], Di Wu[1], Alasdair Crawford[1], Kendall Mongird[1], Mark Weimar[1], Abhishek Somani[1] and Kevin Whitener[2]

[1]*Pacific Northwest National Laboratory, Richland, Washington, USA*
[2]*Portland General Electric, Portland, Oregon, USA*

***Abstract*- This paper presents an assessment of the economic potential of a 5 MW/1.25 MWh Energy Storage System (ESS) installed at the Salem Smart Power Center, a smart-grid technology demonstration facility owned and operated by Portland General Electric in Salem, Oregon. The ESS and the grid conditions in which it operates were modeled using Pacific Northwest National Laboratory's Battery Storage Evaluation Tool to explore tradeoffs between services and to develop optimal control strategies. The analysis resulted in a number of lessons that provide crucial insights into the practical application of ESS.**

***Keywords*- Energy storage, energy storage valuation, valuation methodology, PGE, PNNL, Salem Smart Power Center**

I. Introduction

The proper assessment of potential economic benefits of energy storage systems (ESS) is essential for utilities interested in installing new ESS or investing in the expansion of ESS service capabilities. With an adequate analysis of economic benefits, an ESS project developer would be better equipped to understand how a given ESS would perform against a set of economic opportunities, as well as whether modifications are necessary in design parameters and control strategies to improve returns on investment (ROIs).

The industry values learnings achieved by analyzing deployed systems, as they provide practical and useful lessons. Particularly at this growing phase of the ESS industry when utilities are expanding investment in ESS technologies, learnings achieved from an existing system are particularly valuable. This was the motivation for this paper, which presents the outcome and lessons from an economic benefit assessment of a utility-scale 5 MW/1.25 MWh ESS installed at Portland General Electric's (PGE's) Salem Smart Power Center (SSPC) in Salem, Oregon.

II. The Salem Smart Power Center ESS

The SSPC project, a test and demonstration facility near PGE's Oxford substation in Salem, Oregon, was developed at a cost of around $20M. It was jointly funded by the U.S. Department of Energy (DOE) and PGE, with its principal technology partners EnerDel, Eaton, and Alstom. The facility contains a 5 MW/1.25 MWh lithium ion ESS composed of 20 EnerDel-manufactured SP90-590 modular energy storage racks organized into 5 blocks, with each block containing 4 racks [1]. Each of the racks consist of 18 small drawer-type units, each containing 4 battery modules for a total of 1,440 modules in the system. Each battery module contains 12 series-connected lithium ion cells, which lead to a total of 48 series-connected cells in a drawer unit. Fig. 1 shows the organization of the cells, modules, and racks in a battery block. The system contains 20 inverter banks organized into 5 blocks. Grid interconnection is through the 12-kV side of PGE's Oxford substation.

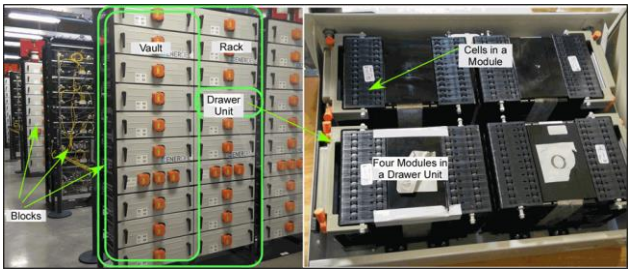

Fig. 1. Salem Smart Power Center ESS.

III. ESS Valuation Methodologies and Cost Estimates

Valuation methodologies and assumptions play an important role in the estimated benefits. Brief descriptions of valuation methodologies, data, and assumptions used for estimation of SSPC use case benefits are provided below. A use case is an application or services offered by an energy storage system (ESS) that provides value to the grid.

A. Energy Arbitrage

Arbitrage is the practice of taking advantage of differences between two market prices. The economic reward is the price differential between buying and selling electrical energy, minus the cost of round-trip efficiency (RTE) losses during the full charging/discharging cycle. The battery system we studied could provide up to approximately 1.25 MWh of energy to bid into the wholesale energy market. Hourly Mid-Columbia Energy Price Index data were obtained from Powerdex for the 2011-2016 time period. Prices during those 6 years ranged from a high of over $220/MWh to a low of $-3.14.

B. Western Energy Imbalance Market

PGE will be joining the Western Energy Imbalance Market (EIM) operated by the California Independent System Operator (CAISO) in 2017 and could use the SSPC as an asset while participating in the EIM. This use case functions very similarly to arbitrage inasmuch as it offers PGE an opportunity to participate in the wholesale pricing of energy. To evaluate the benefit of using the SSPC in the EIM, Pacific Northwest National Laboratory (PNNL) acquired 5- and 15-minute data for the PacifiCorp West load aggregation point nearest the PGE service territory (ELAP_PACW_APND). The data were obtained from the CAISO OASIS system for 2015 to 2016.

C. Demand-Response Benefit

PGE offers a number of demand-response programs in which the SSPC ESS could participate to obtain economic benefits of up to $100/kW-year. In one case, we modeled the benefits using the assumption that PGE can predict demand response events at least 1 hour in advance; in the alternative case, we assumed the ESS must be held at full power awaiting a call between 2 and 6 p.m. during certain months when demand-response events may occur. With a total energy capacity of 1.25 MWh and 300 kWh reserved for primary frequency reserve, 950 kWh remain for demand response. With a 3-hour target window, total demand-response capacity is limited to 317 kW. In 2016, there were eight relevant demand response events ranging from 1 to 3 hours in duration, covering a total of 19 hours.

D. Regulation Up/Down

SSPC, with its ± 5 MW of ESS power capacity, could provide regulation services to the grid. To estimate SSPC regulation up/down benefits, we obtained the regulation prices from a Northwest Power Pool (NWPP) previous PNNL project's production cost analysis [2]. The amount of regulation services possible each hour is limited by both the power and energy capacities of the SSPC. Such constraints have been modeled in the optimal scheduling process.

E. Primary Frequency Response

The SSPC is part of PGE's operational plan for responding to Western Electricity Coordinating Council (WECC)-wide frequency-response events. The SSPC control strategy is designed to generate a 300-kWh response. Based on the set points (high and low) established by a frequency-regulation screen, the SSPC responded 181 times over 13 months, for an average of 13.9 times per month. During roughly 10 months in 2016, PGE registered 18 frequency response events requiring SSPC responses, for an average of 1.8 events per month. Of these events, the SSPC responded 15 times. Thus, the screen governing the SSPC response successfully responded to a frequency-response event 83.3 percent of the time, but triggered nearly eight times as many responses as were required by NERC.

Benefit estimation is performed by taking the weighted average of two recent purchases of primary frequency response services. CAISO recently purchased primary frequency response capabilities from Seattle City Light (SCL) and the Bonneville Power Administration (BPA). The SCL contract transfers 15 MW of frequency regulation to SCL at a contract price of $1.22M, or $81/kW-year [3]. The BPA contract transfers 50 MW/0.1 HZ of frequency regulation to BPA at a contract price of $2.22M, or $44.40 per kW-year [4]. The weighted average of these two values ($52.8/kW-year) was used in the base case, while the SCL value was used as an alternative measure.

We calculated base-case benefits assuming that the frequency-response events cannot be predicted, and therefore, 300 kWh of energy must be held in reserve at all times. We considered an alternative case in which we assumed the events *can* be predicted, thus eliminating the need to hold energy in reserve.

F. Spin/Non-Spin Reserve

The SSPC ESS has the capacity to provide both spinning and non-spinning reserve to balance load and generation during contingencies. To estimate the value of these services, spin and non-spin reserve prices were obtained from the NWPP production cost analysis performed at PNNL [2]. In addition to power capacity limits, these services are also constrained by energy capacity due to the requirement to provide energy at the required power for at least an hour.

G. Volt/VAR and Conservation Voltage Reduction

The Volt Ampere Reactive (VAR) capacity of the SSPC ESS inverter provides local VAR supply and conservation voltage reduction (CVR) benefits. Providing VAR locally from ESS inverters relieves the system of the burden of transmitting VARs from the upstream network. This reduction in burden could be considered a release of the upstream system capacity, which can be monetized based on the utility's cost of capacity. Synching VAR by the ESS inverter can reduce operating voltage and reduce energy consumption that could translate into an economic benefit in terms of the prevailing electricity price.

To estimate the benefit of local VAR support, a model alternating current (AC) system upstream of the PGE Oxford substation was considered in order to achieve a reduction in its VAR supply burden by an amount equal to the VAR supplied by SSPC inverters. This reduction in VAR would then be translated into an equivalent active power capacity using AC system capability curves defined by the relationship among active, reactive, and apparent power capacities, and monetized using PGE's $120/kW-year capacity price [5]. CVR benefit was estimated by monetizing the reductions in hourly active power flow from the Oxford substation using 2016 Mid-Columbia electricity prices. Tests were conducted at the Oxford substation by regulator tapping and inverter control to determine the CVR factor (0.86) for benefit assessment.

H. Valuation Modeling Approach

PNNL's Battery Storage Evaluation Tool (BSET) was used to perform an hourly look-ahead optimization to determine the ESS power schedules with tradeoffs among different services while taking all operational limits into consideration. We then used the simulation to determine the actual battery operation and estimate the co-optimized value of the modeled services. The detailed modeling and formulation of this method can be found in Wu et al. (2015) [6]. As services are provided, the revenue or value derived from the service is logged, as is the time the ESS is engaged in providing each service. The formulation includes energy costs incurred during charging and RTE losses. We assessed the economic benefit for both individual services and bundle services.

I. Estimating ESS Costs and Revenue Requirements

The SSPC was originally conceived as a research and development (R&D) project that would advance PGE's capacity around integration of ESS, smart-grid technologies, and micro-grid resources. Due to the R&D nature of the project and the nascent stage of development of grid-scale lithium ion batteries, system costs reached $20.4M. Considering learning and reductions in battery and component costs, PGE estimates that the SSPC today would cost roughly $10.1M.

PNNL has also considered alternative cost scenarios based on data presented in Lahiri (2017) [7]. These costs are based on deals being monitored by DNV GL[1] and reported in Lahiri (2017), and are stratified somewhat differently from those presented by PGE. PNNL took the mid-point of values presented in Lahiri (2017), applied them to a 20-year battery installation, and estimated the present-value costs of the existing SSPC at $5.4M if built today [7]. Costs were also estimated for 5 MW of power capacity with 5, 10, 15, and 20 MWh of energy capacity at $8.1, $11.8, $15.4, and $19.0M, respectively.

For energy storage to be cost competitive, its benefits must not only exceed its costs, but also all associated revenue requirements, including taxes, debt, and returns to investors. A detailed pro forma for the ESS was prepared to estimate revenue requirements. Major parameters used in the pro forma are presented in Table I.

Based on the combination of costs and assumptions outlined, we determined revenue requirements that accounted for full system costs, including all taxes, debt, and returns to investors and present them in Table II.

TABLE I.
FINANCIAL ANALYSIS PARAMETERS

Parameter	Assumptions
Analysis Time Horizon	20 years
Battery Operating Lifetime	10 years
Federal Income Tax Rate	35%
State and Local Income Tax Rate	7.69%
After-Tax Weighted Cost of Capital	6.32%
Long-Term Rate of Inflation	2.25%
Property Tax Rate	1.4%
Discount Rate	6.32%

TABLE II.
ESS REVENUE REQUIREMENTS

Scenario	Revenue Requirements (Millions)
PGE Actual Expenditures	$28.4
PGE Estimate if SSPC Built Today	14.6
Lahiri 2017 for 5 MW/1.25 MWh ESS	7.9
Lahiri 2017 for 5 MW/5 MWh ESS	11.5
Lahiri 2017 for 5 MW/10 MWh ESS	16.4
Lahiri 2017 for 5 MW/15 MWh ESS	21.3
Lahiri 2017 for 5 MW/20 MWh ESS	26.1

IV. ECONOMIC BENEFITS

An analysis of SSPC historical operation, costs and benefit scenarios suggests that this asset is currently underutilized. With it only using 1.9% of available hours in a month exclusively for primary frequency response, a good deal of value remains unrealized. Though the SSPC

[1] https://www.dnvgl.com/

as originally designed and built is not currently generating positive ROIs, the analysis below demonstrates that if the system were built today at current prices and at an optimally scaled size, benefits would exceed revenue requirements.

A. SSPC Benefits and Revenue Requirements

The first step in estimating the benefits associated with SSPC operation was to evaluate the benefits of each service individually. Table III and Fig. 2 present the results of these individual assessments. The results demonstrate that if the battery were used exclusively for each service, the value of these services could exceed $7.5M in present-value (PV) terms over 20 years. However, the capacity of the ESS to generate value is constrained by its operating characteristics and its ability to provide energy when needed for each application. That is, some services are in conflict and cannot be provided simultaneously.

There is competition for the energy in the SSPC, on both an intertemporal and an application basis. Knowledge of the battery's characteristics and the landscape of economic opportunities matters in terms of optimizing value. To resolve these conflicts, the research team employed BSET. When the model co-optimizes the benefits under the base case, limiting the value to what is technically achievable by the SSPC, economic value declines to $5.9M over a 20-year period in PV terms. Note that in the individual assessments, charging costs are embedded in each value. In the co-optimized case, they are reported separately.

The base case scenario, for which the values are reported in Table III and presented in Fig. 2, employs the following assumptions:

- Arbitrage is run for 2016 using Mid-Columbia and EIM prices, with 300 kWh of energy set aside for primary frequency-response events.
- 317 kW of demand response is provided and the events can be predicted.
- 5 MW of primary frequency response, with 300 kWh of energy set aside at all times for primary frequency response events.
- All ancillary services co-optimized with 300 kWh of energy set aside for primary frequency-response events.
- After all other service-based commitments have been met, the remaining capacity of the SSPC is used to provide Volt-VAR and CVR support, as needed.

The achievable value available to the base case, when co-optimized, is reduced significantly because the energy-to-power ratio of the SSPC is low at 0.25, and roughly one-fourth of its energy must be held in reserve for primary frequency-response at all times. The energy must be held in reserve because primary frequency-response events cannot be predicted. The lack of available energy limits the ability of the SSPC to generate value in more energy-intensive applications such as the ancillary services (e.g., regulation up/down, spin and non-spin reserves).

TABLE III.
INDIVIDUAL VS. CO-OPTIMIZED BENEFITS

Service	Individual	Co-Optimized
Charging Costs		$(449,115)
Arbitrage (Mid-Columbia)	$75,590	$746,299
EIM	$373,778	
Demand Response	$540,259	$428,155
Regulation Up	$727,250	$374,609
Regulation Down	$908,795	$656,706
Primary Frequency Response	$2,971,424	$3,568,826
Spin Reserve	$831,079	$100,622
Non-Spin Reserve	$720,221	$46,124
Volt-VAR/CVR	$393,619	$393,619
Total	$7,542,017	$5,865,846

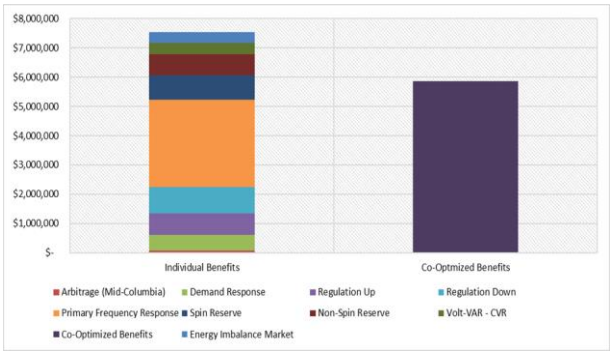

Fig. 2. Individual benefits estimates by use case versus co-optimized benefits.

SSPC benefits for the base case ($5.9M) fall far short of the revenue requirements for the SSPC as originally designed and built ($28.4M) (Fig. 3). It is important to understand, however, that the SSPC was developed as an R&D facility to advance PGE's and the region's understanding of smart-grid technologies, energy storage, distributed energy, and micro-grid systems.

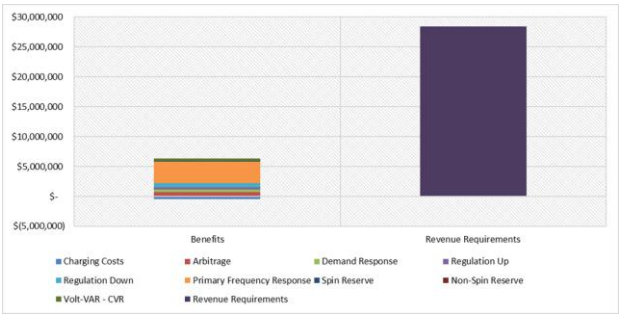

Fig. 3. Base-case benefits and revenue requirements for SSPC.

Table IV and Fig. 4 present the results of a scenario that evaluates costs based on current prices, estimated using Lahiri (2017) [7]. The primary benefit is the one currently being realized by PGE—primary frequency response—which PNNL values at $3.6M over 20 years. However, all other use cases or services yielded an additional $2.3M in currently unrealized benefits over 20 years. Of those services, arbitrage when also bidding into the Western EIM held the most revenue potential at $0.7M, followed by regulation down ($0.7M), demand response ($0.4M), and Volt-VAR/CVR ($0.4M).

TABLE IV
CO-OPTIMIZED 20-YEAR BENEFITS VS. REVENUE REQUIREMENTS (BASE CASE-LAHIRI 2017 COSTS)

Service	Individual	Revenue Requirements
Charging Costs	$(449,115)	
Arbitrage (Mid-Columbia)	$746,299	
EIM		
Demand Response	$428,155	
Regulation Up	$374,609	
Regulation Down	$656,706	
Primary Frequency Response	$3,568,826	
Spin Reserve	$100,622	
Non-Spin Reserve	$46,124	
Volt-VAR / CVR	$393,619	
Total	$5,865,846	$7,893,775

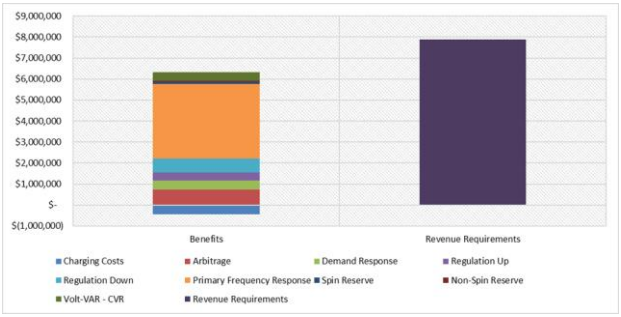

Fig. 4. Benefits and revenue requirements, using current-day pricing, for a 5 MW/1.25 MWh ESS.

The SSPC was originally meant to be operated as a component of a larger micro-grid system, with attention placed on engineering rather than economic goals. Thus, the SSPC holds a small energy capacity (1.25 MWh) in relation to its power capacity (5 MW). With an energy-to-power ratio of only 0.25, it is not well suited to engage in most energy-intensive applications such as arbitrage or ancillary services. Thus, PNNL studied scenarios with energy-to-power ratios closer to industry standards (1.0–4.0).

While expanding the energy capacity increases the costs of the ESS, many system components are defined based on power capacities. Thus, doubling the energy capacity does not double the price. By expanding the energy capacity of the ESS, demand response and the more energy-intensive applications (e.g., arbitrage and ancillary services) generate much more value. By upsizing the energy storage capacity to 5 MWh and 10 MWh, the additional value allows the benefits ($13.3M and $20.3M, respectively) to exceed the system's revenue requirements ($11.5M and $16.4M, respectively). The value would be much higher yet if the ESS were sited in a manner that generated locational benefits associated with outage mitigation or distribution deferral.

B. Application Hours and Values

Though nine value streams are available, the SSPC, when operated in an optimal manner, would remain idle roughly 22 percent of the time. When not idle, it would be most often engaged in arbitrage (1,265 hours), followed by regulation up (1,025 hours) and spin reserve (655 hours). Fig. 5 presents the number of hours the ESS would be engaged in the provision of each service annually. Primary frequency response and demand response provide tremendous value despite the small number of hours engaged each year—17 and 19, respectively. While the SSPC would be optimally engaged in arbitrage and ancillary services 78 percent of the time, those services only generate 27 percent of the total value.

C. Participation in the Western EIM

Two scenarios were considered for bidding the battery energy storage system (BESS) into the Western EIM. One scenario assumed PGE would bid the SSPC into either the EIM or the Mid-Columbia market on an hourly basis to charge the ESS at the lowest price and discharge at the highest price between the two markets. Using EIM data from the PacifiCorp West load aggregation point, doing so would have generated a value of $27,674 in 2016. An alternative scenario was also run in which PGE would bid the SSPC into the EIM on an hourly basis but it would be dispatched by CAISO, subject to 5-minute real-time market (RTM) prices. This scenario takes advantage of ESS flexibility in providing energy more rapidly throughout each hour. This scenario generated a benefit of $152,619 annually, or $2.1M in PV terms, over 20 years. EIM benefits expand to $214,109 annually, or $2.9M in PV terms, over 20 years if the ESS energy capacity expands to 5 MWh.

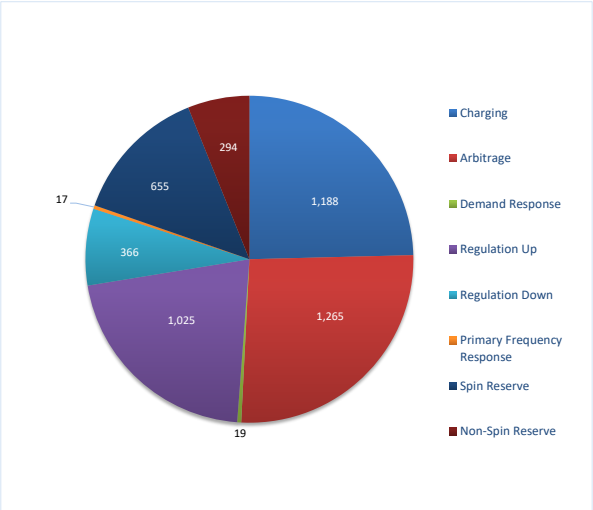

Fig. 5. Hours per service per year.

D. Alternative Scenarios and Sensitivity Analysis

To explore the sensitivity of the results to varying a number of key assumptions, we conducted a series of sensitivity analyses. Fig. 6 shows the various scenarios and their impacts measured in comparison to the base case. Parameters varied for sensitivity analysis include battery capacity, RTE, predictability of a particular event (e.g., frequency response), and price of electricity and ancillary services. Results suggest that changes in the energy capacity and use of current-day prices would profoundly impact the ESS economic benefit.

As shown in Fig. 6, most sensitivity analyses result in benefit improvements, suggesting that the base case was somewhat conservative. The most negative impact is revealed in SA1, when the battery capacity is limited to 750 kWh by setting strict state-of-charge range (20-80 percent) limits. On the positive side, using the higher value for primary frequency response tied to the CAISO contract with SCL would increase benefits by $1.9M over 20 years. Perfect foreknowledge of frequency response events would free up 300 kWh of energy capacity for other applications, resulting in an increase of nearly $600,000 in total benefits. Most other cases (e.g., adjusted RTE, modified discount rate, alternative price years) had a negligible impact on economic returns.

Fig. 7 presents the ROI ratios (defined as PV benefits divided by PV revenue requirements) for the sensitivity analysis cases. Cells shaded red have ROI ratios under 0.5, cells shaded yellow have ROI ratios between 0.5 and 1.0, and cells shaded green represent scenarios with ROI ratios exceeding 1.0. When PGE cost estimates are used in the denominator of the ROI calculations, all fall short of 1.0, meaning that benefits fall short of revenue requirements. With current-day prices [7], the base case ROI ratio is 0.79 and several scenarios generate positive net benefits. When the energy capacity is scaled up to, 10, and 15 MWh, ROI ratios reach 1.15, 1.24, and 1.08, respectively. With 20 MWh, ROI falls below unity. This finding suggests that an energy capacity of 5 to 10 MWh would be optimal in terms of maximizing returns based on the landscape of economic opportunities present. However, increasing the energy capacity of SSPC over a certain limit could have a detrimental impact on the ROI.

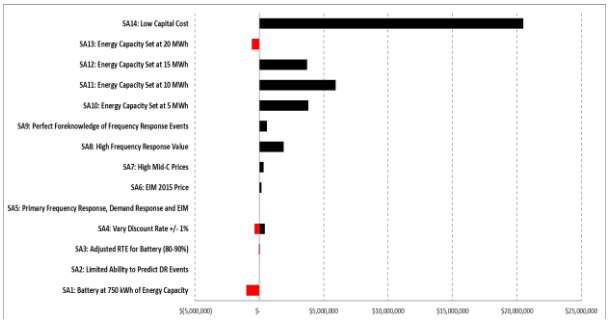

	Low-End	High-End
SA1: Battery at 750 kWh of Energy Capacity	$ (1,007,444)	
SA2: Limited Ability to Predict DR Events	$ (23,928)	
SA3: Adjusted RTE for Battery (80-90%)	$ (37,997)	$ 53,224
SA4: Vary Discount Rate +/- 1%	$ (375,709)	$ 428,565
SA5: Primary Frequency Response, Demand Response and EIM		$ (9,345)
SA6: EIM 2015 Price		$ 164,738
SA7: High Mid-C Prices		$ 334,211
SA8: High Frequency Response Value		$ 1,901,296
SA9: Perfect Foreknowledge of Frequency Response Events		$ 589,890
SA10: Energy Capacity Set at 5 MWh		$ 3,805,708
SA11: Energy Capacity Set at 10 MWh		$ 5,921,969
SA12: Energy Capacity Set at 15 MWh		$ 3,702,353
SA13: Energy Capacity Set at 20 MWh		$ (584,804)
SA14: Low Capital Cost		$ 20,494,044

Fig. 6. Sensitivity analysis results.

	Base Case	Batt-750 kW of Capacity	Demand Response Alternative Constraint	Batt-80% RTE	Batt-90% RTE	Primary Requency Response, Demand Response and EIM	EIM 2015 Price
PGE Actuals	0.21	0.17	0.21	0.21	0.21	0.21	0.21
PGE Today	0.40	0.33	0.40	0.40	0.41	0.40	0.41
Lahiri 2017 Basis	0.74	0.62	0.74	0.74	0.75	0.74	0.76
Lahiri 2017 Basis - 5 MW							
Lahiri 2017 Basis - 10 MW							
Lahiri 2017 Basis - 15 MW							
Lahiri 2017 Basis - 20 MW							

	High Mid-C Prices	Perfect Foreknowledge of Frequency Response Event	High Frequency Response	Batt-5 MWh	Batt-10 MWh	Batt-15 MWh	Batt-20 MWh
PGE Actuals	0.22	0.23	0.27				
PGE Today	0.42	0.44	0.53				
Lahiri 2017 Basis	0.79	0.82	0.98				
Lahiri 2017 Basis - 5 MW				1.15			
Lahiri 2017 Basis - 10 MW					1.24		
Lahiri 2017 Basis - 15 MW						1.08	
Lahiri 2017 Basis - 20 MW							0.90

Fig. 7. ROI for alternative scenarios.

PNNL evaluated the impact of adjusting the energy-to-power ratio of the SSPC upward, from 0.25 (1.25 MWh) to 4.0 (20 MWh). With an energy to power ratio less than approximately 0.5, we observed that the cost is higher than total benefits, thus the ROI is less than 1, as shown in Fig. 8. As the ratio increases, benefits increase at a higher rate than the costs; therefore, ROI continues to increase until the energy-to-power ratio reaches a value of 2. Once the ratio surpasses 2, benefits increase at a lower rate than costs, causing the ROI ratio to decrease. At an energy-to-power ratio of approximately 3.5, costs surpass benefits, bringing the ROI ratio below 1.0.

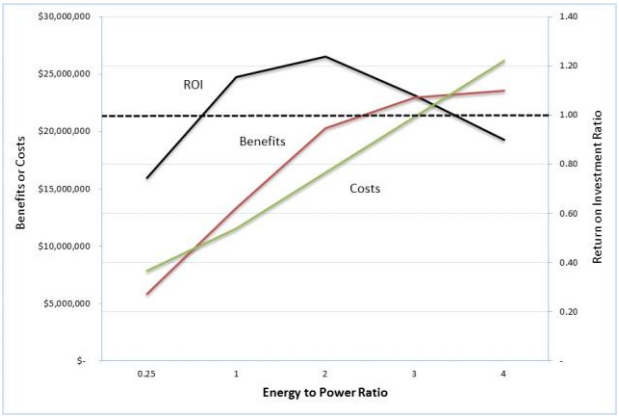

Fig. 8. Impacts of energy-to-power ratio on costs, benefits, and ROI.

V. Conclusion

This assessment examined the financial feasibility of the SSPC by monetizing the values derived from nine services it could provide to PGE and the customers it serves. The ESS and the grid conditions under which it operates were modeled using PNNL's in-house optimization tool, BSET, to explore tradeoffs between services and develop optimal control strategies. The analysis resulted in a number of lessons that provide crucial insights into the practical application of ESS, including:

- The SSPC, which was originally conceived as a research and test facility and built with the prevailing maturity technology level, was built at a cost ($20.4M) that exceeds current-day prices ($5.4M) for a similarly designed and built 5 MW/1.25 MWh system.
- In terms of economic operation, the SSPC is currently underutilized, deployed only for primary frequency response. PNNL modeling indicates that optimal operation of the ESS could generate an additional value of $2.3M over 20 years. It should also be noted that while primary frequency response is the highest benefit application, it requires a response from the SSPC only 17 hours each year. While optimally engaged, the ESS could provide arbitrage and ancillary services 78 percent of the time, but those services currently generate only 27 percent of the total value.
- Participation in Western EIM represents an interesting opportunity for PGE, with a potential to generate $2.1M value in PV terms over 20 years in the 5-minute RTM.
- With an energy-to-power ratio of only 0.25, the SSPC is not well suited to engage in most energy-intensive applications, such as arbitrage or ancillary services. By upsizing the storage capacity to 5 MWh or 10 MWh, the additional value allows the benefits ($13.3M and 20.3M, respectively) to exceed the system's revenue requirements ($11.5M and $16.4M, respectively). For the SSPC, ROI ratios exceeded 1.0 when the energy-to-power ratio fell between 0.5 and 3.5, and peaked at an energy-to-power ratio of 2.0.

This report represents the output of the first of a two-phase effort. Phase II will involve the development of enhanced control strategies to assist PGE in realizing the benefits of energy storage in real time.

Acknowledgements

We are grateful to Dr. Imre Gyuk, the Energy Storage Program Manager in the Office of Electricity Delivery and Energy Reliability at the DOE. Without his office's financial support and his leadership, this project would not have been possible. We also wish to acknowledge the other members of the Grid Modernization Laboratory Consortium team: Dan Borneo, Ben Schenkman, and Ray Byrne of Sandia National Laboratories; Michael Starke of Oak Ridge National Laboratory; and Todd Olinsky-Paul of the Clean Energy States Alliance. We further gratefully acknowledge the useful cost information provided by Sudipta Lahiri of DNV GL. Finally, we would also like to acknowledge the technical assistance provided by other members of the PGE team not acknowledged as authors, including Wayne Lei, Elaine Hart, and Pam Sporborg.

References

[1] Cision PRWeb, "EnerDel's 5 Megawatt Energy Storage System Comes Online as Part of Portland General Electric's Salem Smart Power Project," Last modified June 3, 2013. [Online]. Available: https://www.prweb.com/releases/2013/6/prweb10788962.htm

[2] N. A. Samaan, R. Bayless, M. Symonds, T.B. Nguyen, C. Jin, D. Wu, *et al.*, "Analysis of benefits of an energy imbalance market in the NWPP," Pacific Northwest National Labs, Richland, WA, Rep. no. PNNL-22877, October 2013. [Online]. Available: https://www.pnnl.gov/main/publications/external/technical_reports/PNNL-22877.pdf

[3] CAISO, "California Independent System Operator Corporation Filing of Rate Schedule No. 86, between the CAISO and the City of Seattle," 2016. [Online]. Available: http://www.caiso.com/Documents/Nov22_2016_TransferredFrequencyResponseServiceAgreement_City_Seattle_ER17-411.pdf

[4] CAISO, "California Independent System Operator Corporation Filing of Rate Schedule No. 86, Transferred Frequency Response Agreement between the CAISO and the Bonneville Power Administration," 2016. [Online]. Available from:

http://www.caiso.com/Documents/Nov22_2016_TransferredFrequencyResponseServiceAgreement_BonnevillePowerAdministration_ER17-408.pdf.

[5] Navigant Consulting Inc., "[Draft] Energy Storage Potential Evaluation," Prepared for Portland General Electric, Portland, OR, 2017. [Online]. Available: https://edocs.puc.state.or.us/efdocs/HAA/haa115310.pdf

[6] D. Wu, C. Jin, P. Balducci, and M. Kintner-Meyer, "An energy storage assessment: Using optimal control strategies to capture multiple services," in *Proc. 2015 IEEE Power & Energy Society General Meeting*, Denver, CO, July 2015, pp. 1-5.

[7] Lahiri, S. "Assessing CAPEX for storage projects," Presented at 10th Annual Storage Week, 2017, DVN GN: Oakland, CA.

Update on and Overview of Model Codes and Standards for Energy Storage System Safety

David Conover

Pacific Northwest National Laboratory

902 Battelle Blvd, Richland, WA 99354, United States

***Abstract*- Myriad energy storage system (ESS) technologies are being deployed and developed for future deployment. Successful ESS design, construction, installation, and use in the built environment must address a number of issues—the foremost being safety. Safety is documented and validated through codes, standards, and regulations (CSR). The provisions in these documents typically lag technology development and initial deployment. Until these documents are updated, it can be more challenging to secure approval for an ESS[1] installation because no uniform, consistent, and acceptable means of documenting and validating its safety, in addition to ensuring its continued safety during operation and when decommissioned, is available. This paper provides foundational information for understanding why CSR are important to technology deployment, what CSR are relevant to ESS, and how they are being developed, updated and adopted so stakeholders involved in any way with ESS can further ensure ESS safety in relation to the dynamic nature of ESS development and deployment.**

***Keywords*- safety, codes, standards, technology acceptance, regulations.**

I. Update on and Overview of Model Codes and Standards for Energy Storage System Safety

This paper provides an overview of the topic of codes and standards as related to energy storage systems (ESS) and a little history to provide a framework for understanding how these documents can impact the timely acceptance of ESS while ensuring public safety. Safety-related issues associated with ESS are identified; the documents addressing those issues are highlighted, along with how they are developed and adopted. Finally, information is provided on keeping those documents updated and current as ESS technology evolves and applications increase over time.

United States (U.S.) model codes and standards are developed, published, and regularly updated by voluntary sector (e.g., non-governmental) standards development organizations (SDOs). When adopted, they represent the body of criteria that must be satisfied to design, construct, commission, rehabilitate, operate, maintain, repair, and decommission components of the built environment such as buildings, facilities, products, systems, and equipment therein. This body of adopted criteria is referred to as codes, standards, and regulations (CSR). These criteria are not static but are very dynamic, needing revision and enhancement as new technologies are developed and new issues arise that impact their deployment and use.

The Electricity Storage Handbook (DOE/EPRI 2013) indicates that one of the three biggest challenges hindering adoption of energy storage systems (ESSs) is codes and standards. They directly affect ESS technology (product) and its intended installation/application. Although CSR can focus on other issues such as performance, the acceptability of an ESS from a safety standpoint directly affects whether it can be manufactured and deployed and, if so, how and under what conditions. The administration of CSR and time to approval issues (e.g., documenting and validating compliance) affect the ability to construct and install ESSs in a timely manner. The absence of criteria for evaluation, documentation, and validation of ESS safety can adversely affect those seeking to move ESSs into the market and those responsible for public safety. They have little basis on which to consistently and confidently qualify a system and its installation as being "safe." This 'time lag' between technology development and deployment and the availability and application of CSR that provide needed and relevant criteria poses an ongoing challenge. Existing model codes and standards need to be updated and/or new ones developed to specifically address the range of ESS technologies and installations. After their publication, they have to be adopted as CSR as a basis for uniformly documenting what is safe and determining what can be approved in a consistent and timely manner. In some instances, the lack of specificity limits progress until appropriate safety-related criteria are available; in others, "outdated" criteria can be conservatively applied to the technology, thereby affecting the cost of an ESS installation or limiting the application of an ESS.

Fig. 1 provides a view of how CSR can affect technology development and deployment. All scenarios (A, B, and C) involve up-front investment to bring the technology to market

[1] For the purposes of this paper, ESSs are stationary and can store energy through thermal, mechanical, or electrochemical means for applications in the built environment (e.g., buildings, facilities, industrial processes). Mobile ESSs used for disaster relief and other temporary uses can also be considered "stationary" for the purpose of ensuring system safety.

(negative slope) and then in going to market the generation of income (positive slope). In a "typical" business model (B) where there is some awareness of CSR, while there are no "show stoppers," there is little proactive effort to enhance consideration of the subject technology in CSR. Where CSR are not considered (C), additional investment in technology development and/or generation of research to document technology safety is needed. This increases the time to market, which affects the availability of the technology and requires additional investment. In worst-case situations, CSR can impede the use of the technology because they compromise a basic safety tenet or indirectly by requiring additional unplanned safety considerations. A response to this "time lag" is for the proponents of a technology, in this case ESS, to collaborate early on in development of CSR to conduct needed research to support new CSR criteria in parallel with technology development, as shown in scenario (A). That investment is more than recouped because the necessary CSR are developed and deployed at or near the time the technology enters the market.

When CSR are updated to address new ESS technologies and applications, they can provide a specific, uniform, and repeatable basis for documenting and validating the safety of the ESS technology and its installation (i.e., prescriptive). Note that most CSR allow an approach to compliance by showing that what is proposed is no more hazardous, nor less safe, and performs at least as well as other technologies specifically covered by the CSR (i.e., equivalent performance). While affording a path to approval until the CSR are updated, this path can necessitate the development of criteria by which each entity enforcing the adopted CSR can determine "equivalent safety" associated with a proposed ESS. This can result in proponents of an ESS installation having to provide a customized or "one-off" documentation package for each jurisdiction (approval authority) where an ESS is desired on the customer side of the meter or for each utility on the grid side. In addition, authorities having jurisdiction (AHJs) also may be less inclined to accept this path to compliance because they would have to develop the criteria on which to base "equivalent performance", or consider and approve those suggested by the ESS proponent, and then have to assess the documentation provided by the ESS proponent. The availability of updated and specific CSR to document and validate ESS safety is clearly preferable. That said, it takes time to develop model codes and standards and adopt them as CSR.

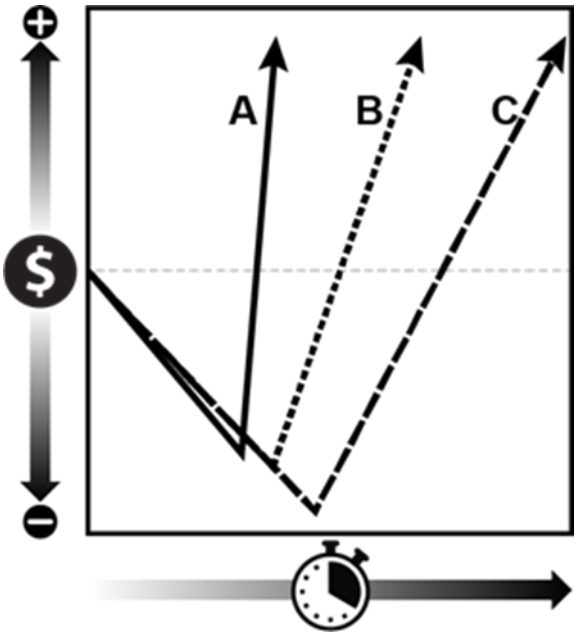

Fig. 1. The value of addressing CSR.

II. Short History of ESSs Relative to CSR

Energy storage has been an integral part of daily life for decades, even centuries. With the advent of electricity, Benjamin Franklin coined the term "battery" to convey the concept of electrical storage. Buildings have historically used batteries to support standby or emergency power requirements. More recently, buildings are using batteries to store electrical energy from renewable energy sources, such as wind and photovoltaic systems, as well as thermal energy from solar or waste heat sources and mechanical energy in flywheels. Although battery safety has been addressed in documents such as the National Electrical Code (NFPA 70), Fire Code (NFPA 1), International Fire Code (ICC IFC), and Underwriters Laboratories standards (UL 1973), until recently they only provided criteria for vented lead-acid batteries. More recent model codes and standards provide criteria for a wider range of batteries and now complete ESSs that include a wide range of ESS technologies. Even with updated model codes and standards available for adoption, the adoption process does take time. Consequently, those adopting them as CSR may still be using older versions of these model codes and standards.

Current U.S. energy, environmental, and economic challenges, coupled with increased globalization of technology, are supporting a very dynamic evolution of new storage technologies and applications. While updated CSR are needed, the development of model codes and standards and their adoption as CSR can be challenging to "speed up," especially when the results of safety-related testing and analysis are needed to form a basis for the criteria in those documents.

In the U.S., the existence of CSR typically occurs through adoption of criteria developed by private sector SDOs. The process involves all stakeholders, including potential adopters, but adopters of these documents can and do develop their own "home grown" CSR. Adoption can occur through governmental vehicles at the federal, state, local, territorial, or tribal levels; through private sector vehicles such as insurance policies, contracts, or incentive programs; and through utilities with respect to equipment that is part of their grid equipment or connected to the grid. After adoption of the CSR, those seeking approval must document compliance with what is adopted to the AHJs having authority for validating compliance (e.g., enforcing the CSR). This introduces another process component—conformity assessment, which focuses on documenting compliance with the criteria that are adopted and then validating that the criteria are satisfied. While adopting entities have the authority to validate compliance and will undertake the necessary enforcement activities to ensure compliance, they will also rely on documentation from third-parties (e.g., testing and listing of products by "approved" agencies or plans and specifications prepared by a registered design professional). This is especially true with respect to ESS products or components manufactured in a single place, then shipped to various sites for installation. Safety issues (traditional and new, due to advances in ESS technology and/or applications) will continue to arise and will have to be addressed.

In summary, the optimum outcome is that CSR provide specific criteria on which to document and validate the safety of ESS at the point in time that ESS initially enters the market. Achieving that outcome, short of drastically changing how the U.S. system of CSR development, adoption and application functions, requires collaboration by all ESS proponents and stakeholders and their participation in the updating of CSR and fostering their adoption and application in parallel to ESS technology development and deployment. A key component of that collaboration is identifying safety issues associated with ESS, conducting research and analysis to develop solutions to those issues and then memorializing those solutions in CSR.

III. Safety Issues Associated With ESSs

A number of safety-related issues are associated with ESSs in general; others are unique to specific ESS technologies (types, chemistries, and capacities/sizes) and their applications. The following application scenarios will affect whether and to what degree a particular safety issue is relevant:

- Location of the ESS in relation to the grid (e.g., customer meter) and whether it is grid-connected
- Location of the ESS in relation to buildings and facilities (e.g., indoors, outdoors, rooftop, below grade, enclosed, etc.)
- Type of building or facility in which an ESS may be located or installed on or adjacent to i.e., single family dwelling, hotel, parking structure, business, industrial)
- Nature of the installation (i.e., rural/remote, urban)
- Application is associated with a new building or an existing building
- ESS is stationary, mobile but "stationary" (i.e., on wheels), or portable.

These systems can be "brand new" or existing systems that may undergo repair, renewal, refurbishment, and recommissioning

The safety issues include:

- Clearances and working space
- Shocks and arc flash
- Structural loading
- Protection against natural and manmade disasters
- Spill control
- Impact protection
- Access to and egress from the ESS area
- Smoke and fire detection and fire suppression
- Separation of ESSs from each other and from other spaces/areas
- Ventilation and exhaust to address temperature and environmental concerns.

The range of ESS technology types, chemistries, sizes/capacities, and potential applications is needed to identify the safety issues associated with each scenario (e.g., technology type, size/capacity, and application), and the research needed to determine how to best ensure the safety issues for each scenario are addressed (e.g., there will be no safety-related incident, or if there is, how it will be effectively managed). When a specific solution(s) is known, model codes and standards can be updated to provide a basis for uniformly implementing the solution(s). When an ESS has been documented and validated as satisfying the criteria in CSR, then its installation can be deemed "safe." Safety includes the minimization of an incident occurring and the ability to effectively address an incident if it does occur.

Safety-related criteria in model codes and standards can be presented in several formats:

- Prescriptive format (e.g., locate the ESS x ft from something)
- Component performance format in which a particular component or portion of the system must provide a particular outcome without specifying

how that is to be achieved (e.g., the ventilation system shall be designed to keep the ESS room temperature during normal operation below x ºF)

- More complete performance format without specifying how it is to be achieved (e.g., the ESS shall be designed and constructed to eliminate all possible electrical shock hazards).

As noted above, the availability of model codes and standards to fully address the safety of any technology or its application in the built environment always lags new technology development and deployment (or even new application of existing technology). It takes time to conduct the necessary research to answer safety-related questions (e.g., how far is a safe x ft clearance or how much ventilation is sufficient?). Even when a complete performance goal is established, it takes time to develop a standard to guide how to uniformly document and verify (through testing and/or analysis) that the goal has been successfully realized. Even though research results and experiences with the technology can inform the development of model codes and standards, there is lag time between their finalization and adoption. Continued growth in ESS technologies and applications drive the ongoing cycle of research, analysis, knowledge, and model codes and standards development and adoption. Hence, all ESS proponents and stakeholders who would collaborate as suggested above to shorten the gap between ESS technology, in relation to CSR that have been adopted and are being applied, need to know the 'target' model codes and standards on which to focus their efforts.

III. What Model Codes and Standards Apply to ESSs and How

Information about model codes, standards, and other related documents can be organized by document scope relative to ESSs from the "macro to the micro" level (Table I). The more "macro" documents are likely to adopt by reference the more "micro" documents. In aggregate, these documents form the basis for documenting and validating the safety of ESSs with respect to the issues noted above, available technologies and today's anticipated applications. These documents will continue to be updated pursuant to SDO-specific processes, which are described on SDO websites and provide every opportunity for input from all interested parties. As noted above it takes time for these documents to be updated and revised and then adopted. Paralleling development of new ESS technologies and applications with these activities can foster timelier and less burdensome ESS deployment. Fig. 2 shows an ESS installation and the relative scope of each of these types of documents.

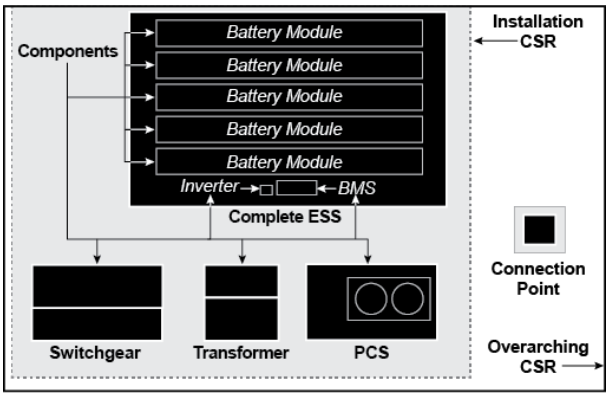

Fig. 2. ESS installation

III. Codes and Standards That Apply to ESSs

Table I identifies documents that enjoy widespread adoption as CSR or are likely to when completed. (See the SDO websites for more detailed information about all the documents included in Table I.)

TABLE I
MODEL CODES, STANDARDS, AND OTHER RELATED DOCUMENTS

Category	Model Codes, Standards, and Related Documents
Overarching codes and standards – the built environment at large that includes, but is not limited to, ESSs	• NFPA 1-2018 (Fire Code). The 2018 edition is finalized and Chapter 52 includes requirements related to ESSs. Public inputs for the 2021 edition will be due in mid-2018. • NFPA 70-2017 (National Electrical Code [NEC]). Article 706 applies to ESSs and Article 480 applies to batteries, in addition to other criteria in the NEC relevant to electrical equipment and installations. A revision process that will lead to the 2020 edition is underway. • 2018 IFC (International Fire Code). Chapter 12 of the IFC covers energy systems and Section 1206 in that chapter covers electrical ESSs. Proposed changes are due January 8, 2018, and the outcome of the code development process, which will occur during 2018, will be the 2021 edition of the IFC. • 2018 IRC (International Residential Code). A section of the IRC covers ESSs and possible changes to that section can be submitted and considered as described above under the IFC. • IEEE C2-2017 (National Electric Safety Code [NESC]). The NESC covers electrical safety for utility systems and equipment. The final date to receive change proposals from the public for revision of the 2017 edition is July 15, 2018. The outcome of the revision process will be the 2022 edition of the NESC. • DNVGL-RP-0043, October 2017 (Safety, Operation and Performance of Grid-connected Energy Storage Systems). This document provides a comprehensive set of recommendations (not a code or standard per se) for grid-connected ESSs.
Codes and standards for ESS installations – the installation of the ESSs relative to other systems and parts of the built environment	• NFPA 855-20XX (Standard for the Installation of Stationary Energy Storage Systems). This standard will cover the safety of all ESSs and their installation in the built environment. It has been drafted and was out for first public input in September 2017. Final approval of NFPA 855 is targeted for June 2018. • NECA 416-2016 (Recommended Practice for Installing Stored Energy Systems). This document describes installation practices for ESSs such as battery systems, flywheels, ultra-capacitors, and smart chargers used for electric vehicle (EV) and vehicle-to-grid applications. It has been published and a new appendix containing a compliance checklist is under development. • FM Global Property Loss Prevention Data Sheet # 5-33 January 2017 (Electrical Energy Storage Systems). This data sheet describes loss prevention recommendations for the design, operation, protection, inspection, maintenance, and testing of electrical ESSs. It focuses primarily on lithium-ion battery technology. Development of an interim revision is planned for 2018 with publication expected in 2019.
Codes and standards for a complete ESS – the entire ESS in the aggregate	• UL 9540[2] (Energy Storage Systems and Equipment). This is a product safety standard for an ESS and was first published November 21, 2016. UL is in the process of creating a bulletin for circulation that includes revision to the standard, and which would include a reference to a newly published UL 9540A – Test Methods for Evaluating Thermal Runaway Fire Propagation in Battery ESS. • ASME TES-1 (Safety Standard for Thermal Energy Storage Systems). This standard provides safety-related criteria for molten salt ESSs. The document has been approved for public review that will close in late February 2018.
Codes and standards for ESS components – components associated with the ESS	• IEEE P1679.1 -2017(Guide for the Characterization and Evaluation of Lithium-Based Batteries in Stationary Applications). This new standard provides appropriate information about safety attributes and operating conditions related to stationary applications of lithium-based batteries. IEEE P1679.2 (Guide for the Characterization and Evaluation of Sodium-Beta Batteries in Stationary Applications). This proposed new standard provides appropriate information about safety attributes and operating conditions related to stationary applications of sodium-beta batteries. • UL 1973 (Standard for Batteries for Use in Stationary, Vehicle Auxiliary Power and Light Electric Rail Applications). A new edition will be published in January 2018. UL 1974 (Evaluation for Repurposing Batteries). The new standard will cover use of repurposed EV batteries for stationary applications and the processes used in such repurposing. A bulletin for the first edition of UL 1974 is expected in early 2018. • UL 810A (Electrochemical Capacitors). The standard covers the safety of electrochemical capacitors, which can be used as an energy source in ESSs. The first edition was published on October 7, 2008, and reaffirmed on March 28, 2017.

[2] UL standards are under continuous maintenance and are updated as warranted.

IV. How Model Codes and Standards Are Developed and Adopted

In the U.S., model codes and standards are developed in the voluntary sector by one SDO or through a co-sponsorship agreement between multiple SDOs. The SDO does not author them; rather it establishes and oversees a process whereby all interested and affected parties, stakeholders, or interested entities, including representatives from all levels of government, can participate in their development. Most SDOs subscribe to the American National Standards Institute (ANSI) essential requirements, which are intended to ensure the SDO provides fair and due process to all interested and affected parties.

The process by which each SDO develops model codes and/or standards is available from each SDO. In general, a process meeting the ANSI essential requirements can be summarized as shown in Fig. 3. After model codes or standards are developed in the voluntary sector, they are available for adoption. Adoption is simply a decision by any decision-making entity that compliance with the adopted model codes or standards is mandatory.

Adoption can occur in many ways, including the following:

- Legislative or regulatory action by a governmental entity (i.e., federal, state, local, Indian Tribe) as a mandatory requirement in all cases or as a condition for program funding
- Action by a utility under its operation as controlled by a Public Utility Commission and acting as the AHJ for systems on the grid side of the meter or simply as the entity connecting to an ESS on the customer side of the meter
- Requirement by an insurance carrier as a condition for insurance coverage
- Condition for licensing (e.g., a state contractor licensing board that adopts and applies particular technical requirements and compliance with those as a condition for licensure)
- Reference in building specifications issued by a building owner/developer or financial institution backing a project
- Anyone considering the application and use of energy storage that, in the absence of any other means of adoption, elects to apply model codes or standards to their project (e.g., self-adoption).

How these adopting agencies or entities exercise their authority varies widely, as does their pre-emptive authority over other bodies or entities and the scope of what they "regulate." While they may adopt model codes and standards and have the authority to amend them (e.g., increase stringency and/or add provisions), they also may choose to develop their own home-grown provisions in lieu of or in addition to the model codes and standards. Ideally, all stakeholders affecting ESS safety can collaborate in the development of model codes and standards and fully support their timely adoption and application in a uniform and consistent manner. The alternative can be a "crazy quilt" of differing requirements that can work against addressing EHS safety in a comprehensive and more timely manner, because those responsible for public safety, in the face of increased ESS deployments and not finding their CSR needs addressed, will generate their own requirements; or worse, be less willing to approve ESS applications until those CSR are updated and available for adoption.

V. Keeping Model Codes and Standards and CSR "Fresh" as ESS Technology and Deployments Grow and More is Learned to Better Address Safety

Multiple initiatives are under way separately within the range of ESS development and deployment and development of model codes and standards and their adoption as CSR. These are typically carried out in series, instead of in parallel as suggested above, and hence can have an impact on the timely acceptance of safe ESSs. While it is very challenging to conduct all the necessary activities (research and development, model code and standard development, and then their adoption and implementation as CSR) in parallel, they can and should be carried out in a coordinated manner that fosters their being addressed in parallel as much as possible. Closing this gap between ESS development and deployment and the availability of CSR needed to document and validate ESS safety can be done but requires collaboration by all ESS proponents and safety stakeholders. Such collaboration can be facilitated by following the ESS safety roadmap, whose goal is to "foster confidence in the safety and reliability of energy storage systems."

The need for a new model code or standard is identified (e.g., one does not exist) by a committee associated with the SDO, an interested and affected party, stakeholder or any entity with an interest in seeing a model code or standard developed. Where a model code or standard already exists, it is updated on a regular schedule as established by the SDO.

The proponents of the new model code or standard prepare relevant documentation for submittal to the SDO for consideration in establishing a new model code or standards project. Where a model code or standard already exists, any interested and affected party can submit proposed changes to the SDO. They are considered in accordance with the SDO procedures. Changes that are approved are included in the next edition of the model code or standard.

The SDO processes the request for a new code or standard through their codes and standards development procedures and either approves, disapproves, or requests additional information.

When approved, the SDO will provide notification of their intent to establish a new model code or standard so that the public can comment on the intended action. If no adverse comments are received, the SDO will initiate development of the new model code or standard, starting with a call for committee members that will be responsible for the development of an initial draft of the model code or standard.

Fig. 3. Summary of the model codes and standards development process.

IV. Summary and Conclusion

ESSs and their potential applications and interrelationships with the built environment will continue to evolve. This will drive the need for more research, testing, and analysis to document safety, and it could raise new safety-related issues. Model codes and standards will continue to be developed and updated regularly to address new technologies and to respond to new information and experiences. They will continue to be available for adoption as CSR, eliminating the need for document adopters to each separately and in parallel conduct the same developmental and updating efforts. Then adopting proponents of ESSs will have to document compliance, and AHJs will have to validate compliance. This process does not end when an ESS is initially commissioned; it continues throughout its first and any subsequent lives—through system renewal, and ultimately, its decommissioning and disposal.

Moving forward requires establishment of an ESS development and deployment goal focused on safety that is respectful of time, identification and satisfaction of information gaps. This has been done through the U.S. Department of Energy OE ESS Safety Roadmap. The realization of a safety related goal requires knowledge of and collaborative involvement in this entire process by all interested and affected parties. As outlined in the safety roadmap this is a dynamic process that is founded on communication and collaboration. On an ongoing basis, all interested parties must have a common and robust understanding of the CSR process and be committed to interacting in that process to foster development and adoption of needed CSR provisions. Concurrently, safety issues need to be identified that are associated with both new technologies being developed and safety-related observations and instances associated with existing ESS installations. Solutions to those issues need to be found and can include research, testing, and analysis, as well as needed modifications to ESS technology designs or installation specifications. Those solutions, in turn, must be memorialized in model codes and standards in as timely a manner as possible, within the processes associated with the relevant SDOs, in addition to making those solutions readily available for application and use in parallel to their consideration in those SDO processes.

The process associated with technology development and deployment and the process associated with the development, adoption, and implementation of CSR are not likely to change drastically. That said, knowing how they each function can go a long way to bridging the gap between ESS technology and CSR criteria. With that knowledge and collaboration in support of a goal, as outlined in the safety roadmap, that gap can be further bridged by addressing technology development and deployment efforts, needed research, analysis and documentation, and development of CSR criteria in parallel. Although challenging, when all stakeholders communicate and collaborate on the needed activities the goal can be achieved.

REFERENCES

[1] D. R. Conover, "Overview of development and deployment of codes, standards and regulations affecting energy storage safety in the United States," Pacific Northwest National Lab., Richland, WA, Rep. no. PNNL-23578, Aug. 2014. Available: https://energymaterials.pnnl.gov/pdf/PNNL-23578.pdf

[2] D. R. Conover, "Inventory of safety-related codes and standards for Energy Storage Systems," Pacific Northwest National Laboratory, Richland, WA, Rep. no. PNNL-23618, Sept. 2014. [Online]. Available: https://www.sandia.gov/ess-ssl/docs/safety/ESS_Inventory_9-15-14_PNNL_23618.pdf

[3] D. R. Conover, "DOE OE Energy Storage Systems safety roadmap focus on codes and standards," Pacific Northwest National Laboratory, Richland, WA, Rep. no. PNNL-27189, Dec. 2017. [Online]. Available: https://www.sandia.gov/ess-ssl/publications/EnergyStorage_safetyroadmap_2017.pdf

[4] Pacific Northwest National Laboratory and Sandia National Laboratories, "DOE OE Energy Storage Systems safety roadmap," Pacific Northwest National Lab. and Sandia National Labs., Richland, WA and Albuquerque, NM, Rep. no. PNNL-SA-126115/SAND2017-5140 R, May 2017. [Online]. Available: https://www.sandia.gov/ess-ssl/publications/EnergyStorage_safetyroadmap_2017.pdf

Determining the Internal Pressure in 18650 Format Lithium Batteries Under Thermal Abuse

Frank Austin Mier[1], Michael Hargather[1] and Summer Ferreira[2]
[1]*New Mexico Tech, Socorro, New Mexico, USA*
[2]*Sandia National Laboratories, Albuquerque, New Mexico, USA*

***Abstract*- Lithium batteries have a well-known tendency to fail violently under abuse conditions which can result in venting of flammable material. Understanding these events can aid in evaluating safety associated with individual battery cells and battery packs when these fluids are vented. The external fluid dynamics of the venting process, including liquid droplets and gases, is related to the internal pressure of the battery cell. In this work, battery case strain is measured on cells under thermal abuse which is then used to calculate the internal pressure via hoop and longitudinal stress relations. Strain measurement is a non-invasive approach which will have no bearing on the de- composition within batteries that leads to thermal runaway. Complementary tests are performed to confirm the strain-pressure relationship by pressurizing 18650 cell caps to failure with an inert fluid. A laboratory setup with a heated test chamber was designed and fabricated to remotely subject cells to heating rates up to 6 ˚C/min. Additional measurements include cell temperature and the test chamber pressure, temperature, and heat flux. Variables explored in these tests include cell chemistry, state of charge, and heating (temperature) rate.**

***Keywords*- Internal pressure, Abuse Testing, Cell venting, Lithium battery, Safety**

I. Introduction

Internal pressure within a battery is an important parameter in describing if and how the venting process will occur when a battery has been subjected to thermal abuse. Among other parameters including opening area size, shape, and fluid density, pressure is key in describing the venting liquid and gas flow fields as well as the criteria for the onset of atomization of vented liquids [1, 2]. Prior work has documented the processes within lithium batteries which occur under thermal abuse with various calorimetry and chemical analysis methods [3]. These tests have also produced experimental measurements on the pressure increase within an enclosed space associated with the venting of 18650 cells. Additional research has performed X-ray computed tomographic imaging within 18650 format cells during thermal runaway to show the gas generation process taking place [4]. A generic burst pressure value of 3,448 kPa has been represented in modeling venting of 18650 cells which includes the use of a choked flow condition at the vent [5]. However, it is important to understand the pressures at which different cell types open, the consistency of the opening pressure, and how the pressure builds up within the cell throughout failure process.

Current research presented here includes two complementary experiments to measure the internal pressure characteristics of 18650 format lithium batteries under thermal abuse conditions. A direct pressurization experiment has been designed to measure the burst pressure and opening area of the vent cap located at the positive terminal of the cells. Another test setup has been constructed to measure the case strain of a battery throughout an entire thermal abuse test to measure the internal pressure time history. From analytical expressions, the non-invasive strain measurements can be used to infer the real time internal pressure within the battery.

II. Direct Pressurization Test Methodology

A. Test Apparatus Design and Instrumentation

Typical battery construction includes a vent mechanism that is crimped in place as part of the positive terminal of a cell. The vents tested here are removed from actual cells using a pipe cutter to separate the cap from the outer battery case. The foil tab which electrically connects the vent cap to the cathode material is then cut, thus completely separating the battery cap. This method is chosen as the entire vent mechanism is left intact. Once removed from the cells, the vent caps retain the battery diameter of 18 mm and have an axial thickness of approximately 4.5 mm. Fig. 1 shows an image of the cap in place on the cell and then removed for direct pressurization testing.

a)  b) 

Fig. 1. (a) An intact 18650 format battery (LG HE2) and (b) the vent cap after removal.

The test apparatus designed and tested here is intended to securely hold vent caps once removed from a battery and create an airtight seal with a source of pressurized air, as shown in Fig. 2. A single vent cap is held firmly between two 7/8-14 UNF sized set screws, and gaskets are used to create a seal. The set screws have a 12.7 mm interior hexagon which allows for fastening while leaving a central opening for unobstructed air flow out of the vents. This design allows for the battery cap to vary in height due to differences in manufacturing tolerance and removal procedure. The cap holder can also accept caps up to 20.6 mm in diameter. A short length of tubing connects the battery cap fixture to a tank which is connected to a pressure regulated source of dry air.

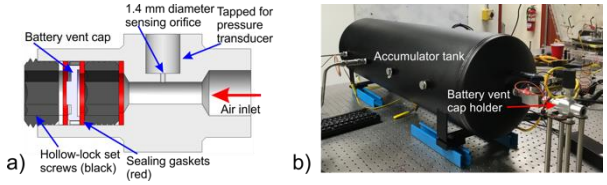

Fig. 2. (a) Schematic representation of the battery vent cap holder and (b) the completed test setup installed at New Mexico Tech.

The center of the battery holder is machined to a precisely known cross-sectional area. A small sensing orifice with a diameter of 1.4 mm allows for measurement of static pressure throughout testing. This feature provides the ability to calculate the opening area of each vent cap. The cross-sectional area at the sensing orifice of 40.0 mm^2 is chosen to be larger than the maximum possible opening area of a battery vent cap, based on a survey of battery end cap designs for cells of interest. This ensures that when venting flow will choke at the vent cap rather than anywhere else within the system.

The direct pressurization test setup is shown in Figure 2(b). Major components included in this setup are the previously described battery vent cap holder, an accumulator tank, pressure regulator, and compressed air cylinder. Air from the cylinder is used to pressurize the tank, vent cap holder, and thus the battery cap itself to a regulated level. While the vent cap has not yet opened, the air within the tank and vent cap holder has no significant velocity as the regulated pressure level is able to be increased very slowly. The accumulator tank has a volume of 76 L which is chosen to minimize transience in pressure values once the vent has opened. A pressure transducer and exposed junction, K-type thermocouple are placed at the opposite end of the accumulator tank from the vent cap holder to measure stagnation pressure and temperature respectively. This location is chosen as gas velocities will be approximately zero at this location once the vent cap opens. Additionally, before vent opening both pressure transducers will be measuring a stagnation pressure as no flow has occurred yet. Once the battery vent opens, the static and stagnation pressure data readings will diverge. Temperature and pressure data are recorded and monitored simultaneously with a National Instruments cDAQ data acquisition system and LabVIEW. Data acquisition rates for the temperature and pressure measurements are 100 Hz and 1 kHz respectively.

B. Calculation of Opening Area

The opening area of the vent cap is inferred via the measured relationship between static and stagnation pressures. Within the test setup, three distinct locations are considered in the analysis: stagnation within the tank, the known cross-section in the vent cap holder, and the opening in the battery vent itself. In most tests, it is expected that the pressure required for the vent to open is also enough to create a choked flow condition. For this to occur, the absolute pressure to open the vent must be 1.89 times atmospheric pressure or greater [6]. As this pressure differential creates a choked flow, it is known that the Mach number of air passing through the vent cap will be fixed at unity until the stagnation pressure drops below 76 kPa gauge (using a value of 86 kPa for atmospheric pressure as measured in the laboratory). The flow will choke at the battery vent cap because it was intentionally designed to have the smallest cross-sectional area within the system.

Once the vent opens and allows air to leave the system, the static pressure measurement taken in the vent cap holder (P_1) will be lower than the stagnation pressure (P_0) at any given instant. Making the assumptions that the flow within the system is isentropic and the air behaves as an ideal gas, the Mach (M_1) number of the flow through the vent cap holder can be calculated via the isentropic flow relation in Equation 1 where γ is the ratio of constant pressure to constant volume specific heats for the air [6, 7]:

$$\frac{P_0}{P_1} = \left(1 + \frac{g+1}{2}\right)^{\frac{g}{g-1}} \tag{1}$$

Once the calculation of Mach number through the vent cap holder is complete, it can be used along with the known cross-sectional area at this location (A_1) and Equation 2 to calculate the area at which the flow is choked (A^*), which is the vent area:

$$\frac{A_1}{A^*} = \frac{1}{M_1}\left(\frac{\frac{g+1}{2}}{1+\frac{g-1}{2}M_1^2}\right)^{\frac{g+1}{2-2g}} \tag{2}$$

If the flow is no longer choked at the vent opening, the Equations 1 and 2 can still be used with the additional

assumption that the flow exits the system through the vent cap with static pressure equal to atmospheric pressure. Accordingly, Mach numbers can be calculated at the vent cap holder (M_1) and vent cap (M_2). Equation 2 will provide area ratios A_2/A^* and A_1/A^* at these two locations. Letting A^* become an arbitrary location for the sonic condition, the vent cap opening area (A_2) can be calculated in terms of the known value for A_1.

C. Validation Series with Known Orifices

A series of orifice plates were fabricated for validation of the opening area calculation methodology. These plates were installed and tested as direct substitutes for the battery vent cap in the test setup. Twenty circular orifices ranging in area from 3.16 mm^2 to 37.4 mm^2 were tested. Additionally, three mock vent orifices seen in Fig. 3 were created representing the intricate geometry and maximum opening area of cells from LG, Panasonic, and A123. The maximum opening area was taken as the series of cutouts on the innermost portion of the vent cap.

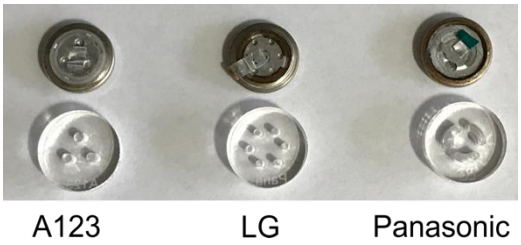

Fig. 3. The internal surface of battery vent caps from 18650 format cells made by LG, Panasonic, and A123 and orifice plates made to mimic the maximum possible opening area.

While tests with battery caps will start from zero gauge pressure within the sealed system and increased until vent opening, the orifice plates do not have a venting mechanism. As such, a ball valve installed between the accumulator tank and the orifice plate was used to manually simulate the opening of a battery vent. To eliminate any erroneous pressure data due to opening the ball valve, the first two seconds stagnation and static pressure readings are ignored. All tests begin with the accumulator tank at approximately 276 kPa to provide a significant amount of time in which the flow is choked.

Initially, three of the twenty circular orifices were chosen for repeated trials to confirm the consistency of the system. The three orifices have areas of 18.5 mm^2, 27.7 mm^2, and 34.5 mm^2 which correspond to standard drill sizes of 11, A, and G respectively. Each orifice was tested five times, and the measured ratio between static and stagnation pressures was used to calculate the opening area. The results of these tests shown in Table I demonstrate the accuracy and repeatability of this experiment.

TABLE I
OPENING AREA RESULTS FROM REPEATED TRIALS

Test	Actual area (mm^2)	Calculated area (mm^2)	Error (%)
11 Drill, Run 1	18.5	19.4	5.1
11 Drill, Run 2	18.5	19.5	5.3
11 Drill, Run 3	18.5	19.5	5.3
11 Drill, Run 4	18.5	19.6	5.9
11 Drill, Run 5	18.5	19.7	6.3
A Drill, Run 1	27.7	28.2	1.6
A Drill, Run 2	27.7	28.3	1.9
A Drill, Run 3	27.7	28.3	1.9
A Drill, Run 4	27.7	28.4	2.2
A Drill, Run 5	27.7	28.4	2.2
G Drill, Run 1	34.5	34.4	0.4
G Drill, Run 2	34.5	34.4	0.4
G Drill, Run 3	34.5	34.4	0.4
G Drill, Run 4	34.5	34.4	0.4
G Drill, Run 5	34.5	34.4	0.4

Individual trials performed on each of the circular orifices show strong agreement between actual and experimentally calculated opening areas throughout the range of possible vent cap opening areas. The results of this validation series are presented in Fig. 4. The orifices designed to resemble the battery vent caps in Fig. 3 show similarly accurate agreement between the actual and calculated opening area.

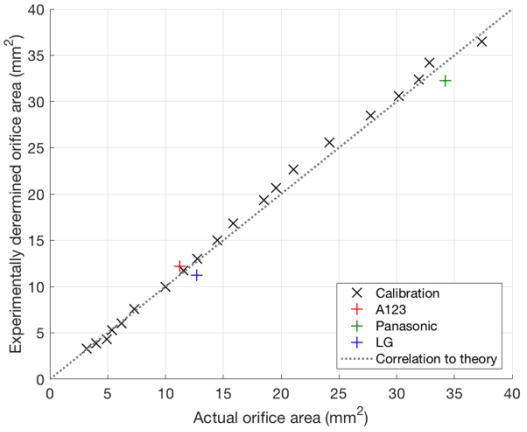

Fig. 4. Comparison between actual and calculated opening areas from the validation series performed on the direct pressurization test apparatus. Both circular and more complex geometries of actual vent can be measured accurately with this methodology.

III. DESIGN AND CONSTRUCTION OF A STRAIN MEASUREMENT TEST FIXTURE

A. Theoretical Basis of Experiment

Strain gauges are used here to perform noninvasive measurement of batteries under thermal abuse conditions.

These gauges are adhered to the battery case with a high temperature rated cyanoacrylate glue as seen in Fig. 5. Fundamentally, a strain gauge operates by changing electrical resistance when it is deformed, which is easily measured by a commercial data acquisition system. Strain measurement allows data to be recorded throughout the entire abuse and eventual thermal runaway process without a need to modify cells which could inherently change how they may react to abuse. The generic nature of this testing approach allows for experiments to be performed on cells of different chemistries and manufacturers.

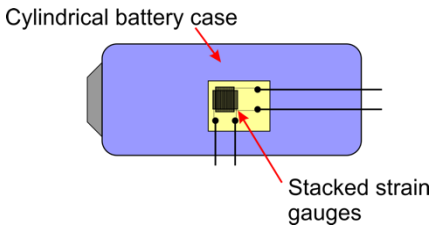

Fig. 5. A schematic representation of the arrangement for how two stacked strain gauges can be mounted to a cylindrical battery. The gauge orientation shown would be used to measure hoop and longitudinal strain.

By treating the outer casing of the battery as a thin walled cylinder, analytic expressions relate hoop (σ_H) and longitudinal (σ_L) stress to the internal pressure (P) within the cell as described by Equations 3 and 4 [8]:

$$s_H = \frac{PD}{2t} \tag{3}$$

$$s_L = \frac{PD}{4t} \tag{4}$$

These equations contain easily measurable geometric constants for the cylindrical battery diameter (D) and case thickness (t). These two stress parameters are converted to strain via the Young's Modulus for the given case material (E). By measuring strain of a battery case under abuse conditions, the internal pressure is inferred.

An important experimental consideration within the range of temperatures observed in thermal runaway events is thermal expansion. The strain measured in experiments can be taken as the sum of the components due to changes in internal pressure and temperature [9]. Expansion along the length and circumference increases the longitudinal and hoop strain measurements respectively. Changes to the length (dl) and circumference (dc) to the battery case as a result of a finite temperature increase (dT) are both forms of linear thermal expansion as described in Equations 5 and 6 [10]:

$$dc = a p D_0 dT \tag{5}$$

$$dl = a l_0 dT \tag{6}$$

The subscript 0 denotes the initial battery length and diameter. The coefficient of thermal expansion (α) is a material property and assumed constant over the temperature changes expected.

By noting that engineering strain (ε) is defined as the change in length to the original length of an object, Equations 5 and 6 may be rearranged to show that the component of case strain due to changes in temperature may be expressed as the product of the thermal expansion coefficient and the finite temperature change. Summing the components of strain due to internal pressure and temperature increases gives Equations 7 and 8:

$$e_H = E\frac{PD}{2t} + a\,dT \tag{7}$$

$$e_L = E\frac{PD}{4t} + a\,dT \tag{8}$$

Equations 7 and 8 represent the measurements that would be taken by strain gauges mounted to a battery as it undergoes thermal abuse. Rearranging these two relations provides Equation 9.

$$P = \frac{t}{4ED}\left(e_H - e_L\right) \tag{9}$$

This expression states that the internal pressure is proportional to the difference of the two strain measurements. Values for cell diameter, case thickness, or Young's Modulus can be measured directly but may require cell disassembly and material testing. However, these parameters may be estimated if experimental strain data can be fixed to a known pressure state of the cell. This could be the battery state at the moment of venting onset where strain is expected to reach a maximum value which can be related to the directly measured burst pressure described in "Direct Pressurization Test Methodology" section. Variability in this estimation between pressure and strain states would be influenced by the results of the direct pressurization testing.

Limitations of this approach could include localized failures within the cell. This could include deformations of interior battery components associated with events such as an internal short. Additionally, gas generation can be localized within the cell prior to failure (e.g. trapped between anode and

cathode layers), leading to non-uniform pressure distribution. To address this, initial tests will be performed with multiple sets of strain gauges on a single cell.

B. Design of Laboratory Setup

A test facility was designed and constructed to measure the external case strain of 18650 format batteries under thermal abuse conditions. The test setup consists of a heated cylindrical chamber with ports for instrumentation and a viewing window seen in Fig. 6(a). A 4 NPT size Schedule 160 steel pipe section is used to create the body of the chamber, and standard pipe flanges are threaded to the ends to provide rigid mounting points for re- movable end caps. The interior space within the chamber is 87 mm in diameter by 305 mm long. There are dedicated end caps for viewing the battery throughout testing and allowing instrumentation pass-throughs. Fig. 6(b) shows the completed instrumentation end cap which has ports for a thermocouple probe to measure chamber gas temperature, three reconfigurable pass-throughs for thermocouples and strain gauge leads, and an inlet and outlet for a remote purge system. Additionally, thermocouples are embedded into the main body of the test chamber to measure the temperature gradient within the steel and thus allow calculation of heat flux.

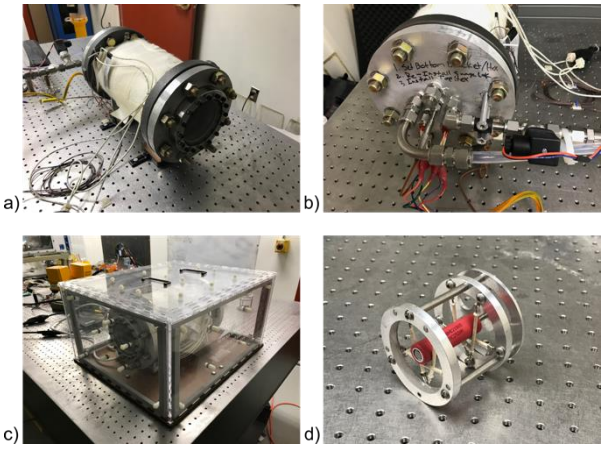

Fig. 6. Images of the test setup installed at New Mexico Tech including (a) the test chamber, (b) instrumentation end cap, (c) insulation structure, and (d) battery holder.

Preliminary testing of the chamber highlighted a need for high total power output from chamber heaters and sufficient insulation of the test chamber. The chamber body is evenly wrapped with nine electrical rope heaters each capable of outputting 260 W as to create even heating within the chamber interior. As achieving relatively high heating rates is important within the chamber to be able to subject batteries to different abuse scenarios, work has gone into insulating the test chamber. A flexible insulation wrap made of fiberglass, ceramic fiber, and Nomex is placed around the test chamber body immediately outside of the rope heaters and secured with stainless steel pipe clamps. The test chamber itself is also placed inside of another rigid insulation structure seen in Fig. 6(c). This structure is fabricated from laser cut acrylic sheeting and has a modular design of double-pane panels. A final step taken in improving heat transfer to batteries is the use of a helium environment inside the chamber. This improves heat transfer significantly as helium has a relatively high thermal conductivity value of 0.142 W/mK compared to a value of 0.024 W/mK for air.

A battery holder was designed and fabricated to securely hold a cell prior to and during venting within the center of the test chamber. Seen in Fig. 6(d), the holder uses high temperature MG wire with a series of aluminum rings and standoffs. This holder fits within inner diameter of the test chamber with minimal movement. The cradle shape of the wire is designed to allow the battery to expand freely throughout testing as to not cause any stress concentrations which would negatively affect strain measurements. A thumb nut and set screw are used in the last aluminum ring to create a hard stop for the battery in case venting causes a thrust which would otherwise cause the cell to move inside the chamber.

Data acquisition is performed with a National Instrument cDAQ system and controlled through LabVIEW. The system is configured to record temperature, strain, and pressure data as well as control the operation of inlet and exit valves used for remote purge of the gas within the chamber after a test. Four J-type thermocouples are embedded in pairs on opposite sides of the chamber wall. Each pair has a thermocouple at a depth of 3.3 mm and 10.1 mm which correspond to roughly 25% and 75% of the wall thickness respectively. K-type thermocouples are used to measure interior chamber gas temperature and surface temperature of the battery on the side of the case and on the positive terminal at the end of the vent cap. Chamber static pressure is also recorded and monitored throughout testing Each strain gauge is wired in a three-wire, quarter bridge configuration with 350 Ω resistors. This arrangement provides adequate thermal compensation as hoop and longitudinal strain values are to be subtracted from each other as previously discussed.

B. Heating Rate Calibration Series

A necessary step in the validation of the test setup was calibrating the system to have predictable interior heating rates as a function of the electrical power output of the heaters. Calibration tests were performed on the test chamber at electrical power values ranging from 468 W to 1,872 W by varying the input voltage to the electrical heaters with a variable autotransformer. Four tests were conducted by heating the chamber for 60 min at power settings corresponding to 20%, 40%, 60%, and 80% of maximum. All tests started with zero gauge pressure and the chamber at room temperature. Temperature and pressure data were recorded throughout.

While setting the heaters at a constant power is inherently a transient process, temperature increases can be approximated as linear to provide a nominal heating rate useful in comparison to other calorimetry testing on lithium batteries. Interior gas temperature increases and associated linear fits for this calibration testing are shown in Fig. 7(a). The nominal heating rates for the calibration tests follows a highly linear relationship with the heater setting as seen in Fig. 7(b) which provides confidence in the ability to interpolate between power settings. Extrapolation of the data yields a maximum possible rate of 6.51 ˚C/min at the maximum heater setting of 2,340 W. However, tests will likely be kept below this rate to minimize the risk of heater failures.

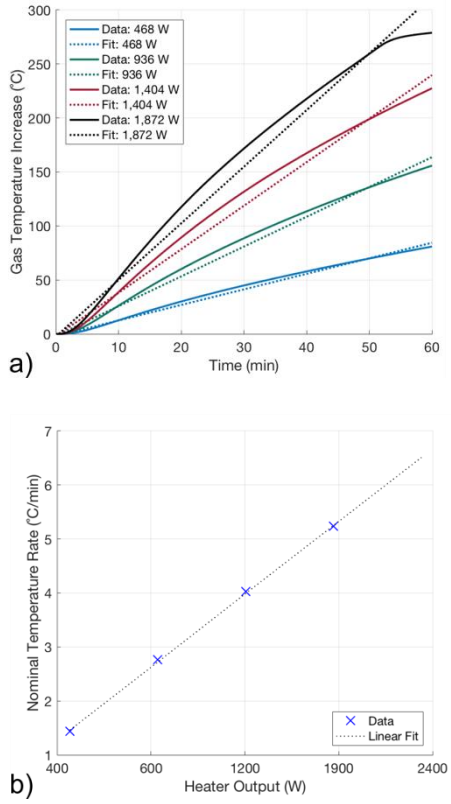

Fig. 7. (a) Gas temperature increase versus time and linear fits for the heating rate calibration test series, and (b) plotting the nominal heating rate versus electrical power input for these tests.

C. Planned Initial Test Series

An initial test series is planned with lithium cobalt oxide LG HE2 cells which should provide a strong baseline for comparison with other battery chemistries. This series will involve using cells charged to 100% SOC by performing charge and discharge cycles. Cells will be subjected to thermal abuse at a rate of 2 ˚C/min and 5 ˚C/min until failure is observed via the onset of venting. Trials will be performed at both heating rates with multiple pairs of strain gauges attached to individual cells to evaluate if there are any localized strain variations. Additional trials will be performed with a single pair of strain gauges on each battery and repeated in triplicate to determine the variation in strain and pressure trends during failure between cells of the same type.

IV. Summary and Conclusions

Understanding the internal pressure of a lithium battery under abuse conditions leading up to and at failure is an important metric in describing safety risks and how the external fluid dynamics of the venting process occurs. Two complementary experiments for describing the internal pressure of 18650 format lithium batteries have been developed and presented here. Both experiments are versatile in the use of actual batteries or their components and are not limited to any certain brands or cell chemistries.

A test apparatus has been built to directly pressurize vent caps removed from live batteries to measure burst pressure and opening area. A series of validation tests has been performed which demonstrates the accuracy of the test setup with circular orifices and the more complicated vent geometries seen on actual batteries. The second experiment uses strain gauges to non-invasively infer the internal pressure within cells which can be subjected to various rates of thermal abuse. This test apparatus has been constructed and calibrated.

Acknowledgements

This work is supported by Sandia National Laboratories and funding comes from the U. S. Department of Energy Office of Electricity under contract PO 1739875. Thanks goes to Heather Barkholtz for supplying battery vent caps used in this testing.

Sandia National Laboratories is a multimission laboratory managed and operated by National Technology and Engineering Solutions of Sandia, LLC., a wholly owned subsidiary of Honeywell International, Inc., for the U.S. Department of Energy's National Nuclear Security Administration under contract DE-NA0003525. SAND2017-10681 C.

References

[1] P. S. Grant, "Spray forming," *Progress in Materials Sci.,* vol. 39, pp. 497-545, 1995.

[2] R. D. Reitz and F. V. Bracco, "Mechanisms of breakup of round liquid jets." In *Encyclopedia of Fluid Mechanics*, Houston, TX: Gulf Publishing Company, 1986.

[3] E. P. Roth, C. C. Crafts, D. H. Doughty, and J. McBreen, "Advanced technology development program for Lithium-Ion batteries: Thermal abuse performance of 18650 Li-Ion cells," Sandia National Labs., Albuquerque, NM, Rep. SAND2004-0584, Mar. 2004.

[4] D. P. Finegan, M. Scheel, J. B. Robinson, B. Tjaden, I. Hunt, T. J. Mason, *et al.*, "In-operando high-speed tomography of lithium-ion batteries during thermal runaway," *Nature Commun.,* vol. 6, pp. 1-10, Apr. 2015.

[5] P. T. Coman, S. Rayman, and R. E. White, “A lumped model of venting during thermal runaway in a cylindrical Lithium Cobalt Oxide lithium-ion cell,” *J. Power Sources,* vol. 307, pp. 56-62, Mar. 2016.

[6] J. D. Anderson, *Modern Compressible Flow with Historical Perspective*, 3rd ed., Boston, MA: McGraw Hill, 2003.

[7] P. Hill and C. Peterson, *Mechanics and Thermodynamics of Propulsion*, 2nd ed., Pearson, 1991.

[8] W. C. Young and R. G. Budynas, *Roark’s Formulas for Stress and Strain*, 7th ed., New York, NY: McGraw Hill, 2002.

[9] A. P. Boresi and R. J. Schmidt, *Advanced Mechanics of Materials*, 6th ed., Hoboken, NJ: John Wiley & Sons, 2003.

[10] F. P. Beer, E. R. Johnston Jr., J. T. DeWolf, and D. F. Mazurek, *Mechanics of Materials*, 5th ed., New York, NY: McGraw Hill, 2006.

An Overview of Tools to Facilitate Documenting and Validating the Safety of an Energy Storage System Installation

Pam Cole
Pacific Northwest National Laboratory, Richland, Washington, USA

***Abstract*- This paper provides an overview of two energy storage system (ESS) compliance tools to help address the acceptability of the design and construction of stationary ESSs, their component parts, and the siting, installation, commissioning, operations, maintenance, and repair/renovation of ESSs within the built environment. These tools assist with the tasks of documenting and validating compliance with codes, standards, and regulations (CSRs) covering ESS safety, both the specific provisions that may address an ESS technology and its application or a situation in which the codes and standards may not provide specific provisions and the documentation and verification of the safety of the ESS are based on it being no more hazardous nor less safe than other ESS or similar technologies that are specifically covered in CSRs.**

***Keywords*- codes, standards, compliance, documentation, verification**

I. INTRODUCTION

Codes, standards, and regulations governing the design, construction, installation, commissioning, and operation of the built environment are intended to protect public health, safety, and welfare. These documents change over time to address new technology and safety challenges, so there is generally some lag time between the introduction of a technology into the market and the time it is specifically covered in model codes and standards developed in the voluntary sector. Development of a new code or standard can take 3 to 4 years from the initiation of the effort until the result is adopted. Typically, this takes on the order of 4 to 5 years and in some cases due to recent efforts to reduce the frequency of adoptions at the state and local level it could be over 6 years before new provisions covering ESS or other technologies are adopted. So, those seeking to deploy energy storage technologies or needing to verify an installation's safety may find it challenging to apply current CSRs to an ESS. Even when CSRs provide specific criteria, those deploying ESS technology must document compliance with the CSRs and those enforcing compliance must be able to verify it with their CSRs.

Under the U.S. Department of Energy's Energy Storage Safety Strategic Plan, developed with the support of the U.S. Department of Energy's Office of Electricity Delivery and Energy Reliability Energy Storage Program by Pacific

Northwest National Laboratory and Sandia National Laboratories, an Energy Storage Safety initiative with collaboration and involvement from many stakeholders has been under way since July 2015. One of three key components of the initiative involves CSRs affecting the timely deployment of safe ESSs. Their timely deployment is focused on how to document and validate compliance with current CSRs and in so doing validate that a proposed ESS installation is safe, as intended pursuant to the CSRs.

A task force was formed under the ESS Safety working group to address documenting and verifying compliance with current CSRs and through their efforts the Energy Storage System Guide for Compliance with Safety Codes and Standards [1] was developed and published in June 2016. In late 2016, another task force of stakeholders involved with the ESS safety initiative was formed, and through their efforts the Energy Storage System Safety–Plan Review and Inspection Checklist [2] was developed and published in March 2017. Acknowledgments of participants in each task force are included in each of the published documents.

As a result of the rapidly increasing demand to deploy stationary ESSs in the commercial and residential sector, the Energy Storage System Safety Working Group stakeholder involvement identified a critical need. The lack of guidance and resources to implement and facilitate new compliance processes in reviewing, documenting, and validating the safety of stationary ESSs is widespread throughout the United States (U.S.) and local jurisdictions that adopt and enforce national model codes and standards. Timely deployment of safe ESS is focused on how to document and validate compliance with current CSRs and, in so doing, validate that a proposed ESS installation is safe as intended pursuant to the CSRs.

Two ESS compliance tools were developed to help address the acceptability of the design and construction of stationary ESSs, their component parts and the siting, installation, commissioning, operations, maintenance, and repair/renovation of ESSs within the built environment. These tools assist with documenting and validating compliance with U.S. CSRs covering ESS safety, both specific provisions that may address an ESS technology and its application or a situation in which the codes and standards may not provide specific provisions and the documentation and verification of

the safety of the ESS is based on it being no more hazardous nor less safe than other ESS or similar technologies that are specifically covered in CSR. These tools are not intended to replace codes and standards. They are intended to simplify and clarify CSR compliance supporting the safe deployment of ESS in the current environment. The following is an overview of each of the compliance tools, a compliance guide, and a compliance checklist, developed under the U.S. Department of Energy's Energy Storage Safety Strategic Plan, with the support of the U.S. Department of Energy's Office of Electricity Delivery and Energy Reliability Energy Storage Program by Pacific Northwest National Laboratory and Sandia National Laboratories.

II. Tool 1: Energy Storage System Guide for Compliance with Safety Codes and Standards

The Compliance Guide (CG) is intended to facilitate the timely deployment of stationary ESSs in accordance with existing safety-related CSRs and other governing (adopted) criteria that are based on voluntary sector standards and model codes that may not have been updated to specifically and prescriptively cover all ESS technologies or their intended applications. In this role, the CG is intended to address challenges related to documenting and verifying compliance with CSRs that have not been updated to more specifically address ESS technologies.

The CG provides 1) assistance to those who need to document compliance with current safety-related codes and standards in order to develop and deploy ESSs and 2) guidance for those responsible for approving and/or accepting ESSs or for verifying their compliance with the same codes and standards on an ongoing basis.

A. Energy Storage System Product and Component Review and Approval

Documenting or validating the safety of an ESS, either as a complete "product" or as an assembly of various components, involves a review of the product, its components, and the manner in which they are combined to create the product. An ESS resembles a product—either a self-contained piece of equipment or an assembly of matched components. The more the ESS is composed of component parts assembled in the field, the greater the reliance on codes and standards that address component installation, rather than complete system installation, as a basis for determining the safety of the ESS (e.g., the ESS "product" is essentially constructed in the field not at a factory). Fig. 1 is a flow chart showing the general process of documenting and validating the safety of an ESS product or component. If no available standards cover the ESS product or its components (or one chooses to not document safety to standards that are available), then alternative methods of evaluating and documenting safety will likely be needed. The various steps associated with reviewing and approving ESS products and components are described below and are covered in more detail in the CG.

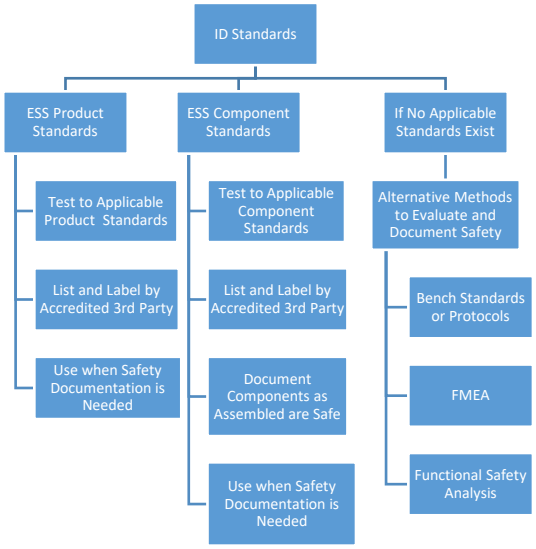

Fig. 1. Review and approval of Energy Storage System Products and their component parts.

1. Determine safety-related testing standards that are applicable to the ESS as a complete prepackaged system or to the components of an ESS when not a complete prepackaged system. These standards will either be included by reference in higher level existing codes and standards applicable to the built environment and or can be adopted and applied separately. Table I is a short list of some of the safety-related testing standards that could be used as a basis for testing and listing systems and system components. More detail about these and additional standards is provided in Appendix C (components) and Appendix D (systems) of the CG. In addition to the standards listed in Table I, specifications and related documents promulgated by utilities may address the acceptability of an ESS for location on or interconnection with the power grid. These standards include IEEE 1547 and may include others beyond those listed in Table I that are adopted by reference in the National Electrical Safety Code (IEEE C2).

Table I
Energy Storage System and Component Standards[1]

Title	Designation
Molded-case circuit breakers, molded-case switches, and circuit-breaker enclosures	UL[(a)] 489
Electrochemical capacitors	UL 810A
Lithium batteries	UL 1642
Inverters, converters, controllers and interconnection system equipment for use with distributed energy	UL 1741

resources	
Batteries for use in stationary applications	UL 1973
Second-use batteries	UL 1974 (proposed)
Recommended practice and procedures for unlabeled electrical equipment evaluation	NFPA[(b)] 791
Standard for interconnecting distributed resources with electric power systems	IEEE 1547
Recommended practice and procedures for unlabeled electrical equipment evaluation	NFPA 791
Outline for investigation for safety for ESSs and equipment	UL 9540
Safety for distributed energy generation and storage systems	UL 3001 (proposed)
Safety standard for molten salt thermal energy storage systems	ASME TES[(c)]-1 (proposed)
a. UL = Underwriters Laboratory b. NFPA = National Fire Protection Association c. ASME TES = American Society of Mechanical Engineers Thermal Energy Storage	

[1]International Electrotechnical Commission (IEC) and other non-U.S. CSRs are not identified in the short list of Table 1 or the more robust list in Appendix C and D of the CG. IEC and other non-U.S. CSRs are outside of the scope of this work.

1. If relevant testing standards are not identified, they may be under development by a Standards Development Organization (SDO) or by a third-party testing entity that plans to use them as the basis for safety testing until a formal standard has been developed and approved by an SDO. Documents that precede formal standards developed by an SDO can be referred to as bench standards, protocols, outlines of investigation, or acceptance criteria. They can provide some guidance on testing until a formal standard is published. In many cases these initial documents form the initial draft of a standard developed by an SDO.
2. As a manufacturer of an ESS or component, conduct internal testing (e.g., self-testing) as required by the standards (or in accordance with bench standards, protocols, or acceptance criteria) applicable to the ESS or component. Then, based on the test results, determine whether the system or component design or construction need to be changed, implement those changes, and re-test/make changes until the system or component tests indicate compliance.
3. In conducting internal tests as a manufacturer, it is probable that those experiences will lead to questions about the test standard being used or suggested changes to improve the usability or accuracy of the standard.
4. Secure the services of an approved third-party testing agency that can test the ESS or component to determine if it complies with applicable standards.
5. When no standard is available with which to evaluate the safety of an ESS or component and a new standard is not under development, a bench standard or protocol may be available or could be developed by a third-party testing agency for use in assessing the acceptability of the system or component from a safety standpoint.
6. Prior to establishing any standard or bench standard, a failure modes and effects analysis (FMEA) could be prepared to document the safety of the ESS or its components from a reliability standpoint based on the application and use of IEC 60812, Analysis Techniques for System Reliability–Procedure for Failure Mode and Effects Analysis. Alternatively, consider the application of NFPA 791, which covers how to assess the acceptability of unlisted electrical equipment.
7. After an ESS or component has been found to comply with one or more appropriate safety standards, bench standards, protocols, etc., via testing by an approved third-party testing agency and their issuance of one or more relevant test reports, the test report can be used as documentation of system/component safety.
8. Secure the services of an approved third-party certification agency that can conduct ongoing monitoring of the continued production of the ESS or component as well as the manufacturer's quality control and manufacturing processes.
9. Through those services, the third-party agency is then in a position to authorize the manufacturer of the ESS or component to list the system or component as complying with the criteria (standard, protocol, etc.) used as a basis for safety testing and label it as such. This will depend on the scope of the safety testing conducted and the findings associated with the review of ongoing production and quality control processes.
10. Use the results from the activities above (testing and listing) when documenting compliance with safety-related codes and standards for any authorities having jurisdiction (AHJs).
11. After documenting or verifying the acceptability of the ESS as a system or individual system components, the safety of their application in, on, or around buildings and facilities must be addressed.
12. Looking toward an actual installation, those who are pursuing application and use of the ESS or components should identify the AHJs that have authority over ESS installation and the CSRs they have adopted to address its system safety.

B. Review the Energy Storage System as a Complete Product

When considering an ESS as an assembly of components, a standard for a complete "product" is likely to refer to various components and component standards within the ESS standard and then simply tie them together. One approach to assessing the safety of the ESS "product" is to confirm that the components meet relevant component standards and then assess the acceptability of their assembly as an ESS. Another approach is to consider the ESS "product" as a black box and how the entire ESS would function as an assembly of components, and then evaluate the ESS "product" against an appropriate standard covering resultant assembly of components. If the ESS "product" satisfies the provisions of the standard and related design criteria and performance metrics, then the components of the ESS would be considered to be in compliance with the standard. Through third-party certification programs, ongoing production of the ESS "product" would be inspected to ensure that subsequent production is identical to the ESS that was tested and found to comply with the standard. Those certification programs would also review and assess the administrative and quality control aspects associated with the manufacturer of the component. When a standard considers the ESS as a complete product, by default it considers performance of one or more components within the requirements of the standard, so the safety of the components is evaluated as a result of testing of the entire ESS.

Standards covering an ESS as a complete product, such as UL 9540, Outline for Investigation for Safety for Energy Storage Systems and Equipment, or ASME TES-1, Safety Standard for Molten Salt Thermal Energy Storage Systems, and the associated conformity-assessment activities to document and validate compliance would be of primary relevance to manufacturers producing an entire ESS "product." But ESS component manufacturers would want to be familiar with those standards to ensure their components comply with them when used in the ESS. Those who assemble a complete ESS "product" onsite from various components would likely have to document compliance on the basis of that standard, so they would benefit from using components that complied with relevant component safety standards. In addition, those who create an ESS "product" onsite by assembling various ESS components may also be more likely to have installation-related codes and standards that address the assembly of the components. Utilities, building regulatory agency staff, and others engaged in validating compliance would have an easier time approving ESS installations when the ESS "product" as a whole is validated as complying with applicable standards. In the absence of such standards, and until they are developed, it is more likely that approval of an ESS "product," whether prepackaged or assembled onsite from various components, would have to be pursued on a case-by-case basis working with the applicable parties involved in documenting and validating the safety of the ESS.

C. Energy Storage System Installation Review and Approval

A review of the installation of an ESS covers what is involved in documenting or validating the safety of an ESS as installed in, on, or adjacent to buildings or facilities. This information does not cover the safety of the ESS as a complete "product" or the safety of the individual components of the ESS (as discussed in the previous section). It covers the installation of the ESS when tested and listed as a complete product or the assembly and installation of the components making up the ESS when the ESS is constructed onsite (as opposed to being a factory-constructed "product"). That said, the installation-related criteria that are part of the ESS "product" or component listing will also apply.

Installation provisions simply cover where and how the ESS interacts with its environment to ensure the surrounding environment is not adversely affected by an incident associated with the ESS and, in turn, that the ESS is not adversely affected by a natural or manmade incident associated with the surrounding environment. When an ESS has not been listed as a complete "product" and instead is an onsite assembly of ESS components, the installation provisions will have a greater impact on the ESS because they will address the acceptability of how the components are aggregated as an ESS onsite to construct the ESS.

The topics in Table II should be addressed when documenting and validating the safety of an ESS installation.

TABLE II
TOPICS ASSOCIATED WITH AN ENERGY STORAGE SYSTEM INSTALLATION

Topic	**Description**
Administration	The scope and purpose of the CSR and how it applies to new and existing ESS installations. These provisions will define what is covered in the CSR and how the provisions will apply to the ESS as a product or components and their installation.
References	Any other code, standard, or regulation document that is related to the installation of the ESS will generally be referenced and as such becomes part of the CSR in which is it referenced.
Definitions	All relevant terms are defined. They can be critical in "sorting out" what does and does not apply to an ESS installation and, if applicable, how the provisions are to be implemented.

ESS equipment and components	How to define the ESS (product, factory-matched components, field designed, and assembled) and what applies to documenting and verifying the safety of the ESS related to any design or construction that takes place offsite (e.g., as manufactured).
Siting	Location in relation to various aspects of the site (e.g., parking, roads, buildings, etc.), as well as criteria relevant to location in, on, or adjacent to one or more buildings.
Interconnection with other systems	Connections to communications, electrical inputs and outputs, and other energy-related systems on the site as well as any interconnections with an electric utility.
Ventilation, exhaust, and thermal management	Air flows, relative pressures, temperature and intake, and exhaust locations associated with the normal operation of the ESS.
Fire protection	Fire and smoke detection, fire suppression, containment of fire and smoke, smoke removal, containment of fluids and effluent from, firefighting operations, access/egress, and signage.
Commissioning	Validating the proper operation of the ESS and all control and emergency systems associated with the ESS.

D. Additional Resources in the Compliance Guide

The CG also covers frequently asked questions in order of when they are likely to occur along the timeline associated with the development and deployment of an ESS. Appendices augment the core materials provided in the body of the CG which include an overview of conformity assessment, a list of standards related to ESS components, entire ESSs, and installation of ESSs. Lists of related standards are subject to change as new codes and standards are developed and existing ones are updated; they are augmented by a monthly report compiled by Pacific Northwest National Laboratory (PNNL) that covers the ESS-related activities of 10 U.S. SDOs.

The ongoing development and deployment of ESS technology, anticipated use of the CG, and future availability of details associated with particular ESS technology installations, mean the CG can be further enhanced as technologies and practices evolve. The author welcomes suggestions for future enhancements of the CG.

III. Tool 2: Energy Storage System Safety – Plan Review and Inspection Checklist

The purpose of the Plan Review and Inspection Checklist (Checklist) is to help AHJs that are validating ESS installations recognize the issues they have to look out for. It could also serve those who have to document the safety of their ESSs installations (e.g., permittees). The Checklist augments the CG and acts as a stand-alone document that can be customized to meet more specific needs of stakeholders/users.

The Checklist is broken down into many sections (listed below) to streamline the plan review and inspection process. Refer to the actual Checklist for all provisions under each section. Figs. 2 and 3 are screenshots showing the Cover Page and ESS Technology Information of the Checklist (the first 2 bulleted items below). The complete Checklist is 30 pages long.

A. Energy Storage System Plan Review/Inspection Checklist Sections

- Cover Page (project name, address, facility owner, ESS owner, type of ESS, ESS owner, ESS operator)
- ESS Technology Information
- Pre-Inspection/Plan Review
- Self-Contained, Prepackaged ESSs
- Pre-Engineered ESSs
- Engineered and Field-Constructed ESSs
- Repairs to Existing ESS
- Additions to Existing ESS
- Renewal or Renovation of Existing ESS
- General Siting of ESS and Associated Equipment, Components and Controls
- Outdoor Installations of ESS and Associated Equipment, Components and Controls
- Rooftop Installations of ESS and Associated Equipment, Components and Controls
- Interior Installation of ESS and Associated Equipment, Components and Controls
- Interconnections with Other Systems
- Ventilation, Thermal Management and Exhaust
- Fire Protection – Fire and Smoke Detection
- Fire Protection – Fire Suppression
- Fire Protection – Fire Containment
- Fire Protection – Removal of Smoke
- Fire Protection – Containment of Fluids
- Fire Protection – Signage
- Commissioning

Energy Storage System (ESS) Plan Review/Inspection Checklist

Date: _____/___/_____

Project Name _____

Address _____

State: _____ County: _____ Jurisdiction: _____

Facility Owner (owner of facility where ESS is installed): _____ I.C.E. #_____

ESS Owner (owner of ESS if different than facility owner):_____ I.C.E. #_____

☐ New System ☐ Addition ☐ Renewal or Renovation ☐ Repair

System Manufacturer(s): _____

System Installer: _____

System Integrator (if one is involved in the project):_____ I.C.E. #_____

System Operator: _____ I.C.E. #_____

System Name: _____

System Address: _____

System Location (in relation to the primary electrical meter): _____

Services Provided: _____

Fig. 2. Energy Storage System Plan Review/Inspection Checklist - Cover Page.

ESS Technology Information			
Type of ESS			
ESS chemistry (if electrochemical)			
Enclosure Type			
Footprint Area (ft.²)			
Weight (lbs.)			
Overall Dimensions L x W x H (ft.)	Length	Width	Height
Rated Continuous Discharge Power (kW)			
Input Voltage into the ESS (VAC)			
Output Voltage (nominal)(VAC)			
Frequency (Hz)			
Number of phases (input and output)	Input	Output	
Duty cycle (if applicable)			
Maximum short circuit current (A)			
Auxiliary (if applicable)	Input voltage (V)	Output voltage (V)	
Auxiliary (if applicable)	Current (A)	Frequency (Hz)	
Rated Discharge Energy (kWh)			
Minimum Discharge Time (min.)			
Maximum Discharge Time (min.)			
Operating Temperature Range (ºF)			
Stored Energy Capacity (kWh)			
Self-discharge Rate (% energy loss/day)			
Liquid Capacity (Gal.) needed for secondary containment of flow batteries			
Special environmental ratings and limitations as applicable	Seismic	Indoor	Outdoor

Fig. 3. Energy Storage System Plan Review/Inspection Checklist – ESS Technology Information.

IV. Conclusion

The ESS industry is rapidly developing new chemistries, system types, and applications. The codes and standards that provide the benchmark for documenting and validating what is and is not considered safe are dynamic and regularly updated. Those documenting and validating ESS compliance must adjust to the ongoing changes. Hence, the CG and Checklist, as they exist today, have a limited "shelf life." They will need regular updating and enhancement as living documents over time. The ESS Plan Review and Inspection Checklist will be further enhanced to reflect the continuing evolution of ESS technology development and deployment, the anticipated use of the CG, and the future availability of details associated with particular ESS technology installations. It will be included in the ESS Guide for Compliance with Safety Codes and Standards and can be accessed at http://www.sandia.gov/ess. The author welcomes suggestions for future enhancements of this document.

The author also encourages all who have a stake in ESS safety to collaborate with the ESS Safety Working Group in the development and deployment of future versions of the CG and Checklist and to identify new resources that foster timely development and deployment of safe ESSs. The CG and Checklist will be updated in 2018 and will include codes and standards updates, new codes and standards development, case studies and new resources such as the ESS Safety Roadmap Focus on Codes and Standards monthly report. Furthermore, based upon feedback received from the ESS Safety Working Group, the CG will also include lessons learned and gaps in knowledge that require research and analysis that can serve as a basis for criteria in those codes and standards.

References

[1] P. C. Cole and D. R. Conover, "Energy storage system guide for compliance with safety codes and standards," Pacific Northwest National Lab. and Sandia National Labs., Richland, WA and Albuquerque, NM, Rep. PNNL-SA-118870/SAND2016-5977R, Jun. 2016.

[2] P.C. Cole and D.R. Conover, "Energy storage system safety: Plan review and inspection checklist," Pacific Northwest National Lab. and Sandia National Labs., Richland, WA and Albuquerque, NM, Rep. PNNL-SA-124486/SAND2017-3066 R, Mar. 2017.

Optimal Control for Battery Storage Using Nonlinear Models

Di Wu, Patrick Balducci, Alasdair Crawford, Vilayanur Viswanathan, and Michael Kintner-Meyer
Pacific Northwest National Laboratory, Richland, WA 99354

***Abstract*- Battery storage systems (BSSs) have become increasingly popular for grid applications due to the growing need for flexibility and reserve in power systems with rapidly developed renewable generation. Successful assessment and deployment of a BSS require optimizing its operation, and thereby, maximizing the potential benefits. In existing studies on economic assessment and optimal scheduling of a BSS, modeling of charging/discharging operation and the corresponding impacts on state-of-charge (SOC) is over simplified, which could result in inaccurate assessment results and even infeasible operation schedules. This paper proposes a general model to capture varying SOC change rate as a nonlinear function of charging/discharging power and SOC level. An optimal control is developed for the BSS based on the proposed nonlinear model. The optimal control using a nonlinear model is compared with a representative linear optimization method using a simplified model through a real-world energy storage evaluation project to show the significance of the proposed method.**

***Keywords*- battery, energy storage system, dynamic programming, nonlinear model, optimization.**

NOMENCLATURE

$E_{\max}$	Battery energy capacity.
K	Number of time periods in optimization time window.
p_k	Power exchange between BSS and grid (measured at the grid connection point) during time period *k*, which is positive when injecting power into grid, i.e., using generator convention.
p_k^{batt}	Rate-of-change of energy stored in the battery at the end of time period *k*, which is positive when the battery is discharged.
$p_{\max}^{+}, p_{\max}^{-}$	Maximum power (i.e., measured at the grid connection point) that can be injected and withdrawn into/from grid, respectively.
$r_{\text{ch}}, r_{\text{disch}}$	State-of-charge (SOC) change rate per 100 kW for charging and discharging, respectively.
$\underline{S}_k, \overline{S}_k$	Lower and upper bounds of SOC during time period *k*, respectively.
s_k	Battery SOC at the end of time period *k*.
ΔT	Time step size.
η^{+}, η^{-}	Discharging and charging efficiency of the battery storage, respectively, including components such as conductor, power electronics, and battery.
$\eta(\cdot)$	Marginal round-trip efficiency as a function of SOC.
λ_k	Energy price of time period *k*.

I. INTRODUCTION

Operation of the electric power sector requires flexibility to realize instantaneous balance between generation and constantly changing demand. Energy storage has been a candidate for meeting such a flexibility requirement for years. With the rapid growth of renewable energy, the inherent uncertainty and variability present difficulties and challenges to power system operators. Recent developments and advances in energy storage and power electronics technologies are making their application a viable solution for grid problems. As many countries place greater emphasis on renewable generation, energy storage is becoming increasingly important and holds substantial promise for transforming the electric power industry.

Many studies have been devoted to optimization and evaluation of BSSs for various grid applications. Studies [1] and [2] are dedicated to various battery technologies and methods of assessing their economic viability and impacts on power systems. In 2007 [3], the authors evaluate the economic performance of NaS batteries for energy arbitrage and flywheels for regulation services, based on fixed utilization factors for NYISO and PJM systems. Reference [4] incorporates realistic CAISO regulation signals and battery responses to yield more granular results. In [5], the authors investigate the application of BSS to relive transmission line thermal constraints, and thereby, increase the transfer capability. Based on a case study, an economic analysis of benefits and costs is provided. Reference [6] presents a distributed algorithm to optimally coordinate energy storage with distributed generators. In [7], an evaluation framework and co-optimization are proposed to assess BSS economic performance considering multiple grid applications simultaneously, including energy arbitrage, balancing services, capacity value, distribution upgrade deferral, and outage mitigation. Reference [8] considers an application bundle, including energy and demand charge reduction. A programming-based method is developed for economic assessment and optimal sizing of behind-the-meter BSSs. In [9], the authors develop a peak-shaving control algorithm to determine battery charging and discharging operation, and then calculate the economic benefits in demand charge reduction. In

[10], an analytical optimal sizing method is proposed based on objective quantitative analysis of costs and benefits for customer-side BSS, which could identify key factors that affect optimal sizing.

These studies optimize the charging/discharging operation to best utilize the limited power and energy capacity of BSS and then assess the economic performance accordingly. Nevertheless, the methods that are used to determine the optimal BSS charging/discharging schedule are not capable of accurately modeling BSS operation. For example, most of these studies (e.g., [5] and [9]) simply use a constant round-trip efficiency (RTE) to capture BSS losses. However, the same RTE with different one-way charging/discharging efficiencies may yield different optimal operating schedules. More importantly, due to the inability to represent one-way efficiencies in optimization, one cannot accurately estimate the SOC during charging (or discharging), and therefore, could obtain an infeasible operating schedule. While the optimal control methods in some existing studies such as [7] are based on one-way efficiencies, they can handle constant efficiencies, but not varying efficiencies. In [11], energy storage is studied for energy and demand charge reduction using a circuit model that expresses battery terminal voltage and current as nonlinear functions of the SOC. The circuit model assumes constant internal voltage and requires significant efforts to identity battery rated energy rated capacity and model parameters. It may not be able to provide required accuracy and is difficult to implement in practice. Furthermore, it is not capable of modeling varying charging/discharging capabilities at different SOC levels. To overcome these limitations, this paper proposes a general BSS model that expresses the SOC change rate as a nonlinear function of charging/discharging power and SOC level. An optimal control method is then developed to utilize the nonlinear model to determine an optimal schedule of BSS operation and evaluate the corresponding benefits.

The rest of this paper is organized as follows: Section II reviews a typical existing method using constant efficiencies to determine the optimal control of a BSS. In Section III, we first discuss the shortcomings and limitations of existing methods with constant efficiency models, and propose a nonlinear model that can more accurately capture the impacts of SOC and operating power on BSS operation. Then, we propose an innovative optimal control method that is capable of incorporating the proposed general nonlinear model for BSS scheduling and evaluation. In Section IV, the proposed and existing methods are used for energy arbitrage analysis in a real-world energy storage project as an example to show the significance of the proposed method. Finally, concluding remarks are offered in Section V.

II. Existing Methods with Constant Efficiency Model

In this section, we review a representative method using a BSS model with constant efficiency to determine optimal battery control for economic assessment and operational scheduling. Because the amount of energy stored in a BSS is limited, the charging/discharging operations at different time periods are interdependent. For example, injecting more energy into the grid in one hour increases the benefits for that hour, but leaves less energy for future use, and therefore may reduce the overall economic benefits. Therefore, the optimal scheduling must be performed over multiple time periods. A BSS also has charging/discharging power capacity, for which different grid services may compete against each other. For example, increasing discharging power for energy arbitrage service decreases the battery's ability to provide other services. Moreover, there are losses associated with a BSS charging/discharging operation, which must be modeled and considered in the optimal scheduling formulation in order to obtain a profitable and effective operating plan.

In the case of energy arbitrage, the objective function is the net benefits of battery charging/discharging for given hourly energy prices over a look-ahead time horizon, as expressed in (1)

$$\sum_{k=1}^{K} \lambda_k p_k \Delta T\,, \tag{1}$$

where p_k is the power exchange between BSS and the grid (measured at the grid connection point) during time period *k*, which is positive when injecting power into grid, K is the number of time periods in the optimization time window, λ_k is the energy price of time period k, and ΔT is time step size. The charging/discharging power must be within the operating range considering both battery and energy conversion system power rating,

$$-p_{\max}^{-} \le p_k \le p_{\max}^{+}\,, \tag{2}$$

Where $p_{\max}^{-}$ and $p_{\max}^{+}$ are the maximum charging and discharging power of the BSS, respectively. The rate of change of energy stored in BSS p_k^{batt} is related to charging/discharging power at grid coupling point p_k using the charging/discharging efficiencies as

$$p_k^{\text{batt}} = \begin{cases} p_k/\eta^{+} & \text{if } p_k \ge 0 \text{ (discharging)}, \\ p_k\eta^{-} & \text{if } p_k < 0 \text{ (charging)}, \end{cases} \tag{3}$$

where η^{+} and η^{-} are the discharging and charging efficiencies, respectively. The change in SOC can be calculated as

$$\Delta s_k = p_k^{\text{batt}} \Delta T / E_{\max}\,, \tag{4}$$

where $E_{\max}$ is the rated energy capacity of the BSS. Finally,

the dynamics of SOC can be expressed as

$$s_{k+1} = s_k - \Delta s_k \,, \tag{5}$$

where s_k is the SOC level of the BSS at the end of time period *k*, and Δs_k expresses the change in SOC during time period k. The SOC level needs to be restricted to be between its lower and upper bounds as expressed in (6), either for safe operation of the BSS or to meet user specifications.

$$\underline{S}_k \le s_k \le \overline{S}_k \,. \tag{6}$$

With the objective function and various constraints, we are now ready to present the optimization problem formulation to determine the optimal charging/discharging operation for energy arbitrage application as follows.

$$\mathbf{P}_1 : \max_{p_k, p_k^{\text{batt}}, \Delta s_k, s_k} \sum_{k=1}^{K} \lambda_k p_k \Delta T \,, \tag{7}$$

subject to constraints from (2) to (6). It has been shown in [7] and [8] that optimization tricks can be applied to convert optimization problem $\mathbf{P}_1$ to a standard linear programming problem, which is then solved to determine the optimal charging/discharging operation.

III. Proposed Optimal Control Method with Nonlinear Model

This section first discusses the shortcomings and limitations of existing methods using constant efficiency and rated discharging/charging power. A general nonlinear model is then proposed to better represent varying charging/discharging power capabilities and efficiencies at different SOC and output power levels. Finally, an optimal control is developed to utilize the proposed general nonlinear battery models for optimal scheduling and economic assessment. The same energy arbitrage application presented in the previous section is again used as an example to better explain and compare the proposed method with the existing method.

In the method presented in Section II, the change in SOC with different charging/discharging power is estimated using battery-rated capacity and constant charging/discharging efficiencies. Such a method is subject to several disadvantages and limitations:

- The energy that can be discharged or charged to the battery depends on discharging/charging power. Using a single rated value $E_{\max}$ for different power operation cannot accurately model the capability of a BSS.
- The feasible charging/discharging power also depends on the SOC. The BSS may not be able to operate at any value within $[-p_{\min},\ p_{\max}]$ for some SOC.
- The overall one-way efficiencies of the BSS need to be estimated based on battery efficiency, inverter efficiency, power for auxiliaries, and other factors. The estimation of each of these components requires approximation and introduces error that can be compounded.
- The charging/discharging efficiency also varies with a BSS operation, which cannot be accurately modeled using constant efficiencies.

A general nonlinear model is proposed to address these limitations, as shown in (8) and (9),

$$p \in \mathcal{P}_s \tag{8}$$

$$\Delta s = f(p, s) \tag{9}$$

where *p* denotes the charging/discharging power from a BSS, $\mathcal{P}_s$ denotes feasible set of *p* for an SOC level of *s*, and Δs denotes SOC change rate, which is a function of *p* and *s*.

Such a nonlinear model can be obtained by experimenting and operating a BSS under various conditions such as operating mode, power, SOC, and temperature. The entire process of constructing the nonlinear BSS model can be automated by programming experiment and using a script to process the recorded data. The SOC level is measured and recorded for different charging/discharging power outputs. With the outputs, we can easily determine the feasible operating power ($\mathcal{P}_s$) at different SOC (*s*), and determine change of SOC (Δs) as a function of charging/discharging power (*p*) and SOC (*s*). As an example, a 1 MW/3.2 MWh vanadium redox BSS is evaluated for an array of charging/discharging power. The corresponding Δs function in (9) is plotted in Fig. 1.

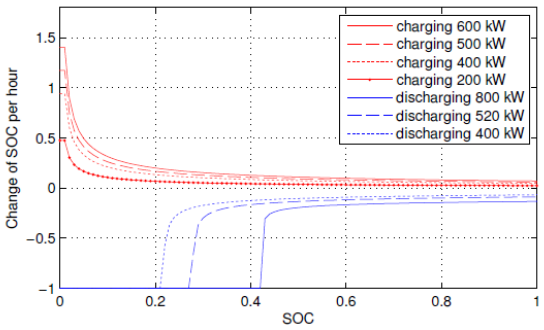

Fig. 1. SOC change rate versus SOC level for different charging/ discharging power levels.

As can be seen, the change in SOC rate varies with the SOC level. At the same SOC level, different charging and discharging power levels also affect the change in the SOC rate. In addition, one can identify the feasible operating power set at different SOC levels in (8). For example, when $s \ge 43\%$, the BSS can be operated on all 7 charging/discharging power levels. When $43 \ge s \ge 28\%$, the BSS cannot be discharged at

800 kW, and Ps only contains the remaining 6 operating power levels.

Based on the nonlinear model, optimal control of a BSS is developed as follows.

For any time period *k*, with 1) the feasible operating power range for different s_k and 2) expression of Δs (analytical or as look-up tables), we can relate the change in SOC in each time period *k* to the operating power and SOC,

$$p_k \in \mathcal{P}_{s_k}, \tag{10}$$

$$\Delta s_k = f(p_k, s_k). \tag{11}$$

Note that the constant efficiency model represented by constraints from (2) to (4) can also be converted to the same form as (10) and (11). Therefore, we can formulate a more simplified but general optimization problem as follows:

$$\mathbf{P}_2: \max_{p_k, \Delta s_k, s_k} \sum_{k=1}^{K} \lambda_k p_k \Delta T, \tag{12}$$

subject to constraints (10), (11), (5), and (6). Such a method removes the need to estimate the rated energy capacity and discharging/charging efficiencies and improves the modeling accuracy related to how different charging/discharging operations affect the SOC. Note that both $\mathbf{P}_1$ and $\mathbf{P}_2$ are deterministic optimization and do not explicitly address the uncertainty associated with the prices. For operation scheduling, one can take the expected value of prices as input and the optimization maximizes the expected benefit. The receding horizon control helps to mitigate the impacts of price uncertainty on the optimal solution.

Compared with $\mathbf{P}_1$, the formulation in $\mathbf{P}_2$ better models the BSS operation, but is more challenging to solve because it is generally a nonlinear and nonconvex optimization problem. The simplest solution strategy is the enumeration method, but this method is generally computationally prohibitive. For example, with a 24-hour look-ahead window and 15-minute time step size, there are 96 time periods the BSS operation needs to be explored. If we discretize the feasible SOC range at each period into 100 values, the number of possible charging/discharging operation combinations is 10,096. The charging/discharging power limits can eliminate some infeasible combinations. Nevertheless, this still leaves us with a possible solution space with extremely high dimensionality. The dynamic programming (DP) method has many advantages over the enumeration scheme. The most important one is the reduction in the dimensionality of the problem. With DP, infeasible combinations can be detected *a priori*, and information about previously investigated combinations can be used to eliminate inferior combinations. This will significantly improve efficiency. A DP algorithm is developed in [11] to minimize the customer electricity bill based on a circuit model. Herein, a DP algorithm is proposed solve the optimization in $\mathbf{P}_2$ using the proposed nonlinear battery model to maximize the revenue from energy arbitrage. The scheduling problem is first divided into stages, and each stage *k* represents a scheduling period (e.g., 15 minutes). Each stage is divided into states $\{s_k\}$. A state represents the SOC level and encompasses the information (including the state trajectory previous to current stage and the corresponding benefit) required to move from one state in a stage to another state in the next stage. At each stage *k*,

1) all feasible operations are first explored.
   a) The feasible operating power at the grid coupling point is determined based on (10).
   b) The corresponding change of the SOC is calculated for different feasible power levels based on (11).
   c) The corresponding SOC is evaluated using (5) and checked against (6) to eliminate any infeasible operation.
   d) The corresponding cost/revenue is calculated for all feasible operating power levels based on the objective function in (12).
2) the maximum arbitrage value in stage *k* with state *J* is then calculated as

$$R(k, J) = \max_I \left[U(k-1, I; k, J) + R(k-1, I)\right] \tag{13}$$

where $R(k, J)$ is the maximal arbitrage value at state (k, J), and $U(k-1, I; k, J)$ is the energy revenue/cost associated with power discharging/charging operation that transits from state $(k-1, I)$ to (k, J).

IV. Case Study

The Washington State Clean Energy Fund (CEF) focuses on deployment and demonstration of energy storage in an effort to explore its role in Washington State and to assess its value to Washington State's utilities and citizens [12]. To maximize the value of the CEF, Pacific Northwest National Laboratory has worked with Washington State and three winning teams, including Avista Utilities, Snohomish PUD, and Puget Sound Energy, to demonstrate and assess a diverse scope of applications for energy storage, such as energy arbitrage, regulation and load following services, Volt/Var control, load-shaping, outage mitigation, and deferment of distribution system upgrade. The evaluation framework together with these demonstration projects will inform and empower other utilities in Washington State and in the region, storage technology developers, and state regulators to prudently and confidently pursue the deployment of energy storage. In this paper, as an example, energy arbitrage assessment is performed for a UniEnergy Technologies battery system to show the significance of the proposed method. The battery system has

been placed and tested at Turner substation in Pullman, Washington. The economic evaluation is performed for a BSS that contains two identical vanadium-flow battery assemblies with total combined ratings of 2 MW/6.4 MWh. While the BSS is capable of providing 6.4 MWh from fully charged to fully discharged, about 10.7 MWh is required to recharge the BSS, resulting in an average RTE equal to 0.6. The SOC change rate versus SOC with different charging/discharging levels for a single assembly (1 MW/3.2 MWh) is plotted in Fig. 1. The Mid-Columbia prices from 2011 to 2015 have been obtained from Powerdex [13] and used for arbitrage analysis in this work.

The optimal charging/discharging operations are determined using 1) optimization $\mathbf{P}_1$ with constant efficiency and discharging/charging power capability (existing method), and 2) optimization $\mathbf{P}_2$ with the nonlinear model (proposed method). The corresponding annual benefits are plotted in Fig 2. As can be seen, the two methods generate very different results. The estimated benefits using the proposed method are much higher than those of the existing method in all 5 years, and the difference is as much as 80% of the annual benefits from the existing method.

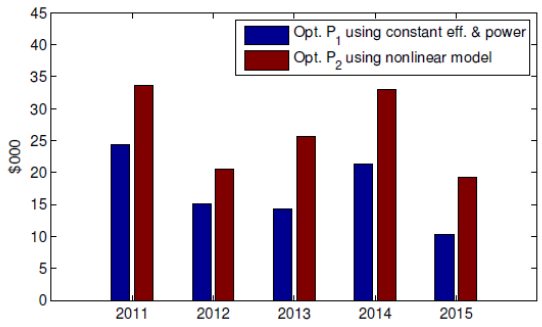

Fig. 2. Annual benefits in energy arbitrage.

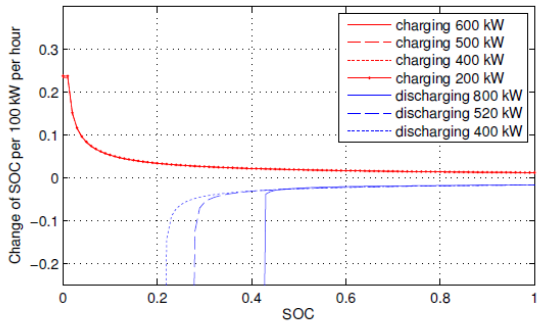

Fig. 3. SOC change rate per 100 kW versus SOC for different charging/discharging power levels.

To understand cause of the difference, the characteristics of a BSS are further explored. The SOC change rate per 100 kW versus the SOC for different charging/discharging power levels is plotted in Fig. 3. This can be understood as an indicator that is equivalent to charging/discharging efficiency; it also shows how much the SOC is reduced (or increased) to obtain 100 kW discharging (or charging) power for per unit time. It is interesting to see that for the MESA 2 BSS, charging (or discharging) at different power levels results in the same efficiency, which only varies with the SOC. When discharging, the operable power capability also varies with the SOC. The marginal RTE at a different SOC can be calculated as

$$\eta(s) = \frac{r_{\text{ch}}(s)}{r_{\text{disch}}(s)} \tag{14}$$

where s denotes SOC level, and $r_{\text{ch}}(\cdot)$ and $r_{\text{disch}}(\cdot)$ are the SOC change rate per 100 kW as a function in SOC for charging and discharging, respectively. The marginal RTE is plotted in Fig. 4.

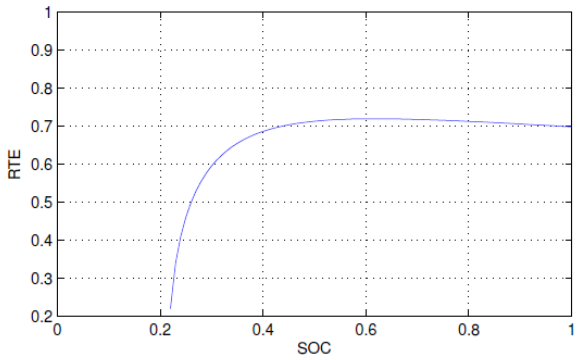

Fig. 4.Marginal round-trip efficiency versus SOC.

As can be seen, as SOC increases from 20% to 100%, marginal RTE increases rapidly before 40%, reaches the maximum around 50%- 60%, and then decreases slightly. It is interesting to note that although cycling a BSS from full to empty and then to full results in an average RTE equal to 60%, a BSS can be operated with a better efficiency when the SOC is above 30%. Therefore, the optimization $\mathbf{P}_1$ using a constant RTE of 60% underestimates the efficiency of a BSS for many possible operations and leaves the BSS on standby for many time periods when arbitrage could be profitable.

To better show this, the energy prices, charging/discharging operations, and SOC from both methods are plotted for two days, in 2015, in Fig. 5.

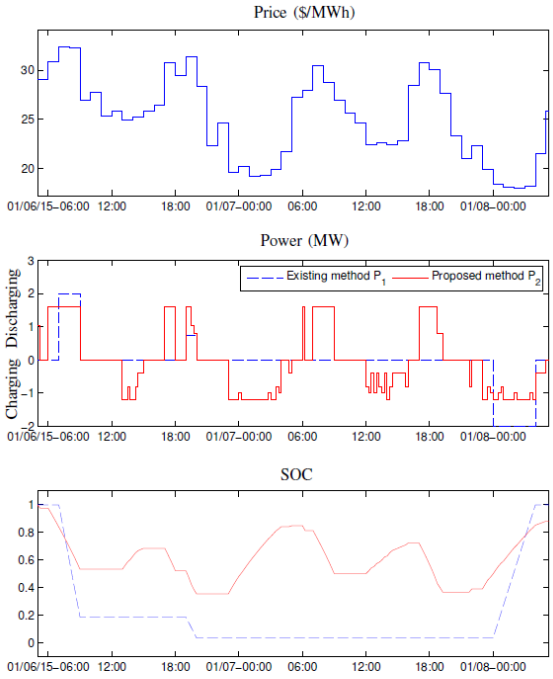

Fig. 5. Charging/discharging operation and SOC in sample days.

The hours at the beginning and end of the sample period correspond to very high and low prices, respectively. Both methods generate similar battery discharging and charging operation at the beginning and end of the sample period because the price difference is big enough compared with RTE and energy arbitrage using BSS is profitable. However, existing method $\mathbf{P}_1$ outputs some infeasible operation. For example, the BSS is discharged at 2 MW from 7 to 9 a.m. and the SOC decreases from 100% to 20%. In fact, the BSS can only be discharged at this full power output within a very limited SOC range. For the other hours, existing method $\mathbf{P}_1$ leaves the BSS in standby most of the time because, using a constant RTE of 60%, the price difference is not big enough to recover 40% losses in energy arbitrage. On the other hand, the proposed method $\mathbf{P}_2$ with a nonlinear model is capable of accurately exploring the BSS operating space at different operating power and SOC levels, takes into account the varying losses, finds profitable operation, and operates the BSS at a higher efficiency region to maximize the benefits from energy arbitrage.

V. Conclusion and Future Work

This paper presents a novel nonlinear battery model and optimal control method for evaluation and operational scheduling of BSS. Compared with existing methods, the proposed method can better capture varying charging/discharging efficiencies and charging/discharging power capabilities, and therefore can generate more realistic and optimal operation of a BSS for grid applications. The case study using a commercial BSS shows that failure to incorporate accurate nonlinear models in optimal scheduling could result in significant errors in assessment of economic benefits and an infeasible operation schedule. In future work, we plan to apply the proposed method with a nonlinear BSS model for other grid applications such as regulation service, distribution deferral, and demand charge reduction.

References

[1] K. C. Divya and J. Østergaard, "Battery energy storage technology for power systems–An overview," *Electr. Power Syst. Res.*, vol. 79, no. 4, pp. 511–520, Apr. 2009.

[2] B. Dunn, H. Kamath, and J.-M. Tarascon, "Electrical energy storage for the grid: A battery of choices," *Science*, vol. 334, no. 6058, pp. 928–935, Nov. 2011.

[3] R. Walawalkar, J. Apt, and R. Mancini, "Economics of electric energy storage for energy arbitrage and regulation in New York," *Energy Policy*, vol. 35, no. 4, pp. 2558–2568, Apr. 2007.

[4] N. Lu, M. R. Weimar, Y. V. Makarov, and C. Loutan, "An evaluation of the NaS battery storage potential for providing regulation service in California," in *Proc. IEEE Power Systems Conf. Expos.*, 2011, pp. 1–9.

[5] A. D. Del Rosso and S. W. Eckroad, "Energy storage for relief of transmission congestion," *IEEE Trans. Smart Grid*, vol. 5, no. 2, pp. 1138–1146, Mar. 2014.

[6] D. Wu, T. Yang, A. A. Stoorvogel, and J. Stoustrup, "Distributed optimal coordination for distributed energy resources in power systems," *IEEE Trans. Autom. Sci. Eng*., vol. 14, no. 2, pp. 414– 424, Apr. 2017.

[7] D. Wu, C. Jin, P. Balducci, and M. Kintner-Meyer, "An energy storage assessment: Using optimal control strategies to capture multiple services," in *Proc. IEEE Power Energy Soc. Gene. Meet*., Denver, CO, Jul. 2015, pp. 1-5.

[8] D. Wu, M. Kintner-Meyer, T. Yang, and P. Balducci, "Economic analysis and optimal sizing for behind-the-meter battery storage," in *Proc. IEEE Power Energy Soc. Gene. Meet*., Boston, MA, pp.1-5, Jul. 2016.

[9] J. Neubauer and M. Simpson, "Deployment of behind-the-meter energy storage for demand charge reduction," National Renewable Energy Laboratory, Golden, CO, Tech. Rep. NREL/TP-5400-63162, Jan. 2015.

[10] D. Wu, M. Kintner-Meyer, T. Yang, and P. Balducci, "Analytical sizing methods for behind-the-meter battery storage," *J. Energy Storage*, vol. 12, pp. 297–304, Aug. 2017.

[11] D. K. Maly and K. S. Kwan, "Optimal battery energy storage system (BESS) charge scheduling with dynamic programming," *IEEE Proc. Sci. Measure. Tech*., vol. 142, no. 6, pp. 453–458, Nov. 1995.

[12] Washington State Department of Commerce, Clean Energy Fund. [Online]. Available: http://classic.commerce.wa.gov/Programs/Energy/Office/Pages/Clean-Energy-Fund-1.aspx

[13] "Powerdex." [Online]. Available: http://www.powerdexindexes.com/

Single-Phase Battery-Buffered Smart Load Controller

Jing Zhang and Ahmed Zurfi

Department of Systems Engineering, University of Arkansas at Little Rock, Little Rock, USA

***Abstract*- This paper presents the design and experiment of a single-phase battery-buffered smart-load (BBSL) controller and its test bench. The motivation for this work is to investigate the design and operation of a BBSL system that will be beneficial for both power grid operation and customers. As a functional experimental system, the developed single-phase BBSL works at a low-voltage level (24 Vac and 48 Vdc) with a fixed-point microcontroller and a LabVIEW-supported test bench. The issues and experimental results include firmware evaluation, line frequency detection with Second-Order-General-Integral Phase-Locked Loop and battery control strategy for primary frequency regulation.**

***Keywords*- battery, smart load, controller, power grid, line frequency**

I. INTRODUCTION

Load-side participation in power system control and operation is becoming more and more important in the power grid operations and research [1]-[3]. In traditional power grids, the control and operation is performed mainly from centralized generation stations and control centers of interconnected areas. Although total effect of loads connected to a grid is almost equal to that of all generators in the same grid, all these loads are generally treated as "passive" components in the grid control. In the model of a power system, loads are generally modeled as stable power flow with switching-on or –off functions. This situation will change because of new challenges to traditional power grids. These challenges include: 1) relative slow development of existing power grids and fast increase of both total electricity consumption and peak loads in recent and coming years; 2) large scale integration of renewable energy with intermittent properties and inverter-based power generation [1]; and 3) increasing load disturbances because of widely synchronizing events [5] or large area natural disasters. In the official definition of a smart grid a decade ago, integration of 'smart' appliances and consumer devices is an important feature to be achieved [8].

Dynamic demand control (DDC) and demand response (DR) are two proposed classes of load-side participation in power system control and operation. DDC proposed in [1] is to apply the traditional load-frequency control strategies [6] of synchronous generators to the demand side. It includes both primary frequency regulation (PFR) and secondary frequency regulation (SFR), in which the deviation of the line frequency from the rated value is detected and used to control load power consumption of appliances. The loads discussed in [1] are the appliances not critical in time-of-use (ToU) within reasonably narrow time periods, such as refrigerators, air conditioners, and water heaters. In this method, load-side dynamic power control will be supplement to the automatic generation control (AGC) so that the system dynamic performance and stability are improved. DDC will help to stabilize a power grid with significant renewable energy penetration.

Based on the description of the Department of Energy website [7], DR is an electricity tariff or program established to motivate changes in electric use by end-use customers, designed to induce lower electricity use typically at times of high market prices or when grid reliability is jeopardized. DR may help to reduce peak load power consumption by encouraging customers to shift their energy demands from "peak load" time. It will also help to increase renewable energy penetration by changing customers' energy behavior.

Although DR is becoming more and more popular in recent years, the effects of DR programs is fairly limited. As discussed in [9], DR requires considerable active efforts of consumers, for example, to pay attention to the energy information, to decide on appropriate actions, and even to add local alternative generation. DDC has not been widely adopted by customers yet. Currently, DDC is proposed only for special loads based on a random control strategy. It may result in some unexpected effect of customers' power consumption. As proposed in [1], the DDC control capability is only effective for under-frequency regulation. Additionally, it requires installation of DDC controllers at the customers' appliances, which may also hamper customers' acceptance.

A reasonable battery storage installed at load-side as an energy buffer will separate the load power consumption from the grid and reduce the impact of DDC and DR on customers. Batteries are a popular type of energy storage. Battery storage systems (BSS) have been widely used in electrical vehicles (EV), wind and solar power generation, substations, and various uninterrupted power supply (UPS). Different from traditional grid-level energy storage, such as pumped

hydroelectric energy storage and compressed-air energy storage, BSS are scalable, mobile, and exchangeable. These characteristics make batteries more suitable for the load-side applications than other energy storage systems. However, up to now, BSS is often a big investment for many customers. The life-time of a BSS is another concern compared to more than 30 years life time of traditional grid-level equipment.

Batteries have been widely used on load-side applications, such as in laptop computers, UPS, and so on. Recently, behind meter battery storage is also commercially available. These applications are mainly for special purposes, for example device mobility or data protection of information systems. In practice, the batteries in such applications are often not fully used because they are not always necessary for system operation. Most people use laptop computers with power plug-in, and an UPS only works when a blackout occurs. The existing applications tell us that customers are willing to invest for attractive features of power supply with batteries though batteries are quite expensive. It is possible for customers to accept batteries as an energy buffer between a power grid and their appliances as long as they believe that the new features are important or beneficial. BBSL technology was proposed in this work with the goal of combining the functions for the load-side participation of power system control and the beneficial features for customers in new load-side application designs. The expected power rating of a BBSL is mainly in the level appliances, from a laptop computer to power supply of a residential house, i.e., from 100 VA to 20 kVA.

The following sections of this paper present the design of a low-voltage functional BBSL controller and BBSL test bench; the high-precision line frequency detection based on Second-Order-General-Integral Phase-Locked Loop (SOGI-PLL); and a control strategy of BBSL for battery with PFR. We also present and discuss the evaluation of firmware, experimental results of line frequency detection, and the experimental result of PFR with state of charge (SoC) control. The contents are organized in the following sections (1) BBSL controller, (2) design of single-phase BBSL controller, (3) firmware description, (4) LabVIEW-based BBSL test bench, (5) experimental results, and (6) conclusions.

II. BBSL Controller

A BBSL controller is designed for a conventional load to implement smart-load features. Its fundamental function is to optimally control the grid power flow to a load by evaluating the states of power grid operation, the load power consumption, and battery storage as shown in Fig. 1.

Equipped with battery storage, a BBSL can be designed to implement DDC and DR automatically and, at the same time, to meet the customers' additional requirements for power supply. The capability is mainly restricted by the energy/power capacity of the installed battery. As an important part of BBSL control, the PFR function is discussed in the following.

Fig. 1. BBSL functional scheme.

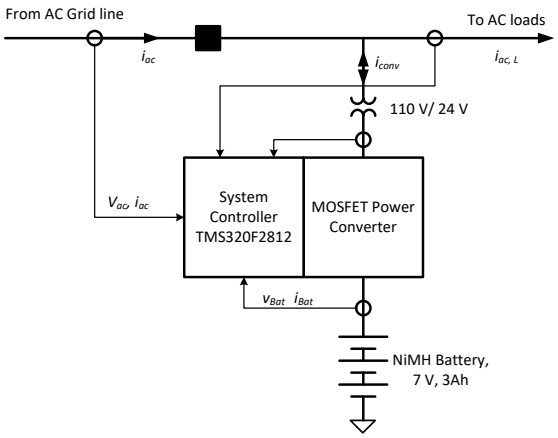

A. BBSL Primary Frequency Regulation

PFR is a widely used control strategy of governors in synchronous generator systems. A governor automatically controls power generation based on line frequency deviation as:

$$\Delta P_g = \Delta P_{set} - \frac{\Delta f}{R} \qquad (1)$$

where ΔP_g and ΔP_{set} are the change of power generation and setting, respectively. Δf is the line frequency deviation from the rating value. R is the regulation constant [6].

Similar to a generator, PFR can also be applied to a BBSL as,

$$P_{grid} = P_{load} + \frac{\Delta f}{R} \qquad (2)$$

where P_{grid} and P_{load} are the grid power delivered to BBSL and the load power consumption, respectively. The difference between the grid power and load power charges or discharges the battery storage. As a load, one restriction is $P_{grid} \geq 0$, or the grid power to a BBSL unidirectional.

There are good reasons to design PFR function so that it will not affect the SoC of the battery storage significantly. PFR is a dynamic compensation of a power grid. The energy storage is used to implement both underfrequency and overfrequency while the SoC is kept around a setting value, for example 80%. The reserved energy stored in the battery

could be used for DR application or UPS function when it is required. By considering this fact, the grid power control in (2) can be modified as:

$$\Delta P_g = \Delta P_{set} + K_{SoC}\Delta SoC - \frac{\Delta f}{R} \qquad (3)$$

where K_{SoC} and ΔSoC are the control gain and deviation of SoC from its setting value of 80%.

All quantities in (1), (2), and (3) are in per unit. The regulation constant is often chosen equal to 0.04. The practical line frequency deviation in normal system operation is generally not more than 0.2 Hz, or 3.3×10^{-3} *pu* for the base line frequency of 60 Hz. The change of the grid power because of PFR should not be more than 0.1 *pu*. Therefore, the base power of the system can be 10 times of the rated power of the battery. For a NiMH battery of 20 watts, it can support load-side PFR at the base power of 200 Watts.

B. Line Frequency Detection

The detection of line frequency is necessary for BBSL load-side PFR. Based on NERC Reliability Standard PRC-024-1, the deviation of line frequency is in the range of ±0.5 Hz for steady state and ±2.2 Hz for dynamic state. However, the frequency deviation is usually around 20 mHz to 40 mHz. The precision of 1 mHz or 0.045% (based on dynamic range of line frequency deviation of 2.2 Hz.) should be reasonable for BBSL applications. It is significant to develop a method to detect the line frequency at such a high precision that is effective in the noisy load environment and easy to be implemented in BBSL controllers at a low-cost. In this work, SOGI-PLL was investigated theoretically and experimentally for the frequency detection. In single-phase inverters, SOGI-PLL is widely used for line voltage synchronization [4].

In a BBSL controller, SOGI-PLL was designed for both phase synchronization and the frequency detection. Because PLL is a closed-loop control system, there is no special restriction on resolution for the frequency detection, theoretically. However, the controller may introduce significant control noise. It requires well-designed filters and the reasonable selection of a sampling rate to detect the frequency for the required precision. In this work the frequency sampling rate is 10 samples per second while the PLL control frequency is 10 kHz. Figure 2 shows the functional block diagram of the SOGI-PLL-based phase synchronization and frequency detection. The detected frequency from SOGI-PLL f_{PLL} is in per-unit with the base value of 60 Hz. The method can easily be applied in a 32-bit fixed-point microcontroller with 12-bit AD converter.

Fig. 2. SOGI-PLL based frequency detection.

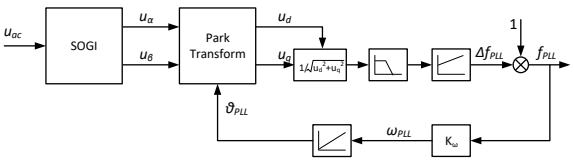

III. Design of Single-Phase BBSL Controller

The goals in designing a BBSL controller test system are 1) to investigate the performance and model of various batteries, 2) to investigate the BBSL control strategies, 3) to evaluate the firmware of a microcontroller and 4) to provide a test bench in the research laboratory. The single-phase BBSL controller at a low-voltage level (24 Vac and 48 Vdc) was designed and developed for safety and economics.

The experimental system shown in Fig. 1 consists of a 200 W, 110 V/24 V transformer, single-phase full-bridge converter, a buck/boost converter, a 7 V/3 Ah NiMH battery, and a digital controller based on TMS320F2812 from Texas Instruments, Inc.

A MOSFET three-phase full bridge inverter developed in the laboratory was used for the single-phase full-bridge inverter and the buck-burst converter as depicted in Fig. 3. Based on the widely used three-phase full-bridge inverter, the design has significant economic advantages for future manufacturing. The control of the single-phase inverter include a SOGI-PLL and a modified proportional-resonant (PR) controller [4]. The SOGI-PLL is designed to evaluate grid voltage phasor and frequency. The evaluated data are fed into the PR controller for the current control of the single-phase inverter. In addition these data are also used in the BBSL controller for the PFR and the early detection of an outage.

Fig. 3. Power circuit of the single-phase BBSL controller.

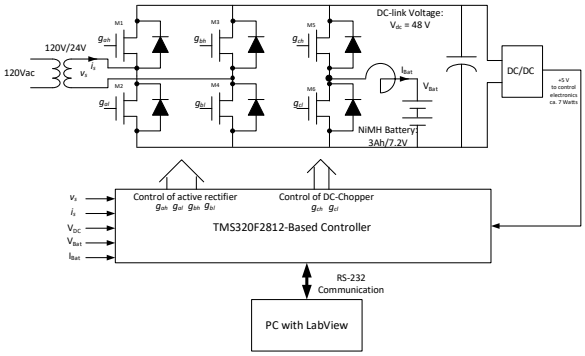

IV. Firmware Description

TMS320F2812 is a fixed-point 32-bit micro-controller. Compared to more advanced 32-bit microcontrollers with floating-point processors, a fixed-point microcontroller is more suitable for the practical design of commercial products with the advantages of low cost and low energy consumption.

The control of active rectifier including SOGI-PLL and PR controller requires much high precision computation. Without a floating-point processor, the functions of IQmath library provided by TI are widely used in the firmware. The main control function operates at 10 kHz, which includes all real-time signal sampling, digital signal processing and control functions. The important control functions for the single-phase active rectifier are SOGI-PLL, PR controller with voltage feedforward compensation, notch filter for detection of DC-link voltage, and conventional proportional-integral (PI) controller. The microcontroller works at the system clock of 150 MHz. The execution time consumption of the main functions is listed in Table I.

The main control function for the real-time control takes 37.2 μs, or 37.2% computation capacity of the microcontroller. In addition, there are functions such as RS-232 data communication, system initialization and analog signal calibration that are not time critical.

TABLE I.
TIME CONSUMPTION OF MAIN FIRMWARE FUNCTIONS

Function	Time (μs)
Main control function	37.2
SOGI-PLL	6.24
Modified PR controller	13.6
PI controller	0.872
Notch filter	0.936

V. LABVIEW-BASED BBSL TEST BENCH

The LabVIEW program allows a desktop computer to realize human-machine interface and system-level control. Through an RS-232 port, the LabVIEW program accesses the microcontroller data for further data processing, graphical display, and data storage, and sends control commands and data back to the microcontroller. The LabVIEW program operates at a much lower control frequency compared to the main function in the microcontroller, such as 1 Hz, which is reasonable for a desktop without a real-time operating system. The obvious advantage with the LabVIEW program is its convenience for development and modification as well as capabilities to use the much more sophisticated functions in network communication and file management provided by a desktop computer.

The LabVIEW program also provides remote-access capability for the test bench. The user can operate and monitor the experiments remotely from a desktop computer. This feature is very helpful for the experiments with battery and BBSL control strategy study because many experiments require 24 hours a day operation.

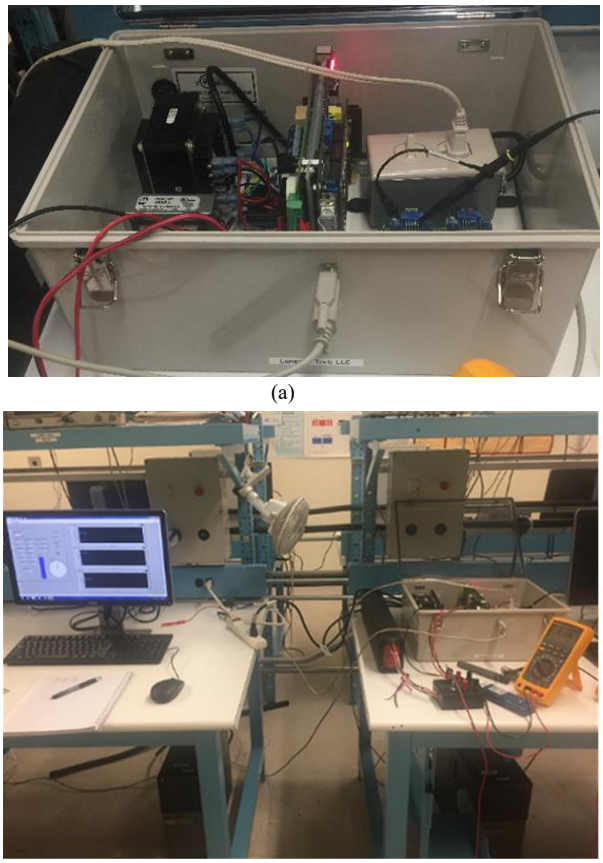

(a)

(b)

Fig. 4. (a) BBSL system (b) and the BBSL test bench.

VI. EXPERIMENTAL RESULTS

Many system experiments have been performed to study the model of NiMH batteries, to confirm the effectiveness of line-frequency detection, and to investigate BBSL strategies such as PFR with battery SoC control. The experimental results of frequency detection and PFR with SoC control are discussed here. The BBSL system is shown in Fig. 4(a) and BBSL test bench in Fig. 4(b). The small fan is the AC load of about 16 watts. The battery used in the experiments is a 7.2 V/3 Ah NiMH battery.

To evaluate the precision of the line frequency detected with SOGI-PLL, FDR frequency data provided by PowerIT lab, University of Tennessee, Knoxville, were requested and used as a reference. FDR frequency data were detected with a high precision grid analyzer [10]. The detected frequency with a SOGI-PLL were compared with the FDR frequency data remotely recorded at the same location (Little Rock, AR72212) and within the same time duration (from 3:47:18 p.m. to 5:27:18 p.m. Central Time on Dec. 30, 2017). The comparison is shown in Fig. 5(a). The blue line is the frequency measured by BBSL controller and the red line the FDR frequency data provided. To take a good look at the

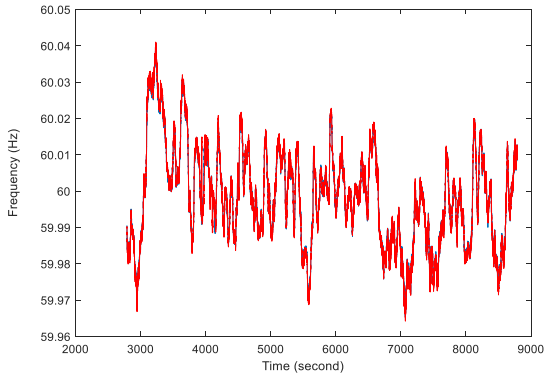

(a)

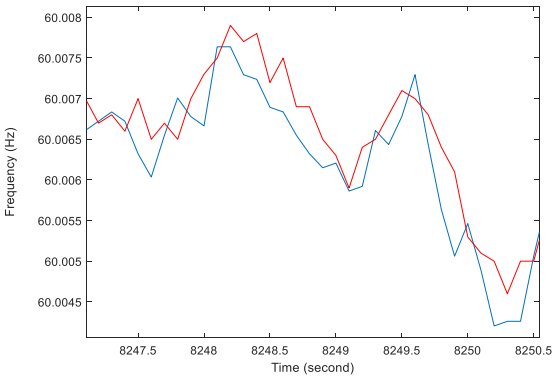

(b)

difference between the two measured frequencies shown in Fig. 5(a), a small section of 3.5 s is magnified and shown in Fig. 5(b). The peak errors between the two measured frequencies are about 0.5 mHz.

Fig. 5. Comparison between BBSL controller frequency evaluation (blue) and FDR frequency data (red).

Fig. 6 shows the experimental results of a primary frequency regulation with battery SoC control realized with the BBSLC test bench. The test began at 1:14:35 p.m., Sept. 4, 2017 and continued for about 2.5 hours. At the beginning of the experiment, the battery is fully charged (100% SoC). In the PFR experiment, the battery SoC is controlled equal to 80% in normal operation. The waveforms include the detected line frequency Freq., the grid power Pgrid, the load power Pload, the battery power regulation Preg, and battery SoC. The battery power is regulated by BBSL controller. When it is positive, it charges the battery. When it is negative, the battery supplies part of the load power.

Because the battery SoC began with 100%, the SoC controller generated a power offset to discharge the battery until the SoC reached about 80%.

In PFR, BBSL controller regulated the battery power based on the detected line frequency deviation with the regulation constant $R = 0.04$ per unit with the base power of 200 Watts. The experimental waveforms show that the BBSL

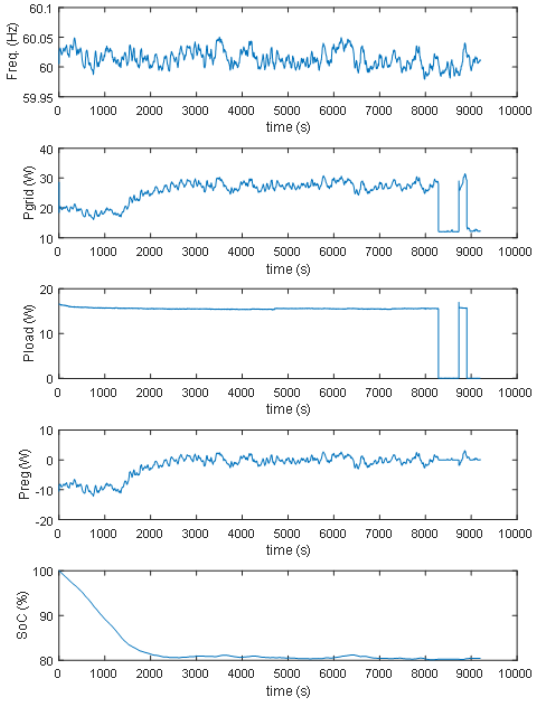

Fig. 6. BBSL waveforms with PFR and SoC control.

PFR was effective until the load was switched off.

In the experiment, the sum of the load power and the battery power was controlled to be not less than zero, which means the load with the battery will never feedback the energy to the power grid. In the experiment, the grid power shown in Fig. 6 included the BBSL controller power consumption of about 11 watts. It was not included in the load power shown in Fig. 6.

VII. Conclusions

Battery-buffered smart loads are proposed in this work. Equipped with a battery storage system, a BBSL is able to implement DDC and DR automatically, which will help the load-side participation of power system control and operation. With battery energy storage, a BBSL will also be designed to realize various customer attractive functions, such as UPS, which may overcome the barriers to customer investment.

A single-phase BBSL controller was designed and the BBSL test bench developed for the experimental study of BBSL operation. The operation of a BBSL with PFR and battery SoC control was investigated. By setting a reasonable gain for SoC control, the battery SoC can be controlled around a desired value while the BBSL operates in PFR. This work also confirmed that the SOGI-PLL can be applied for line frequency detection at a high precision of 1 mHz. The line frequency detected with the test BBSL controller matched the FDR frequency data quite well.

ACKNOWLEDGEMENTS

The authors would like to acknowledge PowerIT lab, the University of Tennessee, Knoxville for providing FDR data for confirming frequency detection.

REFERENCES

[1] Q. Shi, H. Cui, F. Li, Y. Liu, W. Ju and Y. Sun, "A hybrid dynamic demand control strategy for power system frequency regulation," *CSEE J. of Power and Energy Syst.*, vol. 3**,** no. 2, pp. 176–185, June 2017.

[2] A. Kasis, E. Devane, C. Spanias, and I. Lestas, "Primary frequency regulation with load-side participation part I: Stability and optimality," *IEEE Trans. Power Syst.*, vol. 32, no. 5, pp. 3505-3518, Sept. 2017.

[3] A. Kasis, E. Devane, C. Spanias, and I. Lestas, "Primary frequency regulation with load-side participation part II: Beyond passivity approaches," *IEEE Trans. on Power Systems*, vol. 32, no. 5, pp. 3519-3528, Sept. 2017.

[4] V. Blahnik, T. Kosan, and J. Talla, "Control of single-phase AC/DC converter based on SOGI-PLL voltage synchronization," in *Proc. 16th Int. Conf. on Mechatronics - Mechatronika 2014*, p. 1-4.

[5] E. Allen, J. Ingleson, R. Orndorff, B. Starling, and M. K. Thomas, "Frequency disturbances during the Super Bowl: It's more than just what's on the field," *IEEE Power & Energy Mag.*, vol. 14, no. 6, pp. 52-58, Nov.-Dec. 2016.

[6] J. D. Glover, T. J. Overbye and M. S. Sarma, *Power Syst. Analysis & Design*, 6th ed., J. D. Glover, Ed. Boston, MA: Cengage Learning, 2015.

[7] (2018) Demand Response. [Online]. Available: https://energy.gov/oe/activities/technology-development/grid-modernization-and-smart-grid/demand-response

[8] Energy Independence and Security Act of 2007, Pub. L. No. 110-140, § 1301, 121 Stat. 1784 (2007)

[9] G. Schuitema, L. Ryan, and C. Aravena, "The consumer's role in flexible energy systems: An interdisciplinary approach to changing consumers' behavior," *IEEE Power and Energy Mag.*, vol. 15, no. 1, pp. 53–60, Jan.-Feb. 2017.

[10] L. Zhan, Y. Liu, J. Culliss, J. Zhao, Y. Liu, and S. Gao, "Universal grid analyzer design and development," in *Proc. 2015 IEEE Power & Energy Society General Meeting*, 2015, pp. 1-5.

Energy Storage System Dispatching Optimization in Stacked Applications for Utility Grid

Shijie Tong[1], Handa Yangy[2], and William Torre[1]

[1]*Center for Energy Research, University of California San Diego, 9500 Gilman Drive, La Jolla CA, USA*

[2]*Department of Mechanical and Aerospace Engineering, University of California San Diego, 9500 Gilman Drive, La Jolla CA, USA*

Corresponding author: stong at ucsd.edu

***Abstract*- An optimal dispatching algorithm for five different utility grid energy market applications was developed using mixed-integer- linear-programming. This study explores the value propositions of operating an energy storage system (ESS) under each application individually, as well as together, in stacked applications through simulations using market pricing data obtained from the California Independent System Operator. Three different ESSs were simulated at energy-to-power ratios (EtoP) of 2, 4, and 8. In all cases, operation under stacked applications provided the best value proposition, and the effects of EtoP are discussed in light of the current market conditions, as well as potential future market conditions.**

***Keywords*- energy storage systems, dispatching, optimization, mixed-integer linear programming, stacked applications, energy market.**

I. INTRODUCTION

Energy storage systems (ESSs) are becoming crucial components in the modern utility grid as electricity sources shift from fossil fuel power plants to more sustainable but intermittent wind and solar resources. An ESS can provide many services to the grid, such as improving power quality, responding to short-term ramping needs, and matching the load with the demand [1], [2]. Techno-economic analysis on energy applications such as frequency regulation (FQ) [3], energy time shifting, and renewable integration [4] has revealed that cost and cycle life are among the most sensitive factors in designing an ESS for the grid. Battke et al. [5] estimated life cycle costs and their uncertainties for different battery technologies and found different technologies take the cost leaderships in specific applications, yet no single technology surpasses over other solutions by a significant margin. In addition to seeking better and more cost effective ESS solutions, it is also important to investigate better value propositions for grid integrated ESSs to achieve higher adoption [6]. Many studies have been conducted on the dispatching of distributed energy resources, solar plus storage systems, and virtual power plants [7]–[10] to improve ESS performances and economic returns. Atzeni et al. [7] developed an optimization scheme for energy storage, implementing non-cooperative game theory to preserve user privacy. Hoke et al. [11] developed a linear programming-(LP) based optimization scheme for economic dispatching of an ESS in a micro-grid. Nottrott et al. [12] investigated LP optimal dispatching of battery and PV system with load forecasting and local time of use (TOU) utility pricing. Soares et al. [13] proposed a particle swarm optimization to solve a distributed energy resource dispatching problem of large dimension. Dispatching optimization under multiple energy storage applications has also been discussed. For example, Pandvzic et al. [8] provided a case study of stacked energy storage applications by combining long-term bilateral contracts and market participation. Other works investigating the stacked-benefits of ESS have been published [14]–[17]. Previous works mostly focused on the co-optimization of two applications, with one emphasizing on power and the other on energy [15], [16]. In addition, previous works often identified one application as the primary service and treated others as secondary applications in the optimization process [14]. Our work took a market-oriented approach and investigated suitable energy applications at a broader spectrum by considering energy storage service products across retail and wholesale market sectors, with three different pricing tariffs (i.e., retail TOU tariff, wholesale day-ahead (DA) price, real-time-pre-dispatch price) and five distinctive application products.

By combining multiple energy storage applications, different aspects of an ESS's capabilities, including power, energy and fast response, capacities can be better exercised. By incorporating the product design and pricing data of each application from California independent system operator (CAISO) and local utility - San Diego Gas & Electric, the developed dispatching algorithm will provide real-world guidance for energy-management controller design and help evaluate the benefits of energy storage assets deployed on the grid.

II. Energy Storage Applications

As illustrated in Fig. 1, an ESS was simulated to perform five different energy storage applications (e.g., Demand Charge Management (DC), Energy Time Shifting in the DA market, Energy Time Shifting in the Real-time market (RT), Flexible Ramping (FR), and FQ. The five applications cover both the behind-meter retail market and the front-of-meter wholesale market. They cover both lower uncertainty, steadier return services like bulk energy management, and higher uncertainty, greater return services like power quality regulation. It should be noted that the behind-meter and front-of-meter applications don't typically apply to the same ESS because the battery sizes are significantly different and the price is settled from different meters. For the benefit of investigating the performance of stacked applications, the constraint is lifted in this work.

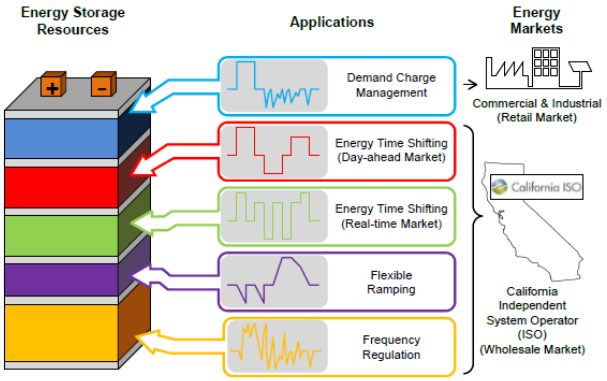

Fig. 1. Five energy storage applications under both retail and whole sale markets; from top to bottom: Demand Charge Management (Blue), Day-ahead Energy Time Shifting (Red), Real-time Energy Time Shifting(Green), Flexible Ramping (Purple), and Frequency Regulation (Orange).

The ***DC*** is an energy service designed for commercial and industrial businesses. The cost of power demand in a billing cycle could be significant because short but large peak load drives up the "demand charge." After implementing an ESS, the demand charge can be reduced by charging an ESS during off-peak usage and discharging during peak usage. If a business is under the TOU tariff, meaning the energy price is different between peak and off-peak hours, the same ESS can also perform energy peak shaving. In this study, a simulated school campus load profile was utilized for the DC application. The average load is 344 kW with a 944 kW peak. During the summer months, from July to September, when school is out of session, the campus will have lower average load demand.

The ***Energy Time Shifting*** application captures the price fluctuation in the market throughout a day, and charges an ESS during off-peak price and discharges during peak price. The DA and RT applications are energy time shifting applications, but implemented in two different market segments. In the DA market, an ESS will submit their bid in the previous day before 10 a.m. The DA market prices are usually more predictable, but the returns are relatively low. In the RT market, an ESS will submit their bid 75 minutes ahead of the clearing interval. The RT price is more difficult to predict, but offers higher potential returns. It fluctuates more, but the returns can be higher.

The ***FR*** products for real-time pre-dispatch and real time dispatch markets were developed in a stakeholder process at CAISO [18]. With the proliferation of renewable resources, the electricity grid has begun to observe a lack of sufficient ramping capability and flexibility. Insufficient ramping capacity on the grid will have to be resolved out of the feasible system-wide schedule or rely on ancillary services and regulation, which will increase the probability of power balance violation. As a result, many utility grids have started considering FR products.

The ***FQ*** is procured by CAISO to obtain regulation capacity each hour, based on the total system-wide demand for power. It is assumed that the system-wide FQ capacity demand is orders of magnitude higher than any single ESS. For that reason, if it is desirable to enter the FQ application, the simulated ESS can procure as much capacity as the ESS allows. The mileage component of the FQ product was created because of a Federal Energy Regulatory Commission order to introduce pay-for-performance measures for regulation products on the grid [19]. The mileage is a way to reward devices that can fluctuate and match load profiles more accurately. It is defined as the sum of the absolute values of the regulation control signal movements.

III. Optimization Algorithm

A mixed-integer linear programming algorithm was implemented to develop the optimization solver. The algorithm dispatches the energy storage resources among the applications by maximizing the revenue (minimizing the cost) from stacked applications:

$$\underset{P,W}{\text{minimize}} \quad J(P,W) \tag{1a}$$

$$\text{subject to } A(P,W) \leq B \tag{1b}$$

$$Aeq(P,W) = Beq \tag{1c}$$

where J is the cost function. A, B, Aeq, Beq are composed matrices to form the inequality and equality constraints. By committing the resources to different applications, the ESS can earn a collective of revenues

described in the following equation:

$$J(P,W)=\sum_{i=1}^{N}\sum_{k=1}^{K}J_{ene,k,i}(p_{k,i},w_{k,i}) + \sum_{i=1}^{N}\sum_{k=1}^{K}J_{app,k,i}(p_{k,i},w_{k,i}) \quad (2)$$

For each application, there are two types of revenues: the energy revenue, with subscript ene, is from the price differences between buying and selling energy; the application revenue, with subscript app, is based on the specific service that an ESS performs. k is the application index: $k=1,2,...,5$ refers to DC, DA, RT, FR, FQ applications, respectively. *i* is the time index. For this optimization task, each time step has an interval of 15 minutes and an optimization horizon of 24 hours, which gives *N* = 96. *P* are continuous variables representing the ESS charging and discharging. In each time interval, there could be either charging (with superscript +) or discharging (with superscript −) actions, their differences are the actual ESS power (with superscript 'o'). The ESS power output is confined by the power constraints:

$$p_{k,i}=\{p^{o}_{k,i},p^{+}_{k,i},p^{-}_{k,i}\} \quad (3)$$

$$p^{o}_{k,i}=p^{+}_{k,i}-p^{-}_{k,i} \quad (4)$$

$$0\le p^{+}_{k,i}\le \overline{p_k} \quad (5)$$

$$0\le p^{-}_{k,i}\le \underline{p_k} \quad (6)$$

$$0<\sum_{k=1}^{K}p^{+}_{k,i}<\overline{p_k} \quad (7)$$

$$0<\sum_{k=1}^{K}p^{-}_{k,i}<\underline{p_k} \quad (8)$$

where $\overline{p_k}$ and $\underline{p_k}$ are power limits for ESS charging and discharging, respectively. And collectively, the ESS's state-of-charge must be limited within the energy constraints:

$$SoC_i=SoC_0+\sum_{i=1}^{n}\sum_{k=1}^{4}(\frac{\eta p^{+}_{k,i}-p^{-}_{k,i}}{Q})\Delta t + \sum_{i=1}^{n}\frac{\eta\frac{900}{M_i^{+}}p^{+}_{5,i}-\frac{900}{M_i^{-}}p^{-}_{5,i}}{Q}\Delta t \quad (9)$$

$$\underline{SoC_{bat}}<SoC_{bat,i}<\overline{SoC_{bat}} \quad (10)$$

The time interval Δt is 15 minutes in this study. η is battery round trip efficiency. *Q* is battery capacity. The $SoC_{bat,0}$ is the initial state-of-charge. The $\underline{SoC_{bat}}$ and $\overline{SoC_{bat}}$ are the upper and lower SoC limits, respectively. For FQ application, the reserved power capacity $\frac{900}{M_i^{+}}p^{+}_{5,i}$ and $\frac{900}{M_i^{-}}p^{-}_{5,i}$ were used instead of the actual clearing power. Five applications were considered for stacking. Based on the product design of each application, additional constraints and revenue models were implemented.

The DC application is the only behind-meter application among the five. Because an ESS needs to be scaled to match the simulated commercial and industrial load data, the power limits for DC application were set to be 100kW Also, because the metering is $(\overline{p_1}=\underline{p_1}=0.1MW)$. separate from the other applications, the DC application can only purchase energy at the local TOU price. One way to apply this restriction is to enforce the daily net *SoC* change to be zero:

$$\sum_{i=t_0}^{t_{end}}(\frac{\eta * p^{+}_{1,i}-p^{-}_{1,i}}{Q})\Delta t=0 \quad (11)$$

where $t_0=00:00$ and $t_{end}=23:45$ in hh : mm are the start time and stop time. The DC energy revenue (cost) is based on grid consumption reduction:

$$J_{1,ene}=\sum_{i=1}^{N}E_{tou}(p^{o}_{1,i})\Delta t \quad (12)$$

where E_{tou} is the TOU pricing. The application revenue is based on the cost reduction from demand charge:

$$J_{1,app}=E_{dc}(max(p^{o}_{1,i}+L_i)-max(L_i)),i=1,2,..,N \quad (13)$$

where E_{dc} is the demand charge cost per in $\$/MW$. L is the load consumption. Because the demand charge cost settles monthly, which is a longer optimization horizon compared to the rest of the applications. A simplified approach was implemented to estimate a peak load Lpk for each month, and penalizes the cost function whenever the grid load exceeds the Lpk. The cost function in (11) is now simplified for optimization with shorter interval:

$$J_{1,app}=E_{dc}max\{p^{o}_{1,i}+L_i-Lpk_i,0\},i=1,2,..,N \quad (14)$$

The ***Energy Time Shifting*** applications in the DA market and the RT obtain the energy revenue through buying and selling in the respected markets:

$$J_{2,ene}=\sum_{i=1}^{N}E_{da}(p^{o}_{2,i})\Delta t \quad (15)$$

$$J_{3,ene}=\sum_{i=1}^{N}E_{rt}(p^{o}_{3,i})\Delta t \quad (16)$$

where the DA market has a E_{da} bidding interval of 1 hour and the bidding must be submitted 1 day ahead before 10 a.m. to enter the market. The RT utilizes E_{rt} the real-time pre-dispatching price that has a bidding interval of 15 minutes, and the bidding must be submitted 75 minutes ahead to enter the market. Both markets are location specific. In this study, the local marginal pricing data from the La Jolla node (*LAJOLLA_6_N*007) from CAISO were utilized. The dispatcher is also applicable to other locations if the local marginal price of that node is given.

The ***FR*** application energy revenue utilizes the same pricing data as the RT:

$$J_{4,ene} = \sum_{i=1}^{N} E_{rt}(p_{4,i}^{o})\Delta t \tag{17}$$

The application revenue of FR comes from ramping up/down service. Based on the product design, resources will submit FR bidding according to the ramping requirement for the next bidding interval and get paid by the clearing price of the accepted bidding. For simulation purposes, the algorithm utilized the ramping up/down shadow prices from CAISO as the ramping clearing prices and assumed that the ESS always won the bid:

$$J_{4,app} = -\sum_{i=1}^{N}(E_{fr,down}\Delta p_{4,i}^{+} + E_{fr,up}\Delta p_{4,i}^{-})\Delta t \tag{18}$$

$$\Delta p_{4,i}^{+} = max\{(p_{4,i}^{o}) - (p_{4,i-1}^{o}), 0\} \tag{19}$$

$$\Delta p_{4,i}^{-} = max\{-(p_{4,i}^{o}) + (p_{4,i-1}^{o}), 0\} \tag{20}$$

where $E_{fr,down}$ and $E_{fr,up}$ are the FR down and ramping up shadow prices. Δp_4^{+} and Δp_4^{-} are the ramping down and ramping up movements performed in each bidding interval.

The ***FQ***'s application revenue is generated from two types of payments: capacity and mileage. The capacity payment comes from the amount of power capacity reserved for FQ application to dispatch, represented by The mileage payment PC_{fq}. comes from the actual mileage dispatched by the system coordinator. The typical FR control signal has a time interval of 4 s. Given 1 h as an application time interval for FQ, the mileage of a FQ resource output is calculated within the interval, indicated in the following equation as AGC time step *j*, which should not be confused with the higher-level optimization time step *i*:

$$\begin{aligned} M_i^{\pm} &= \sum_{j=1}^{900} \frac{|p_{5,j}^{\pm}|}{PC_{fq,i}^{\pm}} \\ &= \frac{900|p_{5,i}^{\pm}|}{PC_{fq,i}^{\pm}} \end{aligned} \tag{21}$$

Given that the mileage data *M* is available from CAISO market, we can back calculate PC_{fq} based on average power p_5. As a result, the revenue function of FQ application can be represented as:

$$\begin{aligned} J_{5,app} = & \\ & (C_{fq}^{+}\sum_{i=1}^{N}\frac{900}{M_i^{+}}p_{5,i}^{+} + C_{fq}^{-}\sum_{i=1}^{N}\frac{900}{M_i^{-}}p_{5,i}^{-})\Delta t \\ & + (E_{fq}^{+}\sum_{i=1}^{N}900p_{5,i}^{+} + E_{fq}^{-}\sum_{i=1}^{N}900p_{5,i}^{-})\Delta t \end{aligned} \tag{22}$$

where $\frac{900}{M_i^{\pm}}p_{5,i}^{\pm}$ calculates the reserved regulation up/down capacity. $C_{fq}^{\pm}$ and $E_{fq}^{\pm}$ are capacity payment price and mileage payment price respectively. The FQ application's energy revenue utilizes the same pricing data as the DA market.

$$J_{5,ene} = -\sum_{i=1}^{N} E_{da}(p_{5,i}^{0})\Delta t \tag{23}$$

The market data from Jan. 1st to Dec. 31st of 2016 were scraped from the CAISO web API for DA, RT, FR, FQ applications and TOU tariff and demand charge pricing information from San Diego Gas & Electric was utilized for DC application. Since the FR application is under development, the shadow prices for ramping up/ramping down revenue was used instead. A set of forecasted pricing data was generated, by applying time delay and moving average to the true data. For the day ahead market, the signal was estimated using data from 2 days ahead.

$$\widetilde{E}_{da,i} = \frac{\sum_{j=1}^{n} E_{da,i-j-191}}{n} \tag{24}$$

For the RT, the signal was estimated using data from one day ahead.

$$\widetilde{E}_{rt,i} = \frac{\sum_{j=1}^{n} E_{rt,i-j-95}}{n} \tag{25}$$

IV. Results and Discussion

An ESS model of 1 MW/2 MWh was used ($Q = 2MWh$, $p_k = \underline{p_k} = 1MW$). The round trip efficiency η is assumed to be 90%. Fig. 2 shows the 7 days of ESS dispatching power profiles among all five applications. The color coded bars (blue: DC, Red: DA, Green: RT Purple: FR

Orange: FQ) indicate whether applications are charging (positive) or discharging (negative) in each time interval.

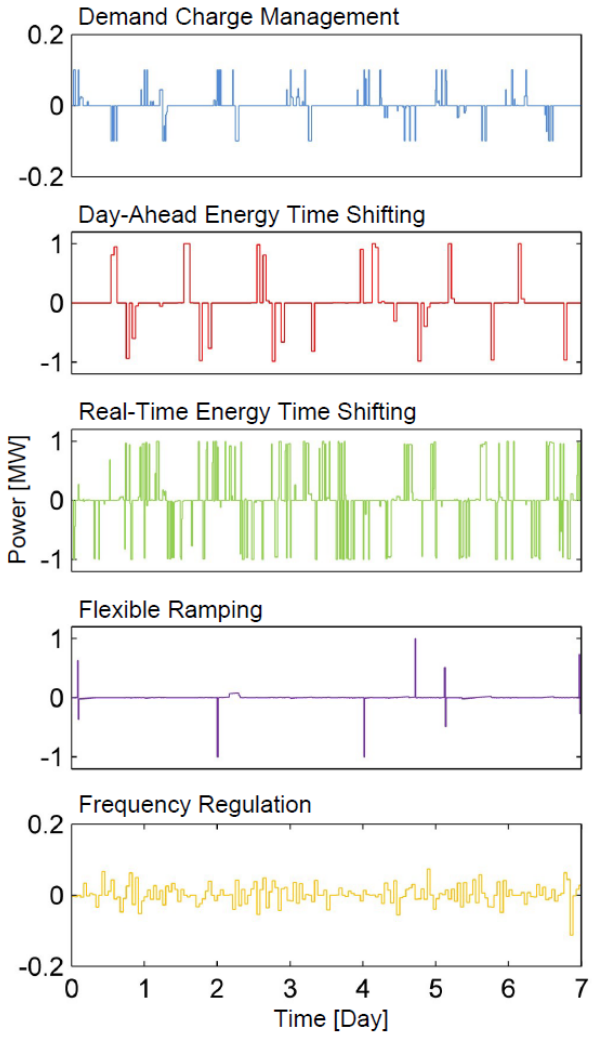

Fig. 2. Dispatching duty cycles of each energy service under stacked applications; from top to bottom: Demand Charge Management (blue), Day-ahead Energy Time Shifting (red), Real-time Energy Time Shifting (green), Flexible Ramping (purple), and Frequency Regulation (orange).

The dispatcher was able to operate the ESS system based on economic incentives of different applications. The DC application mainly reduces the peak load demand. When peak load is not present, it will also dispatch the ESS to perform peak shaving based on the TOU price. The DC application only activates for a short period of time each day. The DA and RT application need to move bulk energy in and out of the ESS, and as a result, they are mutually exclusive and occupy most of the ESS time. For the FR application, when the ramping demand occurs, the ESS will capture it by reserving ramping up or ramping down capacity for the next interval and performing the ramping to earn extra revenue. The FQ application mainly dispatches the ESS's power capacity. It is compatible with the rest of the energy-focused applications and stays active throughout the course of the simulation. As shown in Fig. 3, for stacked and single use applications, their power profile and energy throughput are largely similar. Under stacked applications, a 1 MW/2 MWh ESS will dispatch about 2 cycles per day and earn average revenue of $398 each day, over 100% more compared to only participating in the RT application, at the similar cost of ESS usage. Further simulation was conducted of three ESSs of the same peak power (1 MW) and round trip efficiency (90%) but at different EtoP of 2, 4, and 8 respectively.

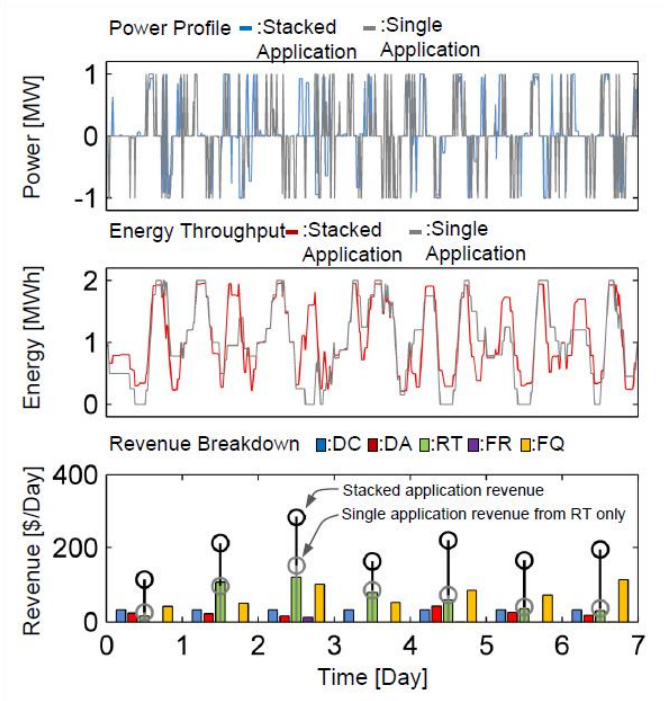

Fig. 3. Comparison between the stacked application and single real-time energy shifting application; from top to bottom: Dispatching power profile, Energy throughout, and Revenue breakdown.

As shown in Fig. 4, the black marks indicate the stacked daily revenues and the gray marks indicate the stacked daily revenues, excluding FQ. For long duration ESSs, they earn a higher portion of bulk energy management applications revenue from the total revenue mix. For short duration ESSs, they earn a higher portion of power applications revenue from the total revenue mix. However, under the current market, the revenue from FQ application are more profitable than the rest of the applications. As a result, extending the ESS duration from 2 hours to 8 hours only improves revenue by 30%. However, as the market progresses, the regulation market capacity will soon be filled; if excluding revenue from the FQ application, extending the ESS duration from 2 hours to 8 hours will improve its revenue by over 72%. It should be noted that because the FR application is still under development, the economic benefit of performing FR service is still possibly

underestimated.

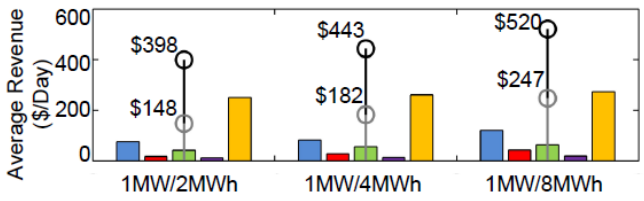

Fig. 4 Comparison among the revenues of three Energy Storage Systems with different durations of 1-hour, 2-hour and 3-hour. Colored bars: revenue breakdown of the applications. Black mark: stacked revenue. Gray mark: stacked revenue, excluding the frequency regulation application.

V. Conclusions

This work developed an optimal dispatching algorithm using mixed-integer-linear-programming to operate an ESS under five different utility grid energy market applications. The study shows that operation under stacked applications provides better value proposition compared to single use application. Further simulation unveils system performances under various energy to power ratios representing different types of ESS solutions.

To improve the dispatching algorithm, further work can be performed on acquiring more application data to develop a better market forecasting model using machine learning techniques. In addition, for applications like RT energy shifting, FQ, and flexible ramping, stochastic models can be constructed to account for uncertainties in the market participation process and help design a dispatcher weighing expected earnings and earning covariances.

Acknowledgements

The research team gratefully acknowledges the funding from Advanced Research Projects Agency-Energy (ARPA-E) under Grant No. DE-AR0000520. A.O. The authors would like to express their gratitude to Peter Klauer from CAISO and Spence Gerber from Olivine, Inc. for providing guidance on the CAISO market simulation. The authors would also like to acknowledge Prof. Y. Shirley Meng, Prof. Graham Elliott, and Daniel Davies at the University of California San Diego whose work was influential in deciding on, and producing the application duty cycles used in this study.

References

[1] *DOE/EPRI 2013 Electricity Storage Handbook in Collaboration with NRECA*, A. A. Akhil, G. Huff, A. B. Currier, B. C. Kaun, D. M. Rastler, S. B. Chen, *et al*., Sandia National Labs., Albuquerque, NM, July 2013, pp. 1-26.

[2] J. Eyer and G. Corey, "Energy storage for the electricity grid: Benefits and market potential assessment guide," Sandia National Labs., Albuquerque, NM, Rep. no. SAND2010-0815, Feb. 2010.

[3] R. L. Fares and J. P. Meyers, "Economic operational planning of grid-connected battery energy storage," *ECS Trans.*, vol. 45, no. 26, pp. 1–16, Jun. 2013.

[4] E. Hittinger, J. Whitacre, and J. Apt, "What properties of grid energy storage are most valuable?" *J. Power Sources*, vol. 206, pp. 436–449, May 2012.

[5] B. Battke, T. S. Schmidt, D. Grosspietsch, and V. H. Hoffmann, "A review and probabilistic model of lifecycle costs of stationary batteries in multiple applications," *Renewable and Sustainable Energy Reviews*, vol. 25, pp. 240–250, Sept. 2013.

[6] A. S. Tsagkou, E. D. K. D. I. Doukas, D. P. Labridis, A. G. Marinopoulos, and T. Tengnér, "Stacking grid services with energy storage techno-economic analysis," in *PowerTech, 2017 IEEE Manchester*, Jun. 2017, pp. 1–6.

[7] I. Atzeni, L. G. Ordóñez, G. Scutari, D. P. Palomar, and J. R. Fonollosa, "Demand-side management via distributed energy generation and storage optimization," *IEEE Trans. Smart Grid*, vol. 4, no. 2, pp. 866–876, Jun. 2013.

[8] H. Pandžić, I. Kuzle, and T. Capuder, "Virtual power plant midterm dispatch optimization," *Applied Energy*, vol. 101, pp. 134–141, Jan. 2013.

[9] L. Xiaoping, D. Ming, H. Jianghong, H. Pingping, and P. Yali, "Dynamic economic dispatch for microgrids including battery energy storage," in *Power Electron. for Distributed Generation Systems* (PEDG), *2010 2nd IEEE Int. Symp. on. IEEE*, pp. 914–917.

[10] H. Hao, D. Wu, J. Lian, and T. Yang, "Optimal coordination of building loads and energy storage for power grid and end user services," *IEEE Trans. Smart Grid*, vol. 9, no. 5, pp. 4335-4345, Jan. 2017.

[11] A. Hoke, A. Brissette, S. Chandler, A. Pratt, and D. Maksimović, "Look-ahead economic dispatch of microgrids with energy storage, using linear programming," in *2013 1st IEEE Conf. Technol. for Sustainability (SusTech)*, pp. 154–161.

[12] A. Nottrott, J. Kleissl, and B. Washom, "Storage dispatch optimization for grid-connected combined photovoltaic-battery storage systems," in *Power and Energy Society General Meeting, 2012 IEEE*, pp. 1–7.

[13] J. Soares, M. Silva, T. Sousa, Z. Vale, and H. Morais, "Distributed energy resource short-term scheduling using signaled particle swarm optimization," *Energy*, vol. 42, no. 1, pp. 466–476, Jun. 2012.

[14] A. Dubey, P. Chirapongsananurak, and S. Santoso, "A framework for stacked-benefit analysis of distribution-level energy storage deployment," *Inventions*, vol. 2, no. 2, p. 6, Mar. 2017.

[15] B. Cheng and W. Powell, "Co-optimizing battery storage for the frequency regulation and energy arbitrage using multi-scale dynamic programming," *IEEE Trans. Smart Grid*, vol. 9, no. 3, pp. 1997-2005, Sept. 2016.

[16] K. Anderson and A. E. Gamal, "Co-optimizing the value of storage in energy and regulation service markets," *Energy Systems*, vol. 8, no. 2, pp. 369–387, Sept. 2017.

[17] D. Wu, C. Jin, P. Balducci, and M. Kintner-Meyer, "An energy storage assessment: Using optimal control strategies to capture multiple services," in *Power & Energy Society General Meeting, 2015 IEEE*, pp. 1–5.

[18] L. Xu and D. Tretheway, "Flexible ramping products," 2012. [Online]. Available: http://www.caiso.com/documents/draftfinalproposal-flexiblerampingproduct.pdf

[19] S. Tao, "Business requirements specification," 2012. [Online]. Available: https://www.caiso.com/Documents/BusinessRequirementsSpecification-pay-PerformanceYearOneDesignChanges.pdf

Controlling Energy Storage Systems: Lessons Learned from the Washington Clean Energy Fund Demonstration Projects

Jan Alam[1], Patrick Balducci[1], Vilayanur Viswanathan[1], Alasdair Crawford[1], Di Wu[1], Trevor Hardy[1], Kendall Mongird[1]

[1]*Pacific Northwest National Laboratory, Richland, Washington, USA*

***Abstract*- Washington State Clean Energy Fund energy storage demonstration projects created opportunities for learning various aspects of Energy Storage Systems (ESSs), including its control for optimum economic return under various conditions. As the lead for ESS use-case analytics program in the ESS demonstration projects, the authors experienced practical aspects of ESS control in terms of control strategy development, control systems deployment, and performance during actual operation. This paper presents some of the learning opportunities availed from the demonstration projects along with a few key lessons for the benefit of the broader energy storage community.**

***Keywords*- Washington CEF, ESS control strategy, control system, ESS performance, power and SoC deviation**

I. Introduction

With all its advantages of being a source of fast and on-demand power supply, Energy Storage Systems (ESS) are being considered by utilities and industry players as a means of enhancing the efficiency and resilience of electric power systems. As a device with certain physical constraints, and then subject to the complexities of grid interfacing, and finally with the expectations to fulfill deployment objectives, ESS installations require significant considerations for their control. To successfully control an ESS for a given service, the control strategy needs to be appropriate, the control system it will run through needs to be well-understood and reliable, and the ESS needs to perform as anticipated during the design of the control strategy. As one could imagine, all of these elements may be affected by practical issues and hence, achievement of ESS deployment goals may be challenging.

Lessons from field demonstrations on the control aspects mentioned above could provide useful insights and guidance on designing and deploying effective and reliable control systems. This paper presents the learning opportunities obtained and key lessons learned by the authors on ESS control from the Washington State Department of Commerce Clean Energy Fund (CEF) demonstration projects across the state of Washington. Various use cases relating to ESS application for bulk energy, ancillary services, and distribution grid efficiency and reliability improvement were run at different utility sites. Experience from these field demonstrations would help better understand practical requirements of ESS control for different ESS services. Lessons that particularly relate to deviations between desired and actual ESS power, and estimated and actual State of Charge (SoC) that were observed during use case tests are presented and discussed for the benefit of the energy storage community.

The paper will first provide an overview of the CEF program and the ESS demonstration project sites. This will be followed by a description of the type and scope of learning opportunities from experience at CEF demonstration sites with practical lessons from use case testing performed to date. Finally, the paper will conclude with a general outline of how these experiences, observations, and lessons could enhance the ESS community's understanding of ESS control.

II. Washington CEF Program and ESS Demonstration Projects

In 2013, the Washington State Legislature appropriated funding for the advancement of renewable energy technologies throughout the state [1]. A Smart Grid grant of $15M was created from that funding to support efforts by three Washington utilities (Avista Utilities, Snohomish Public Utility District, and Puget Sound Energy) to install ESS to help with outage mitigation and renewable integration issues. Below are brief descriptions of these participating utilities and their ESS projects. The locations of the ESS demonstration sites at these three utilities' service area are identified in Fig. 1.

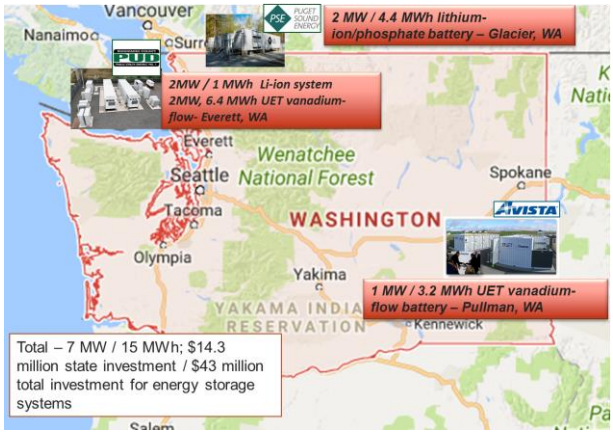

Fig. 1. Washington CEF ESS Demonstration Project site locations.

A. Avista Utilities

Avista Utilities, an investor-owned utility in the Pacific Northwest region, serves more than 600,000 electric and natural gas customers over a service territory of 30,000 square miles in eastern Washington, northern Idaho and parts of southern and eastern Oregon—an area with a total population of 1.6 million. With a $3.2M grant from Washington CEF and $3.8M of matching funds, Avista installed a 1 MW/3.2 MWh flow type ESS near Avista Turner substation, which is connected to Schweitzer Engineering Laboratories' (SEL's) premises in Pullman, Washington [2]. The SEL facilities and its ESS are shown in the top panel of Fig. 2. This ESS will serve as a critical resource to supply uninterrupted power to SEL loads during transition between one feeder and another, and also as backup power during outages at the upstream network. The ESS is built on advanced Vanadium Redox flow battery technology developed by Pacific Northwest National Laboratory (PNNL) and further improved and commercialized by Uni Energy Technology (UET). This technology consists of a thermally stable, aqueous system with no risk of thermal runaway. Commercially named "Uni.System" [3-4], each of these ESS units consists of five 20-foot factory-integrated standard containers, of which four contain the battery stacks and the fifth houses the Power Conversion System (PCS). The four containers of battery stacks are connected in series to form a string. Each unit of Uni.System provides 500 kW of power for up to 4 hours, with peak power capability of 600 kW and maximum energy capability of 2.2 MWh. There are two Uni.System units at the Avista ESS installation.

Fig. 2. Avista ESS at SEL manufacturing plant (top) and PSE ESS at Glacier Substation (bottom) provide critical backup power and outage mitigation support.

B. Snohomish Public Utility District

Snohomish Public Utility District (SnoPUD) is located approximately 20 miles north of Seattle and serves over 327,000 electric customers and 19,000 water customers over 2,200 square miles of service territory. SnoPUD received $7.3M from the Washington CEF towards installation of two ESSs [5] - both built using Modular Energy Storage Architecture (MESA) and are identified as MESA 1 & MESA 2. SnoPUD's motivation behind the ESS projects was to acquire assets with capabilities to help integrate renewable energy resources with their network, and could be fully integrated with their control systems. MESA 1 ESS is comprised of 2 × 1 MW, 0.5 MWh lithium-ion battery system installed at SnoPUD's Hardeson substation. One of the 1 MW banks is manufactured by Mitsubishi and GS Yuasa, the other by LGChem. MESA 2 is built on Vanadium Redox flow battery technology and consists of two UET-supplied Uni.System units, each with a 2 MW/6.4 MWh capacity.

C. Puget Sound Energy

Puget Sound Energy (PSE) provides electric and natural gas services to more than 1.7 million customers over a 6,000 square-mile service area, primarily in the Puget Sound region of western Washington. Headquartered in Bellevue, Washington, PSE's service area is home to some of America's most recognized and respected businesses, including the Boeing Commercial Airplane Group, Microsoft, and Amazon.com. With $3.8M funding from the CEF Smart Grid Grant and $5.8M of their own, PSE installed a 2 MW/4.4 MWh

lithium-ion ESS near its Glacier Substation [6]. Glacier is a small, geographically isolated town in northern Washington state that suffers frequent outage of electricity supplied by a long, exposed 55 kV transmission line, vulnerable to severe storms and falling trees [7]. This situation makes the Glacier ESS, with its outage mitigation capabilities, highly important and valuable to PSE. The ESS at Glacier substation was integrated by Renewable Energy Systems Americas, Inc. (RES Americas), with lithium-iron phosphate ($LiFePO_4$) cells manufactured by BYD[1]. The system consists of four containers, each having six strings connected in parallel through a 500 kW bi-directional converter manufactured by BYD (model BEG500KTL-U). Bottom panel of Fig. 2 shows an image of the ESS with four containers and the electrical interconnection with Glacier substation.

III. ESS Control Learning Opportunities

PNNL is leading the Use Case Testing and Analytics effort under the Washington CEF program and is responsible for scoping the use cases for each of the participating utilities. Use case testing process of a service starts with designing a duty cycle that represents the charge/discharge operations an ESS will be subjected to while engaged in that specific service. Therefore, one of the first learning opportunities encountered was in the design of control strategies.

The next step is to implement the designed duty cycle through a control interface. This step presents opportunities to learn about different control systems, particularly how the participating utilities implemented these systems onsite, and how they impact the fulfillment of the utilities' deployment goals.

Finally, during the execution step of the duty cycle, there are opportunities to learn how practical operational issues of a given system influence the ESS performance. In-service performance provides critical information about the ESS that will help researchers to model ESS performance more accurately, leading to better control strategies to meet deployment objectives. Fig. 3 illustrates these three elements related to ESS control and the following sections enlarge on them.

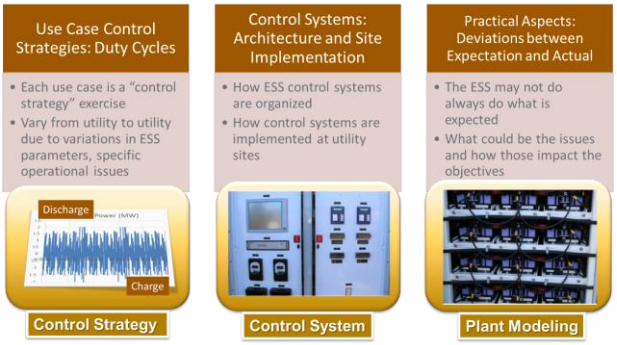

Fig. 3. Types of control learning opportunities gained from Washington CEF ESS demonstration projects.

IV. Control Strategy Development

Use cases under the Washington CEF program are built upon a variety of power system services, such as bulk energy applications (e.g., energy arbitrage, system capacity support), ancillary services (e.g., regulation), distribution system services (e.g., investment deferral by peak shaving, load shaping), and Volt/VAR applications. Controlling a given ESS for a particular use case at a specific utility requires a unique duty cycle, and provides an opportunity to go through a control strategy design exercise. A generic list of the use cases included in the CEF program can be found in Fig. 4. The control strategies were developed using either a rule-based approach or an optimization-based approach, as described below.

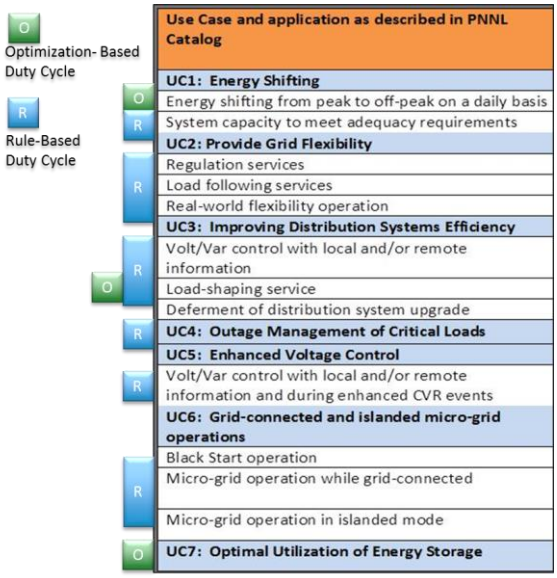

Fig. 4. Washington CEF use cases.

A. Rule-Based Approach

Generally, control strategies of the use cases that did not explicitly require an optimization to be performed were modeled using rule-based approaches. For instance, providing

[1] http://www.byd.com/usa/energy/

capacity support during a system-wide peak, or performing a load shaping service. System wide peak support duty cycle is developed by studying the system peak hours for a given utility and the ESS was controlled to discharge power at different length of periods (e.g. 1-4 hours) with adequate charging to maintain SoC level. Load shaping could take a variety of forms, and both types of control approaches (rule-based, and optimization-based) can be used to develop duty cycles for this service. For the rule-based approach, a strategy was set up to charge and discharge the ESS to reduce the gap between peak and valley of the load profile to make it flatter. The logic was to reduce efforts of control and regulating devices to manage these two opposite scenarios. A schematic of the rule-based load shaping duty cycle using historical load data and the result of performing that duty cycle is presented at the top panel of Fig. 5. As observed, the gaps between peaks and valleys of the load profile (brown: original, violet: with ESS) reduced by charging/discharging the ESS as per the duty cycle (green).

As one would understand, different approaches can be adopted to develop a rule-based duty cycle for a given service. PNNL focused on finding the appropriate match for the utility and the scenario under consideration. Ancillary service use cases (e.g., Regulation, Load Following) were developed using the rules of power system dynamics. Data (e.g., Area Control Error, Wind Generation) supplied by the participant utilities was used so that the duty cycles developed resemble the dynamics of that particular system, and the ESS is tested to the situations it would be subjected to in actual operation.

Outage mitigation and micro-grid operation use cases were also tested using rule-based duty cycles. ESS performance in these services depend on how effectively the ESS control performs in conjunction with distribution automation system. For CEF use case analytics program, these tests were performed based on U.S. Department of Energy test protocol using historical load and outage data. While CEF program scope did not require an actual outage to be conducted for these use case tests, PNNL closely engaged with the utilities in planning, execution, and analyzing results of similar tests conducted by the utilities for their own purposes. Precise timing of distribution system switching operations and ESS load pick-up was found to be very important for this type of services.

B. Optimization-Based Approach

An optimization-based approach is used for use cases that inherently require optimization to be performed for benefit maximization. Energy arbitrage is a classic example of such a use case because it involves maximizing the revenue from "buy low, sell high" transactions. Duty cycle for optimization-based load shaping service under CEF has been designed by minimizing payment to the balancing authority to reduce the gap between scheduled and actual load. A more complex and comprehensive use case is the optimal bundling of multiple services to maximize revenue from ESS operation. PNNL's in-house Battery Storage Evaluation Tool (BSET) has been used to develop optimization-based control strategies. A schematic of the optimization-based duty cycle development process using BSET is shown in the bottom panel of Fig. 5.

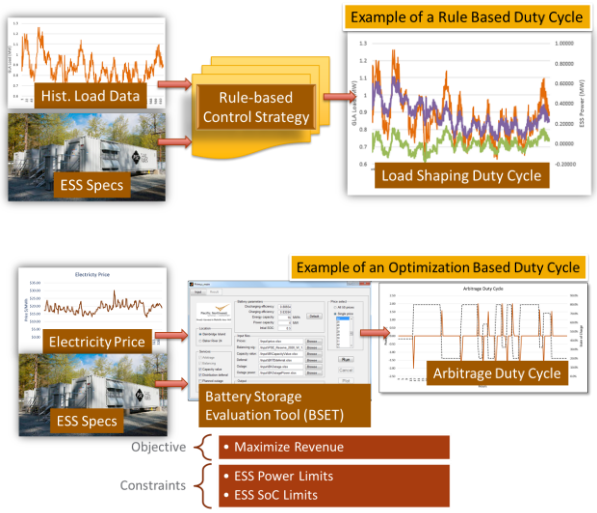

Fig. 5. Rule-based (top) and optimization-based (bottom) control strategies for ESS duty cycle development.

IV. Control Architecture and Site Implementation

Understanding the control architecture, systems, and equipment used for ESS control and how they interface and interact with a utility's existing control systems or SCADA is highly important. During the testing process, PNNL experienced multiple interruptions because control systems at different levels (e.g., Battery Management System [BMS], and inverter controller) failed to communicate and interact properly. Without adequate understanding of the control systems and their interoperability issues, it could be difficult to operate ESS reliably to achieve expected benefits. The following paragraphs outline the architecture and equipment used to control ESS at each of the CEF program utility sites.

A. Control Architecture

CEF demonstration projects (except Glacier ESS) deploy a two-layer control architecture for their ESS control systems (represented in Fig. 6). The top layer consists of an optimal scheduler that features capabilities to incorporate economic aspects (e.g., electricity price and/or other financial inputs) and ESS technical parameters to optimally run the ESS. An optimal scheduler can schedule multiple ESSs and other distributed resources. The bottom layer consists of controllers for each individual ESS, which perform detailed control and monitoring functions (e.g., charge/discharge, ramping, maintaining SoC) in coordination with the BMS. Of the three utilities, SnoPUD and PSE used the control and communication architecture proposed in MESA. A detailed discussion of MESA appears later in this paper.

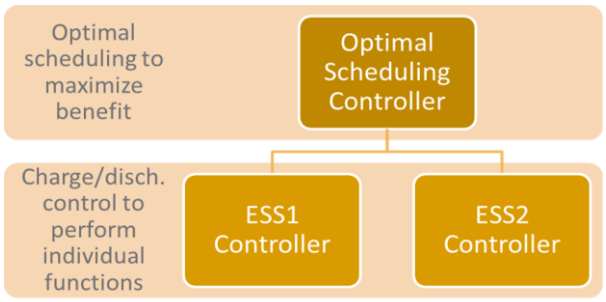

Fig. 6. General control architecture used at Washington CEF ESS projects.

B. Avista ESS Control System

Avista's UET flow batteries installed at SEL facilities are controlled using a Siemens PLC-based control system. A site controller using the Simatic WinCC Open Architecture (OA) SCADA system is installed for visualization and operation of processes. One site controller can control up to 100 strings of UET batteries. Each string, consisting of four batteries, one power conversion system, cooling system, and communications system, is controlled by a Simatic S7-1500 PLC which accomplishes day-to-day operational functions (e.g., charge and discharge control, SoC management, and reactive power control) of each ESS unit. A schematic of the control architecture is shown in the top panel of Fig.7.

Avista is in the process of deploying an optimization controller (the SPIRAE Wave™ [2]) as the top-layer controller (see Fig. 6) to optimize the ESS operation for maximizing the benefit of various services tied with their deployment goals. To compare with the architecture in Fig. 6, control layers in Fig. 7 are identified with dashed boxes.

C. SnoPUD and PSE ESS Control Systems

ESS Control systems at SnoPUD and PSE are built on MESA standards. At the planning stage, SnoPUD explored different standards for software and control system integration of ESS and experienced lack of adequate open standards [8]. Therefore, in collaboration with a number of partners, MESA – an open, non-proprietary standard was developed that helps accelerate interoperability, scalability, safety, quality, and affordability in energy storage components and systems.

The MESA standard has two major components. One is "MESA-ESS," which addresses ESS configuration management, ESS operational states, and the applicable ESS functions of IEEE 1815 (DNP3) profile for advanced DER functions. The other is "MESA-Device," which addresses how energy storage components within the ESS communicate with each other and other operational components and is built on the Modbus protocol.

SnoPUD deployed 1Energy-Intelligent Controller (1E-IC) built by 1Energy, which has been acquired by Doosan GridTech that renamed the controller "DG-IC". Supervisory control, including optimal control for different use cases, is performed by Doosan's Distributed Energy Resources Optimizer (DG-DERO™), a management system that optimally aggregates economic values from fleets of ESSs and other distributed resources. Built-in operating modes of DG-IC include Market-based Charge/Discharge, Frequency Correction, Spinning Reserve, Forecast Assurance, Power Following, Peak Power Limiting, Power Factor Correction, Volt/VAR, Volt/Watt, Power Smoothing, Islanding, and SoC Maintenance. A schematic of the DERO and DG-IC control deployment is shown at the bottom panel of Fig. 7. PSE deployed DG-IC without DERO at its Glacier ESS.

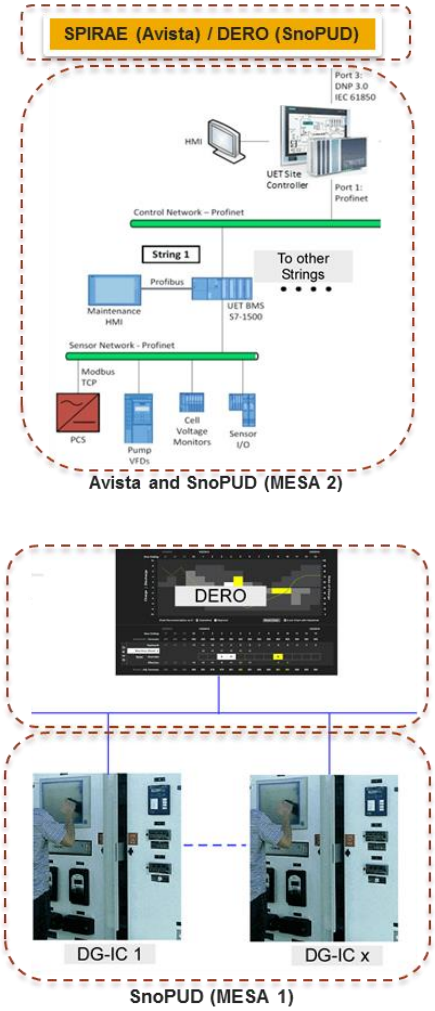

Fig. 7. Control system deployment at Washington CEF ESS project sites.

[2] http://www.spirae.com/microgrid/about-microgrid

V. Deviation Between Expected and Actual Performance of ESS

In the process of running use case tests, it was observed that the ESS may perform differently in actual operation than predicted during the design of control duty cycles. This might create unacceptable engineering and economic outcomes. Analysis of these deviations using test results can provide useful insights on ESS performance, and more importantly, how performance could drift from that anticipated. Two such examples of deviation between expected and actual performance are presented below.

A. Scheduled and Actual Power Input

While engaged in providing a service, an ESS is expected to charge/discharge at scheduled rates over a given horizon of time. However, during the course of use case testing under the CEF program, deviations were observed between scheduled and actual power output at multiple instances. An example is shown in Fig. 8 in which the ESS was commanded to charge at a certain power level, but it charged at a lower level than commanded. Similar deviations were observed for discharging operations as well, as identified in Fig. 8. Discussion with utility personnel on these incidents helped in the development of some hypotheses on the cause (e.g., conflicts between different scheduling modes in the control system), but no definitive cause was identified.

Examination of SoC profiles from the past and future operations did not provide any evidence to support the idea that these particular deviations were caused by BMS interventions to prevent overcharging or overdischarging. Failing to follow a power command properly could be economically detrimental for power intensive applications (e.g., regulation), which happens to be a major component of ESS revenue for many deployment sites and therefore, needs to be treated with importance. With energy intensive applications, this could result in having inadequate amount of energy (or empty space) and could affect economic benefit achievement.

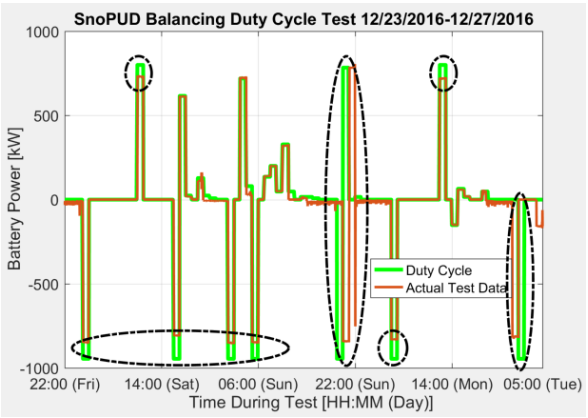

Fig. 8. Deviation between scheduled and actual power output of ESS.

B. Predicted and Actual SoC

Deviation between predicted and actual SoC could usually be observed with real world ESS because the SoC depends on many physical parameters (e.g., charging/discharging rate, temperature) during operation and could largely vary with time. If not tracked and corrected time to time, these variations could cause the SoC to exceed recommended operational bounds. If there are not enough protective features enabled in the BMS, an ESS could operate outside recommended SoC limits for longer than its designed tolerance, which could shorten its lifetime. Fig. 9 illustrates such an instance extracted from a 28-days-long use case test. The red circle between August 3 and 5 identifies a situation where the SoC went down to 1 percent, which is typically not recommended.

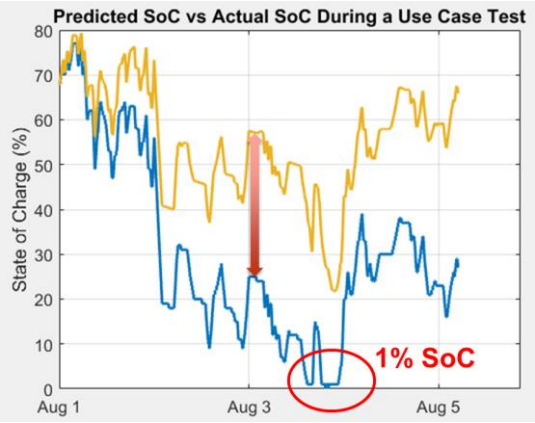

Fig. 9. Deviation between actual and expected SoC.

The researchers use PNNL's advanced nonlinear battery model to predict SoC profile over the test period and adjust the duty cycle as necessary to keep the SoC within limits. The same practice was exercised for the use case shown in Fig. 9. However, analyzing data from this low SoC event suggested that the ESS' performance drifted from the previously used performance parameters used for SoC prediction model and therefore failed to predict the SoC limit violation. This suggests that a check and balance of ESS performance parameters while developing and deploying a control strategy could be useful for ensuring operation within specifications. Another important lesson from this incident is that the monitoring and protection features in the BMS should be enabled to send alarm to the operators, and if required, execute a shutdown to save the ESS from possible damage.

VI. Conclusion

Three utilities across the state of Washington (Avista, SnoPUD and PSE) installed ESS, partially funded by the Washington State Department of Commerce under Washington CEF program. This paper presented the learning opportunities and key lessons in three areas of ESS control based on the Washington CEF ESS demonstration projects – control strategy development, control system deployment, and practical

challenges with ESS control during operation.

Duty-cycle development for Washington CEF use-case testing essentially consists of exercises in developing control strategies for the various types of ESS services (e.g., bulk power, ancillary services, and distribution support). With the variations of economic and technical constraints including ESS parameters from one to another utility, the same use case could take different forms and therefore different control strategies will be needed for duty cycle development. Depending on the nature of a given use case, either optimization- or rule-based, control strategies could be used to develop the test duty cycle. The physical process of conducting use-case testing by running the duty cycles through ESS control systems provides opportunities to understand how control systems are designed, implemented, and integrated with a utility's existing control system or SCADA. Such exercises yield valuable insights on control and communication failure that can help achieve more reliable ESS operation.

Further, deviations between expected and actual performance (e.g., between commanded and actual power, predicted and actual SoC) of the ESS during testing provide opportunities to learn what practical challenges exist in ESS control. Information obtained by analyzing these deviations is vital in modeling and predicting ESS performance more accurately so that ESSs operate within acceptable parameters and impart values estimated.

While the learning opportunities and lessons presented in this paper relate to Washington CEF demonstration projects, they are likely applicable to many other ESS projects of similar size and complexity, both across the USA and in other parts of the world. The authors hope the lessons learned from these projects help to improve control system performance for existing ESS projects, and to develop new control systems for future projects.

ACKNOWLEDGEMENT

We are grateful to Dr. Imre Gyuk, the Energy Storage Program Manager in the Office of Electricity Delivery and Energy Reliability at the U.S. Department of Energy. Without his office's financial support and his leadership, this project would not be possible. We wish to acknowledge the other members of the Grid Modernization Laboratory Consortium team: Dan Borneo, Ben Schenkman, and Ray Byrne of Sandia National Laboratories; Michael Starke of Oak Ridge National Laboratory; and Todd Olinsky-Paul of the Clean Energy States Alliance. We would like to acknowledge the valuable support from utility personnel (Avista: John Gibson/Caitlin Greeney/Darrel Richardson, SnoPUD: Kelly Wallace, PSE: Kelly Kozdras/Shane Richards) in providing information on use case test runs, control system issues, interruptions, etc.

REFERENCES

[1] Washington State Department of Commerce, "Clean Energy Fund: Program Status per 2EHB1115 (2015), Section 1028(11)," Washington State Department of Commerce, Olympia, WA, 2015, accessed July 26th 2017 at http://www.commerce.wa.gov/wp-content/uploads/2017/04/Commerce-Clean-Energy-Fund-2017.pdf

[2] (2015) Avista Corporation News Release. "Avista's Energy Storage Project is energized by Governor Inslee." accessed November 16th 2017 at http://avistacorp.mwnewsroom.com/News/in/Avista%E2%80%99s-Energy-Storage-Project-is-energized-by-Go.

[3] UniEnergy Technologies (UET), "Uni.System™ grid-scale energy storage Solution," UniEnergy Technologies, LLC, Mukilteo, WA, 2016, accessed September 18 2017 at http://www.uetechnologies.com/images/product/UET_UniSystem_Product_Sheet_reduced.pdf.

[4] UniEnergy Technologies (UET), "Maximizing grid value through UET energy storage for utilities, microgrids, commercial & industrial," UniEnergy Technologies, LLC, Mukilteo, WA, 2015, accessed September 18 2017 at http://www.uetechnologies.com/images/product/UET_Product_IntroSheet.pdf.

[5] Snohomish Public Utility District, "Energy Storage Project: A new model of battery architecture," Snohomish County Public Utility District, Everett, WA, 2016, accessed November 16 2017 at http://www.snopud.com/Site/Content/Documents/energystorage/energystorage_factsheet_1017.pdf.

[6] Puget Sound Energy, "Glacier Battery Storage Project," Puget Sound Energy, Bellevue, WA, 2017 accessed November 16 2017, at https://pse.com/inyourcommunity/pse-projects/system-improvements/Documents/Glacier_BatteryStorage/GlacierBattery_FactSheet_Oct2017.pdf.

[7] RES Americas, "Case study: Glacier Energy Storage Project," Renewable Energy Systems, Ltd., England, UK, 2016. accessed August 23 2017 at http://www.resgroup.com/media/2410/glacieresscasestudy_042517.pdf.

[8] J. Zyskowski, "Overview and Lessons Learned from Snohomish County PUD's First Energy Storage Project," Snohomish County Public Utility District, Everett, WA, 2016, accessed July 14 2017 at https://www.snopud.com/Site/Content/Documents/energystorage/SnoPUD-EnergyStorage013115.pdf.

How Battery Energy Storage Displaces and Replaces Conventional Generation – Trajectory of Storage Providing Supplemental Services, to Essential Services, to Full Replacement of Generation

Michael Jacobs
Union of Concerned Scientists
Two Brattle Sq. Cambridge, MA 02138-3780, United States of America

***Abstract*—The trajectory of energy storage substituting for conventional generation can be traced from actual practices, and projected further from demonstrated capabilities. Demonstration projects from 1987 proved benefits from utility-connected operations. Niche markets developed after 2005, further raising confidence and capabilities. With demonstrated efficiencies and supportive policies, U.S. battery storage installations began to serve as generation. This paper traces this trajectory, and suggests that retiring old generation and making replacements with storage-backed variable renewable generation is a viable technical option.**

***Keywords*— grid applications, policy, markets**

I. Introduction

The trajectory of energy storage substituting for conventional generation can be traced from actual practices, and projected further from demonstrated capabilities. The deployment of energy storage instead of fossil-fired generation is an important shift in the electric power industry, even if begun incrementally and first in niche applications. The implications of this on system planning, expansion, operations, and on energy markets have not been defined. The private and public stakeholders making new power capacity investment decisions should recognize this technological change could be a revolution.

From 1987 to 2005, a very small number of grid-scale battery systems were installed on power grids. Rare demonstration projects, provided proof that battery energy storage could be used in a utility system. Today, procurements, planning and announcements for utility-scale battery storage systems are widespread.

In US and Japan, a series of successful battery installations demonstrated a variety of storage technologies. Often these were connected at end-user locations, provided valuable learning and field experience. Important milestone projects date back to the 1987 installation of a 500 KW lead acid battery at the Crescent Electric Membership Cooperative in North Carolina, a distribution-only utility. A 10 MW, 40 MWH lead acid battery at Southern California Edison substation at Chino, CA demonstrated beginning in 1988 the fast response of storage could reinforce a transmission system. The 20 MW, 14 MWH lead acid battery installed in 1994 on the island grid of Puerto Rico provided utility PREPA with reserves and frequency control. This demonstrated how a battery can operate on a power system as an alternative to generation, and that was done with battery technology comparable to the Chino installation [1].

Development and demonstration projects in Japan soon followed, though with different emphasis. Utility KEPCO and manufacturer Sumitomo demonstrated vanadium flow batteries for peak shaving on in commercial customer settings from 1999. At the same time, utility TEPCo and manufacturer NGK began operating sodium-sulfur projects. Japanese installations alongside wind generation equipment proved the capability of energy storage in flywheels and flow batteries to provide generation services.

II. Overview of Storage Progress

A. How did this happen and What Does This Mean?

As the power industry demonstrates confidence in the increased functions of inverters and long-duration energy storage, decision-makers face the reality of storage replacing conventional power plant capacity with storage.

The record of the past decade shows energy storage making incremental replacement of the features, functions and roles of conventional generation. Initial commercial storage deployments provided operational flexibility to manage forecast errors and output variability. In Hawaii, limits set out in 2006-2007 on windfarm variability led to storage systems designed for high-power, low-energy application of smoothing short-term output. At the same time, a generation owner in Chile began to add storage to provide spinning reserves for contingency response previously provided by unloaded generator capacity.

The successes started to come through the identification of specialized functions provided by conventional generators that could be done economically by available or emerging storage technology. Confidence from initial projects led to more

installations, followed by changes in assumptions and practices regarding the functions of megawatt (MW)-scale storage systems and fast-responding inverters with power-factor control supporting voltage. While most of the early grid installations and defined niches were not related to renewable energy, the potential for clean energy from intermittent sources combined with reliability attributes from energy storage soon grew from concept to reality.

By examining how energy storage has quickly matured from filling just a few functions in the past to understanding how in the present battery storage is a full participant in resource adequacy planning, utility industry observers and participants can prepare for a future where fuel-burning powerplants are replaced by storage systems, and the energy can be provided by variable renewable energy sources.

B. What Is the Storage Asked to Do?

Throughout the discussion in support of energy storage deployment, the role and use cases for storage have sought to clarify the functions for energy storage on the grid [2]. This range of options available from energy storage, and the breadth of discussions is important, but should not become an overwhelming distraction. Rather than starting with storage as a many-talented tool and asking how to value many functions, the successful paths to deployment have been found where necessity or value is in the simulation or replacement of a traditional power system asset that is particularly scarce, expensive or difficult to provide. Where planners or stakeholders can determine the performance specifications for the needed power system component, this becomes the benchmark for comparisons with energy storage designs suited to fill that need. Identification of high value needs has proven to be a quicker means to identifying real-world applications for storage than an inventory of features and benefits abstractly available from storage technology.

III. Trajectory of Experience

A few trail-blazing efforts have opened markets to successful energy storage deployments. Each of these innovations sought to optimize existing grid assets by taking on a specific cost-effective role for storage. In doing so, these each established a commercial demonstration of battery storage providing a function previously provided by conventional generators. Cumulatively, this creates a trajectory suggesting that storage additions are reducing the operation of existing power plants, reducing additions of conventional power plants, and ultimately that storage can be combined with renewable energy supplies to replace existing conventional plants.

One of these explored and established a hold on an ancillary service in U.S. markets managed and operated by independent system operators (ISOs). That service, frequency regulation, proved to be attractive in PJM, the ISO serving the region from northern Illinois to North Carolina and New Jersey. Another set of niches developed in isolated areas of northern Chile and in Hawaii, where generator reserves and related services are not easily obtained. The final proving ground in very recent years is California, where public policies directing utility procurements of energy storage capacity have demonstrated competition between storage types, and between storage and any other asset class capable of providing resource adequacy.

A. Path to US Ancillary Services Market

The separation of generation from transmission in the U.S. by Order 888 of the Federal Energy Regulatory Commission (FERC) created a small number of ancillary services required to operate the power supply. The wholesale energy markets that formed after this decision defined and priced these services with varying levels of precision and differentiation. As storage technology companies made practical advances, their initial market development efforts focused on commercial opportunities that value the speed of response and short-lasting power output, rather than substantial amounts of stored energy. The supply of frequency regulation service, a short-term balancing of supply and demand needed for the grid operators to maintain the desired frequency (e.g. 60 hz in North America), proved to be a good match between emerging energy storage capabilities and higher value in the range provided by energy markets.

Combined efforts in 2006-2007 by Beacon Power, start-up manufacturer of flywheel energy storage units, Pacific Northwest National Laboratories (PNNL), Bonneville Power Administration, California Energy Commission and California Independent System Operator successfully demonstrated the benefits of flywheel storage technology and argued for a higher value for rapid, accurate response to grid operator direction for frequency regulation. These efforts were reported in two reports published in 2008 characterized California ISO regulating units' characteristics; determined the value of fast responsive resources, and compared efficiency of fast regulation units with the hydro units. One critical finding established a fast responding resource is more efficient than the average hydro power units used for regulation, allowing a smaller amount of fast acting capacity to substitute for a larger amount of hydro capacity, or even less-responsive thermal capacity [3], [4].

Beacon Power and global utility conglomerate AES Corporation led a campaign to present an economic case for compensation for faster, more accurate performance of frequency regulation with advocacy at FERC, ISO-New England and PJM.

Beacon installed a small storage facility (initially 1 MW) on a distribution line in New England in 2008. At the same time, lithium-titanate battery manufacturer Altairnano began work under a 2007 agreement with AES to validate and then deploy a MW-scale battery for frequency regulation at the headquarters of PJM [5], [6]. Each of these installations were designed specifically for frequency regulation needs. Frequency regulation is unusual in the realm of ancillary energy services because of the need to move small amounts of energy in both

directions.

FERC took notice and at the same time (2011) PJM took steps through its stakeholder process to reward more accurate and faster regulation resources. In 2010 FERC began a technical review of frequency market designs, value and benefits. The resulting rule in Order 755 directed the organized markets to change the measurement and compensation of frequency regulation service [7]. FERC, as regulator of rates and markets where they exist, designed this policy change in 2011 to foster explicit competition by energy storage with grid generation capacity held for this function. How the markets implemented FERC's order varied, but ultimately the economics of these frequency regulation markets were affected by the small size and limited demand for frequency regulation capacity.

Absent new technologies, frequency regulation and other ancillary services are provided by conventional generation holding some fraction of generating capacity in reserve for dispatch in response to instruction from the grid system operator. On the mainland U.S., all the ancillary services total 5- 10% of the costs of wholesale energy. PJM is the largest market for frequency regulation from storage, but in 2013, the first year of implementing the frequency market design changes of Order 755, PJM had installed generating capacity of 183,095 MW and PJM's daily average quantity of frequency regulation service needed was 784 MW, a decline from 943 MW in 2012 [8]. PJM indicated at the outset that the need for capacity reserved and used for this service would be lower: "fast following resources decrease the total regulation requirements necessary to maintain reliability requirements" [9]. As the PNNL studies has indicated, the PJM experienced efficiency gains from the fast and accurate provision of frequency regulation. This benefit, which PJM reported as an average of 2.6 MW of slower capacity replaced by 1 MW of fast regulation resource, allowed PJM to lower daily procurements [10].

In terms of the money in PJM's wholesale electricity market, the cost of providing the specific function of frequency regulation is roughly 0.5% of total price of a megawatt-hour (MWh) [11]. In New England, where the existing practices for tracking performance were adopted by FERC in Order 755, the frequency regulation requirement range for ISO-NE was 50 – 170 MW on a power system of roughly 25,000 MW. The risks of over-supply in such small markets were better anticipated in New England, and soon realized in PJM.

B. Storage in generation role on small grids

Providing reserves is an appropriate application for battery energy storage, given the good match between battery storage system capabilities and grid requirements for this service. Reserves are used relatively infrequently, for a defined period. Generally, reserves are deployed from generating capacity that is synchronized but unloaded. Rapid response is important, if not critical, to grid support. Where the grid is small and capacity constrained, these attributes are scarce and more valuable than on a large system with numerous generators partially loaded at any time.

Early examples of commercial energy storage deployment to displace conventional generation were in isolated grids where very small generator fleets are limited in capability and capacity limits constrain grid operations. These early deployments, installed between 2009 and 2011, take the place of conventional generation providing reserves.

Important cases in northern Chile and in Hawaii, illustrate where energy storage provides ancillary services otherwise required from generators, allowing conventional generation to either 1) increase output to serve load (Chile) or 2) not operate as the combination of renewable generator provides energy and the battery energy storage system (BESS) provides reserved capacity (Hawaii).

C. Battery systems in Chile provide spinning reserve

The power systems of the northern mining region of Chile and the Hawaiian Islands are smaller grids in isolated areas. High prices or unmet demand for energy in these locations helped support the selection of battery (BESS) to provide modest amounts of reserves.

In Chile's Atacama Desert, AES is one of many generation providers in the Northern Interconnected System, which has 3,700 MW total generation. Power system constraints limited the energy and capacity available to meet growing demand from the energy-intense mining industry in the region [12]. Each generator on this system has an obligation to maintain capacity unloaded as reserves. All else equal, an economically competitive generator would make more energy sales if the obligation to provide reserves is shifted to a storage system. Two BESS installations by AES Gener in Chile provide this alternative source of reserves. A 12 MW/4MWh BESS integrated with AES Gener's Norgener power plant in 2009 and the larger Angamos BESS (20MW/5MWh) installed in 2011 provide immediate response to frequency deviations and continue to discharge while supply balance is restored [13]. AES increased the available capacity of its Norgener plant by 20 MW with operational performance improvements provided by the 20 MW BESS. Reports by the grid operator indicate this BESS is among the most reliable and provides for quicker restoration and stability of the system compared to reserve capacity provided by thermal plants [14]. These BESS provide a substitute for conventional generation, and have demonstrated the function known in the U.S. as primary frequency response, which is sometimes mentioned as an "essential reliability service."

D. Battery systems in Hawaii smooth renewables

The power system in the Hawaiian Islands offers opportunities for energy storage and renewable energy not found elsewhere in the U.S. Each island's grid is separated from any other; oil is the dominant fuel used in generation; and state policies drive increasing use of renewable energy. The resulting prices are high compared to the mainland, and the push for renewable energy is very pronounced in the market and in

policy. The results in less than 10 years have been the inclusion of storage in renewable energy projects to modify wind and solar generation from the original description of "as available" energy into a closer approximation of conventional generation.

The physical constraints of Hawaii make the integration of variable renewable energy on the electric grid more challenging. The largest of the island grids, on Oahu, is 1,000 MW. The grids on the islands of Maui and Hawaii are 250 – 300 MW and the Kauai grid is 125 MW. Starting Oahu combustion turbine units requires 15 minutes. On the island of Hawaii, steam units predominate, so reserves are slow-moving [15]. These conditions result in very limited sources of flexibility or ancillary services and a utility policy of requiring ramp-rate controls on renewable generators.

The increased use of windpower in Hawaii led the utility to impose a limit on the rate of change in energy production in power purchase agreements for new renewable generators. These ramp-rate limits effectively created a requirement for new generators to provide frequency response and spinning reserves in proportion to their intra-hour variability. As a practical matter, planning to mitigate variability for windfarms planned on slopes was inexact. Rather than estimating and mitigating the aggregated, and partially offsetting, movement of all sources of variability this required a solution dedicated to each individual windfarm.

Hawaii received considerable attention regarding renewable energy as energy storage and renewable energy integration technologies emerged. In April 2008, the National Renewable Energy Laboratory signed a memorandum of understanding with First Wind to establish a Remote Research Affiliate Partner Site at First Wind's Kaheawa Wind Power on Maui. First Wind, the developer most active in Hawaii at the time, soon invested in a 1.5 MW/1 MWh BESS for a pilot demonstration of windfarm smoothing at that site.

This pilot led to planning and eventual deployment of full-scale 15MW/10 MWh BESS for 30 MW windfarm on Oahu. Prior to installation in 2011, developer made decisions regarding control algorithms and recognition in interconnection planning for control including using the planned BESS to meet a need for fast response to manage grid conditions after a transmission fault on the line connecting the loads and new windfarm on the North Shore of Oahu. This latter set of functions involved voltage and frequency stabilization functions not available from a generator.

Also in 2011, the Kauai utility purchased a 1.5 MW/1 MWh unit from the same BESS vendor to address variability from a growing number of solar installations, an on-going need for frequency response, as well as spinning reserves. Kauai subsequently made additional procurements of energy storage, and solar projects combined with storage as it progressed from 5% of its energy coming from renewable energy to present level of 36% [16]. Two such projects, from SolarCity/Tesla (17 MW solar, 13 MW/52MWh storage) and AES (28 MW solar, 20 MW/ 100 MWh storage), are designed to meet utility system evening peak for several hours [17].

IV. California Events Accelerate Storage As Peaker Unit

One indicator of the contemporary acceptance and confidence in utility-scale storage is the continued procurement of peaking generation built entirely from energy storage. This stage has been established in California through a mixture of state policies and events in the energy market.

California leadership in energy policy dates from at least the late 1970's and hosted the first boom in renewable energy in the U.S. in the 1980's. Attention turned to storage in the last several years, with policy action in the form of a commitment in law: SB2514, enacted in 2010. Implementation of this law, directed by the California Public Utility Commission (CPUC) in 2013, laid out a 7-year schedule for procurements in three broad categories, for the three investor-owned utilities totaling 1,325 MW under contract by 2020. This proved to be a minimum as events and additional legislation came to pass.

Industry expectations regarding the role of storage as an alternative to peaking generation changed when Southern California Edison (SCE) announced the results of its 2013 Local Capacity Resource procurements in late 2014. SCE selected 260 MW of energy storage, 100.5 MW in front of the meter, at a time when the regulatory obligation was to acquire 50 MW of storage resources in that process. This five-fold greater commitment to storage for reliability needs, instead of generation, was a distinct signal that was noticed.

A. 2016: Year of Further Gains

State policy actions taken in 2016, combined with utility procurement activity, provide a foundation for energy storage as peaking power plant. In February, SDG&E (he utility serving San Diego area) released an energy storage procurement for local capacity requirements totaling 140 MW [18]. In May, in response to an emergency created by the failure of the natural gas storage facility at Aliso Canyon, the CPUC ordered expedited energy storage procurement suitable for meeting resource adequacy. This led to SDG&E contracting for another 37.5 MW/150 MWh of battery energy storage [19]. Another 57 MW of BESS with 4-hour duration was purchased by SCE under the direction of the Aliso Canyon resolution.

B. Hybridization by generator manufacturers

Recent energy storage deployments by generator equipment manufacturers demonstrate another turning point in the substitution of BESS for conventional generation. Present (October 2016) state-of-art technology adoption includes manufacturer General Electric (GE) hybridization of storage with their LM aeroderivative generators to improve the performance of peaking plants [20].

With short duration storage now understood as providing ancillary and essential services, GE is delivering hybrid plants with storage and a gas turbine integrated in a system with a single set of controls. The GE hybrid system uses the storage to provide the reliability capabilities of the gas generator with

instantaneous response, regardless of whether the unit is started and burning fuel when response is needed.

General Electric completed a hybrid battery-gas turbine system installation at a site in Norwalk, Calif., for SCE. The system combines two 50 MW LM6000 gas turbines with a 10 MW, 4.3 MWh battery storage system. Manufacturers of internal-combustion generators Caterpillar, Cummins and Wartsila have all recently announced offerings of hybrid generation systems combining storage and conventional generation [21].

V. End-Stage Long-Duration Storage and Renewable Generation

If the trajectory described here is the accumulation of incremental steps, this is appropriate as power system expansion planning is incremental. However, there is a difference in assumptions and modeling for a changing future where incremental capacity and services are predominantly attributed to a BESS while the energy is provided from one or more variable renewable sources. Lessons learned from the past decade of assessing the capabilities and roles for energy storage can be applied to current questions.

A. Prospects for Repowering Old Generation with BESS in Critical Locations?

As part of a recent analysis of options for replacing an old generating facility in the Chicago area, UCS and students at the University of Wisconsin-Madison considered the potential role of storage. While the question was posed as, "can storage and renewables replace a major water-front fossil generator?" the analysis required a series of smaller questions, including one familiar in this discussion, what is the storage asked to do? Further, should the replacement mimic the production pattern of the plant undergoing replacement? In effect, how much energy is needed and how much on-peak capacity is needed?

Multiple feasible combinations of storage with renewable generation can provide capacity, energy, and ancillary services, as well as unpaid “essential services” in satisfaction of power system performance expectations. The value of the replacement will likely be higher with a production pattern and capacity characteristics that are matched to the local system. To make a realistic assessment, the needs for voltage support in the area must be included.

The capabilities and characteristics of replacement resources in this sort of change in generation resources is the subject of the NERC Essential Reliability Services Task Force (ERSTF) created in 2014. proposed measures to guide change in the generation mix. The ERSTF summarized the needs for this kind of assessment as frequency response, ramping energy output, and voltage support [22]. As the narrative above describes the expanding role for energy storage as a replacement for conventional generation, all of these identified needs are obtainable from BESS.

Analysis of options for the Waukegan Generation Station in northern Illinois illustrates 4- hour duration storage paired with variable renewable generation for full satisfaction of reliability and capacity market requirements. More refined study is needed, but clearly energy storage is quickly meeting critical milestones to satisfying these expectations. In addition, NERC’s essential services have been confirmed in field testing of utility-scale commercial deployment of inverters at solar facilities [23].

Conclusion

In a very short time, energy storage facilities have demonstrated all the capabilities required of generation on the U.S. power grid in commercial deployments. Taken discreetly, the reliability contributions of conventional power plants are available from battery energy storage systems. When combined with renewable energy generation, this combination is equivalent to that the operating characteristics of the conventional generation sources that are being replaced.

References

[1] A. Akhil, S. Swaminathan, and R. K. Sen., “Cost analysis of energy storage systems for electric utility applications,” Sandia National Laboratories, Albuquerque, NM, rep. no. SAND97-0443, Feb.1997.

[2] M. Deal, S. Churchill, L. Chaset, and C. Villarreal. “Electric energy storage: An assessment of potential barriers and opportunities,” California Public Utilities Commission, San Francisco, CA, Jul. 2010.

[3] Customized Energy Solutions, Sustainable Energy Advantage, Daymark, and Alevo Analytics, “State of Charge: Massachusetts Energy Storage Initiative,” Massachusetts Department of Energy Resources, Boston, MA, 2016.

[4] Y. V. Makarov, J. Ma, S. Lu, and T. B. Nguyen, “Assessing the value of regulation resources based on their time response characteristics,” Pacific Northwest National Laboratories, Richland, WA, rep. no. PNNL-17632, June 2008.

[5] Y. V. Makarov, B. Yang, J. G. DeSteese, S. Lu, C. H. Miller, P. Nyeng, *et al.*, “Wide-area energy storage and management system to balance intermittent resources in the Bonneville power administration and California ISO control areas,” Pacific Northwest National Laboratories, Richland, WA, rep. no. PNNL-17574, Jun. 2008.

[6] Altairnano, “Advanced Energy Storage Systems for frequency regulation.” Altair Nanotechnologies, Inc., Cody, WY, 2016. [Online]. Available at: http://en.escn.com.cn/Tools/download.ashx?id=130

[7] Federal Energy Regulatory Commission (FERC), “Frequency regulation compensation in the organized wholesale power markets,” Washington, DC: Federal Energy Regulatory Commission, Order 755, 2011.

[8] Monitoring Analytics, LLC. “2013 State of the Market Report for PJM,” PJM Interconnection, LLC, Norristown, PA, p. 292, 2014.

[9] PJM, “Order No. 755 Compliance Filing,” 2012, p, 8. [Online]. Available: https://elibrary.ferc.gov/idmws/common/opennat.asp?fileID=12908780

[10] PJM, “Performance based regulation: Year one analysis,” 2013. [Online]. Available: https://www.pjm.com/~/media/documents/ferc/2013-filings/20131016-er12-1204-004.ashx

[11] Monitoring Analytics, “2013 State of the Market Report for PJM,” 2013, p. 12. [Online]. Available: http://www.monitoringanalytics.com/reports/PJM_State_of_the_Market/2013.shtml

[12] Center for Economic Load Dispatch of Northern Interconnected System, “2010 Annual Report – Statistics and Operation,” 2010. [Online]. Available: http://www.cdec-sing.cl/html_docs/anuario2010/pdf/SING2010EN.pdf

[13] Businesswire, “AES combines advanced battery-based energy storage with a traditional power plant,” May 2012. [Online]. Available: http://aesenergystorage.com/2012/05/03/aes-combines-advanced-battery-based-energy-storage-with-a-traditional-power-plant/

[14] Energy Storage Association, “AES Energy Storage Angamos Battery Energy Storage System (BESS),” 2011. [Online]. Available: http://energystorage.org/energy-storage/case-studies/aes-energy-storage-angamos-battery-energy-storage-system-bess

[15] Hawaiian Electric Company, Inc., “Investigation of HECO, HELCO, and MECO related to the major power outages of October 15-16, 2006,” 2006. [Online]. Available: https://dms.puc.hawaii.gov/dms/DailyActivityReport.jsp?reportDate=04/01/2010

[16] Kauai Island Utility Cooperative, “Overview,” Touchstone Energy Cooperatives, 2017. [Online]. Available: http://website.kiuc.coop/content/overview

[17] J. Spector. “AES’ new Kauai solar-storage ‘Peaker’ shows how fast battery costs are falling,” Greentech Media, January 16, 2017. [Online]. Available: https://www.greentechmedia.com/articles/read/aes-puts-energy-heavy-battery-behind-new-kauai-solar-peaker

[18] SDG&E, “Energy Storage System request for offers,” 2016. [Online]. Available: https://www.sdge.com/sites/default/files/documents/634880294/2016%20SDGE%20PrefRes%20RFO%20Energy%20Storage.pdf?nid=17216

[19] California Public Utilities Commission. Resolution E-4798. August 18, 2016. [Online]. Available: http://docs.cpuc.ca.gov/PublishedDocs/Published/G000/M165/K861/165861595.PDF

[20] General Electric, “GE unveils world’s first battery storage & gas turbine hybrid with Southern California Edison,” October 4, 2016. [Online]. Available: http://www.genewsroom.com/press-releases/ge-unveils-world’s-first-battery-storage-gas-turbine-hybrid-southern-california

[21] P. Maloney, “Gas plant makers embrace batteries with hybrid machines,” Utility Dive, July 25, 2017. [Online]. Available: http://www.utilitydive.com/news/gas-plant-makers-embrace-batteries-with-hybrid-machines/447655/

[22] NERC, “Essential reliability services task force measures framework report,” 2015. [Online]. Available: http://www.nerc.com/comm/Other/essntlrlbltysrvcstskfrcDL/ERSTF%20Framework%20Report%20-%20Final.pdf

[23] C. Loutan, V. Gevorgian, *et al.* “Using renewables to operate a low-Carbon grid: Demonstration of advanced reliability services from a utility-scale solar PV plant,” California ISO, 2016 [Online]. Available: https://www.caiso.com/Documents/UsingRenewablesToOperateLow-CarbonGrid.pdf

Mike Jacobs develops recommendations and strategy to shape electricity markets and policies to encourage demand-side and renewable energy. Prior to coming to UCS, Mr. Jacobs worked at two renewable energy and energy storage companies that together built four storage facilities in Hawaii. Two of these facilities demonstrated grid support and transmission capabilities. While on the staff of the American Wind Energy Association, he led settlement efforts at the Federal Energy Regulatory Commission to streamline generator interconnection rules for wind and distributed generation. He has served on the boards of renewable energy organizations and the Northern Maine Independent System Administrator.

Technology Assessment of Stationary Electricity Storage Technologies for Different System and Time Scales

Xiaojin Zhang[#1], Andrea Abdon[*2], David Parra[#3], Martin K. Patel[#4], Christian Bauer[#5], Jörg Worlitschek[#6],

[#]*Technology Assessment Group, Laboratory for Energy Systems Analysis, Paul Scherrer Institute*
PSI, Forschungsstrasse 111, 5232 Villigen, Switzerland
[#]*Energy Efficiency Group, Institute of Environmental Sciences, University of Geneva*
1205 Geneva, Switzerland
[#]*Thermal Electricity Storage Group, Lucerne University of Applied Sciences & Arts*
Werftestrasse, 6002 Luzern, Switzerland
**Energie360*
Aargauerstrasse 182, 8048 Zürich, Switzerland

***Abstract*— Electricity storage (ES) has the potential of introducing several energy system benefits [1], but different technologies offer various services which can be traded on different markets. In this study, a combined assessment methodology is proposed, enabling a benchmark comparison of stationary electricity storage technologies (pumped hydro storage, advanced compressed air storage, power-to-gas-to-power, li-ion battery) for different time and system scales, considering their technical, economic and environmental performance.**

***Keywords*— electricity storage, stationary application, life cycle assessment, techno-economic assessment**

The results [2][c] show that for short-term time scale (0.01 h), battery stands out with an advantage in terms of levelised costs, while Advanced Adiabatic (AA-) and Isothermal (I-) Compressed Air Energy Storage (CAES) have relatively low life cycle Greenhouse Gas (GHG) emissions. For the medium-term time scale (4.5h), I-CAES shows the best performance for small scale systems, while for large scale systems, Pumped Hydro Storage (PHS) and AA-CAES show excellent performance. In the long-term time scale (seasonal) scenario, Power-to-gas-to-power (P2G2P) has lower levelised costs due to low or avoided investment for storage of gas, but higher GHG emissions than other technologies. If existing reservoirs can be utilized for PHS, it can be economically competitive to P2G2P for seasonal storage. However, storage capacity required for seasonal storage should also be taken into account, for which P2G2P has more flexibility.

I. Introduction

Increasing penetration of renewable electricity has been one of the reasons for very low electricity costs on the European electricity spot markets in recent years [3]. Growing renewable energy production has been also a challenge for grid operators in terms of transmission and distribution loads. A potential remedy to the temporal mismatch of supply and demand is electricity storage (ES) [4][1][5], which has led to an increased research effort during recent years as several reviews show [1][6][7]. Although there has been studies investigating different storage technologies, comparative assessment from both techno-economic and life cycle environmental perspective is lacking. Past assessment has also rarely taken into account the application of storage, and many of them are focusing on battery technologies for small-scale applications such as in mobility.

This study therefore complements the previous investigations with a combined assessment of stationary electricity storages, considering both techno-economic and environmental performance. Levelised cost (EUR/kWh) and life cycle greenhouse gas emissions (CO_2 eq/kWh) of electricity from storage are quantified as performance indicators, representing economic and environmental performance respectively. The study focuses on electricity storage technologies that can be applied for stationary applications, including pumped hydro storage (PHS), advanced adiabatic- and isothermal-compressed air electricity storage (AA- and I-CAES), a type of lithium-ion battery suitable for stationary application, and power-to-gas-to-power (P2G2P). Consideration of technologies' current and potential future (2020-2030) performance, at different storage time scales are taken into account. Storage time scales include short- (0.01 hr), medium- (4.5 hr) and long (seasonal, 2160 hr) time scales, representing frequency control (21 cycles per hour), shifting the consumption between peak and off-peak time during the day (1 cycle per day), shifting the consumption between summer and winter time during the year (1 cycle per year with 12 hours per day for 6 months), respectively. There are

Andrea Abdon, David Parra and Xiojin Zhang are co-first authors of this work.

[c] This is a summary of the work that is published in Energy, volume 139, page 1173–1187 in 2017 (https://doi.org/10.1016/j.energy.2017.07.097).

also two system scales (characterized by discharge power): 1 MW, which represents relatively decentralized storage systems, and 100 MW, which represents more centralized storage systems. A sensitivity analysis is incorporated in order to understand the variability of the results, driven by the ranges of key input parameters, including lifetime, system round-trip efficiency, costs, stored electricity type and cost. The goal is to understand the relative environmental and economic implications considering not only the technologies, but also the application and system scales.

The three storage operational scenarios and two storage system scales are outlined in the table below, together with the corresponding number of cycles, and annual electricity supply from storage.

TABLE I.I
STORAGE OPERATIONAL SCENARIOS AND SYSTEM SIZES WITH ANNUAL ELECTRICITY PRODUCTION AND NUMBER OF CYCLES PER DAY OR PER YEAR. TS: TIME SCALE.

1 MW	**Short TS 0.01h**	**Medium TS 4.5h**	**Long TS 2'160h**
Cycles	20 per day	1 per day	1 per year
Annual Energy Supply from Storage	81 MWh	1'643 MWh	2'160 MWh


100 MW	**Short TS 0.01h**	**Medium TS 4.5h**	**Long TS 2'160h**
Cycles	20 per day	1 per day	1 per year
Annual Energy Supply from Storage	8'091 MWh	164'250 MWh	216'000 MWh

II. METHODOLOGY

In the techno-economic analysis, levelised cost of electricity storage (LCOES) is quantified as economic performance indicator for comparison of the considered storage technologies. This parameter is computed as following:

$$LCOES = (CAPEX + OPEX \cdot AF) / (W \cdot AF) \quad (1)$$

$$AF = (1 - (1 + i)^{-n}) / i \quad (2)$$

Where:

CAPEX = capital expenditures

OPEX = operational expenditures

W = annual energy output (kWh) of storage

= number of cycles per year * discharge power *time of discharge (time-scale)

AF = Annuity Factor

i = discount rate

n = lifetime (years)

Discount rate is set to be 5%, and lifetime is specified for each technology individually. In line with previous investigations, the operational expenditures include the cost of electricity [8] [9]. In order to evaluate the impact of electricity cost on the LCOES, calculations with high (0.15 EUR/kWh) [1], low (0 EUR/kWh) [2] and medium (0.10 EUR/kWh) electricity costs are performed. In addition, a sensitivity analysis considering the range of investment and operational costs, efficiency and lifetime is also carried out for which the values of input parameters are summarized in Table 2.4.

The environmental performance of ES technologies is assessed using ISO-compliant attributional Life Cycle Assessment (LCA) [10]. The functional unit is 1 kWh of electricity supplied from storage. The impact on climate change, estimated in life cycle greenhouse gas emissions (in carbon dioxide equivalents) per kWh of electricity supply from storage, according to IPCC 2013 [11] as implemented in Simapro 8.0.4.30, is used as the evaluation criterion for the environmental performance. The system boundary covers the life cycle of each storage system, including the production of materials required to manufacture the storage facility, the energy consumption during the operation of storage, the maintenance and the end-of-life disposal and treatment. The sources of life cycle inventory (LCI) data vary between technologies. The foreground LCI data are partially based on previous work of the authors, and partially based on literature with adjustments on technology specifications and performance in order to ensure the consistency of evaluation. The background database used is ecoinvent version 3.1 [12]. The types of electricity being stored include electricity produced by wind turbines and solar photovoltaics and average grid supply in Switzerland. Supply from wind turbines in Switzerland has the lowest life cycle GHG emissions (18 g CO_2 eq./kWh), and the supply from Swiss grid (representing the consumption mix including electricity imports from neighboring countries) is associated with the highest life cycle GHG emissions (115 g CO_2 eq./kWh [13]). Thus, the lower and higher limits of GHG emissions in the sensitivity analysis results correspond to Swiss wind power and the Swiss grid mix being stored. In sensitivity analysis where variation of electricity type is not considered, average grid supply in Switzerland is used.

More details on technology-specific assumptions can be found in [2].

[1] Price estimate based on PV generation cost
[2] Price assumed to be zero for periods of low demand and high supply of renewable electricity

III. Results

The combined assessment results are presented in this conference paper, while more detailed results on LCOES and life cycle GHG emissions can be found in [2] separately. In the figures below, the combined assessment results including both LCOES and life cycle GHG emissions per kWh of supply from storage are shown on y and x axis respectively, in the form of box charts in Fig. 3.5 (considering efficiency, lifetime, costs and without considering the cost and type of electricity) and Fig. 3.6 (considering efficiency, lifetime, cost, cost and type of electricity) for the large and small scale systems. As it is shown, the range of performance increases a lot when the cost and type of electricity are taken into account.

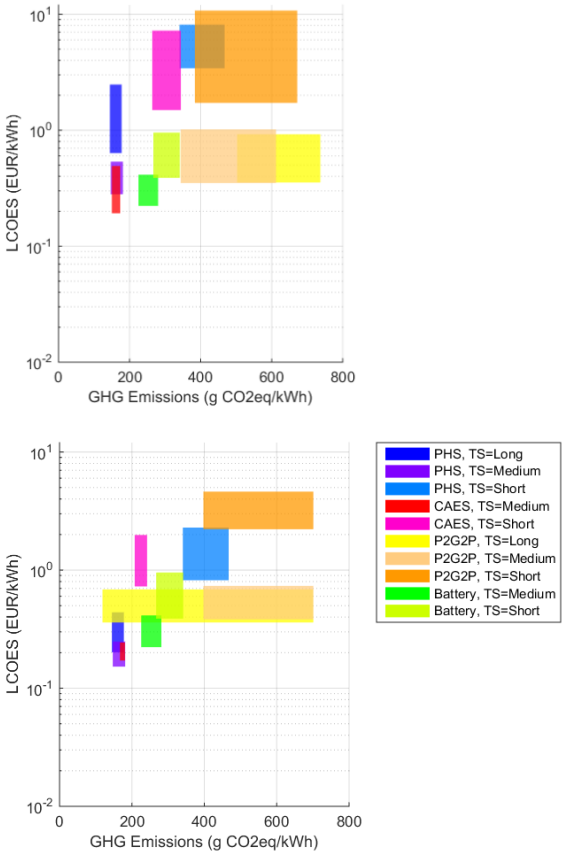

Fig. 3.5 Combined results considering all technical factors (lifetime, efficiency, and costs) and Swiss grid mix supply at an electricity cost of 0.10 EUR/kWh; left: 1 MW systems; right: 100 MW systems (Fig.s with results split into short-, medium- and long- time scale can be found in Appendix A)

When only the technological factors (lifetime, efficiency, costs) are considered (Fig. 3.6), preference of technologies for certain application is relatively obvious. For the short time scale, the Li-ion battery has the lowest LCOES and CAES has lowest GHG emissions; LCOES of battery can be up to 94% lower than those of CAES, while life cycle GHG emissions of CAES can be comparable or up to 39% lower than those of the battery. For medium storage, a different ranking of technologies with an overall better technology performance is shown compared to short time scale. CAES and PHS become more attractive than the battery for the large scale system, while for small scale system, all these three technologies have potential to be the preferred technology. For the long time scale, P2G2P shows a poor performance compared to PHS for large scale system, but for small scale system, P2G2P shows in general lower LCOES and higher life cycle GHG emissions than PHS. However, it should be kept in mind that the opportunities for seasonal storage in Switzerland using PHS in practice are limited as very large storage volumes are required, which are constrained by the topography, social and political conditions.

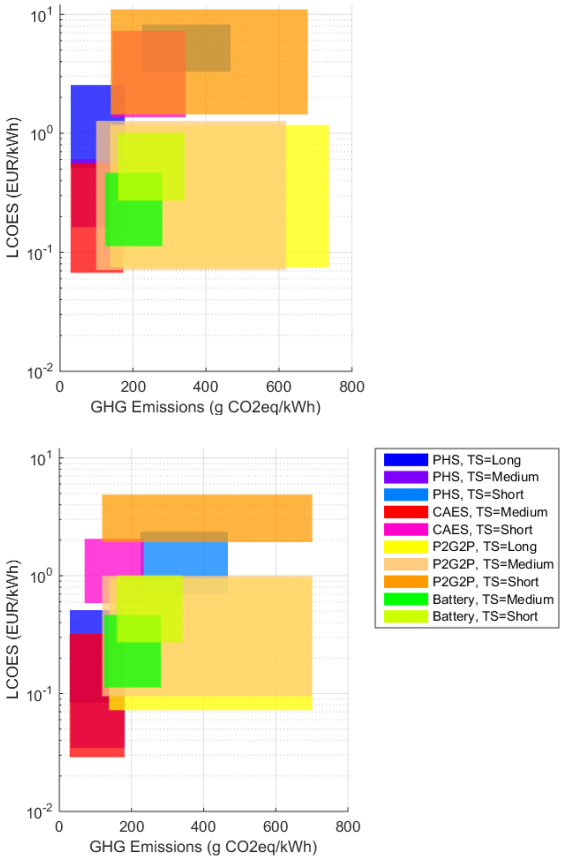

Fig. 3.6 Combined results considering all technical factors (lifetime, efficiency, and costs) as well as electricity cost range and types (Swiss wind electricity and Swiss grid supply (based on consumption mix)); left: 1 MW systems; right: 100 MW systems (Fig.s with results split into short-, medium- and long time scale can be found in Appendix A).

The ranking of technologies becomes less clear when electricity cost and type are taken into account (Fig. 3.6) the performances of technologies overlap a lot more with each other than results considering technological factors only (Fig. 3.5). The lower the system efficiency is, the higher the impact of electricity variation on storage technology performance is. Therefore, P2G2P stands out with its potential wide range of performance, due to its lowest system efficiency and the important role of

electricity type stored. In other words, storing renewable electricity with low or zero cost and low life cycle GHG emissions via P2G2P could result in an overall competitive solution despite of the comparatively low system efficiency.

IV. Conclusions and Future Research

In this study, a comprehensive methodology combining techno-economic and environmental life cycle assessment for stationary electricity storage technologies under various application scenarios is demonstrated. LCOES and life cycle GHG emissions are quantified for each storage technology and scenario.

In terms of LCOES, Li-ion battery shows the lowest cost for short time scale (0.01 h). Together with I-CAES, Li-ion battery might also be economically attractive for the medium time scale (4h) for small systems (1 MW), while for large systems (100 MW), PHS and AA-CAES show lower LCOES. For the seasonal storage at small scale, P2G2P may outperform PHS due to lower investment costs. The P2G2P technology can be also economically more attractive than PHS for large systems, when the electricity cost is close to zero.

In terms of life cycle GHG emissions, when the ranges of system lifetimes and efficiencies are considered, I- and AA-CAES have lower emissions than other technologies for short time scale, and it is very closely followed by Li-ion battery; for medium time scale, the emissions of PHS and CAES can be comparatively low; whereas for long time scale, PHS has lower emissions than P2G2P. Storing electricity from renewable sources with low GHG intensities substantially reduces the emissions of P2G2P, making it much more competitive with other technologies, especially in short time scale. In general, most storage technologies can contribute to a reduction of overall system GHG emissions, if intermittent renewable electricity is stored and subsequently replaces conventional grid supply that is produced by fossil fuel to a large extent.

Considering both LCOES and life cycle GHG emissions, when Swiss grid mix supply with an assumed cost of 0.10 EUR/kWh is stored, the current results show that for the short time scale, Li-ion battery and CAES technology are the most attractive options, whereas for medium time scale, both PHS and AA-CAES are more attractive for large systems due to comparable emissions and lower LCOES than other technologies. For small systems, I-CAES has better potential performance than the other technologies. The long time scale results show that large-scale PHS is more attractive than P2G2P due to substantially lower emissions, although the capacity required for seasonal storage shall also be taken into account for which P2G2P may have more flexibility; for small scale systems, LCOES of P2G2P are lower, while PHS performs better in terms of life cycle GHG emissions. In the case of storing renewable electricity with zero marginal costs and low GHG intensity, P2G2P performance improves and may be comparable or better compared to other technologies for medium and long time scales.

In conclusion, this study demonstrates the potential of several emerging electricity storage technologies becoming serious competitors for incumbent storage systems, although it should be kept in mind that higher uncertainties of input data presently cannot be avoided for emerging technologies (e.g., AA-CAES and I-CAES as well as P2G2P) due to limited real applications. The result shows the great importance of storage applications and the variations of electricity type and cost in storage technology assessment. It also gives an overview on relative ranking of technology performance for different applications.

Assessing techno-economic benefits and life cycle emissions of electricity storage technologies under dynamic conditions, and how to establish and compare scenarios with combined applications within one storage system need to be further analysed. Our present scope is limited to the context of Switzerland, but the assumptions and methodology framework used in this study can be extended to other technologies and/or regions. In addition, the methodology applied in this study can also be expanded with other performance measures such as levelized value or complementary environmental indicators, and comparison with other alternatives for storage, such as grid expansion, in order to further enrich the evaluation of stationary electricity storage.

Acknowledgement

The work has been carried out by the funding support from The Swiss Competence Centre for Energy Research for Storage of Heat and Electricity (SCCER-HaE) from 2014 to 2016, by Hochschule Luzern funding, and by the Energy System Integration (ESI) platform of Paul Scherrer Institute.

References

[1] X. Luo, J. Wang, M. Dooner, and J. Clarke, “Overview of current development in electrical energy storage technologies and the application potential in power system operation,” *Appl. Energy*, vol. 137, pp. 511–536, Oct. 2014.

[2] A. Abdon, X. Zhang, D. Parra, M. K. Patel, C. Bauer, J. Worlitschek, “Techno-economic and environmental assessment of stationary electricity storage technologies for different time scales,” *Energy*, vol. 139, pp. 1173–1187, Nov. 2017.

[3] E. Fanone, A. Gamba, and M. Prokopczuk, “The case of negative day-ahead electricity prices,” *Energy Econ.*, vol. 35, pp. 22–34, Jan. 2013.

[4] R. K. Edmunds, T. T. Cockerill, T. J. Foxon, D. B. Ingham, and M. Pourkashanian, “Technical benefits of energy storage and electricity interconnections in future British power systems,” *Energy*, vol. 70, pp. 577–587, Jun. 2014.

[5] J. K. Kaldellis and D. Zafirakis, “Optimum energy storage techniques for the improvement of renewable energy sources-based electricity generation economic efficiency,” *Energy*, vol. 32, no. 12, pp. 2295–2305, Dec. 2007.

[6] D. O. Akinyele and R. K. Rayudu, “Review of energy storage technologies for sustainable power networks,” *Sustain. Energy Technol. Assessments*, vol. 8, pp. 74–91, Dec. 2014.

[7] H. Chen, T. N. Cong, W. Yang, C. Tan, Y. Li, and Y. Ding, “Progress in electrical energy storage system: A critical review,” *Prog. Nat. Sci.*, vol. 19, no. 3, pp. 291–312, Mar. 2009.

[8] F. Klumpp, “Potential for large scale energy storage technologies – Comparison and ranking including an outlook to 2030,” *Energy Procedia*, vol. 73, pp. 124–135, Jun. 2015.

[9] V. Jülch, T. Telsnig, M. Schulz, N. Hartmann, J. Thomsen, L. Eltrop, and T. Schlegl, “A holistic comparative analysis of different storage systems using levelized cost of storage and life cycle indicators,” *Energy Procedia*, vol. 73, pp. 18–28, Jun. 2015.

[10] The International Standards Organisation, “Environmental management — Life cycle assessment — Principles and framework,” *Iso 14040*, pp. 1–28, 2006.

[11] IPCC, 2013: *Climate Change 2013: The Physical Science Basis. Contribution of Working Group I to the Fifth Assessment Report of the Intergovernmental Panel on Climate Change* [T. F. Stocker, D. Qin, G.-K. Plattner, M. Tignor, S. K. Allen, J. Boschung, *et al.* (eds.)]. Cambridge University Press, Cambridge, United Kingdom and New York, NY, USA, 2013.

[12] Cut-Off System Model. (2014) [Online]. Available: https://www.ecoinvent.org/database/system-models-in-ecoinvent-3/cut-off-system-model/allocation-cut-off-by-classification.html

[13] K. Treyer and C. Bauer, “Life cycle inventories of electricity generation and power supply in version 3 of the ecoinvent database-part II: electricity markets,” *Int. J. Life Cycle Assess.*, vol. 21, no. 9, pp. 1255–1268, Sept. 2016.